THE DEVELOPMENT AND APPLICATION OF A NEW HIGH PRECISION GC-IRMS TECHNIQUE FOR N_2O-FREE ISOTOPIC ANALYSIS OF ATMOSPHERIC CO_2

By

Dominic Francesco Ferretti

A thesis

submitted to the Victoria University of Wellington

in the fulfilment of the

requirements for the degree of

Doctor of Philosophy

Victoria University of Wellington

1999

Abstract

A new GC-IRMS technique has been developed for isotopic and mixing ratio analysis of atmospheric CO_2. The technique offers for the first time, N_2O-free, high precision (<0.05 ‰) analysis of $\delta^{13}C$ and $\delta^{18}O$ from small whole-air samples. On-line GC separation of CO_2 and N_2O from these small samples is combined with IRMS under elevated ion source pressures. A specialised open split interface is an integral part of the inlet system and ensures a continuous flow of either sample gas or pure helium to the IRMS. The analysis, including all flushing, uses a total of 45 ml of an air sample collected at ambient pressure. Of this, three 0.5 ml aliquots are injected onto the GC column, each providing ~0.8 nmol CO_2 in the IRMS source. At this sample size, $\delta^{13}C$ precision obtained is at the theoretical shot-noise limit. Demonstrated precisions for $\delta^{13}C$, $\delta^{18}O$, and CO_2 mixing ratio (all measured simultaneously) are 0.02 ‰, 0.04 ‰ and 0.4 ppm respectively. The initial results from an inter calibration exercise with Atmospheric Research at the Commonwealth Scientific and Industrial Research Organisation (CSIRO), Australia achieved the International Atomic Energy Agency (IAEA) target precision for $\delta^{13}C$. During this exercise, agreement for $\delta^{18}O$ and CO_2 mixing ratio was outside the IAEA and World Meteorological Organization (WMO) target precisions for these species, however, when the measurement uncertainties of the two laboratories were considered, the differences were not significant. An inter comparison program using air samples collected at Baring Head, New Zealand and Cape Grim, Australia was also established with CSIRO and $\delta^{13}C$, $\delta^{18}O$ and CO_2 mixing ratio showed excellent agreement when combined measurement uncertainties were considered. Further inter comparisons with the Carbon Cycle Group at the National Oceanic and Atmospheric Administration Climate Monitoring and Diagnostics Laboratory (NOAA CMDL), the Institute of Arctic and Alpine Research (INSTAAR), and Scripps Institution of Oceanography (SIO) were also established. No significant differences for $\delta^{13}C$ were observed during these inter comparison programs. Therefore, these preliminary measurements suggest that the current situation between these laboratories for $\delta^{13}C$ comparisons from whole-air in glass flasks may be improved compared to the 1995 IAEA inter comparison from whole-air in high-pressure cylinders. Following these inter calibration and inter comparison exercises, temporal and spatial variations in the mixing ratio and isotopic composition of atmospheric CO_2 were determined over a large region of the Pacific Ocean to demonstrate the successful use of the GC-IRMS technique. Temporal variations were observed at

long-term monitoring sites in the Southern Hemisphere (Baring Head, Cape Grim, and Arrival Heights, Ross Island, Antarctica). Seasonal cycles of CO_2 mixing ratio and $\delta^{13}C$, with amplitudes of ~1 ppm and ~0.05 ‰ respectively, were measured at Baring Head. A decline in $\delta^{13}C$ of ~-0.1 ‰/year was observed at Arrival Heights between 1997 and 1999. Spatial variations in the Pacific Ocean were investigated by shipboard sampling programs between ~62 °S and ~32 °N. These data were consistent with a Southern Ocean sink between ~43 °S and ~57 °S. In addition, inter hemispheric gradients of $\delta^{13}C$ and CO_2 mixing ratio in March and September 1998 were determined and the position and intensity of the SPCZ and ITCZ were important for the strength of these inter hemispheric gradients. Measurements performed during an upper tropospheric flight from New Zealand to Antarctica show elevated CO_2 levels and depleted $\delta^{13}C$ compared to samples obtained in the marine boundary layer over this region. A small-scale application of the technique measured soil-respired CO_2 in a New Zealand Mountain Beech forest from 150 ml sample flasks that were filled to ambient pressure. These measurements determined a difference between the $\delta^{13}C$ source signature from the young and old trees of ~0.3 ‰, which was in the correct direction but of smaller magnitude than that expected. The small sample requirements of the GC-IRMS technique ease sample collection logistics for varied research. Since initial results from an inter calibration exercise with CSIRO obtain the IAEA target precision for $\delta^{13}C$, and the technique has demonstrated its ability to successfully monitor atmospheric CO_2 species from small whole-air samples, without contamination by atmospheric N_2O or the use of cryogen, the technique will be a powerful tool in global carbon cycle research.

Acknowledgements

I would like to express my sincerest thanks to my two supervisors, Dr Dave Lowe of NIWA and Dr Jim McGregor of VUW for their invaluable expertise and assistance throughout the course of this research.

The nature of the research of this PhD has required the direct and indirect assistance of many people and without their help this research would not have been possible. Inter calibration and inter comparison exercises with other laboratories occur as a result of the assistance and co-operative spirit of many people. The same can be said for Pacific region measurements. These people are listed below and are sincerely thanked for their help.

- The entire TROPAC group at NIWA, especially Gordon Brailsford, Ross Martin, Rob Knobben, Rowena Moss, Tony Bromley, Jill Cainey, Sylvia Nichol, Martin Manning, Tom Clarkson, Peter Bergamaschi and Antony Gomez.
- Expert technical advice on isotope ratio mass spectrometry from: John Hayes, Woods Hole Oceanographic Institute; and Willi Brand, formerly of Finnigan MAT, GmbH and now at Max-Planck-Institut für Biogeochemie.
- The assistance of CSIRO Atmospheric Research Australia is gratefully acknowledged and Colin Allison and Roger Francey are especially thanked for their expertise. Also Lisa Cooper for freight and analysis of the extra ICP flasks.
- Tom Conway, Ken Massarie, Ed Dlugokencky and Constance Prosotko-Bell of the Carbon Cycle Group at NOAA CMDL.
- Jim White and Bruce Vaughn of INSTAAR.
- Dave Keeling and Allane Bolenbacher of SIO.
- The Captain and crew of the *Argentina Star* (P & O Nedlloyd shipping company) in addition to Carolyn Walker for sample collection.
- Mike Harvey for collecting samples onboard *R.V Tangaroa* in the Southern Ocean
- RNZAF Hercules crew and Antarctic New Zealand staff, for aircraft sampling and logistical support for Antarctic sampling at Arrival Heights.
- The NIWA IT staff for providing excellent computing facilities and assistance.
- The NIWA – VUW Center of Excellence for Atmospheric and Climatic Research for providing the research grant which made this work possible.
- Jeanette Ida for her sensational support and proof reading ability.

Publications

Sections of work presented in this thesis have been reported in the following publication:

- D.F. Ferretti, D.C. Lowe, R.J. Martin, and G.W. Brailsford, A new GC-IRMS technique for high precision, N_2O-free analysis of $\delta^{13}C$ and $\delta^{18}O$ in atmospheric CO_2 from small air samples, *Journal of Geophysical Research*, in press, accepted 13 Oct 1999.

List of Figures

List of Tables

1 Introduction and scope of the thesis

1.1 Introduction

Human activities have released billions of tonnes of *greenhouse gases*[*] into the atmosphere since the industrial revolution [*IPCC*, 1996]. This has raised greenhouse gas levels far above those of the 10,000 year stable period before this time. For example, over the last two hundred years, the dominant *anthropogenic*[†] greenhouse gas, carbon dioxide (CO_2) has increased significantly, rising by ~30 %, from a mixing ratio of ~280 parts per million (ppm) to its current level of ~360 ppm [*Etheridge et al.*, 1996].

These rising greenhouse gas levels have been caused by the release of carbon to the atmosphere from industrial and agricultural activities (*e.g.* fossil fuel combustion and deforestation). This has perturbed the balance of the carbon cycle, which has large, naturally varying fluxes that have existed in near balance over periods of millennia.

Because these greenhouse gases are radiatively active in the atmosphere, rising greenhouse gas levels have led to the enhanced greenhouse effect. The resultant additional heating to the Earth's surface may lead to global warming with substantial consequences to the Earth's climate. The degree of this global warming is uncertain and is the focus of many research programs worldwide.

As the level of atmospheric CO_2 has risen, the isotopic composition of atmospheric CO_2 has changed because a greater fraction of atmospheric CO_2 is now of fossil fuel origin, which is isotopically lighter than ambient atmospheric CO_2 [*Keeling*, 1973; *Friedli et al.*, 1986; *Siegenthaler and Oeschger*, 1987]. Due to such isotopic differences for CO_2 from different sources, measurements of these isotopic signatures therefore provide valuable information. In terms of atmospheric CO_2, monitoring its mixing ratio and isotopic composition enables estimates to be made of the spatial and temporal variations in, and the magnitude of, biospheric and oceanic sources and sinks of carbon [*Ciais et al.*, 1995a, b; *Francey et al.*, 1995]. More extensive measurements (both mixing ratio and isotopic) are required to better distinguish between these sources and sinks [*Conway et al.*, 1994]. This improved quantification is necessary to provide more accurate and precise assessments and predictions of the future state of the atmosphere.

---

[*] Greenhouse gases are radiatively active gases that are transparent to incoming short-wave solar radiation, but which trap some of the outgoing long-wave terrestrial radiation

[†] Produced as a result of human activities

A main limitation to the accuracy and precision of global carbon cycle models is the fact that collected data is very sparse. The logistics and costs of providing extensive global coverage are too great for an individual laboratory to easily undertake and therefore a cooperative international effort is required. However, attempts to do this by "seamlessly merging" measurements into one extensive data set are limited by the accuracy and precision of the measurements obtained from many laboratories. This is because many laboratories fall short of the formally agreed target precisions set by the World Meteorological Organization (WMO) and the International Atomic Energy Agency (IAEA) [*Francey and Rayner*, 1998].

Currently, difficulties exist in the techniques and calibration strategies used to measure CO_2 species. The traditional technique for measuring atmospheric CO_2 isotopes (dual-inlet IRMS) requires relatively large (μmol) samples of CO_2. This usually isn't a problem for routine measurements, but does hinder inter calibration programs which are essential to enable the merging of laboratory measurements. During CO_2 sample extraction, nitrous oxide (N_2O) is transferred as a contaminant. Therefore, a correction for N_2O must be applied to the isotopic measurements. This correction varies mainly as a function of the amount of N_2O compared to CO_2 in the sample and is about an order of magnitude larger than the precision required in the measurement. Other factors, *e.g.* the relative ionisation efficiency for N_2O versus CO_2, which is specific to individual mass spectrometers, also affects the N_2O correction. Unfortunately, not all laboratories use identical N_2O correction procedures and a standardised correction procedure needs to be used by *all* laboratories, as recommended by *Allison et al.*, [1995]. In addition, the sample extraction requires cryogen use, which is both costly and increases the human workload required to maintain the supply.

Analysis of N_2O-free samples avoids these problems completely. At present, one spectroscopic technique is available for contaminant-free isotopic measurements in atmospheric CO_2. This Fourier transform infrared spectroscopy (FTIR) technique is capable of performing carbon isotope ratio measurements in background levels of atmospheric CO_2 [*Esler*, 1997]. However, because the precision of this technique is about an order of magnitude larger than that required for monitoring the isotopic composition of atmospheric CO_2, and because the oxygen isotope ratio of CO_2 cannot be measured at present, the technique is currently limited to restricted applications.

Therefore, it can be seen that, for isotopic analyses of CO_2, there is a need for an experimental technique that utilises small samples and offers contaminant-free isotopic analysis without off-line sample preparation involving cryogen use. Such a technique

should operate to a high level of precision and be internationally inter calibrated to allow the merging of its data with that from traditional techniques and from other laboratories worldwide.

The work presented in this thesis describes the development of such a technique. In addition, inter calibration and inter comparison exercises and some applications of the technique are presented to demonstrate its successful use on both large and small-scales.

1.2 Scope of the thesis

Chapter 2

- Reviews the field that the major application of this new technique will contribute to (the Earth's atmosphere and climate change).
- Reviews detail the following subjects: climate and the climate system, the Earth's atmosphere, perturbations to the natural state of the atmosphere, atmospheric CO_2, and the stable isotopes of CO_2: $\delta^{13}C$ and $\delta^{18}O$.

Chapter 3

- Reviews the history of isotope measurements by mass spectrometery, including dual-inlet IRMS and GC-IRMS.
- Defines the notation and standard gases used.
- Introduces isotope chromatography.
- Describes the experimental development of a new GC-IRMS technique for monitoring the mixing ratio and isotopic composition of atmospheric CO_2. Description of the inlet system, analysis procedure, and operational running of GC-IRMS is given. In addition, discussion of important points of the optimal configuration development including CO_2 – N_2O separation, maximisation of signal to noise ratio and reproducibility are given. Sufficient information is provided to enable replication of the technique from the details presented here.
- Presents the details of the technique performance (observed versus theoretical).

Chapter 4

- Discusses the limitations of current inter calibration programs.
- Details why high precision inter calibration is necessary for global monitoring of atmospheric CO_2 and therefore an important requirement for a new technique.

- Describes a high precision inter calibration exercise between the GC-IRMS technique and a traditional dual-inlet IRMS technique at CSIRO. This performs the initial stages of the inter calibration and evaluates the performance of the GC-IRMS technique with respect to the traditional techniques.
- Presents inter comparisons with other laboratories currently measuring atmospheric CO_2 species. This further assesses the performance of the GC-IRMS technique and compares operational flask air-sharing programs that were established during the work of this thesis.
- Investigates possible reasons for the discrepancies observed between laboratories and summarises areas that require further investigation.

Chapter 5

- Presents measurements made by the technique of the temporal and spatial variations of atmospheric CO_2 species in the Pacific Ocean region. This demonstrates its operational use and its capability of providing useful measurements to the field of carbon cycle research.
- Demonstrates a small-scale application of the GC-IRMS technique for soil-respired CO_2 to show its use for varied research different to that originally designed.

Chapter 6

- Summarises the thesis.
- Provides conclusions of:
  - the GC-IRMS technique for atmospheric CO_2.
  - the inter calibration and inter comparison exercises that were established.
  - the applications of the technique.
- Gives possibilities for future research using GC-IRMS.
- Provides an overall conclusion.

2 Background

Because the major application of the new GC-IRMS technique presented in this thesis is to monitor changes to the global carbon cycle and the climate system, it is necessary to first describe these areas in detail to provide the required background for these applications.

2.1 Climate and the climate system

Climate is usually defined to be the average weather for a specified area, described in terms of the mean and other statistical quantities that measure variability over a specified period (usually decades). Many components contribute to the climate system (Figure 2.1).

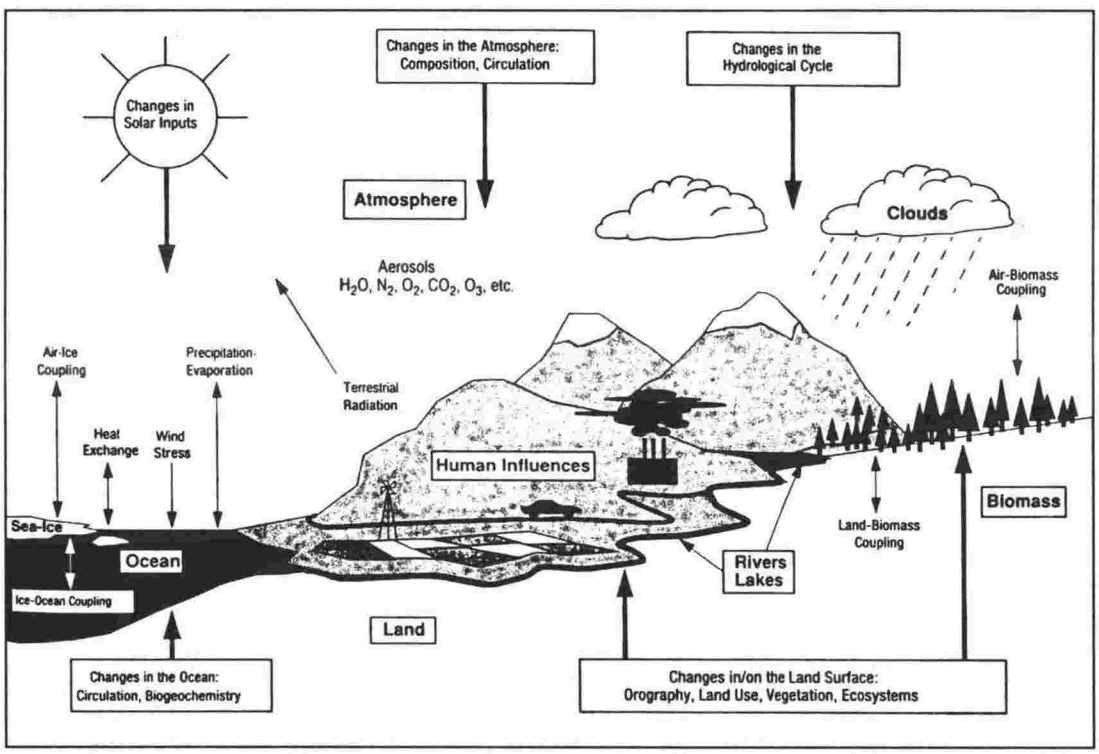

Figure 2.1 Components of the global climate system (bold), and their processes (thin arrows) and some aspects that may change (bold arrows) [*IPCC*, 1996].

The internal components of the climate system are the *atmosphere*, the terrestrial and marine *biosphere* (plants, animals, litter, detritus and biota), the *hydrosphere* (oceans, rivers, fresh and saltwater lakes, soil moisture, vadose water*, ground waters and atmospheric vapor) and the *lithosphere* (rocks, soils and sediment). Some external factors

* Water in the Earth's crust above the permanent groundwater level

of the climate system are the Sun and its output, the Earth's rotation and its slowly changing orbit, the geographic features on the land and the mass and basic composition of the atmosphere and oceans. These components determine the mean climate, which may vary from natural causes. External forces on the climate system as a result of human activities (*e.g.* increases in atmospheric greenhouse gases) may modify the climate system and their potential effects are uncertain. This aspect of atmospheric change is the field that the work of this thesis contributes to.

2.2 The Earth's atmosphere

2.2.1 Structure

The Earth's atmosphere is a relatively thin layer of gas (~100 km thick) surrounding the planet Earth (of radius ~6370 km). It is divided into 4 main regions: the *troposphere, stratosphere, mesosphere* and *thermosphere*, primarily based on temperature gradients (Figure 2.2).

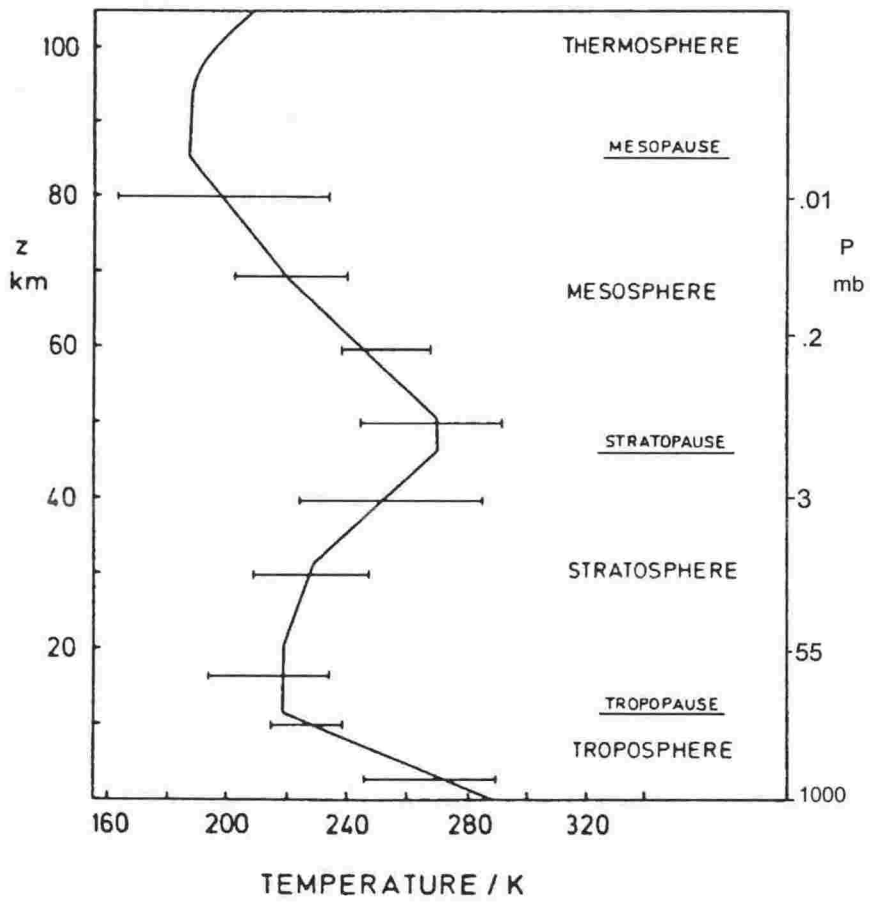

Figure 2.2 Vertical temperature and pressure structure of the atmosphere [Adapted from *Warneck*, 1988]. The solid curve is the U.S. Standard Atmosphere, and the horizontal bars indicate the range of monthly means observed between the equator and pole.

Atmospheric pressure falls exponentially with altitude, and ~90 % of the mass of the atmosphere is contained in the lowest layer of the atmosphere, the troposphere. Here, the temperature decreases with altitude at a relatively uniform rate. Because of this temperature gradient, the troposphere is unstable to convection. Therefore the troposphere is "well mixed" because efficient vertical mixing of gases occurs within it. The altitude of the tropopause depends strongly on latitude, varying from ~15 km in equatorial regions to ~10 km in Polar Regions. It also varies a small amount with season (< 2 km) and meteorological conditions [*Warneck*, 1988]. Temperature rises with altitude in the stratosphere due to the absorption of solar radiation, mainly by O_3 and O_2, and subsequent heating. This temperature inversion results in very slow vertical mixing and a vertically stratified structure within the stratosphere. Ninety nine percent of the mass of the atmosphere is contained in this lowest ~50 km of the troposphere and stratosphere. Above the stratopause, in the mesosphere, temperature again decreases with altitude to the mesopause. The outermost region of the atmosphere, the thermosphere, has no well-defined upper boundary and temperature increases to ~1000 ^{o}C at 250 km, but this varies widely with solar activity. The large temperature increase with altitude in the thermosphere is due to the absorption of most high-energy solar radiation reaching the atmosphere by N, O, N_2 and O_2 above 100 km. Another well-known region of the atmosphere is the *ionosphere*. This electrically conducting region which exists from ~60 km upward, with no defined upper boundary, is utilised for the transmission of radio waves. The electron concentration in the ionosphere varies with day and night and solar activity and its maximum occurs at ~400 km.

2.2.2 Composition

Of the Earth's dry atmosphere, 99.98 % is composed of the three main gases; Nitrogen, Oxygen and Argon. The remaining 0.02 % is composed of the minor constituents of the atmosphere that are referred to as *trace gases* of which the *greenhouse gases* are part (Table 2.1). Water vapor varies from ~3 ppm to ~4 % by volume.

Table 2.1 Composition of dry, unpolluted air [Adapted from *Manahan*, 1994].
Only major greenhouse gases are given. Greenhouse gas values are at early 1990 levels.

Gas	Abundance	Major source
[a]Nitrogen (N_2)	78.08 %	Biogenic
[a]Oxygen (O_2)	20.95 %	Biogenic
[b,c]Argon (Ar)	0.934 %	Radiogenic
[b,d]Carbon dioxide (CO_2)	350 ppm	Biogenic, Industrial
[c]Neon (Ne)	18.18 ppm	Interior
[c]Helium (He)	5.24 ppm	Radiogenic
[c]Krypton (Kr)	1.14 ppm	Interior
[d]Methane (CH_4)	1.6 ppm	Biogenic
[d]Nitrous oxide (N_2O)	300 ppb[e]	Biogenic
[d]Carbon monoxide (CO)	~120 ppb	Photochemical, anthropogenic
[c]Xenon (Xe)	87 ppb	Interior

[a]Major components

[b]Minor components

[c]Noble gases

[d]Greenhouse gases

[e]Parts per billion

The major components of the atmosphere are long lived. Noble gases are permanent in the atmosphere (except for helium, which is slowly escaping), while the anthropogenic greenhouse gases are variable and increasing. CO is not a direct greenhouse gas, but as it influences the oxidative state of the atmosphere and the removal of CH_4 and some other greenhouse gases, it therefore indirectly influences the greenhouse effect [*IPCC,* 1995].

2.2.3 Circulation

The large-scale atmospheric circulation of the atmosphere is shown in Figure 2.3.

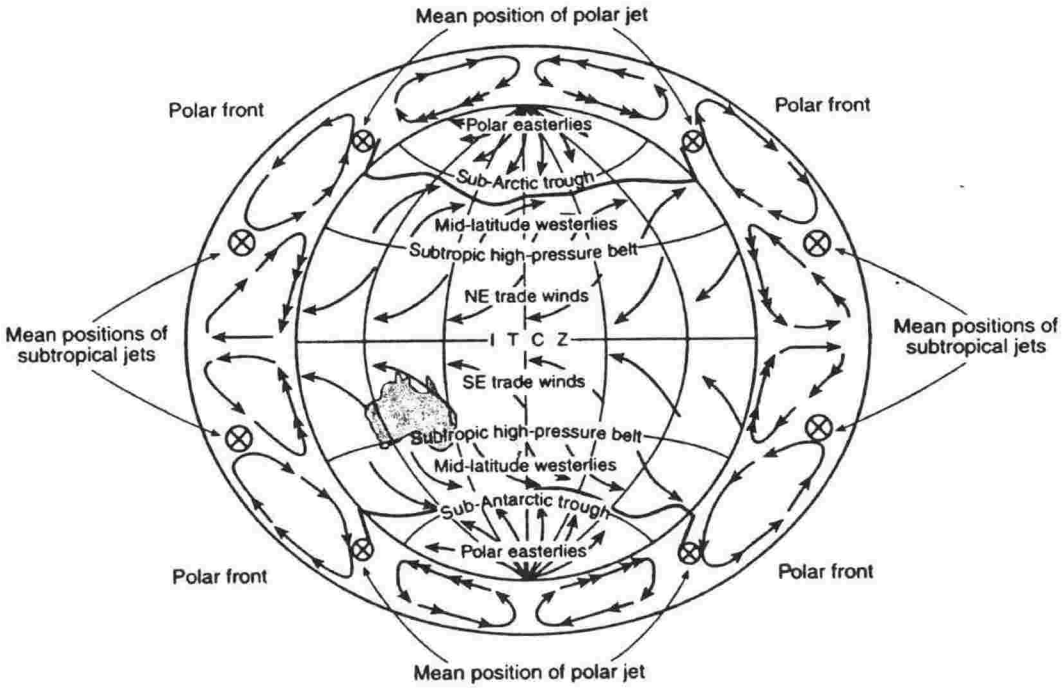

Figure 2.3 General circulation of the global atmosphere [*Sturman and Tapper*, 1996].
Single headed and double headed arrows in the cross sections indicate wind components from the West and East respectively. The *Inter Tropical Convergence Zone (ITCZ)* is the meteorological equator and in this region, ascending air separates two thermally forced "Hadley" cells. The air at high levels develops a considerable westerly component as it moves poleward, cooling and subsiding, reaching a maximum of ~200 km/h in the *subtropical jet stream.* In addition, some of the air descends to the surface at this latitude, forming the *subtropical high-pressure belt* zone. Between this zone and the equatorial low-pressure zones, lie the *trade-wind easterlies.* From the subtropical high-pressure belts, some of the subsiding air moves poleward at low levels, gaining a westerly component because of Coriolis deflection, giving rise to the *mid-latitude-westerlies.* This relatively warm poleward-moving air eventually encounters and rises over colder denser air flowing equatorward from the poles in a region defined as the *polar front.*

Interhemispheric exchange in the troposphere is seasonal and is related to the position of the ITCZ. Here, the inter-hemispheric mixing is slow and the ITCZ forms an effective "barrier" between the two hemispheres. Limited global transport occurs in the upper troposphere but gases that have sufficiently long lifetimes are relatively well transported after entrainment into the stratosphere. The tropospheric-stratospheric exchange rate is ~1.5 years for both hemispheres and the inter-hemispheric exchange rate is ~1 year in the troposphere and ~3.5 years in the stratosphere [*Warneck*, 1988]. In both hemispheres, the troposphere is both horizontally and vertically well mixed. The stratosphere is only horizontally well mixed because the strong temperature inversion present inhibits vertical motion.

2.3 Perturbations to the natural state of the atmosphere.

Over the last ~200 years, the human population has grown exponentially from ~0.6 billion in 1700 to ~6 billion in 1999, and is expected to reach ~9 billion by the year 2050 [*U.S. Bureau of the Census, International Data Base*, http://www.census.gov/ipc/www/worldpop.html]. Strongly correlated with population growth over this period since the industrial revolution is the onset of many anthropogenic activities, which perturb the atmosphere from its natural state. These perturbations and associated effects are divided into inter-related areas of urban pollution, acid rain, ozone depletion and the *greenhouse effect*. In this background chapter, only the greenhouse effect is investigated.

2.3.1 The Greenhouse Effect

Most of the electromagnetic energy reaching the Earth originates from the Sun's surface – the photosphere. Of this, only ~40 % lies in the visible spectrum that we see (~400 to 700 nm). Of the rest, ~10 % occurs at wavelengths shorter than the visible spectrum and ~50 % occurs at wavelengths longer than the visible spectrum. Of this solar spectrum, absorption by various gases, primarily H_2O, CO_2 O_3 and O_2 (in addition to N_2, N, O, NO, N_2O, CO and CH_4, which also exhibit small absorption spectra) occur in the atmosphere. This causes the solar irradiance reaching the Earth's surface to be lower from that incident at the top of the atmosphere (Figure 2.4).

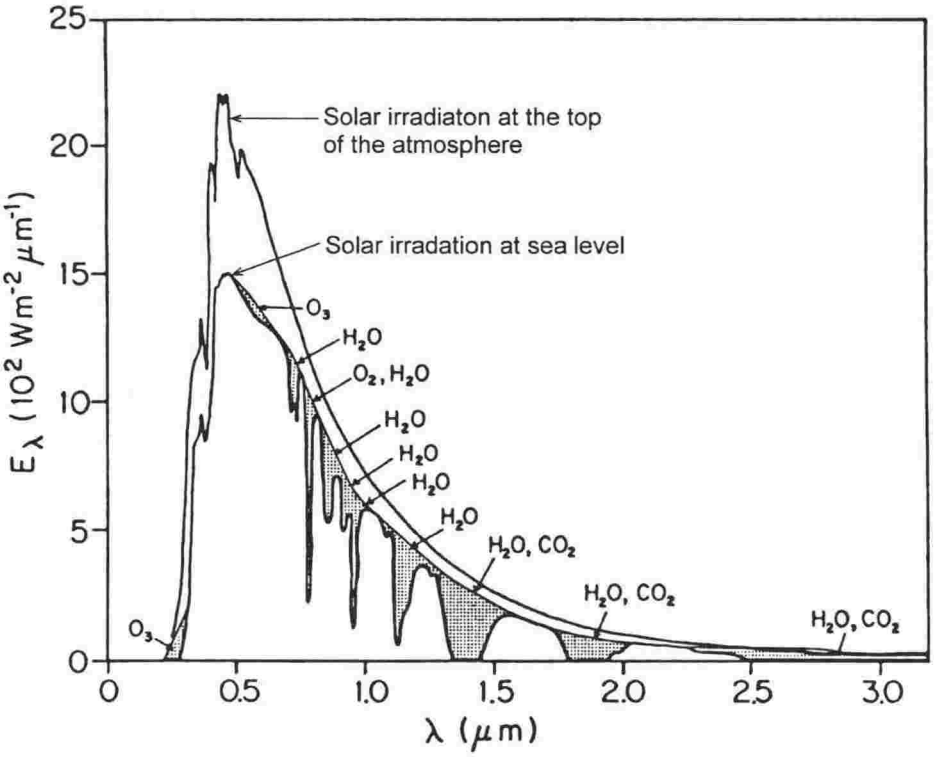

Figure 2.4 Spectral distribution of solar irradiation at the top of the atmosphere and at sea level [Adapted from *Peixoto and Oort*, 1992].

The shaded areas represent absorption by various atmospheric gases. The unshaded area between the two curves represents the portion of solar energy backscattered by air, water vapor, dust and aerosols and reflected by clouds. The plot is for average atmospheric conditions with the Sun at zenith.

Just as the Sun emits electromagnetic radiation over a wide rage of frequencies, so does the Earth. However, the temperature of the Earth-atmosphere system (~255 K) is much lower than that of the photosphere of the Sun (~6000 K). Due to Wein's displacement law, the intensity peak of the Earth's radiation field occurs at a longer wavelength than that of the Sun (Figure 2.5 (a)). The energy emitted from the Earth-atmosphere system is referred to as longwave, thermal infrared or *terrestrial radiation*, some of which is absorbed by greenhouse gases.

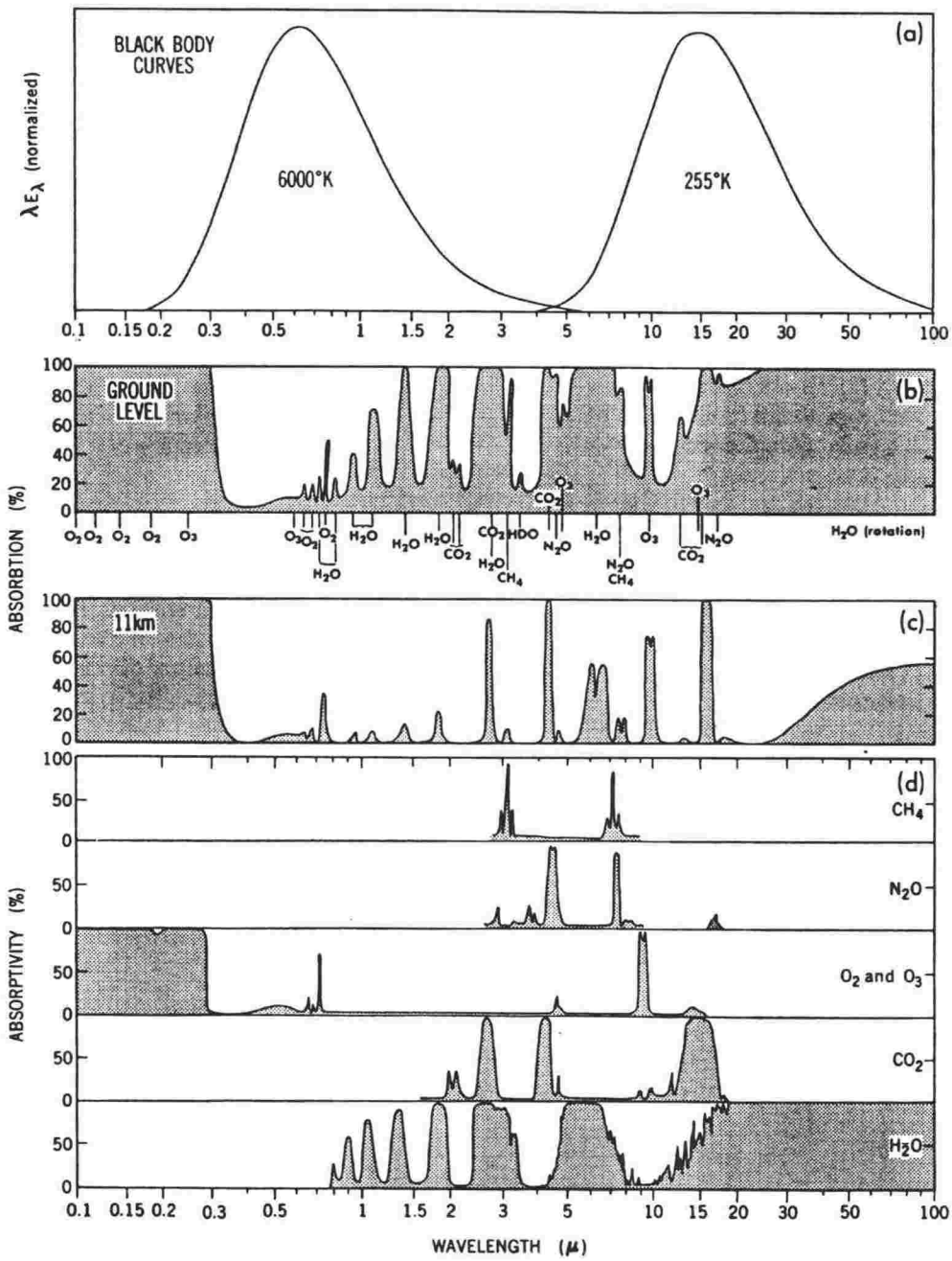

Figure 2.5 Black body curves for solar and terrestrial radiation and absorption spectra [*Peixoto and Oort*, 1992].

(a) Black body curves for solar radiation (assumed to have a temperature of 6000 K) and terrestrial radiation (assumed to have a temperature of 255 K). Absorption spectra for (b) the entire vertical extent of the atmosphere (c) the portion of the atmosphere above 11 km and (d) the various greenhouse gases over the entire vertical extent of the atmosphere.

Terrestrial radiation shorter than ~7.5 μm and longer than ~14 μm is almost completely removed by tropospheric H_2O. The region between ~7.5 μm and ~14 μm where the atmosphere is relatively transparent (apart from the O_3 band) is defined as the *atmospheric window*. Greenhouse gases absorb terrestrial radiation over various wavelength bands within the 7.5 - 14 μm atmospheric window (*e.g.* CO_2 absorbs very strongly at ~15 μm

and less strongly but more significantly, in terms of greenhouse warming, at ~10 μm [H_2O absorbs at many frequencies throughout the 7.5 - 14 μm region]).

Greenhouse gases warm the Earth's surface by absorbing terrestrial radiation from the Earth (that would otherwise be lost to space) and re-radiating some of it back to Earth (Figure 2.6). Without this process known as the *natural greenhouse effect* life would not be possible, as the Earth's average surface temperature would be ~33 °C colder than at present [*IPCC,* 1995].

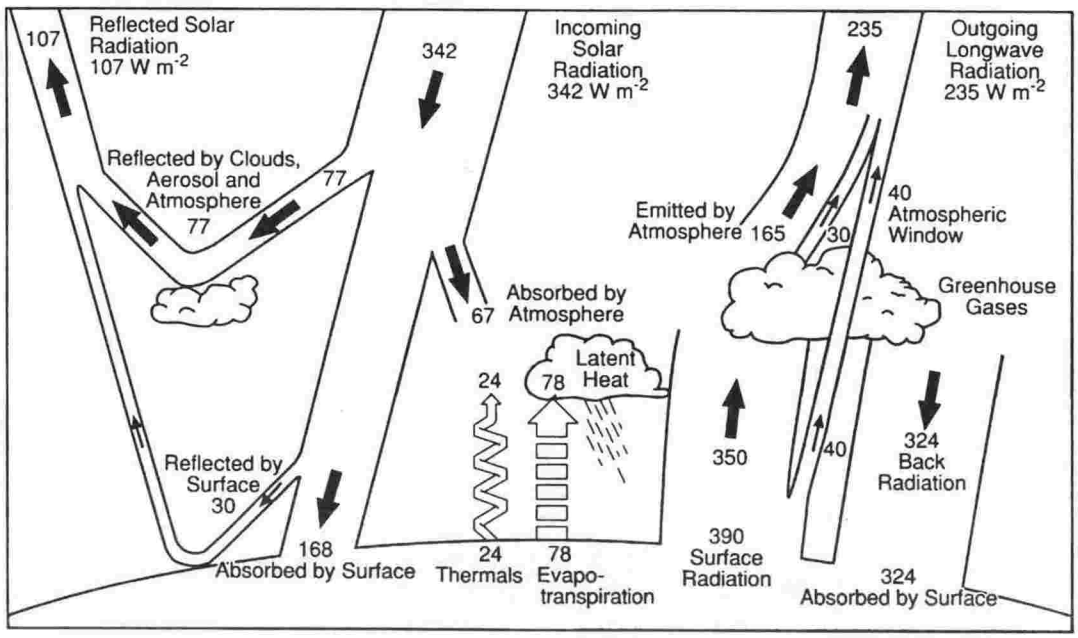

Figure 2.6 The Earth's radiation and energy balance [*IPCC*, 1996].
The incoming solar radiation of 342 Wm^{-2} is partially reflected by clouds, the atmosphere, and the Earth's surface. Forty nine percent of the net incoming solar radiation is absorbed and warms the Earth's surface, of which some is returned to the atmosphere as heating and evapotranspiration. The remainder is terrestrial radiation, most of which is absorbed and re-emitted by greenhouses gases in the atmosphere, producing the greenhouse effect.

2.3.2 Radiative forcing and global warming potentials

Since the industrial era began in the mid-nineteenth century, anthropogenic activities, such as biomass and fossil fuel burning, deforestation and cement production, have released billions of tonnes of CO_2 into the Earth's atmosphere [*IPCC*, 1995]. Consequently, the increased greenhouse gas levels present in today's atmosphere re-radiate back to Earth a greater fraction of terrestrial radiation that would otherwise be lost to space. This results in what is termed the e*nhanced greenhouse effect,* which has the potential to warm the Earth's average temperature with substantial consequences to the

climate system. These changes in greenhouse gas levels (also aerosol and O_3), in addition to naturally occurring solar-variability, perturb the planetary radiation budget leading to what is known as a *radiative forcing*. Processes that tend to warm the atmosphere produce a positive radiative forcing (*e.g.* increasing trace gas levels leading to the enhanced greenhouse effect). Processes that tend to cool the atmosphere produce a negative radiative forcing (*e.g.* increasing tropospheric sulfate which has the direct effect of scattering incoming radiation and the indirect effect of acting as cloud condensation nuclei (CCN) so that cloud coverage is increased and a greater fraction of incoming solar radiation is reflected).

The *global warming potential (GWP)* index is defined as the cumulative radiative forcing between the present and a chosen horizon time, caused by a unit of a greenhouse gas emitted now, expressed relative to a unit of reference gas (normally CO_2). GWPs are listed for a range of gases in Table 2.2.

Table 2.2 Global Warming Potentials for important greenhouse gases [*IPCC*, 1996].
The GWP is on a mass basis and is referenced to the absolute GWP for CO_2. Typical uncertainties are ~± 35 % relative to the CO_2 reference. (The GWP for CH_4 includes indirect effects of tropospheric ozone production and stratospheric water vapor production).

		GWP		
Species	Lifetime	20 years	100 years	500 years
CO_2	*See footnote	1	1	1
CH_4	12±3	56	21	6.5
N_2O	120	280	310	170

The differences in GWPs for different gases are a result of two factors. First, greenhouse gas lifetimes vary depending on the mode and rate of destruction or removal in the atmosphere. Therefore, a gas that has a longer atmospheric lifetime will have an impact over a longer period and therefore its cumulative impact will be greater. Second,

* In contrast with most anthropogenic compounds that are destroyed chemically in the atmosphere, CO_2 has a different rate of uptake for different sink processes and therefore no single "lifetime" for it can be defined. CO_2 is therefore well mixed in the atmosphere, and as reservoir exchange rates vary from a few years, to thousands of years, consequences of anthropogenic CO_2 perturbations will be long lived and much slower than the initial response of the carbon system of ~5 years (deduced from the rate of $^{14}CO_2$ removal) [*IPCC*, 1995].

the spectral region in which absorption occurs and the extent of saturation are important. Some spectral bands for CO_2 are already saturated (Figure 2.5). Thus, the absorption caused by additional CO_2 will be small. A similar effect occurs if absorption takes place in a region already mostly saturated by some other species such as water vapor or CO_2. Using CH_4 as an example, the relationship between added CH_4 and additional radiative forcing is more linear because it is much less abundant than CO_2 and none of the absorption bands are saturated. This partly explains why the GWP for CH_4 is much larger than that of CO_2.

Based on knowledge of greenhouse gas levels in the past and at present, estimates of radiative forcings for each of the greenhouse gases (Figure 2.7) are derived by applying a formulae that gives radiative forcing (W/m^2) as a function of mixing ratio. GWPs indicate the relative importance of current emissions of the main anthropogenic greenhouse gases.

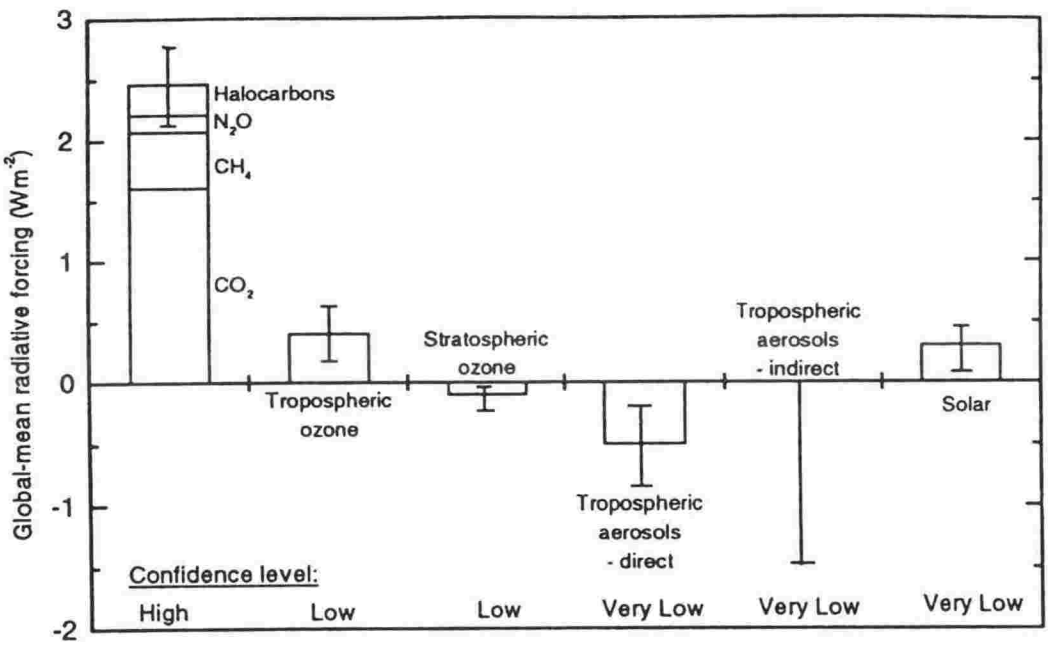

Figure 2.7 Globally and annually averaged estimates of anthropogenic radiative forcings [*IPCC*, 1996]. The radiative forcings are due to changes in greenhouse gases, aerosols and solar variability from pre-industrial times to the present. The height of the bar represents a mid-range estimate of the forcing which is given with uncertainties represented by the error bars. An indication of the relative confidence level in each of the estimates is given below each bar.

The order of relative importance for the main anthropogenic greenhouse gases is: CO_2, CH_4, N_2O and the various halocarbons.

2.4 Atmospheric Carbon Dioxide

2.4.1 The carbon cycle

Carbon is exchanged between its main reservoirs: the atmosphere, biosphere, hydrosphere and lithosphere (Figure 2.8).

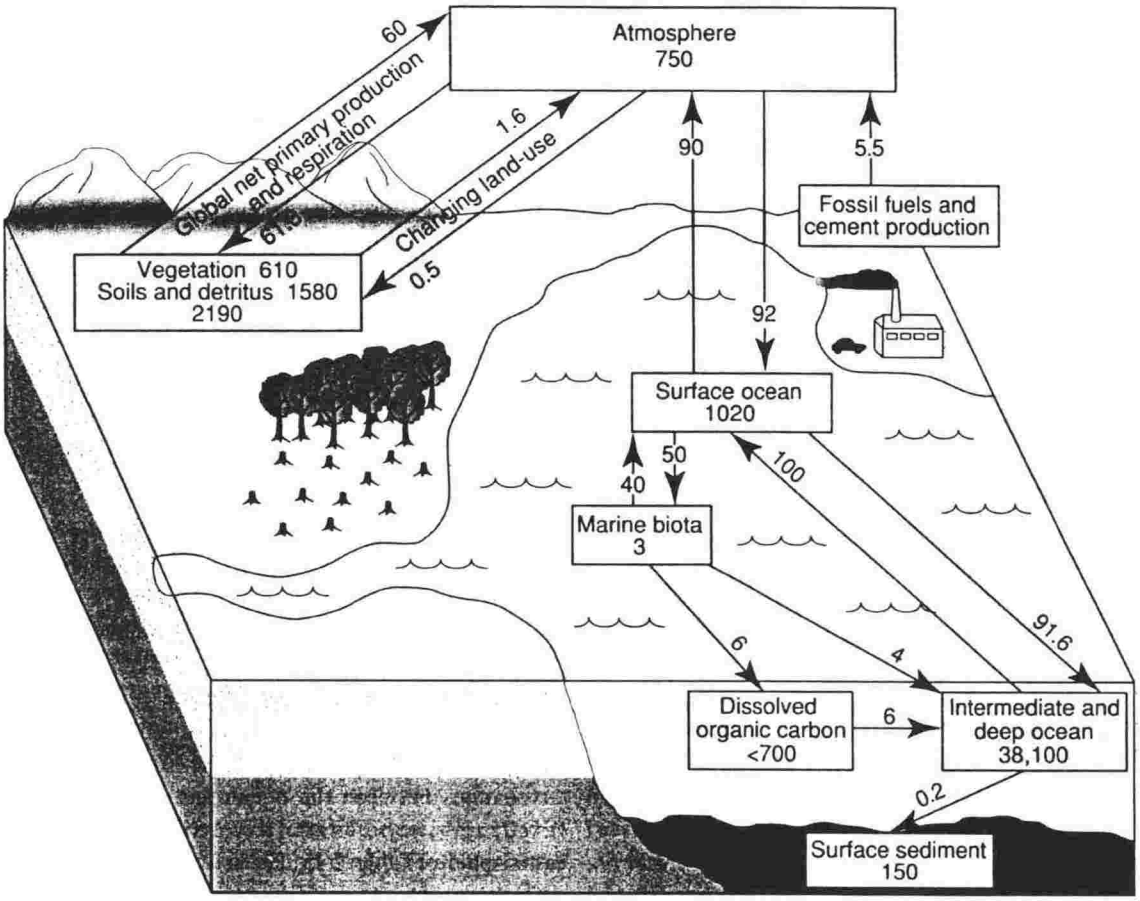

Figure 2.8 The global carbon cycle [*IPCC*, 1995].

Reservoirs (GtC) and fluxes (GtC/year) relevant to anthropogenic perturbation as annual averages over the period 1980 to 1989 are shown. The component cycles are simplified and are subject to considerable uncertainty. In contrast to the static view represented by this diagram, the carbon system is dynamic and is coupled to the climate system on seasonal, interannual and decadal time-scales.

The largest of these reservoirs, the lithosphere, contains ~150 × 10^6 GtC* in the interior of the Earth since its formation. This is in addition to elemental and organic carbon and carbonates that are formed by oceanic deposition. Small exchanges between the lithosphere and the other reservoirs occur at a slow rate through ocean sedimentation, carbonate and silica weathering, and volcanism. The next largest carbon reservoir, the hydrosphere (most of which is the oceans), contains ~38,000 GtC in the form of dissolved

* 1GtC = 1 billion tones of carbon = 1 × 10^{12} kg of carbon)

CO_2 and carbonates. Because much of the flux from the surface ocean is re-disolved in the top layers of the ocean, the hydrosphere cycles its carbon with the deep ocean slowly (over millennia). Furthermore, inorganic carbon (derived mainly from dead marine biota which are partly deposited as ocean-floor sediment) is cycled over millennia. The top layers of the ocean cycles faster (less than a year to decades) because the gross two-way fluxes of carbon are much larger than the net fluxes. The biosphere and atmosphere, with reservoirs of 2,200 and 750 GtC respectively, have the fastest carbon cycling fluxes in the global carbon cycle (the turnover time for the biosphere varies from less than a year to decades, while the time spent in the atmosphere for a CO_2 molecule is ~4 years).

Of the 750 GtC of carbon in the atmosphere (more than 99 % of which is CO_2) ~20 % is annually exchanged with the ocean and terrestrial biosphere. In the absence of anthropogenic inputs, global exchanges of carbon were in near balance for periods of millennia [*IPCC*, 1995], implying nearly constant reservoirs. This balance in the carbon cycle has been disturbed by anthropogenic activities that transfer carbon (mainly as CO_2) into the atmosphere. This carbon is then cycled between the atmosphere, hydrosphere and the terrestrial biosphere with varying turnover times. The effects on the carbon cycle and global climate are long lasting because carbon cycling in the terrestrial and oceanic biosphere occur slowly, over time-scales from decades to millennia. One of the main reasons for these long-lasting effects is that a large amount of the carbon transferred to the atmosphere is derived from the burning of (carbon-containing) fossil fuels. Over the last ~200 years, the release of these fossil fuels, which took millions of years to form, has disturbed the global carbon cycle. This disturbance will persist for periods of geological time scales until new fossil deposits are formed. However, carbon transfer to the atmosphere because of deforestation can potentially be restored to the terrestrial biosphere over decades during the growth of a new forest.

A strong effort by many atmospheric research groups worldwide is currently being undertaken to evaluate the effects of changes to the global carbon cycle on the Earth's climate. Measurements and observations of atmospheric, oceanic and biospheric parameters and events (especially of greenhouse gases; the subject of this work) are essential to accurately assess the present state of the atmosphere and the rate and manner in which it is changing. In addition, these measurements are essential to provide global climate models with the high-precision, high-resolution data required to more accurately predict the future state of the atmosphere.

2.4.2 The CO_2 budget

The *CO_2 budget* describes the perturbation to natural fluxes, assumed to be in balance, in terms of the sources and sinks of excess atmospheric CO_2 (Table 2.3). These estimated changes in emissions and fluxes between the main reservoirs allow the changing components of the global carbon cycle to be determined.

Table 2.3 The average annual CO_2 budget for 1980 to 1989 [*IPCC*, 1995].
Fluxes and reservoir changes of carbon are expressed in GtC/year and error limits correspond to an estimated 90 % confidence interval.

CO_2 sources	**GtC/year**
(1) Emissions from fossil fuel combustion and cement production	5.5 ± 0.5
(2) Net emissions from changes in tropical land use	1.6 ± 1.0
(3) Total anthropogenic emissions (1) + (2)	7.1 ± 1.5
Partitioning amongst reservoirs	
(4) Storage in the atmosphere	3.2 ± 0.2
(5) Ocean uptake	2.0 ± 0.8
(6) Uptake by northern hemisphere forest	0.5 ± 0.5
(7) Additional terrestrial sinks (CO_2 fertilisation, nitrogen fertilisation, and climatic effects) (3) – [(4) + (5) + (6)]	1.4 ± 1.5

Emissions from fossil fuel combustion and cement production are well quantified due to documented emissions inventories. Net emissions from tropical land use changes are difficult to measure or model and are more uncertain. The sink terms describe the way in which the carbon cycle is dealing with the extra anthropogenic carbon and its *partitioning* amongst the various reservoirs. Storage of CO_2 in the atmosphere is determined with reasonable precision by global monitoring of the tropospheric CO_2 mixing ratio. This is possible because atmospheric CO_2 is well mixed and the CO_2 mixing ratio is relatively homogeneous. Only ~1 % of atmospheric carbon storage is from other carbon containing compounds (*e.g.* CH_4, CO and hydrocarbons), which are neglected in the carbon budget. The atmospheric storage accounts for almost half of the total anthropogenic emissions. Ocean uptake (~2 GtC/year) is difficult to determine because it is a very small fraction of the gross ocean-atmosphere flux (~120 GtC/year). Uptake by Northern Hemisphere forest is also difficult to quantify and contains a large uncertainty. Uptake by Southern Hemisphere forest is also another likely contributing factor that could potentially draw

down ~0.2 ± 0.2 GtC based on the Northern Hemisphere to Southern Hemisphere land mass ratio of 2.5:1

The last term in Table 2.3, sometimes called the "missing sink", accounts for storage of carbon not easily accounted for and at this stage not accurately known. This storage is due to CO_2 fertilisation, nitrogen fertilisation and climatic effects. CO_2 fertilisation occurs due to the presence and availability of increased atmospheric CO_2 levels for enhanced plant growth, which may increase terrestrial carbon storage. Intentional fertilisation of agricultural lands and deposition of nitrogen, from fossil fuel production and other anthropogenic processes, also increase plant growth and hence terrestrial carbon storage. However, it is not known if photosynthesis and respiration would increase at equal rates, and therefore the total carbon pool size may experience no net change. Climate effects may also influence terrestrial carbon-uptake through plants (photosynthesis) and subsequent release (respiration in vegetation and soils) such that uptake is more active in warmer periods, than in cold, with resultant higher carbon storage. Decadal variations in climate may cause natural changes in carbon storage, acting in conjunction with, or even in opposition to, anthropogenic effects (this effect is separate from potential changes in carbon storage arising from direct greenhouse gas induced climate changes).

Other than the increase in atmospheric carbon storage (which can be measured directly) components of the carbon cycle can be determined by the following methods:

- Direct determination of the carbon content rate of change in atmospheric, oceanic and terrestrial carbon reservoirs.
- Indirect assessment of the fluxes between the atmosphere, ocean, and terrestrial biosphere by means of carbon cycle model simulations.
- Interpretation of tracers, such as the isotopic composition of atmospheric CO_2.

The determination of the components of the carbon cycle and the partitioning between oceanic and terrestrial carbon sinks, need to be more accurately and precisely determined to enable global carbon cycle and climate model predictions to be made with higher confidence [*Francey et al.*, 1995]. This can be performed with high precision isotopic measurements of atmospheric CO_2 [*Conway et al.*, 1994]. Furthermore, the history of atmospheric CO_2 that is described in the following sections is essential for understanding changes within the carbon budget over time. Quantifying the continuing changes of atmospheric CO_2 is also vital to the understanding and future predictions of the global carbon cycle and climate system response.

2.4.3 The history of atmospheric CO_2

For the 10,000 year period before the industrial revolution in the mid-nineteenth century, the *mixing ratio* of atmospheric CO_2 was stable ~280 ppm [*IPCC*, 1995]. More recently, release of CO_2 into the atmosphere from fossil fuel and biomass burning, changing land and cement production have annually transferred billions of tonnes of CO_2 into the atmosphere. This has raised the mixing ratio of atmospheric CO_2 by ~30 % to ~360 ppm in 1996 (Figure 2.9).

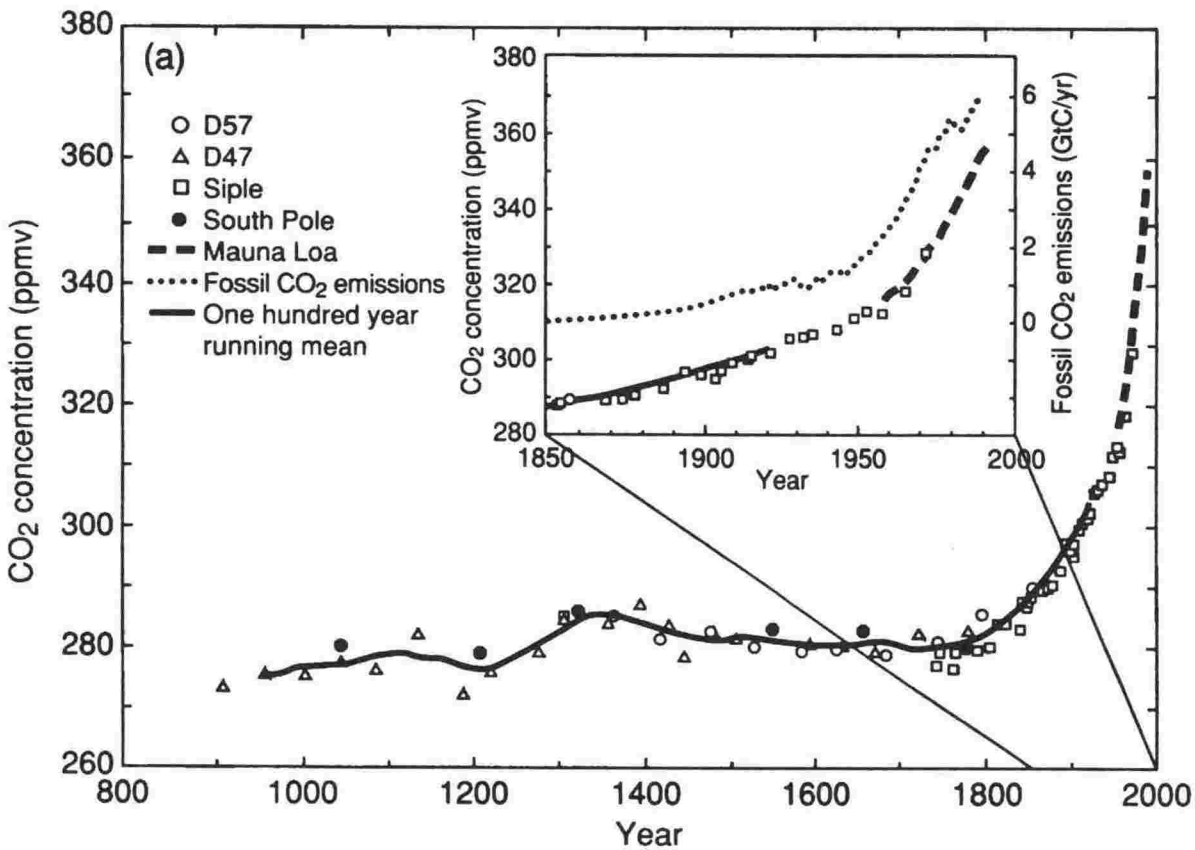

Figure 2.9 CO_2 mixing ratios since 1000 AD from ice core records (D57, D47 and Siple, Antarctica) in addition to the modern atmospheric CO_2 record since 1958 at Mauna Loa, Hawaii [*IPCC*, 1995].
The inset shows the period from 1850 in more detail, including CO_2 emissions from fossil fuel burning. The smooth curve is based on a 100 year running mean.

Because of inter annual variability in exchange fluxes between the terrestrial biosphere, oceans and the atmosphere, the CO_2 growth rate fluctuates (Figure 2.10), but globally, the level of atmospheric CO_2 continues to grow (Figure 2.11). The current average atmospheric growth rate is ~1.5 ppm/year or 0.4 %/year [*Tans et al.*, 1998].

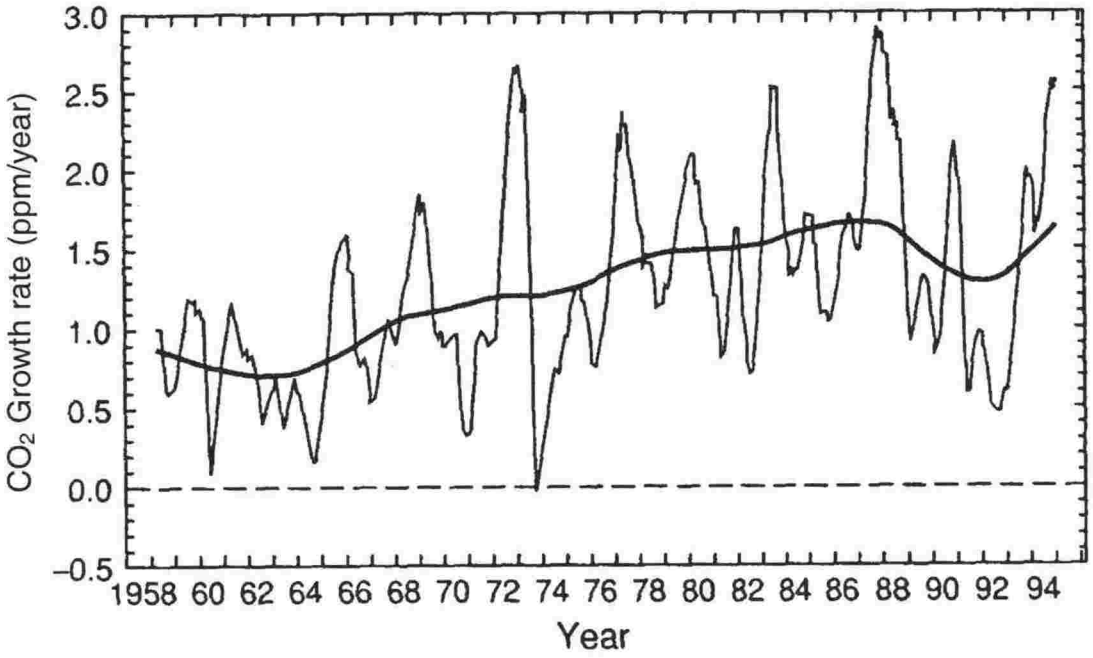

Figure 2.10 Growth rate of CO_2 mixing ratio since 1958 at Mauna Loa, Hawaii [*IPCC*, 1996]
The smooth curve shows the same data, but filtered to suppress variations on time scales less than ~10 years. The data is from C.D. Keeling and T.D Worf of SIO and P.Tans of NOAA CMDL.

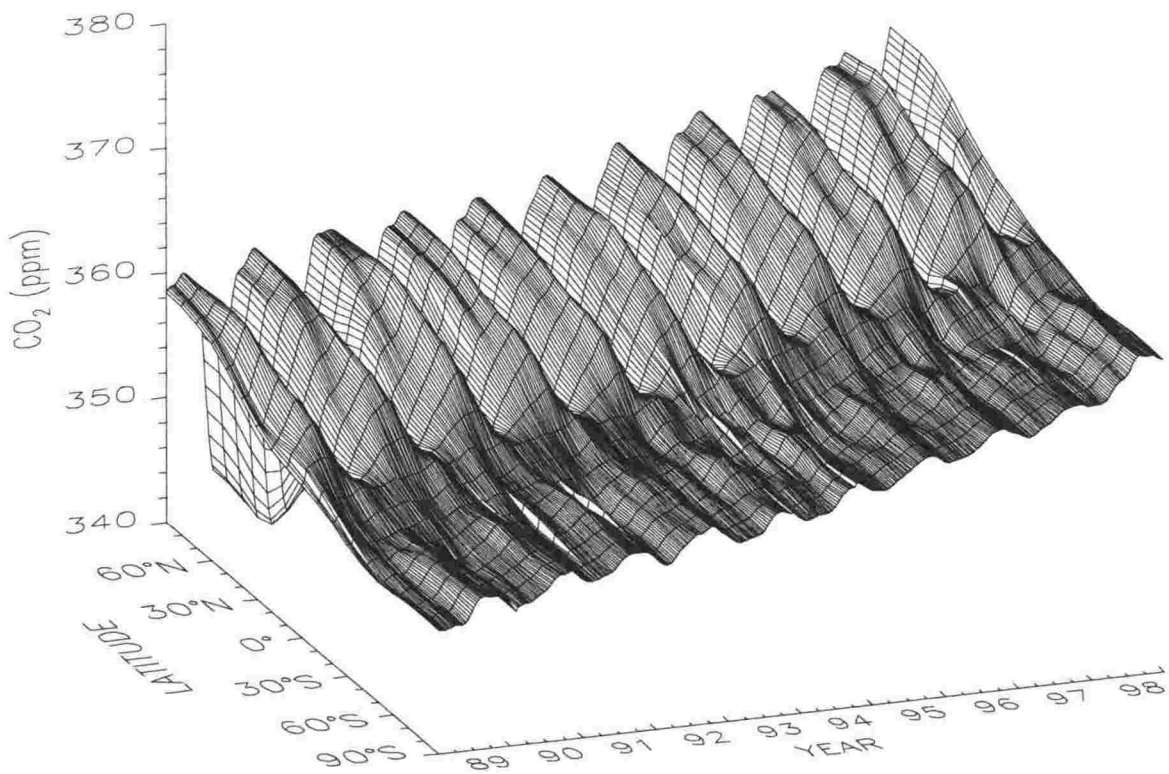

Figure 2.11 Three-dimensional representation of the latitudinal distribution of atmospheric CO_2 in the marine boundary layer [*Carbon Cycle Group, NOAA CMDL* website: http://ccg.cmdl.noaa.gov].
Data is from the NOAA CMDL cooperative air-sampling network. The surface represents data smoothed in time and latitude.

The higher atmospheric CO_2 mixing ratios in the Northern Hemisphere and resultant large north-south gradient exist because most anthropogenic CO_2 emissions (mainly fossil fuel release) occur in the Northern Hemisphere. This imbalance of sources between the Northern and Southern Hemispheres accounts for the growing difference of CO_2 mixing ratio between the hemispheres [*IPCC*, 1995]. The larger amplitude of the CO_2 seasonal cycle in the Northern Hemisphere is mainly due to the larger land mass of the Northern Hemisphere, which has a greater annual uptake of carbon during the growth season and larger human population and emissions. The atmosphere also exhibits a large inter-hemispheric asymmetry, which is mainly due to uptake during the growth seasons for the Northern and Southern Hemispheres being out of phase.

2.4.4 Current analysis techniques of atmospheric CO_2 mixing ratios

Presently there are two main analytical techniques used for the determination of atmospheric CO_2 mixing ratios: 1) non-dispersive infrared (*NDIR*) spectroscopy, and 2) gas chromatography separation of CO_2 before reduction to CH_4 and detection by flame ionisation detector (*GC-FID*). In addition to these, a Fourier transform infrared spectroscopy (*FTIR*) method has recently been developed [*Esler*, 1997]. NDIR and GC-FID both operate to precision levels of ~± 0.07 ppm in 360 ppm or ~± 0.02 % [e.g., *Steele et al.*, 1996; *Francey et al.*, 1996]. FTIR operates to a slightly lower precision of ~± 0.11 ppm in 360 ppm or ~± 0.03 % [*Esler*, 1997].

Of the two main techniques, NDIR analysis is more common for in situ analysis and is used at many background air pollution sites [e.g., *Tans et al.*, 1998]. NDIR instruments are also used for analysis of flasks collected from global networks and other sample platforms such as aircraft [e.g., *Francey et al.*, 1996] and ships [e.g., *Conway et al.*, 1994].

NDIR works by passing infrared radiation through the sample gas of interest. Gas filters selectively absorb radiation passing through this mixture depending on their absorption bands (*e.g.* CO_2 absorbs strongly at ~4.3 mm). The integrated absorbed energy is measured over the bandwidth passed by the gas of interest, and the detector generates a current that is proportional to the CO_2 mixing ratio.

GC-FID is a relatively straightforward technique which first separates the CO_2 from the sample gas by GC and then uses a heated nickel catalyst at ~400 ^{o}C (a methaniser) to reduce CO_2 to CH_4 that is detected by a FID.

FTIR utilises a Michelson interferometer that partially transmits and partially reflects the incident source beam at a beamsplitter, at which interference occurs. The intensity of

the beam reaching the detector is measured as a sinusoidal variation because a mirror moving at constant velocity causes the path differences to alternately constructively and destructively interfere. This changing intensity with time (as the mirror is moving at constant velocity) is called the interferogram. The single beam spectrum is given from the interferogram by calculating the cosine Fourier transform of the intensity of the beam striking the detector as a function of the path difference. Beer-Lambert's Law is applied to calculate the resulting transmittance, which is related to the absorption coefficient of the sample at a certain frequency, the pathlength through the sample, and the mixing ratio of the absorbing species. For a mixture of many components which do not chemically interact, absorptance is additive and thus, it is possible to determine the mixing ratios of all absorbing species in the sample from a single spectrum. Mixing ratio measurements are made by comparing spectra, which pass through the interferometer, with, and without the presence of sample gas. Furthermore, high accuracy FTIR measurements are obtained by comparing spectra with that from calibration gas, the composition of which is accurately known. Therefore, FTIR can be used to simultaneously measure the mixing ratio of CO_2, CH_4, N_2O and CO.

2.5 The Stable Isotopes of CO_2 : $\delta^{13}C$ and $\delta^{18}O$

Carbon and oxygen both have three principal naturally occurring isotopes (Table 2.4). It is therefore possible for CO_2 to exist in eighteen isotopomeric forms varying in molecular weight from (m/e) 44 to 50. ^{14}C is radioactive with a half-life of ~5730 years and is termed a radioisotope. All other isotopes given in Table 2.4 are not radioactive and are termed *stable isotopes*.

Table 2.4 The natural isotopes of carbon and oxygen [Adapted from *Hoefs*, 1997].

Isotope	Natural abundance (%)
^{12}C	98.89
^{13}C	1.11
^{14}C	$< 1 \times 10^{-10}$
^{16}O	99.76
^{17}O	0.038
^{18}O	0.20

The ratio of the carbon and oxygen isotopes, ^{13}C to ^{12}C and ^{18}O to ^{16}O respectively are commonly expressed in the delta notation. These are referred to as $\delta^{13}C$ and $\delta^{18}O$ and expressed relative to a known reference as per mille (‰) deviations from a reference in the relationship (*e.g.* for $\delta^{13}C$):

$$\delta^{13}C_{sample} = 1000\,(R_S / R_r - 1)\,‰ \qquad (2.1)$$

where R_S is the $^{13}C/^{12}C$ ratio in the sample and R_r is the $^{13}C/^{12}C$ ratio in the reference.

Sample measurements are typically made via a working reference gas containing CO_2 that is calibrated relative to an international primary standard (*e.g.* NBS19; a $CaCO_3$ sample which evolves CO_2 of a known isotopic composition from a reaction with phosphoric acid at 25 °C). NBS19 is distributed for the calibration of $^{13}C/^{12}C$ and $^{18}O/^{16}O$ variations by the International Atomic Energy Agency (IAEA), Vienna, Austria [*Gonfiantini et al.*, 1995]. Any gas containing CO_2 with isotope ratios traceable to this international standard may be used as a *working reference gas* providing the link to the V-PDB (Vienna Peedee Belemnite) scale that is widely used.

2.5.1 Geophysical significance

Isotope ratio measurements provide information that is not accessible from mixing ratio measurements alone. This is because physical and biological processes fractionate between different isotopomers in distinct ways. For example, in the photosynthesis process, uptake occurs faster for $^{12}CO_2$ than for $^{13}CO_2$ (this is because heavier isotopes have a lower zero-point energy than lighter isotopes, therefore the chemical bonds formed

by lighter isotopes are weaker and thus lighter isotopes react more readily than heavier isotopes). In respiration, the process is reversed (although the fractionation is much smaller). Thus, daily and seasonal variations in $\delta^{13}C$ occur due to plant photosynthesis and respiration. In addition, different types of plants fractionate CO_2 by a different amount. On the basis of whether the carboxlyation step proceeds through a 3-carbon or a 4-carbon intermediate, plants are divided into two main types, referred to as C3 and C4 plants respectively. Most plants are the C3 type and fractionate atmospheric CO_2 (which has a $\delta^{13}C$ of ~-8 ‰) by ~-18 to ~-20 ‰ resulting in plant tissue with $\delta^{13}C$ of ~-26 to ~-28 ‰. C4 plants are not as abundant (*e.g.* grasses, corn and sugar cane) and fractionate by ~-5 ‰ and therefore have plant tissue of ~-13 ‰. The $\delta^{13}C$ of coal and crude oil is about the same as living C3 plant matter at ~-28 ‰. Negligible fractionation occurs during the combustion of these products so the $\delta^{13}C$ of CO_2 released into the air from fossil fuel burning is also depleted and has a $\delta^{13}C$ of ~-28 ‰.

$\delta^{18}O$ of atmospheric CO_2 are strongly influenced by land biota because CO_2 and water exchange both in leaves and in soils. Therefore, $\delta^{18}O$ is useful for studying the global carbon cycle as it is sensitive to the processes by which the global biosphere absorbs (by photosynthesis, leaf water enriched in $\delta^{18}O$) and respires CO_2, depleted in $\delta^{18}O$ [*Ciais et al.*, 1997a]. Thus $\delta^{18}O$ has the potential to be quantitatively used to separate respiration from photosynthesis in carbon cycle studies [*Tans et al.*, 1998]. Further discussion on the use of $\delta^{18}O$ isotopes in atmospheric CO_2 is given in the following section.

By using the above information and monitoring both the mixing ratio and isotopic composition of CO_2, it is possible to determine whether variations are of anthropogenic, oceanic or biologic origin. More specifically it enables estimates to be made of the *spatial* and *temporal* variations in, and the relative magnitudes of, biospheric and oceanic carbon sources and sinks [*Ciais et al.*, 1995a, b; *Francey et al.*, 1995]. In addition to measurements of the CO_2 mixing ratio, more extensive isotopic measurements are required to distinguish between sources and sinks [*Conway et al.*, 1994] and hence provide accurate assessments and predictions of the future state of the atmosphere. This is the focus of many research strategies worldwide and is also the main contribution this work can potentially undertake.

2.5.2 The history of $\delta^{13}C$ and $\delta^{18}O$ in atmospheric CO_2

Simultaneously with CO_2 mixing ratio growth since the industrial era, the isotopic composition has changed (Figure 2.12). This is because a greater fraction of atmospheric

CO_2 is now of fossil fuel origin which has an associated carbon isotopic value of ~-27 ‰ which is more negative (depleted in ^{13}C) than atmospheric CO_2 which currently has a carbon isotopic composition of ~-8 ‰ [*Keeling*, 1973; *Friedli et al.*, 1986; *Siegenthaler and Oeschger*, 1987].

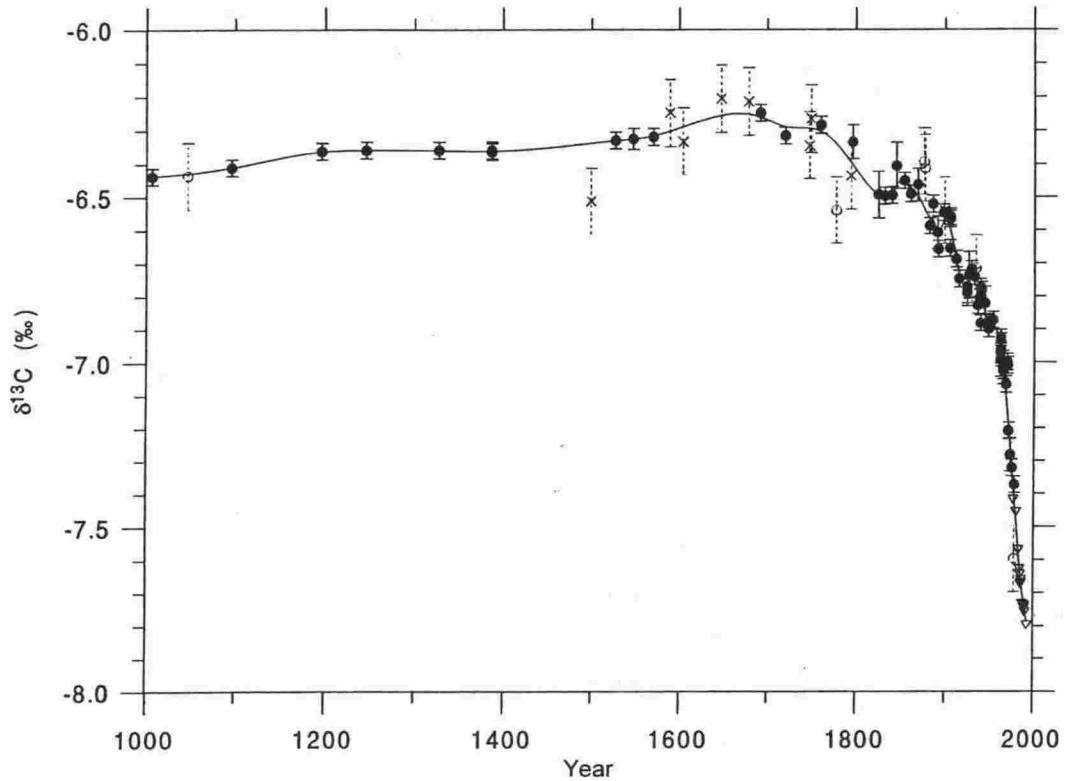

Figure 2.12 $\delta^{13}C$ over the last 1000 years from ice cores and firn air from Law Dome, Antarctica [*Francey et al.*, 1999].

The density and statistical error of the data weight the smoothing spline, so that its effective smoothing is ~130 years before 1800 AD and 25 years after 1800 AD. Crosses indicate ethanol contaminated samples, open circles are other rejections.

In the Northern Hemisphere, seasonal cycles of $\delta^{13}C$ and $\delta^{18}O$ are large (*e.g.* for $\delta^{13}C$: ~0.35 ‰ over the period 1979 to 1984 at Mauna Loa, Hawaii, 21 °N [*Keeling et al.*, 1995]; and ~0.70 ‰ at Point Barrow, Alaska, 71 °N, over the period 1984 to 1993 [*Francey et al.*, 1995]). In Southern Hemisphere mid latitudes, the seasonal cycles of $\delta^{13}C$ and $\delta^{18}O$ are smaller, ~0.15 ‰ and ~0.4 ‰ peak to peak respectively [*Francey et al.*, 1987, 1995; *Keeling et al.*, 1995]. This smaller variation in the Southern Hemisphere is due to a smaller plant and human influence and less landmass. At the South Pole an even smaller seasonal cycle of ~0.05 ‰ is observed [*Murayama, et al.*, 1998; *Keeling et al.*, 1995; *Francey et al.*, 1995]. A global view of $\delta^{13}C$, which summarises measurements for a global network of measurements, is given in Figure 2.13.

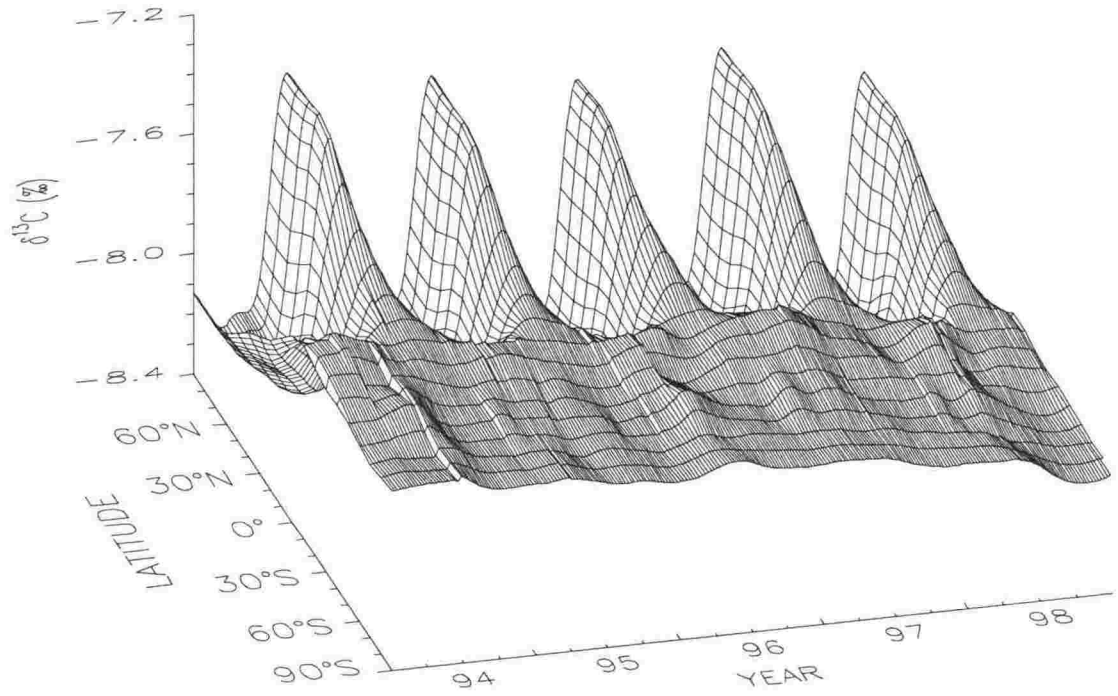

Figure 2.13 Three-dimensional representation of the latitudinal distribution of the carbon composition of atmospheric CO_2 in the marine boundary layer [*Carbon Cycle Group, NOAA CMDL* website: http://ccg.cmdl.noaa.gov].

The stable isotope measurements were performed at INSTAAR, CU using air samples provided by the NOAA CMDL cooperative air-sampling network. The surface represents data smoothed in time and latitude. $\delta^{13}C$ are expressed relative to the VPDB-CO_2 standard.

As atmospheric $\delta^{18}O$ are influenced strongly by land biota, values vary considerably with location globally (Figure 2.14).

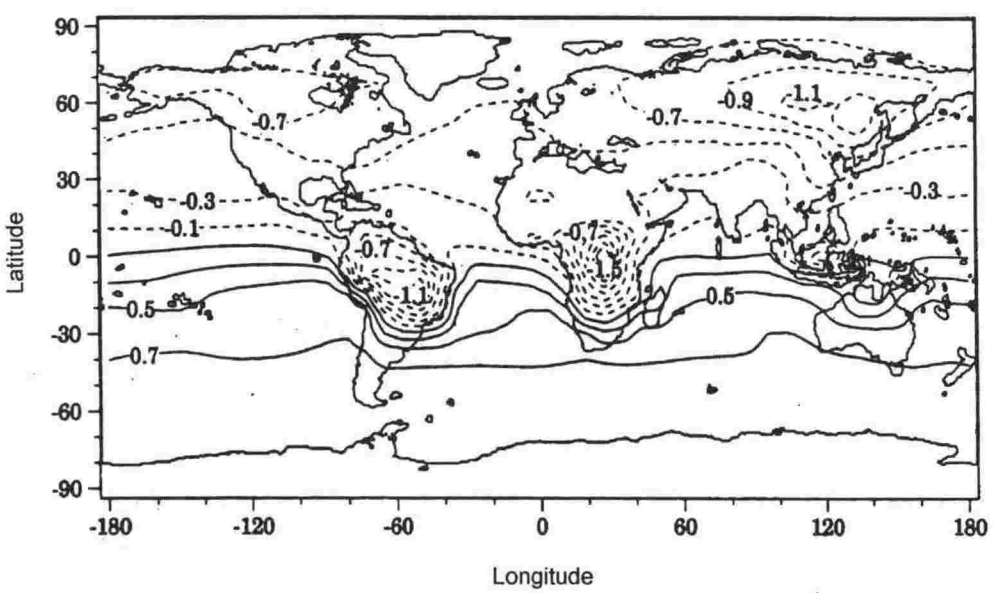

Figure 2.14 Annual mean $\delta^{18}O$ in CO_2 at the surface level [*Ciais et al.*, 1997b].

$\delta^{18}O$ shown are the combination of all reservoirs: terrestrial fluxes, air-sea exchange, and anthropogenic CO_2 emissions.

Atmospheric $\delta^{18}O$ are more depleted over land where active plant growth is present. The Northern Hemisphere is therefore more depleted overall than the Southern Hemisphere, because its larger landmass has a larger effect.

The $\delta^{18}O$ seasonal variation (Figure 2.15) is due to the effect of plant photosynthesis and respiration, in addition to soil-respired CO_2. Due to the larger landmass in the Northern Hemisphere, the $\delta^{18}O$ variation is larger in the Northern Hemisphere compared to that of the Southern Hemisphere.

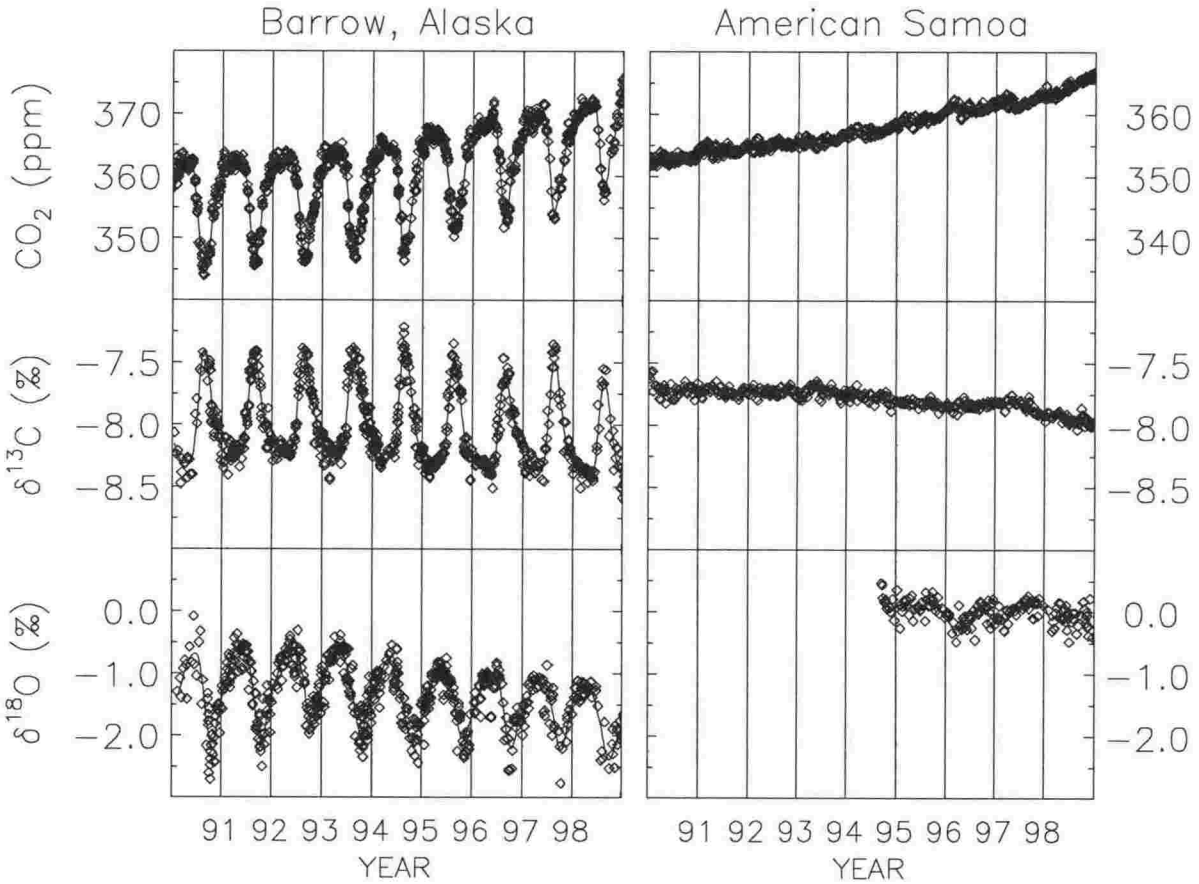

Figure 2.15 Time series showing the variation in atmospheric CO_2, $\delta^{13}C$, and $\delta^{18}O$ in the marine boundary layer [*Carbon Cycle Group, NOAA CMDL* website: http://ccg.cmdl.noaa.gov].
Data are shown for Barrow, Alaska (71.32 °N) and American Samoa (14.25 °S). The stable isotope measurements were performed at INSTAAR, CU using air samples provided by the NOAA CMDL cooperative air-sampling network. The surface represents data smoothed in time and latitude. $\delta^{13}C$ is expressed relative to the VPDB-CO_2 standard.

Observing the relationship between atmospheric CO_2 species (Figure 2.15), we see that a striking anti-correlation exists between the seasonal cycles of CO_2 and $\delta^{13}C$. This anti-correlation is a reflection of terrestrial photosynthesis and respiration. Because of the different uptake rates for carbon isotopes during photosynthesis (^{12}C faster than ^{13}C), the carbon isotope ratio of the CO_2 left behind in the atmosphere becomes enriched in ^{13}C (*i.e.*

$\delta^{13}C$ shifts to more positive values). This explains why during the summer growth period in the Northern Hemisphere, CO_2 mixing ratio falls, while $\delta^{13}C$ simultaneously rises.

The $\delta^{18}O$ cycle can change dramatically from year to year, most likely because it is subject to strong opposing forces of respiration (depleted in ^{18}O) and photosynthesis (leaf water enriched in ^{18}O) [*Tans et al.*, 1998]. For example, at the end of the growth season, when photosynthesis slows and the biosphere becomes a net source to the atmosphere, the respired CO_2 from soils is "still pulling" down atmospheric $\delta^{18}O$ (because moisture at high latitudes is depleted in ^{18}O). This signature, can therefore be detected in $\delta^{18}O$ of respired CO_2 [*Ciais et al.*, 1997a] and can be used to increase understanding of photosynthesis and respiration processes and carbon cycle studies, *e.g.* to provide information about when photosynthesis stops and how much relative magnitude of plant and soil respiration.

2.5.3 Current analysis techniques of $\delta^{13}C$ and $\delta^{18}O$ in atmospheric CO_2

Currently there is only one method available for isotopic analysis of $\delta^{13}C$ and $\delta^{18}O$ in atmospheric CO_2. This dual-inlet isotope ratio mass spectrometry (IRMS) technique is capable of performing high precision isotopic measurements of atmospheric CO_2. However, the technique has the following disadvantages: large sample requirements, cryogen use; co-extraction, analysis, and post correction of contaminating atmospheric N_2O. These are discussed in detail in the following chapter.

For $\delta^{13}C$ measurements only, the following spectroscopic techniques are available: Tunable Diode Laser spectroscopy (TDL), Non dispersive infrared spectroscopy (NDIR), and Fourier transform infrared spectroscopy (FTIR). These techniques work on the principle that the distributions of vibrational and rotational energy states of a molecule are affected by the isotopic composition of that molecule. With the absorption of a photon of certain infrared energy, low-mass isotopes are excited to a higher vibrational energy state. With the absorption of a photon of a lower infrared energy, than was required for the lower mass isotope, high-mass isotopes are also excited to a higher vibrational energy state. The rotational constant is also slightly different for each isotope. Therefore, each isotope has its own rotational-vibrational infrared spectrum. Analysis of specific features in these infrared spectra (*e.g.* rotational absorbance lines) can be used to determine the isotopic composition of a gas sample.

TDL works by tuning the laser frequency over a small range in the infrared region that contains one or more absorbance lines of the isotope species to be measured. $\delta^{13}CO_2$ has been measured by this technique to a precision of 4 ‰ [*Becker et al.*, 1992]. Using a

different laser technique called laser optogalvanic spectroscopy, $\delta^{13}CO_2$ in 5 % CO_2-in-N_2 samples have been measured to a precision of 0.2 ‰ [*Murnick and Peer*, 1994].

NDIR spectrometers have been used to measure CO_2 in exhaled human breath for diagnostic purposes based on ingestion and metabolism of a ^{13}C-labelled drug. The performance of such a technique measures $\delta^{13}C$ to a precision of ~0.4 ‰ from 500 ml breath samples containing ~4 % CO_2 [*Koletzko et al.*, 1995].

The most recent and high precision measurements of $\delta^{13}CO_2$ by FTIR have been reported by *Esler* [1997]. This technique works as described in section 2.4.4 and is capable of performing isotopic measurements of $\delta^{13}C$ in background levels of atmospheric CO_2 to a precision of 0.1 ‰.

All of these techniques require larger samples than that of the new technique presented in this thesis. In addition, only isotopic analysis of $\delta^{13}C$ in atmospheric CO_2 is possible, ($\delta^{18}O$ information can not currently be measured). Furthermore, low obtainable precision, which is at least an order of magnitude larger than that required for high precision atmospheric CO_2 monitoring, currently limit the techniques to restricted applications.

As dual-inlet is the only existing technique to successfully measure atmospheric CO_2 isotopes, and because it could potentially be replaced by the new technique presented in this work, it is discussed in detail before the experimental development of the new GC-IRMS technique is presented in the next chapter.

3 Experimental

3.1 Mass spectrometry

3.1.1 Background

In the early 1900s, *mass spectrometry* (MS) was developed in approximately the same period as the discovery of isotopes. Over the first half of the 1900s, MS research concentrated on the physical properties of matter (characterisation of molecular structure and amount, elemental composition and spatial arrangement) and determination of the "natural" abundances of the elements. At this point it was perceived that once all of the isotopic abundances of the elements were completed, there would be no further use for MS [*Svec*, 1985]. However, in the 1930s before the isotopic abundances of all the elements had been determined, the MS analysis of *stable isotopes* as tracers was yielding important breakthroughs in the bio-sciences [*Clarke*, 1948]. The first observation of isotopic variations linked to material sources and systematics was by *Nier and Gulbransen* [1939] who detected that the concentration of ^{13}C is greater in carbonates than in organic carbon. This isotope variation linked to natural processes is now widely known throughout environmental science and is used in research as diverse as soil and plant respiration, dietary studies of ancient humans and animal food webs, nitrification rates in forests, biodegradation, and climate history of the Earth [*Brenna et al.*, 1997].

All polybaric* elements of the periodic table can be isotopically analysed by MS at high precision by one of three instrument types; *static gas* or *noble gas* instruments, *thermal ionisation MS* (TIMS) for metals, and *gas IRMS* (Isotope Ratio Mass Spectrometery) for light elements. Mass spectrometers used for structural studies are termed *organic MS*. All mass spectrometers can measure isotopic abundances, however, only IRMS instruments perform these measurements at high precision (generally defined as standard deviation in the range 4 – 6 significant figures) [*Brenna et al.*, 1997]. IRMS instruments are used to measure the small variations associated with natural processes at high precision. However, this is at the expense of flexibility compared to scanning MS techniques that deliver a full mass spectrum in seconds.

IRMS instruments can only accept the analyte in one of a limited number of pure gases (*e.g.* CO_2, N_2, O_2, H_2, SO_2 for analysis of $^{13}C/^{12}C$, $^{15}N/^{14}N$, $^{18}O/^{16}O$, $^{3}H/^{2}H$, $^{34}S/^{32}S$ respectively). The disadvantage of this requirement is that time consuming (sometimes off-line) sample extraction and/or conversion to one of these pure gas forms is needed. In

* Occurring at several different pressures.

addition, relatively large sample sizes are required and the extraction/conversion, transfer and sample handling of the pure analyte must be carefully performed to avoid isotopic fractionation and sample contamination. Detailed discussion of these traditional *dual-inlet IRMS* techniques, with respect to measuring isotopes of atmospheric CO_2, are discussed in section 3.1.2.

The high precision *dual-inlet IRMS* techniques introduced in the late 1940s, dominated IRMS for four decades. Over this time, instrument system performance and precision have improved. Fundamental changes were introduced to IRMS in the 1980s and are now sparking a revolution in IRMS. These changes allow detailed analysis of complex mixtures and offer many advantages over traditional techniques. These hybrid techniques between *gas chromatography* (*GC*) and IRMS are discussed in section 3.1.3 and form the basis of the technique developed in this work.

3.1.2 Dual-inlet IRMS

Dual-inlet IRMS was first available in 1950 where the system devised by Murphey [1947], for the analysis of gas diffusion rates, was incorporated into the classical analytical IRMS instrument design of *McKinney et al.*, [1950] (Figure 3.1).

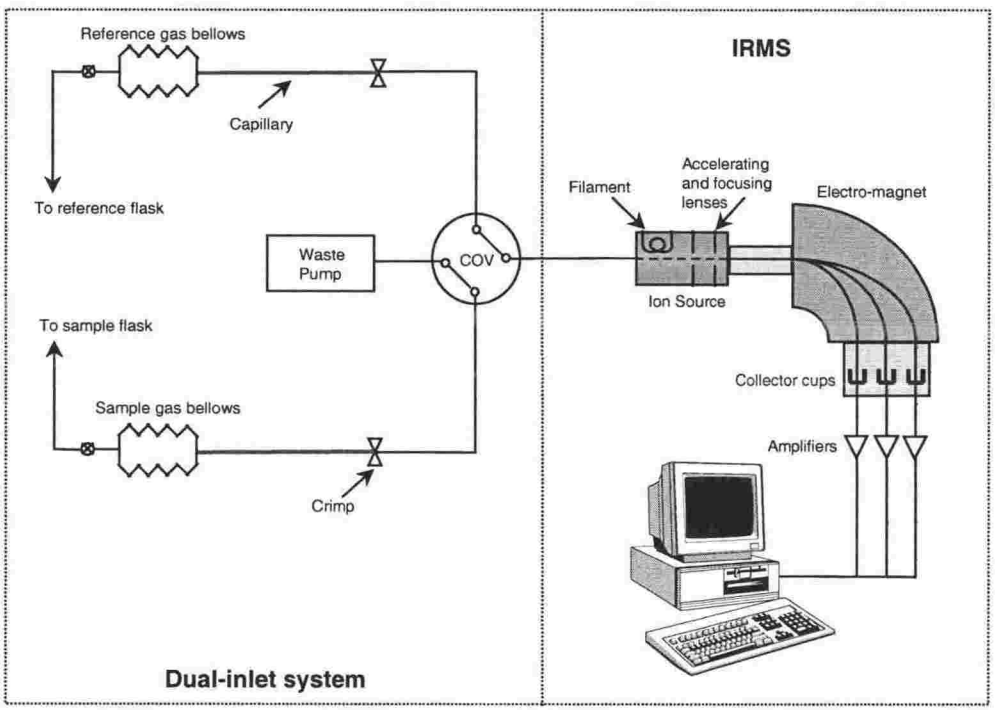

Figure 3.1 Classical dual-inlet system for use with IRMS

Two variable-volume metal bellows gas reservoirs introduce the sample and reference gases at carefully matched rates through capillary inlet lines to the ion source of the IRMS. These bellows balance the inlet pressures so that both gases enter the ion source at the same flow rate and pressure. This is necessary to ensure detected signal intensities of the major ion beams of both reservoirs are as identical as possible to minimise instrument non-linearity. The capillaries have a crimp immediately prior to the ion source so that the flow resistance can be set to allow the sample and reference flow rates to be matched. The dimensions of these capillaries are chosen to maintain viscous flow conditions so that the isotopic composition of the gas in the inlet remains unchanged throughout the period of analysis [*Halstead and Nier*, 1950]. A changeover valve (COV) toggles the flow of each of the two capillaries, to either the ion source or the waste line of the IRMS using one or the other for each flow path, and then switching flow paths. This ensures that a constant flow through the capillaries and equivalent pressures in both reservoirs are maintained at all times. An electron impact *ion source* that is designed and tuned to maximise ionisation probability, ionises analyte molecules which are accelerated and focused into a beam which enters the analyser section (molecules that are not ionised are pumped away to vacuum). The extracted ions have a kinetic energy given by:

$$\text{K.E.} = \tfrac{1}{2}\, mv^2 = eV \qquad (3.1)$$

where m is the mass of the ion, v is its velocity, e is the charge of the ion, and V is the applied voltage to the ion source.

The ions enter the flight tube between the poles of an electromagnet and are deflected by the magnetic field, **B**. Only ions of mass-to-charge ratio that have equal centrifugal and centripetal forces pass through the flight tube, *i.e*:

$$ev\mathbf{B} = mv^2/r \qquad (3.2)$$

where r is the radius of curvature of the ion path and is equal to

$$r = mv/e\mathbf{B} \qquad (3.3)$$

Rearranging (3.3) for v, squaring and substituting into (3.1) we see that the mass (m/e) of the ions reaching the detector can be varied by changing either V or **B,** *i.e*:

$$m/e = \mathbf{B}^2 r^2/2V \qquad (3.4)$$

For the measurements of the isotopes of CO_2^+ the magnetic field, **B** is set so that the major ion currents (m/e 44, 45 and 46) are simultaneously centered on the entrance slits of the respective detector cups. The detected ion currents are measured simultaneously and continuously by a multiple Faraday cup arrangement, where the cups are lined up in fixed radii along the image plane of the magnetic sector.

Dual-inlet measurements are made by admitting a standard gas to the ion source and allowing the signal to stabilise to a plateau level, at which data are collected. After a pre-set measurement time the COV cycles and the measurements are repeated for the sample gas. This process is repeated a number of times so that high precision measurements of the isotopic ratios can be made of the sample relative to the reference.

Typically, dual-inlet IRMS analysis requires (sometimes off-line) sample extraction using relatively large (μmol) samples of CO_2 for high precision (0.01 ‰ for $\delta^{13}C$) [*Allison and Francey*, 1995; *Ciais et al.*, 1995a; *Keeling et al.*, 1995]. These sample requirements are restrictive for some experimental applications. However, with specialised automated and on-line cryogenic trapping procedures, such as those used at CSIRO Atmospheric Research, smaller CO_2 samples of ~0.4 μmol are routinely measured with this same high precision [*Francey et al.*, 1996].

For dual-inlet analysis, CO_2 is typically extracted from the air sample in two stages. First, the air sample passes at reduced pressure through a cold trap at liquid nitrogen temperature (-196 °C). This condenses CO_2 (and nitrous oxide, N_2O) while the non-condensable gases in the sample (*e.g.* N_2, O_2, Ar, CH_4, CO etc.) are pumped away to vacuum. Second, the trap is warmed to ~-80 °C so that the trapped gases (excluding H_2O) are released for IRMS analysis. As the vapour pressure versus temperature relationship of CO_2 and N_2O are so similar, CO_2 and N_2O separation is not possible during the extraction process for dual-inlet IRMS analysis. Therefore, both CO_2 and contaminating-N_2O are introduced to the IRMS. Because N_2O has the same molecular mass as CO_2, both gases therefore contribute to the measured signals at m/e 44, 45 and 46.

A correction for N_2O must therefore be applied to dual-inlet measurements of CO_2 isotopes. This correction is a function of three factors. First, the amount of N_2O compared to CO_2 in the sample. Second, its stable isotopic composition (the variance of which is assumed negligible). Third, the ionisation efficiency of N_2O relative to CO_2 in the IRMS, which changes with filament age and may be specific to each machine.

Accurate and precise CO_2 and N_2O mixing ratio measurements are required for each sample. This is because an error of ~5 % in the N_2O/CO_2 ratio corresponds to an error of ~0.01 ‰ in the determination of $\delta^{13}C$ [*Mook and Jongsma*, 1987]. Most laboratories easily obtain this level of accuracy and precision for N_2O/CO_2 ratio measurements, but the potential for error exists. In addition, not all laboratories use identical N_2O correction procedures [*Allison et al.*, 1995]. When comparing dual-inlet IRMS $\delta^{13}C$ and $\delta^{18}O$ data between laboratories, a direct comparison becomes difficult, and if an erroneous or different N_2O correction is made by one or both laboratories, the direct comparison is impossible. To solve this problem and source of error, either a standardised correction procedure must be used by *all* laboratories, as recommended by *Allison et al.*, [1995], or analysis of N_2O-free samples must be achieved.

3.1.3 GC-IRMS

The problems resulting from impure sample analysis can be potentially solved by on-line contaminant separation prior to IRMS introduction. The earliest reported work using on-line chemical alteration before IRMS analysis, was in 1976 where a gas chromatograph was coupled to an organic MS for monitoring aspirin and its metabolites following separation [*Sano et al.*, 1976]. Later, a system designed for biological work yielded sufficient precision to detect methane isotope ratio variability in natural biological sources where the signal is large [*Matthews and Hayes*, 1978]. Two important features missing from these techniques were: 1) the ability to handle transient gas signals at low abundance, without a significant loss of precision; and 2) computerised data acquisition/processing, capable of handling the large amounts of data. Extensions to pre-concentrated amounts of trace gases, for example, CH_4 [*Merritt et al.*, 1995] and NMHC [*Rudolph et al.*, 1997] were significantly more advanced than the initial attempts but were achieved with relatively poor precision compared to dual-inlet IRMS.

For gas analysis by these techniques, GC separation is performed using an inert carrier gas such as helium. For some applications, the sample conversion occurs prior to this step (as for dual-inlet sample preparation, but by a minaturised version) before GC separation. Following separation, the analyte is directed to the IRMS via an *open split interface,* which is essentially a gas switching device that enables a continuous flow of helium to enter the IRMS during non-sample periods to avoid IRMS contamination.

Many techniques that combine some form of on-line sample preparation prior to IRMS have been developed since the late 1970s. Such techniques have been referred to as

irmGCMS (isotope ratio monitoring Gas Chromatography – Mass Spectrometery), CF IRMS (Continuous Flow Isotope Ratio Mass Spectrometery) or GC-IRMS (Gas Chromatography – Isotope Ratio Mass Spectrometery). These techniques have wide and varied applications and no standardised nomenclature has yet been agreed upon as shown below:

- GC-IRMS or irmGC/MS. GC separation prior to IRMS (irmGCMS sometimes includes on-line sample combustion and/or pre-concentration and tends to be used for applications with widely varying backgrounds).
- GCC-IRMS. GC combustion – IRMS (more specific name for the above).
- GCMS. Used for identification rather than isotope ratio determination.
- LC-IRMS. Liquid Chromatography - IRMS, (also LCC-IRMS).
- CSIA. Compound Specific Isotope Analysis, (another name for GCC-IRMS).
- PSIA. Position Specific Isotope Analysis, (used for measurements of intramolecular isotope ratios).

GC-IRMS has been used to describe the work presented in this thesis. In the remainder of this chapter, the design, construction and operation of the GC-IRMS technique are detailed. In this description of the technique, the main factors responsible for precision, accuracy, and reproducibility are discussed. A presentation of results from replicate analyses of reference gas is given to demonstrate the precision and accuracy of the technique (with respect to internal reference gases that have assigned values from traditional methods). In addition, measurement precision of whole-air samples is compared to the theoretical shot noise limited precision over a range of sample sizes.

3.2 Reference gases and assignment of the measurement scale

In this work, the calculation procedure initially used was that of *Santrock et al.*, [1985], but following IAEA recommendations [*Allison et al.*, 1995], the theoretically based relationship of *Craig* [1957] between the $^{17}O/^{16}O$ and $^{18}O/^{16}O$ ratios in sample and reference gases was used. However, no significant differences in $\delta^{13}C$ and $\delta^{18}O$ were observed in a comparison of both calculation procedures over the range of values presented here.

Two clean, whole-air samples collected at Baring Head, New Zealand are used as working reference gases for the technique. Unlike previous GC-IRMS systems, whole-air, rather than pure CO_2, is used as a reference gas. This procedure eliminates sources of

possible error as it ensures identical introduction of the reference and sample gas (injection, separation, drying and Gaussian peak shape, rather than introduction of pure CO_2 in the form of a "square" peak) to the IRMS. In addition, problems associated with storing pure CO_2 at high pressure (*e.g.* formation of liquid CO_2 and resultant fractionation) are avoided by using a reference gas that contains CO_2 at ambient levels in whole-air. These whole-air reference gases were collected using an oil free compressor [*Mak and Brenninkmeijer*, 1994], dried to a dew point of about -80 °C with phosphorous pentoxide (P_2O_5), and stored at high pressure in 27 litre aluminum cylinders, AIRCO (BOC Gases Inc, NJ, USA). The first reference gas, (AIR1) was collected in September 1996 and regulated by a VICTOR® gas regulator (Specialty Products Division, USA), the second, (AIR2) was collected in February 1995 and regulated by an Air Products specialty gases regulator (Air Products and Chemicals, Inc, USA).

Reference gas CO_2 mixing ratio values were assigned from multiple analyses on NIWA's* CO_2 GC. The reference gas of this GC is relative to the WMO X93 mole fraction scale assigned from calibration measurements performed at the central calibration laboratory (SIO) in 1988. Therefore the assigned GC-IRMS reference gas values are relative to this scale. The assigned CO_2 mixing ratios of AIR1 and AIR2 are (356.44 ± 0.09) ppm and (404.19 ± 0.13) ppm respectively.

The isotopic compositions of the GC-IRMS reference gases were assigned by collecting three sub-samples of air from AIR1 and AIR2 in 0.5 litre glass flasks fitted with high vacuum valves with Teflon® PFA (Perflouroalkoxy) o-rings (Glass Expansion, Pty. Ltd, Victoria, Australia). These sub-samples were then sent to CSIRO Atmospheric Research for dual-inlet IRMS analysis. The isotopic compositions of these sub-samples were assigned using the CSIRO CG92 reference scale that is calibrated against NBS-19 and hence traceable to V-PDB CO_2 [*Allison and Francey*, 1999]. Combining the analyses of the sub-samples, the isotopic composition of CO_2 in AIR1 was assigned to be $\delta^{13}C$ = (-7.614 ± 0.029) ‰ and $\delta^{18}O$ = (0.020 ± 0.017) ‰. The isotopic composition of CO_2 in AIR2 was assigned to be $\delta^{13}C$ = (-8.192 ± 0.021) ‰ and $\delta^{18}O$ = (-2.549 ± 0.067) ‰. The errors in the isotopic composition are the standard deviations of the sub-sample analyses and do not contain possible systematic errors associated with collection of the sub-samples.

---

* The National Institute of Water and Atmospheric research Ltd., New Zealand (the laboratory at which the GC-IRMS technique was developed at).

3.3 Air sample collection

For GC-IRMS analyses, *routine* air samples are collected in 2 litre glass flasks that are fitted with ultra high vacuum valves and inert Teflon® PTFE (Polytetralouroethylene) o-rings (Glass Expansion Pty, Ltd. Victoria, Australia). A metal bellows pump (Senior Flexonics, Metal Bellows Division, Sharon, MA, USA) is used to fill the flasks to a pressure of ~100 kPa. Sample storage in the flasks is typically for a period less than two months. To avoid any chance of ^{18}O exchange between H_2O and CO_2 which destroys the $\delta^{18}O$ signal by the following exchange:

$$H_2{}^{18}O + C^{16}O_2 \leftrightarrows H_2{}^{16}O + C^{16}O^{18}O \qquad (3.5)$$

the air samples are chemically dried with magnesium perchlorate, $Mg(ClO_4)_2$. This chemical drying agent was chosen to dry the air samples without any detectable change to the gas composition [*Francey et al.*, 1996]. Furthermore, the configuration of the drying trap was chosen to suit that of the inter comparison program with CSIRO detailed in section 3.4.1. The in-line drying trap (200 mm × 20 mm i.d.) contains ~60 g of $Mg(ClO_4)_2$ which is replaced with fresh chemical after a measured H_2O absorption (weight gain) of 3 – 4 g (5 – 6 %).

Working references and routine samples were collected at Baring Head background air pollution station situated on the south coast of the North Island of New Zealand (41.4 °S, 174.9 °E). Air sample collection at Baring Head is further described in sections 4.5.1 and 5.2.1.2.

3.4 Isotope chromatography

Peak detection is performed from the major ion beam (m/e 44) because it has the best signal-to-noise ratio. The instantaneous rate of change of the signal is determined using a five point linear regression for each data point which are collected every 0.25 s. The beginning and end of each peak is then determined based on a slope threshold of 0.02 mV/s.

Sample related ion currents are determined by subtracting the background from the gross signal at each point. For each individual peak, its individual background values are determined and used in the calculation for that individual peak. The individual

background, which is constant across the width of each peak, is defined as the lowest running five-point average among the 20 points immediately preceding the peak start.

Small differences in vibrational-energy-shifts associated with the condensation of isotopically distinct species occur in chromatography processes. Intramolecular vibrations can either be red shifted (attractive interaction) or blue shifted (repulsive interaction). Solutes containing the heavy isotope will have slightly higher energies and vapour pressures, and thus elution times will be shorter [*Ricci et al.*, 1994]. This effect is observed in a plot of the instantaneous 45/44 ratio (Figure 3.2 (a)).

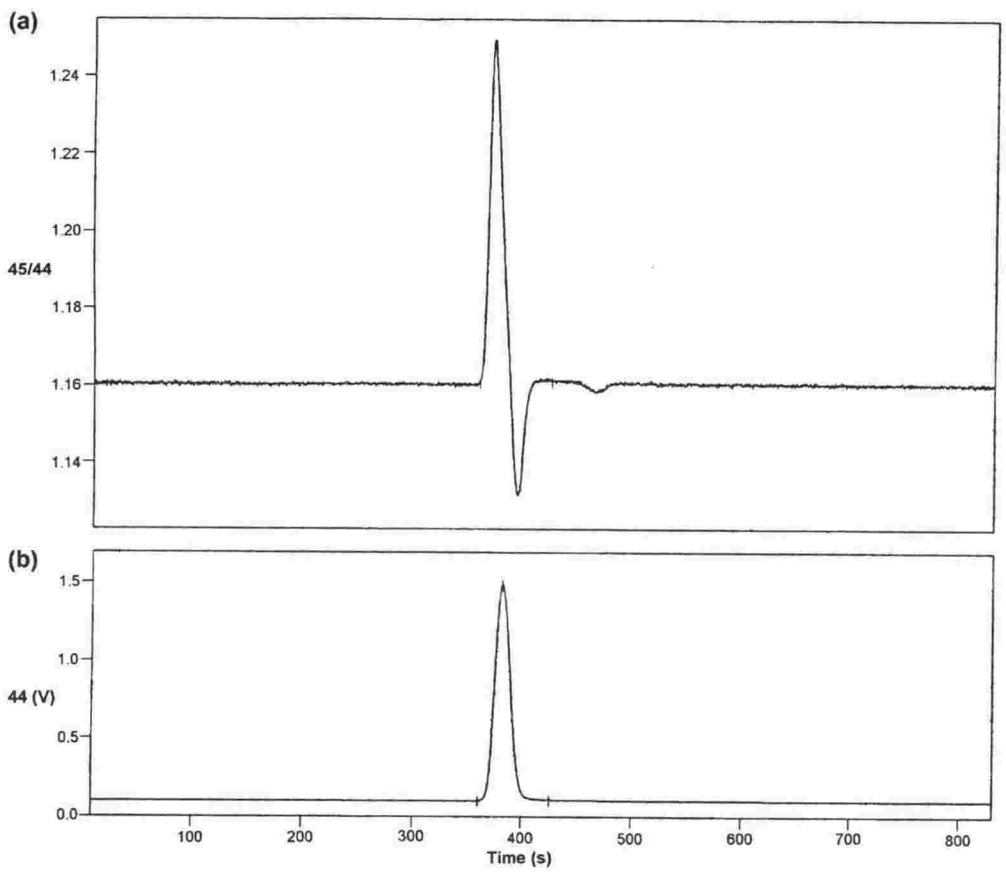

Figure 3.2 (a) Instantaneous mass-45/mass-44 ion-current ratio and (b) major ion current m/e 44 for an aliquot of AIR2 as detected by the GC-IRMS technique.

The isotope chromatograpy of Figure 3.2 demonstrates how the beginning of the peak is enriched in ^{13}C compared to the end of the peak which is depleted in ^{13}C (*i.e.* $^{13}CO_2$ molecules pass through the column faster than $^{12}CO_2$ molecules). This difference, by which the $^{13}CO_2$ peak precedes the $^{12}CO_2$ peak (Δt_r) is accounted for by methods previously described by *Ricci et al.*, [1994]. This peak integration software fits a parabolic function to each of the three detected signals and shifts the integration intervals for m/e 44, 45 and 46 to align with m/e 45.

3.5 GC-IRMS system

The GC-IRMS system couples a GC to an IRMS via a specialised open split interface (Figure 3.3).

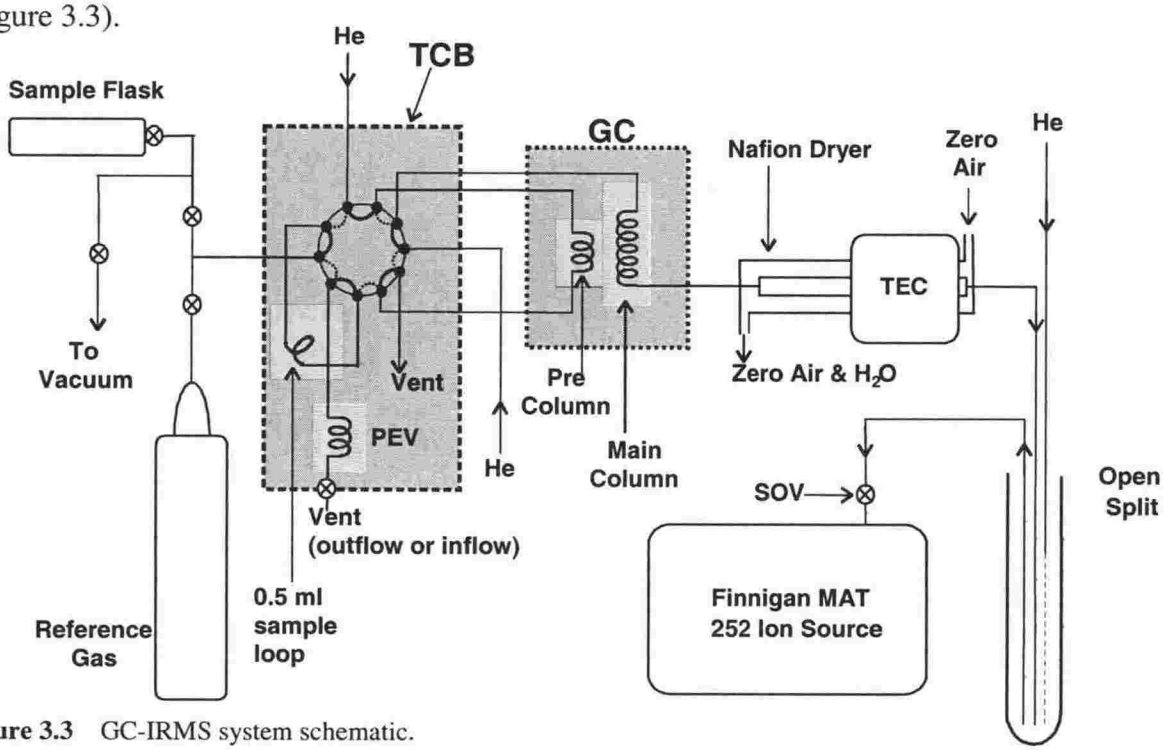

Figure 3.3 GC-IRMS system schematic.

The 10 port valve and adjacent plumbing are enclosed in a Temperature Controlled Box (TCB) at (35.00 ± 0.02) °C to increase reproducibility and automatically switches between load/back flush (solid loops), and inject (dashed loops). Pressure equilibration of sample gas before injection to the GC column occurs in the Pressure-Equilibration-Volume (PEV). After GC separation, gas effluent flows through a Nafion™ drier and enters the open split. The Nafion drier is cooled by a Thermo-Electric Cooler (TEC) and is purged by a counter current flow of clean, dry "zero"air. To enable gas stream switching, the sample and purge helium capillaries alternately move into the immediate proximity of the tip of the transfer capillary, which is permanently positioned at the bottom of the open split. The open split has two positions: 1) ***'open split in'*** (sample capillary extended, helium capillary retracted, as shown in the figure) – the IRMS receives undiluted GC sample effluent; 2) ***'open split out'*** (sample capillary retracted, helium capillary extended) – the IRMS receives pure helium. The Shut-off-valve (SOV) is closed to enable operation of the IRMS in dual-inlet mode.

The 10 port valve (Valco Instruments Co. Inc. Houston, TX, USA) was operated pneumatically to switch between load/back flush, and inject, into the HP5890 Series II GC (Hewlett Packard, Avondale, PA, USA). Switching between sample/reference gases, and vacuum on/off was performed with pneumatic valves (Nupro Company, Willoughby, OH, USA) controlled by a Lab View™ program run from Windows 95™. Reference gas flow rates were controlled at 60 ml/min by high-pressure regulators previously described in section 3.2 (page 36). Sample aliquot introduction into an evacuated sample loop and Pressure-Equilibration-Volume (PEV) before injection is described in section 3.6.

Separation was performed with a packed column: Porapak-Q, 3.66 m × 1.59 mm o.d. (1.016 mm i.d.), stainless steel (SS), 80/100 Mesh with a 1.83 m pre column of the same material (Alltech, Deerfield, IL USA). This was used at a temperature of 41 °C with a flow rate of the Helium carrier gas through the analytical column during injection of 3.0 ml/min. Before each reference or sample aliquot injection the column was back-flushed with Helium at 3.5 ml/min.

After GC separation, sample gas enters the open split interface via a Nafion drier that is discussed further in section 3.8.2.1. Two independent air-actuated pistons provide linear movement for both the sample capillary (deactivated quartz glass, 0.32 mm i.d., flow rate 3.0 ml/min) and the helium purge gas capillary (deactivated quartz glass, 0.32 mm i.d., flow rate 5 ml/min). Transfer of sample gas or purge helium from the open split to the IRMS was through a deactivated quartz glass *transfer capillary*, 0.11 mm i.d., 1 m long (SGE, International Pty Ltd, Ringwood, Victoria, Australia) at a flow rate of ~0.3 ml/min. Obtainable precision was found to be critically dependent on the open split design, which is further discussed in section 3.8.2.2. The inlet to the ion source for GC-IRMS was through a shut-off valve (SOV) enabling IRMS use in both dual-inlet and GC-IRMS modes.

Isotopic analysis of CO_2 was performed by a MAT 252 IRMS (Finnigan MAT, Bremen, Germany) with an accelerating potential of 10 kV. This IRMS utilises a Multi Element - Multi COllector (MEMCO) system with Faraday cups connected to feedback resistors of 3×10^8 Ω, 3×10^{10} Ω and 1×10^{11} Ω to simultaneously measure m/e 44, 45 and 46 ion currents respectively. The IRMS was tuned for a compromise between maximum sensitivity and minimum non-linearity as later discussed in section 3.8.3.1. In the course of the development, new Finnigan source-slits were installed to the IRMS, the advantages of which are later discussed in sections 3.7, 3.8.1 and 3.8.3.1.

3.6 Analysis procedure

To reduce the effect of instrumental drift between successive GC-IRMS analysis, pure CO_2 from the dual-inlet bellows is admitted to the IRMS source, and a peak center is performed at ~1.3 V (~4.3 nA) m/e 44 before each analysis is started.

Routine analysis is provided by injection and analysis of: 1) a reference gas aliquot 2) three aliquots of a sample and 3) a second aliquot of the same reference gas. The detected peaks of the reference gas aliquots are set to the assigned values (section 3.2, page 36) and the average 44/45, 46/44 ratios and areas of the two reference gas aliquots are used to

calculate $\delta^{13}C$, $\delta^{18}O$ and the CO_2 mixing ratio of the sample. This bracketing of the sample aliquots with reference gas aliquots reduces the effect of any instrumental drift that may occur during the period of analysis.

During the analysis procedure the sample loop and adjacent plumbing (see Figure 3.3) is first purged with reference gas for 30 seconds at a flow rate of 60 ml/min. The flow is then stopped and pressure equilibrates for 5 seconds, after which injection through both the pre column and main column occurs for 230 seconds. Following injection, the pre column is back-flushed for 270 seconds. Meanwhile at ~60 seconds before the eluting CO_2 peak, the open split interface switches from directing pure helium to the IRMS to directing sample effluent to the IRMS. Integration of the CO_2 peak follows. Approximately 45 seconds after the final integration point of the CO_2 peak, the open split re-directs the flow to the IRMS to pure helium.

For sample gas aliquots, the sample loop and adjacent plumbing are evacuated rather than pressure flushed. To ensure peak reproducibility the same amount of gas must be introduced to the IRMS for each sample aliquot. Thus, each sample aliquot must be at the same pressure, volume and temperature (PVT). To facilitate this, a vacuum is applied to the sample flask valve, through the 0.5 ml sample loop and into a 5 ml PEV (Figure 3.3). After introduction of the sample aliquot to the sample loop, the PEV valve is opened to enable sample loop equilibration to ambient pressure. For above ambient samples, outflow from the PEV to the laboratory atmosphere occurs, and for samples at or below ambient pressure, inflow from the laboratory atmosphere into the PEV occurs. This equilibration is necessary to ensure that sample/reference gas injections are at the same PVT. During this equilibration for samples collected at or below ambient pressure, the PEV is necessary to avoid contamination by stopping "suck-back" or inflow of laboratory air into the sample loop. Furthermore, during sample loop filling, up to 5 ml of sample gas purges through the sample loop to ensure that no residual from a previous sample or reference gas is injected as a contaminant.

Initially for each new sample, the PEV valve is closed and all inlet plumbing to the flask valve is evacuated by a turbo molecular pump to ~0.01 Pa. This volume is filled, re-evacuated and re-filled with the gas to be measured before an analysis commences. The vacuum pump connection then switches from turbo to roughing pump for the automated run. After the reference gas injection and 450 seconds prior to each subsequent sample injection, the PEV valve is closed and the PEV, sample loop and adjacent plumbing are evacuated. Typically, a vacuum of ~0.02 Pa is obtained in this time, after which the vacuum inlet is closed and the sample valve opens – filling the sample loop, PEV and

adjacent plumbing. To ensure equilibration between the sample flask and sample loop, the sample valve remains open for 30 seconds. Pressure equilibration of each sample aliquot to ambient pressure then occurs by opening the PEV valve for 5 seconds.

Total sample usage is 45 ml for routine analysis (3 aliquots) of air samples collected at ambient pressure. This usage is high compared to the total amount actually injected onto the column (three 0.5 ml aliquots) and is currently limited by the 15 ml inlet volume of the sample loop, PEV and adjacent volume of the 0.762 mm i.d. SS tubing. For air samples collected to 100 kPa (as described in section 3.3, page 38), total sample usage is 90 ml for routine analysis. This higher total sample usage (compared to that required for air samples collected at ambient pressure) is because the 15 ml inlet volume is filled to the pressure at which the sample was collected at (*i.e.* ~100 kPa above ambient pressure), rather than ambient pressure. Although sample collection to 100 kPa uses more gas, it suits an inter comparison of the technique developed in this work with existing methods at CSIRO.

To avoid sample contamination during pressure equilibration of each sample aliquot, inflow of laboratory air into the inlet volume must not pass beyond the PEV. To ensure this, after extraction of a sample aliquot, the inlet pressure must not be lower than 33 kPa below ambient pressure. Many different combinations of sample flask volumes and filling pressures enable this (*e.g.* for an air sample collected at ambient pressure, the sample flask volume must be greater than 150 ml).

3.7 Operational running of GC-IRMS and dual-inlet

The IRMS used in this work is used for both dual-inlet and GC-IRMS. After running in dual-inlet mode, the switch to GC-IRMS introduces large amounts of impurities into the IRMS. This is because when running in dual-inlet mode, gas stagnation in the transfer capillary occurs and impurity levels increase (the most problematic being water). Switching from dual-inlet to GC-IRMS therefore introduces these impurities to the IRMS.

Mass spectrometers experience what is often described as *memory effect* or *scale compression*. This is due to the fact that CO_2 molecules are "sticky" in the ion source of an IRMS and therefore take much longer than many other gases (with the exception of H_2O vapour) to pump away. During dual-inlet IRMS the memory effect lengthens the required pumping time between the sample-reference gas changeovers to ensure that mixing of the two gases is avoided. This results in a longer analysis time for dual-inlet measurements. Furthermore, impurities, which accumulate during periods in which the SOV valve is closed, are introduced into the IRMS when changing from dual-inlet to GC-

IRMS modes and these take longer to clear from the IRMS due to the memory effect (it was observed that a background of m/e 18 < 2 pA is required before high precision analysis can be obtained). With a standard MAT 252 source kit, a switch-over from dual-inlet to GC-IRMS required about two days. For the switch-over to dual-inlet, about 1 day was required.

A new source slit material has been developed by Finnigan to reduce the memory effect. After its installation in the NIWA MAT 252, the switch-over from dual-inlet to GC-IRMS was reduced to ~8 hours (from ~2 days with the old source slits) and the GC-IRMS to dual-inlet switch-over was reduced to ~2 hours (from ~1 day with the old source slits). This significant decrease in down time during mode switching increases the running efficiency of the mass spectrometer.

Occasionally, after very large exposures to impurities (*e.g.* after changing a filament where the ion source of the IRMS is exposed to the laboratory atmosphere), pumping alone is not enough to remove the impurities in an acceptable amount of time. In this case, the COV and source-block require baking out to drive the water molecules off the metal surfaces of the IRMS. Baking in GC-IRMS mode was observed to be more effective than in dual-inlet mode. This is attributed to the continuous flow of dry helium helping to remove the impurities, even with a higher source pressure. In extreme cases, the transfer capillary and SOV also require baking. This is performed by gently heating the transfer capillary and SOV taking care not to overheat the transfer capillary – SOV connection that is made with a 1.588 mm to 0.4 mm VG2 graphite-vespel reducing ferrule (Alltech. Deerfield, IL, USA). Stainless steel capillaries are easily baked by passing a current through them. However, the physical dimensions of these capillaries (~1.6 mm o.d.) limit the performance of the open split, discounting the possibility of using these for this application.

3.8 Development of optimal configuration

3.8.1 Separation of CO_2 and N_2O

For mixing ratio measurements only, CO_2 and N_2O can be separated by a GC column and detected separately by a Flame Ionisation Detector, (FID) for CO_2 (after conversion to CH_4) and an Electron Capture Detector, (ECD) for N_2O [*Weiss*, 1981]. However, such a method for detection by IRMS is not easily possible due to the similarity between the two gases and identical masses of the isotopomers of CO_2 and N_2O.

GC separation of CO_2 and N_2O from ambient air samples for IRMS is difficult. This is because N_2O typically elutes on the tail of the 1000-times larger CO_2 peak. This problem is made worse by the enhanced tailing of the CO_2 peak in the IRMS due to the memory effect.

Before the installation of the new source slits to the NIWA MAT 252 IRMS, the following column phases were tested for CO_2 – N_2O separation and were found to be unsuccessful: 1) Molecular sieve, 2) Carbosphere and 3) HayeSep-D. Molecular sieve caused serious fractionation destroying the $\delta^{18}O$ information, had poor peak integration characteristics and produced bad precision (however, of note was the observation that N_2O eluted first, the only column to do this). Carbosphere required temperature ramping which was unable to be controlled at the required level of reproducibility and HayeSep-D would not provide adequate separation.

Porapak-Q was also tested with the old slits and was found to provide the best separation. For an analysis of acceptable length, complete CO_2 – N_2O separation was not possible and some overlap was present (Figure 3.4).

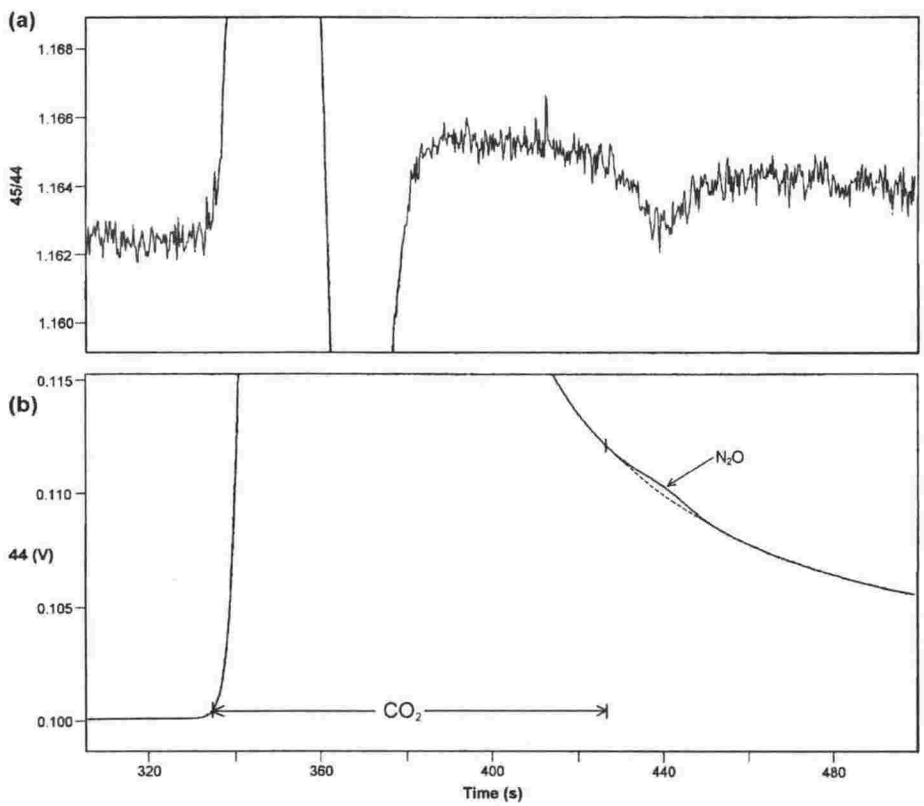

Figure 3.4 CO_2-N_2O separation with the old MAT-252 source-slits.

(a) 45/44 isotope ratio and (b) mass 44 chromatogram. The tick marks show the boundaries of the CO_2 peak integration. The 1000-times smaller N_2O peak, which is just visible as a small blip on the large CO_2 tail and clearly seen in the 45/44 ratio plot, is not completely separated from the integrated CO_2 peak.

The new source-slits reduced the memory effect and increased the CO_2 – N_2O separation such that complete separation of N_2O from the integrated CO_2 peak was possible (Figure 3.5). This enabled N_2O-free determinations of $\delta^{13}C$ and $\delta^{18}O$ in atmospheric CO_2.

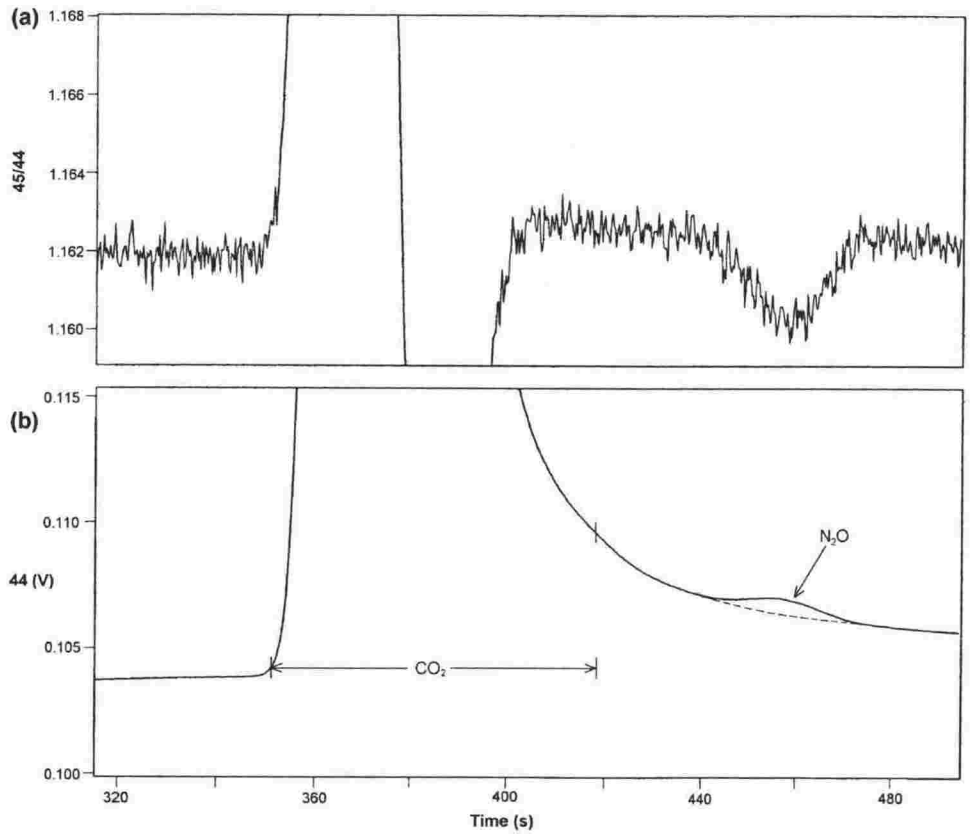

Figure 3.5 CO_2-N_2O separation with the new MAT-252 source-slits
(a) 45/44 isotope ratio and (b) mass 44 chr ıatogram. The tick marks show the boundaries of the CO_2 peak integration. The 1000-times smaller N_2O peak is separated from the integrated CO_2 peak to enable N_2O-free determinations of $\delta^{13}C$ and $\delta^{18}O$ in atmospheric CO_2.

The GC column used to achieve the CO_2 – N_2O separation was a Porapak - Q, 3.66 m × 1.59 mm o.d. (1.016 mm i.d.), SS, 80/100 Mesh packed column with a 1.83 m pre column of the same material (Alltech). This was used at a temperature of 41 °C with a flow rate of helium carrier gas through the main column during injection of 3.0 ml/min.

3.8.2 Maximisation of signal to noise ratio

3.8.2.1 Contamination and carrier gas purity

High carrier gas purity is required to minimise background contamination and noise. This was achieved with the use of an in-line gas purifier (ALL-Pure Helium Purifier, Alltech) to purify Zero Grade (ZG) helium (He > 99.995 %, BOC gases Ltd., New Zealand). This enabled a reduction of contaminants (CO, CO_2, O_2, H_2O and NMHCs) from ppm levels to ppb levels. Such performance enabled the replacement of the higher cost Ultra High Purity (UHP) helium initially used (He > 99.9995 %, BOC gases, New Zealand Ltd). Savings from the lower cost ZG helium covered the cost of the purifier within about a year of GC-IRMS work. Therefore, future operating costs are minimised because column contamination is reduced and the life of the GC column is extended.

Entrainment of laboratory air into the inlet system results in increased background levels, increased noise, and loss of precision. This is mainly because laboratory air is relatively "wet" and the formation of HCO_2^+ molecules according to:

$$^{12}C^{16}O_2 + H_2O \rightarrow H^{12}C^{16}O_2 + OH^{\cdot} \qquad (3.6)$$

(and similarly for $^{13}CO_2$) in the ion source contribute to loss of precision and accuracy for CO_2 isotope measurements [*Leckrone and Hayes*, 1998]. Thus, it is imperative for high precision results to maintain the inlet system completely leak free and dry. Extensive measures were necessary to achieve the required background levels (*e.g.* gold plated ferrules were used to ensure a gas tight seal in some parts of the inlet system, 10 port Valco valve). The inlet to the ion source was made completely leak free by replacing the original MAT 252 SOV (SMOV Micro control valve, SGE International Pty Ltd, Ringwood, Victoria, Australia) with one that was rated for high vacuum, (MCV, SGE). This was necessary as the original contained a Teflon® seal, which leaks under the high vacuum of about 5×10^{-4} Pa directly on the SOV when running in GC-IRMS.

The drying capability of the original Nafion drier used was low and background m/e 18 levels were about three times higher than the level required (m/e 18 are required to be < 2 pA for high precision). This Nafion drier, Nafion™ (Registered) MD - Series Gas Drier (Perma Pure Inc., Toms River, NJ, USA) had dimensions of 0.6 mm i.d., 0.8 mm o.d., and 200 mm long and was mounted coaxially inside a glass tube 4 mm i.d., 6 mm

o.d., using reducing "T-unions" (SGE 6.350 mm to 1.588 mm union) and was purged with UHP helium at ~10 ml/min.

IRMS background water levels were minimised and maintained at a constant level by passing all GC effluent through a higher performance Nafion drier. This consisted of a 610 mm long, 0.76 mm i.d., Nafion tubular membrane in a 1.59 mm o.d. stainless steel sheath. Clean, dry "zero" air (dew point < -80 °C) purges the Nafion drier at a flow rate of ~100 ml/min. The Nafion purge flow (~100 ml/min) is high compared to the sample flow (~3 ml/min) to ensure high drier performance [*Leckrone and Hayes*, 1997]. A ThermoElectric Cooler, (TEC) (Tropicool, Christchurch, New Zealand) cooled the second half of the Nafion to 0 °C. By cooling the Nafion, the vapour pressure in equilibrium with the membrane decreases and the effectiveness of the drying is enhanced [*Leckrone and Hayes*, 1997]. The addition of the TEC decreased the dew point of the emerging dried gas from ~-45 °C to about < -80 °C corresponding to a drop in background water (m/e 18), as measured on the most sensitive detector in the MAT 252, from 2.2 volts to 1.030 volts (2.2 pA to1.03 pA).

3.8.2.2 Open split design

The open split interface is an integral part of the GC-IRMS system as it forms the critical GC to IRMS link and allows the continuous flow of either sample gas or pure helium into the mass spectrometer. The original open split assembly (Figure 3.6), (Finnigan MAT Combustion Interface II), was designed for general use and compromised the obtainable precision for this application.

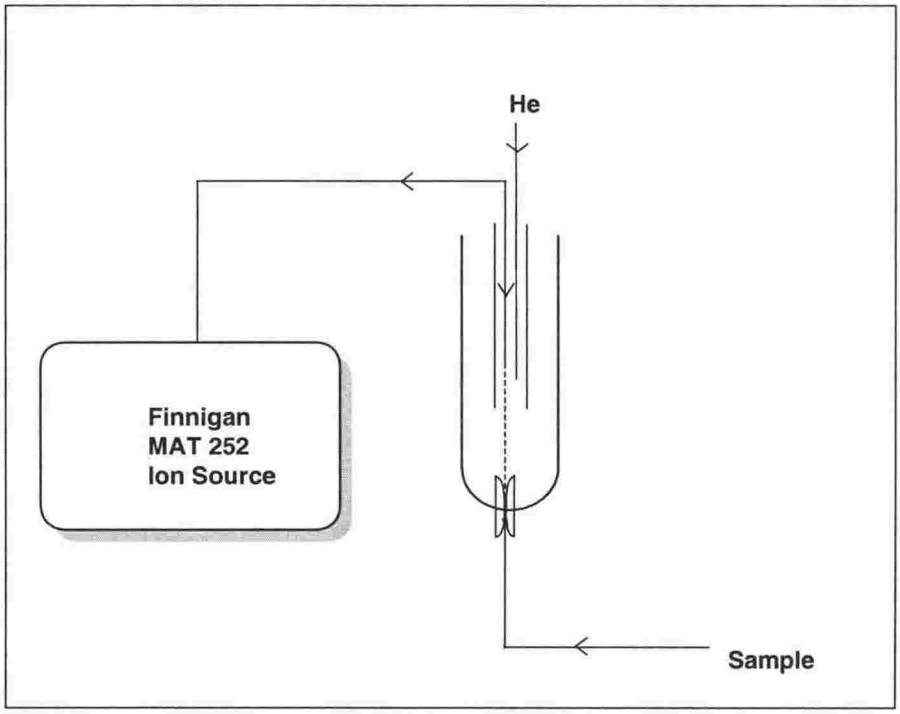

Figure 3.6 The Finnigan MAT Combustion Interface II open split.
An air-actuated piston provides the linear movement of the MS inlet capillary. The capillary has two positions: 1) ***'open split in'*** (dashed line); the mass spectrometer receives the full effluent stream from the GC; 2) ***'open split out'*** (solid line) the MS outlet capillary is retracted to a position 20 – 25 mm from into an inner glass tube and within ~2 mm above the continuous stream of helium purge gas.

With the Finnigan open split configuration, laboratory air was entrained into the open split, resulting in contamination of the IRMS. In addition, high sample dilution (due to the high helium purge rate of up to 15 ml/min that was required to reduce laboratory air entrainment and unwanted GC effluent) affected the sample:helium dilution in the open split and reduced the signal to noise ratio. Furthermore, the placement of the helium capillary relative to the sample capillary was critical to the amount of contamination in the open split and the background noise. The placement of the helium capillary had to be in the correct position (to within less than a millimetre) to ensure that the IRMS receives uncontaminated helium. During development, frequent removal and replacement of the capillaries was necessary for measuring column and purge helium flow rates. Replacing the capillary in exactly the same place was not easily possible and time was wasted finding the optimum position again.

The design and implementation of a new open split (previously shown in Figure 3.3) minimised entrainment, contamination and sample dilution and maximised reproducibility and precision. The open split is like a miniature Pyrex® glass test tube, open at the top, with dimensions: 60mm long, 1.9 mm o.d., 1.3 mm i.d. Gas stream switching, previously described in Figure 3.3 (page 40), enables a high signal to noise ratio. The split ratio is

~1:9, *i.e.* of the sample effluent that enters the open split at 3.0 ml/min, only ~10 % of this enters the ion source at 0.3 ml/min (this factor is currently limited by chromatography and not the open split design). Thus, in the technique described here, and for samples at current atmospheric levels, ~8 nmol CO_2 is injected onto the GC column and ~0.8 nmol of this enters the IRMS source.

3.8.3 Reproducibility

3.8.3.1 Sensitivity and non-linearity

The sensitivity of an IRMS is the measure of how many molecules of sample or reference gas are needed to generate an ion measured at the collectors. The more sensitive the IRMS is, the fewer molecules needed to generate an ion, and for a given sample size, an increased signal to noise ratio and higher precision is possible.

The initial sensitivity was ~1500 to ~1700 molecules/ion. With the installation of the new source slits, the sensitivity increased by ~20 % to ~1200 molecules/ion. This enabled larger peak areas and correspondingly better precision.

Tuning and linearity measurements are made in dual-inlet mode under an ultra high vacuum of $\sim 3 \times 10^{-7}$ Pa. If these measurements are then applied to GC-IRMS with a higher source pressure of $\sim 6 \times 10^{-4}$ Pa and a continuous flow of helium into the IRMS, the tuning requirements change. Over the 2 to 7 Volt (6.7 to 23 nA) range for m/e 44 typically achieved when running in dual-inlet mode, a non-linearity of 0.03 ‰·Volt^{-1} was easily achieved. However, achieving this level, or even ~0.1 ‰·Volt^{-1} non-linearity in the normal GC-IRMS operating region below 1.5 Volts (5 nA), was very difficult.

The sensitivity measured in dual-inlet mode (with an electron energy of 97.2 Volts, a trap voltage of 50.0 Volts, and a low ion extraction [325 potentiometer setting]) was ~1570 molecules/ion. In this mode a non-linearity of 0.17 ‰·Volt^{-1} and 0.44 ‰·Volt^{-1} for $\delta^{13}C$ and $\delta^{18}O$ respectively was observed over the 1 to 3 Volt range. Using the same settings (electron energy etc) and switching from dual-inlet to GC-IRMS, non-linearity worsened to 1.03 ‰·Volt^{-1} and -0.78 ‰·Volt^{-1} for $\delta^{13}C$ and $\delta^{18}O$ respectively. However, if the IRMS was tuned whilst running in GC-IRMS* for maximum sensitivity and

---

* GC-IRMS non-linearity is measured by performing multiple runs and for each run the sample is diluted in the open split to vary the peak height over a range of voltages typically experienced when running in GC-IRMS. This gives a more accurate indication of linearity rather than performing the non-linearity test introducing varying amounts of bellows CO_2 to the IRMS source.

minimum non-linearity with a higher ion extraction (577 potentiometer setting) a significantly improved non-linearity results (0.07 ‰·Volt^{-1} and -0.15 ‰·Volt^{-1} for $\delta^{13}C$ and $\delta^{18}O$ respectively). In addition to the improved non-linearity with GC-IRMS tuning, the sensitivity increased to about 1100 molecules/ion.

GC-IRMS tuning achieves low non-linearity and high sensitivity in comparison to dual-inlet tuning and has been used for all results presented. However, the maximum obtainable non-linearity for GC-IRMS is lower than that achieved by dual-inlet. Therefore, sample and reference sizes should be as close as practically possible to minimise the effect of this non-linearity.

3.8.3.2 Temperature and pressure effects

Reproducibility and precision of measured CO_2 mixing ratio are strongly affected by temperature and pressure variations that occur for each eluting peak during GC-IRMS analysis. Due to IRMS non-linearity, $\delta^{18}O$ and $\delta^{13}C$ measurements are also affected.

Observed laboratory pressure variations were minimal and occurred over a relatively long time compared to that required for GC-IRMS analysis (a change of ~1 hPa per day). Laboratory temperature variations were proportionally larger than pressure variations both in the extent of the variation and in the frequency (a change of ~1 °C per hour).

Temperature variations change the value of the high-precision resistor that regulates the magnet current in the MAT 252 [*Brand*, personal communication, 1999]. The detected signals are therefore affected because magnetic field strength variations cause the ion beam to be shifted. This was clearly demonstrated by the observation that under dual-inlet conditions, the background water signal (m/e 18) varies with the same period and relative amplitude as the temperature cycle in the laboratory.

The GC-IRMS background noise is further magnified due to variations in open split entrainment. This occurs because the relative pressure difference between the slightly above ambient pressure open split (due to the purge helium) and the laboratory are affected by temperature variations. This further highlights the need for a well-designed open split so that minimal (if any) entrainment and IRMS contamination occurs.

The effects of laboratory temperature variations were minimised by stabilising the inlet system temperature to < 0.2 °C/hour. Insulation of the inlet system from the reference gas regulators through to the open split achieved this. In addition, temperatures were stabilised in the transfer capillary and SOV to < 0.1 °C/hour by insulation of the section. Furthermore, the sample loop, PEV and adjacent plumbing were maintained at a stable

temperature of (35.00 ± 0.02) °C by enclosing this section within an insulated, temperature controlled box (TCB), see Figure 3.3. Temperature control to this level within the TCB was achieved with the use of an external GC temperature sensor and 40 Watt cartridge heater. A 2 Watt electric fan circulated air within the box and two thermal masses of 150 ml water and 1.6 kg brass, were positioned in the box. These measures reduced the uncontrollable temperature effects due to laboratory air temperature variations and improved technique precision.

3.8.4 Analysis Time

The analysis time* is determined by the requirements for: adequate N_2O – CO_2 separation, high signal to noise ratio, and a sufficient number of reference and sample aliquots for good measurement statistics, and to reduce instrumental drifts. Increasing the carrier flow rate in the column decreases the analysis time. However, reduced separation and increased sample dilution occurs, which lowers the signal strength, reduces the signal to noise ratio, and hence lowers precision. A balance between the analysis time, adequate separation, dilution and precision was achieved at an analysis time of 40 minutes and was comparable to that required for dual-inlet analysis.

Using the technique described here, mass spectrometers that have a large memory effect may not be used (without modification) to obtain high precision N_2O-free isotopic analyses of atmospheric CO_2 in short analysis times.

3.9 Technique performance

Maximum performance can be evaluated by considering the *shot-noise limit*. This is based on ion collection statistics and refers to the precision that would be obtained if the ion beam was the only significant noise source [*Peterson and Hayes*, 1978]. Simplified expressions for the shot-noise-limited precision (σ_δ) expressed as functions of the integrated m/e 44 signal area (^{44}A, Volt·s) for a MAT-252 IRMS from *Merritt and Hayes* [1994] are:

$$\sigma_\delta^2 = 0.00892/^{44}A \qquad (3.7)$$

---

* Includes the time required for extraction of CO_2 from the air sample.

and if the integrated ion currents of the reference and sample are not equal then:

$$\sigma_\delta^2 = 0.00446(1/^{44}A_{\text{reference}} + 1/^{44}A_{\text{sample}}) \quad (3.8)$$

To provide an indication of technique performance, results from replicate analyses of the reference gases are first presented.

Table 3.1 GC-IRMS replicate analyses of (a) AIR1 versus AIR1 and (b) AIR2 versus AIR1. The differences (Δ) from assigned values (CSIRO for isotopes and NIWA GC for CO_2 mixing ratio, detailed in section 3.2, page 36) are given in the last line of the table.

	(a)			(b)		
	$\delta^{13}C$ (‰)	$\delta^{18}O$ (‰)	CO_2 (ppm)	$\delta^{13}C$ (‰)	$\delta^{18}O$ (‰)	CO_2 (ppm)
	-7.60	0.03	355.7	-8.18	-2.60	403.9
	-7.60	0.09	356.7	-8.15	-2.47	405.1
	-7.64	0.05	356.1	-8.20	-2.50	405.3
	-7.62	0.03	356.4	-8.21	-2.52	404.8
	-7.66	-0.05	356.8	-8.17	-2.52	404.4
	-7.61	0.03	356.2	-8.17	-2.47	404.6
	-7.64	0.02	356.8	-8.22	-2.45	404.7
	-7.62	-0.01	355.7	-8.18	-2.52	404.2
	-7.65	0.05	356.3	-8.21	-2.47	404.5
	-7.61	0.00	356.9	-8.22	-2.47	404.9
Average	-7.63	0.02	356.4	-8.19	-2.50	404.6
Standard deviation	0.02	0.04	0.4	0.02	0.04	0.4
Δ	-0.02	0.00	-0.1	0.00	0.05	0.4

The replicate analyses show the precision of the technique to be:

- 0.02 ‰ for $\delta^{13}C$
- 0.04 ‰ for $\delta^{18}O$ and
- 0.4 ppm for CO_2 mixing ratio

An indication of the differences between measurements from GC-IRMS and those from traditional techniques is also given by the replicate analysis of the reference gases. The

measured differences between GC-IRMS isotopic analysis and CSIRO assigned isotopic values from dual-inlet analysis, were less than 0.02 ‰ for both $\delta^{13}C$ and $\delta^{18}O$ when measuring AIR1 versus AIR1 and AIR2 versus AIR1. When measuring AIR2 versus AIR1, the differences increased to 0.05 ‰ for $\delta^{18}O$ ($\delta^{13}C$ differences remained below 0.02 ‰). The measured differences between GC-IRMS mixing ratio analysis, and NIWA assigned mixing ratio values from GC analyses, were less than 0.1 ppm when measuring AIR1 versus AIR1 but increased to 0.45 ppm when measuring AIR2 versus AIR1. These differences must however, be considered in association with the uncertainty of each measurement (some of this difference may be due to GC-IRMS measurement uncertainty and some of may be due to the uncertainty associated with the assigned values of the reference gases). Taking these into account, the observed differences are not significant for the CO_2 species measured.

The standard deviation of ten air samples (chosen at random from more than 100 samples) collected at Baring Head are presented in Table 3.2.

Table 3.2 Standard deviation (st dev) from GC-IRMS analyses of air samples collected at Baring Head, New Zealand and comparison to the theoretical shot-noise limited (SNL) $\delta^{13}C$ precision.

Sample CO_2[a] (nmol)	Sample Area (V·s)	$\delta^{13}C$ st dev (‰)	$\delta^{18}O$ st dev (‰)	CO_2 st dev (ppm)	SNL[b] (‰)
0.800	21.1	0.01	0.03	0.4	0.021
0.794	21.6	0.04	0.01	0.3	0.020
0.819	21.2	0.02	0.03	0.4	0.020
0.813	22.0	0.02	0.04	0.4	0.020
0.817	22.2	0.01	0.04	0.2	0.020
0.816	21.5	0.03	0.03	0.4	0.020
0.815	21.6	0.02	0.02	0.3	0.020
0.815	22.2	0.03	0.06	0.6	0.020
0.814	21.3	0.03	0.06	0.2	0.020
0.799	21.4	0.01	0.04	0.4	0.020
	Average	**0.02**	**0.04**	**0.4**	**0.02**

[a]Source CO_2

[b]Caculated from (2.7), Reference gas used: AIR1, area = 21.3 V·s.

The standard deviation of the three species measured for these air samples are equivalent to that of the replicate analyses, indicating that the sampling and storage process does not introduce any further detectable (non-systematic) errors.

The theoretical shot-noise-limited $\delta^{13}C$ precision has been calculated for these routine samples for various CO_2 mixing ratios (Table 3.2). Comparing the observed and theoretical shot-noise-limited $\delta^{13}C$ precision, it is evident that the technique performs at the shot-noise limit of 0.02 ‰.

It is also useful to evaluate the technique performance over a range of sample sizes. Differing amounts of CO_2 were introduced to the ion source of the IRMS by varying the open split dilution. The split ratio of 1:9 was varied by introducing reference and sample CO_2 with the sample helium capillary extended and increasing the open split helium purge flow from the normal 5 ml/min to ~20 ml/min. Replicate analyses of AIR2 by this method are shown in Figure 3.7.

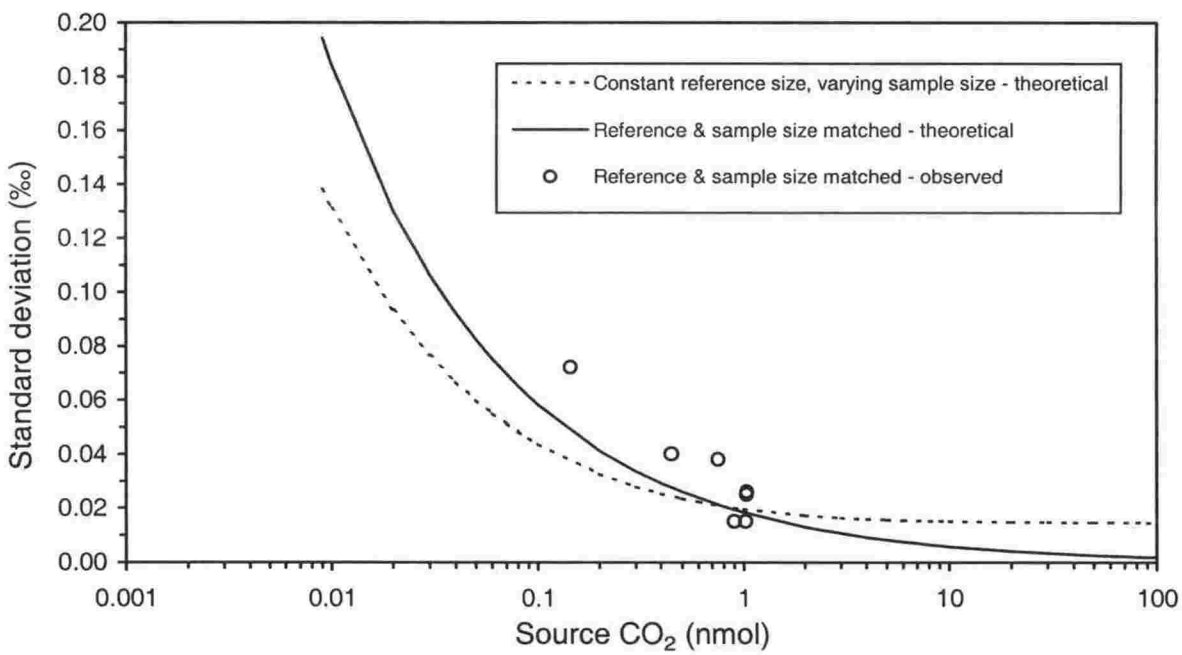

Figure 3.7 Observed and theoretical (shot-noise limited) standard deviations for varying amounts of CO_2 in the IRMS source.

Over the observed range of ~150 pmol to ~1 nmol CO_2 in the source, the technique performs within a factor of ~1.3 of the shot-noise limit. At the lower limit of ~150 pmol CO_2 in the source, the technique performs within a factor of ~1.5 from the shot-noise limit. This indicates that the effects of noise or systematic error become more significant at these lower sample sizes.

It can be seen from the theoretical prediction (Figure 3.7) that by increasing the amount of gas reaching the IRMS source (while maintaining matched reference and sample volumes), higher performance (*i.e.* lower standard deviation) is possible. This performance however, is ultimately limited by IRMS detector overload which, for eluting CO_2 peaks from the experimental technique presented here in a MAT 252, would occur at ~4 nmol CO_2 in the source. A shot-noise limited precision of 0.01 ‰ is theoretically possible with ~3 nmol CO_2 in the source. This would be possible by this technique if the split ratio could be reduced to ~1:2.2.

Also evident from the theoretical prediction (Figure 3.7) is that if unmatched reference and sample gas volumes are admitted to the IRMS source (reference gas volume fixed and sample gas volume increased) no significant improvement to performance is possible. However, operating in this regime, improved technique performance is possible when analysing reduced sample volumes. This is an advantage for some applications measuring $\delta^{13}C$ from very small samples.

3.10 Summary and discussion

The development of a new GC-IRMS technique for high precision isotopic analysis of $\delta^{13}C$ and $\delta^{18}O$ in atmospheric CO_2 has been completed. Difficulties experienced by the traditional dual-inlet technique, in correcting for interfering N_2O mass contributions, have been overcome by complete CO_2-N_2O GC separation before introduction to the IRMS.

The transient sample introduction to the IRMS of the small samples used by GC-IRMS mean that fewer ions are detected than for dual-inlet and theoretical measurement precision is therefore lower. However, high precision was achieved with careful design to maximise signal to noise ratios and reproducibility.

Small samples can be measured by GC-IRMS (up to three orders of magnitude smaller than those required by dual-inlet). For routine analyses of ambient samples the total sample usage is 45 ml and collected ambient sample volumes as low as 150 ml can be introduced to the inlet system and analysed without contamination. This minimum sample volume is limited by inlet dead volume and can potentially be further reduced with the use of very-low-volume valves and plumbing.

The GC-IRMS technique performed at the theoretical shot-noise limit for both replicate analyses of reference gases, and for analysis of air samples collected at Baring Head. No significant differences between GC-IRMS measurements and those from traditional techniques were determined over the range of values measured. Furthermore, the air

sample collection and storage procedure did not introduce any detectable (non-systematic) errors to the measurements.

GC-IRMS measurements of $\delta^{13}C$ and $\delta^{18}O$ are performed to a precision of 0.02 ‰ and 0.04 ‰ respectively which meets the requirements of global carbon cycle research. In addition, a simultaneous CO_2 mixing ratio is measured to a precision of 0.4 ppm. This eliminates the need for off-line analysis on another instrument, unless higher precision is required.

The technique presented here has the potential to perform isotopic analysis of $\delta^{13}C$ in atmospheric CO_2 to a precision of 0.01 ‰ by admitting ~3 nmol CO_2 in the IRMS source. This could be obtained by reducing the split ratio from its current value of 1:9 to ~1:2.2.

Simple comparisons, between GC-IRMS and traditional technique measurements, of the type presented in this section, do not address the important issue of long-term inter calibration that is essential for atmospheric CO_2 measurements. To achieve this, a high precision inter calibration program with CSIRO has been established in addition to flask air-sharing inter comparison exercise with CSIRO and other laboratories. The strategy and results of these programs are presented in the following chapter.

4 Inter calibration and inter comparison exercises

4.1 Introduction

The aim of this chapter is to further investigate the performance of the new GC-IRMS technique. The initial stages of inter calibration and inter comparison exercises with traditional techniques and other laboratories achieve this. In addition, the ultimate goal of this work is to merge GC-IRMS data with that from these traditional techniques and other laboratories worldwide.

The literature currently available about the topic of this chapter is somewhat confusing and the terms "inter calibration" and "inter comparisons" have been used loosely. To avoid further confusion these terms are now defined as they have been used in this work.

- *Calibration*

  The assignment of a *measurement scale* to laboratory measurements. This measurement scale is what the analysed data values are reported to (*e.g.* the measurement scale for stable isotopes of atmospheric CO_2 might be the CG92 scale or the VPDB-CO_2 scale and for CO_2 mixing ratio, it might be the WMO X93 scale. The assignment of a measurement scales to the GC-IRMS technique has been previously discussed in section 3.2 (page 36).

- *Inter Calibration*

  Inter calibration is achieved between two or more laboratories when the laboratories have compared high precision measurements of gas composition over a range of values and have formally agreed upon their conformity over this range. Any further measurements over this range are therefore directly comparable between the laboratories. Inter calibration generally involves a high number of replicate analyses from pure CO_2 or whole-air stored in high-pressure cylinders of which the composition has been very precisely determined. These multiple analyses provide better measurement statistics compared to 'one-off' routine measurements. The inter calibration exercise presented here utilises whole-air stored in a low pressure tank.

- *Inter Comparison*

  Inter comparison measurements are performed by what are normally referred to as *Inter comparison programs* (*ICPs*) and the term "flask-air-sharing inter comparisons" is also used to describe these programs, which utilise high frequency

routine measurements from air samples obtained by operational monitoring programs. ICPs investigate the differences that arise in attempts to monitor spatial and temporal variations in atmospheric CO_2 species. The differences that arise are most likely caused by different laboratory calibrations, analyses procedures, and flask sampling programs. ICPs provide additional information to inter calibration exercises and enable the long term monitoring of operational measurement programs and measurement scales. Problems can be detected as they arise which enables them to be quickly rectified. In some previous cases, cylinder inter comparisons have been performed between laboratories to investigate the differences between laboratories in air measured from cylinders.

This chapter first discusses the reasons why high precision inter calibration is necessary for global monitoring of atmospheric CO_2 and the limitations of current inter calibration programs. This background provides the reasons why inter calibration is an important requirement for the new GC-IRMS technique if it is to be used to globally monitor the mixing ratio and isotopic composition of atmospheric CO_2.

A description of the methodology and presentation of the initial results from a high precision inter calibration exercise that was established between the GC-IRMS technique and a traditional dual-inlet IRMS technique at CSIRO is then given. These initial stages of the inter calibration exercise evaluate the performance of the GC-IRMS technique with respect to the traditional techniques.

Results from inter comparison exercises with other laboratories currently measuring atmospheric CO_2 species are then presented to further assess the performance of the GC-IRMS technique and compare operational flask air-sharing programs established during this work.

Further investigations of the possible reasons for the discrepancies observed between laboratories are given and areas that require further investigation are discussed.

4.2 Background

By using atmospheric transport models, together with global carbon cycle models which use mixing ratio and isotopic measurements of atmospheric CO_2 as inputs [e.g., *Ciais et al.*, 1995a], estimates of the natural and anthropogenic CO_2 fluxes can be derived to increase our understanding of the global carbon cycle. Unfortunately, the uncertainty associated with the flux estimates derived from global carbon cycle models is high and

sometimes as large as the flux itself [e.g., *IPCC,* 1995]. This is because the sites are sparse, the temporal continuity is lacking at some sites, and not all sites have data over the same time period. In addition, poor data quality means that only some of it can be used in global carbon cycle models (*e.g.* although atmospheric CO_2 species are measured at ~100 sites globally, the number of sites producing data of high enough quality (defined in following text) for integration into global carbon cycle models is limited to ~25 [*Francey and Rayner*, 1998]). To reduce the biases due to spatial and temporal deficiencies in the sampling network, excellent spatial resolution and temporal continuity are required [*Conway et al.,* 1994].

The financial costs and logistics of obtaining high frequency data at many sites worldwide are obviously very high, and such an exercise cannot be easily undertaken by a single laboratory. Therefore, to successfully address this problem a cooperative international approach is required. Such an approach has been established by some laboratories (*e.g.* the Carbon Cycle Group at the National Oceanic and Atmospheric Administration Climate Monitoring and Diagnostics Laboratory (NOAA CMDL) cooperative program to globally represent data in GLOBALVIEW [http:// cmdl.noaa.gov]). However, such integration of independent data sets is very difficult because inconsistencies exist between different measuring laboratories (*e.g.* differences in calibration scales, sample collection, analysis techniques, and data processing). Several other laboratories have recently engaged in inter comparison programs to examine these differences (*e.g.* the Stable Isotope Laboratory at the Institute of Arctic and Alpine Research (INSTAAR), NOAA CMDL and Atmospheric Research at CSIRO [*Steele, et al.,* 1996]; Atmospheric Environment Service, Canada (AES) and CSIRO [*Francey et al.,* 1999]; and NOAA CMDL, INSTAAR and the Centre des Faibles Radioactivités at the Laboratoire de Modélisation du Climat et de L'Environnement, France (CFR-LMCE) [*Gaudry et al.,* 1996]). These inter comparison programs have highlighted inconsistencies, the causes of which are difficult to identify. Further work is therefore required to achieve the goal, which is to "seamlessly merge" independent data sets with confidence to enable the accuracy and precision of global carbon cycle source – sink partitioning calculations to be increased.

For global atmospheric CO_2 monitoring programs to meet this goal, a dedicated approach is required. Programs initiated by the WMO and IAEA aim to achieve this goal, but have not yet obtained it. New programs that utilise high frequency inter calibration and inter comparison exercises, such as the GLOBAL-HUBS proposal that is derived from CLASSIC-AL [*Francey and Rayner,* 1998] and recently accepted at the WMO experts

meeting in Stockholm, Sweden, August 1999, [*Francey*, personal communication, 1999] are required to achieve this goal quickly and effectively.

For the successful merging of atmospheric CO_2 mixing ratio data from different sites, the WMO recommends that inter-laboratory target precisions of 0.05 ppm or better are necessary to achieve a network precision of 0.1 ppm [*WMO*, 1987]. This target precision refers to the average temporal values (*e.g.* annual or seasonal) and large-scale values (*e.g.* model grid scale to hemispheric) and is comparable to that capable from many laboratories. However, this target precision has not yet been achieved worldwide (Figure 4.1) as significant inter calibration differences exist between laboratories.

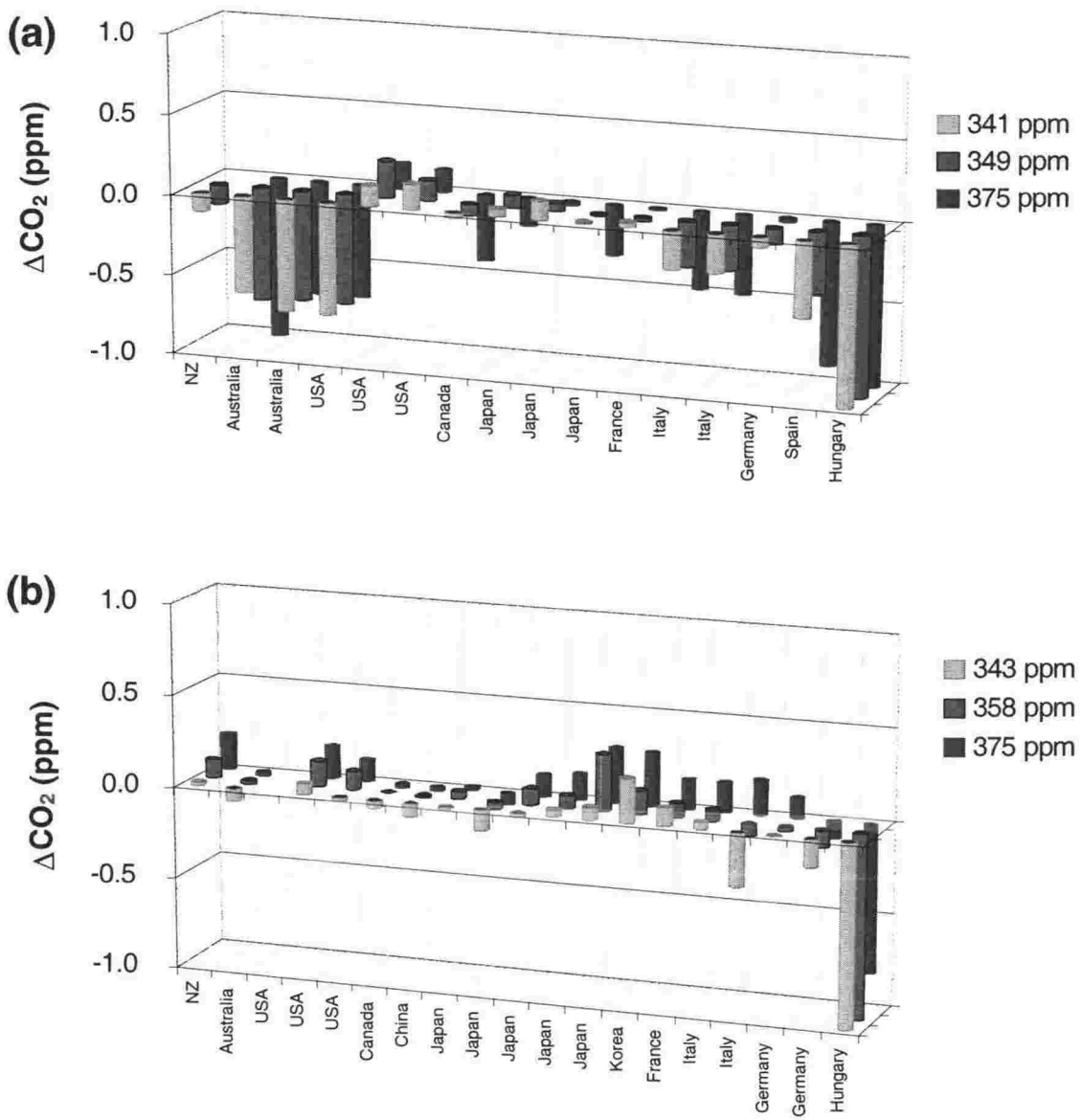

Figure 4.1 WMO inter calibrations of atmospheric CO_2 measurement laboratories in (a) 1991-1993 and (b) 1995-1997 (From *Francey and Rayner*, [1998] and adapted from WMO technical reports [*Pearman*, 1993; *Peterson*, 1997].

ΔCO_2 are measured differences from mixing ratios assigned from NOAA CMDL by gravimetric dilution.

Few laboratories are within the target precision of 0.05 ppm and some laboratories are far from this goal. In addition, possible non-linearity problems are evident in many laboratories that measured lower values for low mixing ratio gas and elevated levels for high mixing ratio gases. However, this could be a problem with the gravimetric dilution technique used in the assignment of the mixing ratio values at NOAA CMDL because it may have assigned incorrect values to the tanks, and independent verification of this technique is therefore necessary.

In addition to the unsatisfactory situation with the calibration of atmospheric CO_2 mixing ratios, calibration of the isotopic ratio $\delta^{13}C$ in atmospheric CO_2 also falls short of the level required. In 1995 an IAEA working group stated a need to report $\delta^{13}C$ so that comparisons of different collection sites (spatial) to a precision of ~0.01 ‰, and a comparison of the long-term behavior (temporal) to a precision of ~0.005 ‰ are possible, with only slightly relaxed requirements for $\delta^{18}O$ [*Allison et al.*, 1995]. This requirement is so high because an error of only 0.024 ‰ in $\delta^{13}C$ measured globally corresponds to a source sink partitioning error of 1 GtC [*Tans et al.*, 1998].

The 1995 IAEA inter comparison during CLASSIC (Circulation of Laboratory Air Standards for Stable Isotope inter Comparisons) between four laboratories with the longest history of isotopic analysis of atmospheric CO_2 (Figure 4.2) indicates the nature of the situation for $\delta^{13}C$ measurements at this time.

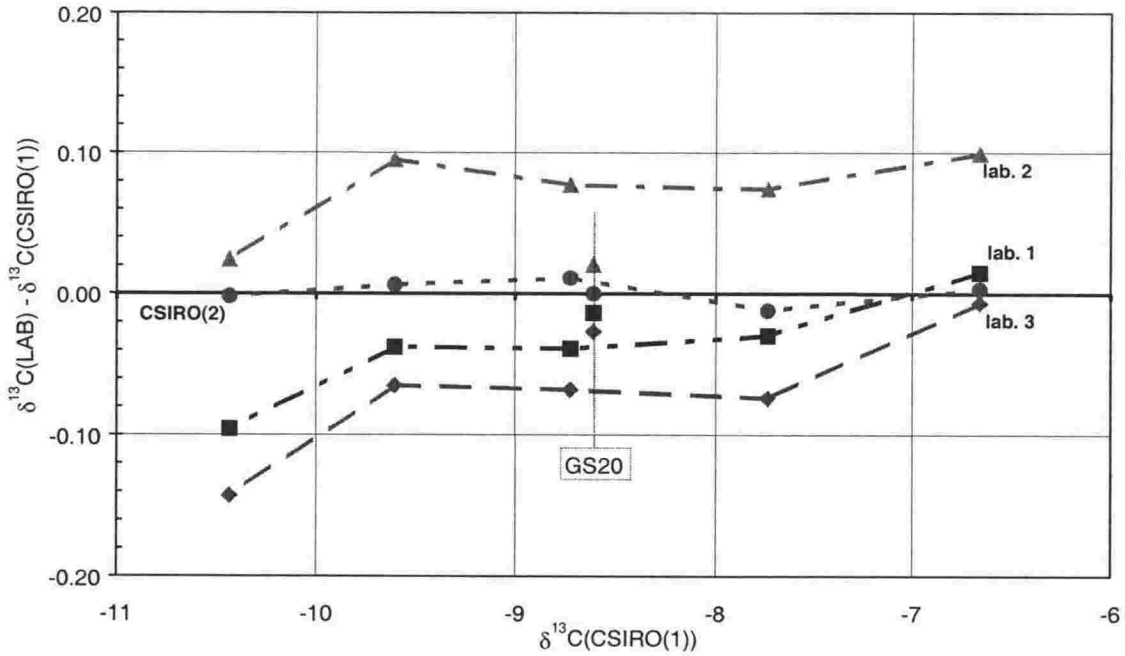

Figure 4.2 IAEA inter comparison of $\delta^{13}CO_2$ using both pure-CO_2 (GS20) and whole-air in high-pressure cylinders during the 1995 CLASSIC exercise [From *Francey and Rayner*, 1998].
Differences are from $\delta^{13}C$ measured before circulation. CSIRO(2) refers to analysis after circulation. $\delta^{13}C$ is related to CO_2 mixing ratio difference from ambient values by ~-0.05 ‰ppm^{-1}. USA and Japanese measurement laboratories are referred to by number only.

In this CLASSIC inter comparison exercise, differences for pure-CO_2 samples (GS20) were outside the target precision for whole-air by a factor of two. Differences for measurements from whole-air samples from high-pressure cylinders were much larger; up to ten times the target precision. This suggests that, in this comparison there may have been serious differences with extraction and analysis techniques of CO_2 from whole-air for dual-inlet analysis. Calibration scale offsets may have also been responsible for some of the observed differences. In addition, there also appears to be a non-linearity issue that is different between the laboratories.

When examining an operational flask-air-sharing inter comparison (Figure 4.3), where the measurement precision is low (individual measurements) but the frequency is high, the differences are worse than that observed in the CLASSIC inter comparison of air in high-pressure cylinders described above because the scatter is larger.

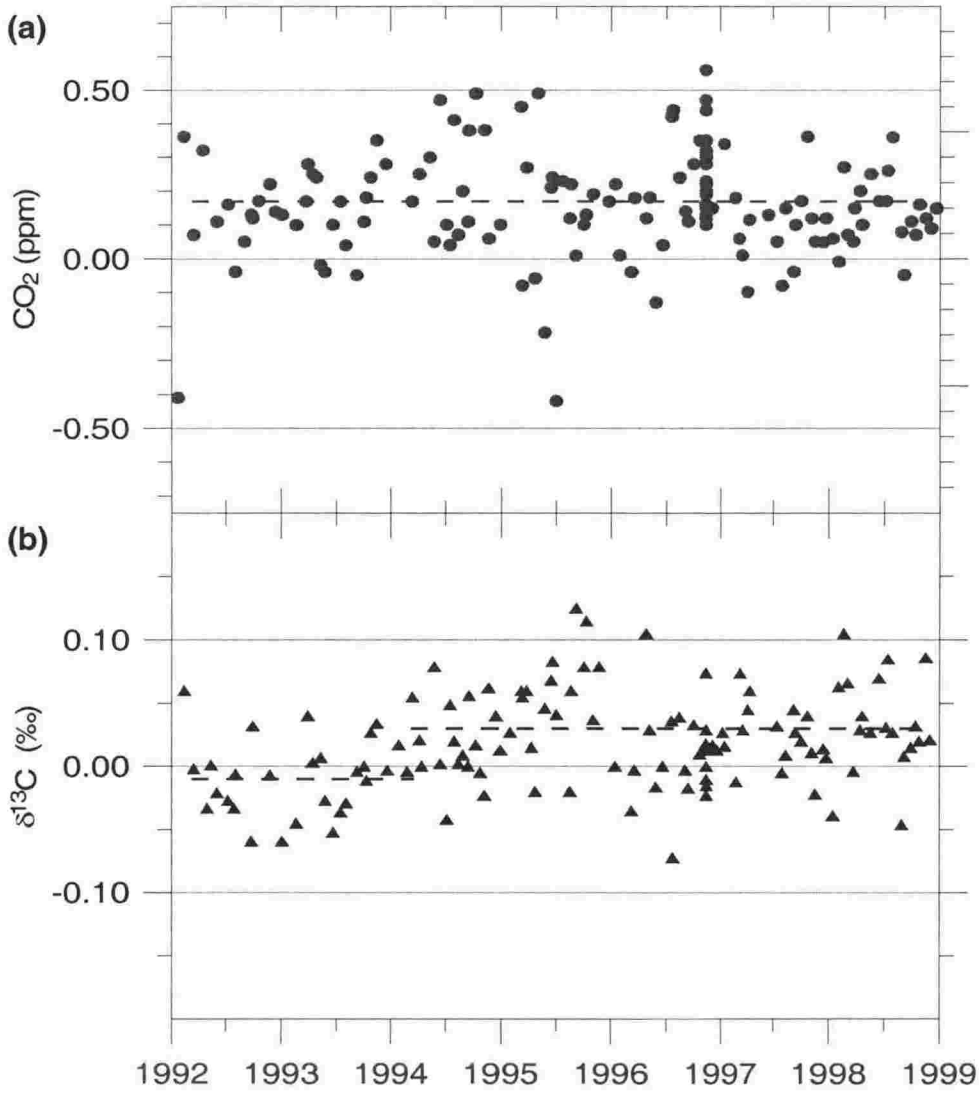

Figure 4.3 (a) (CSIRO-NOAA CMDL) measured CO_2 differences on Cape Grim air from the same flask as a function of flask collection date. (b) (CSIRO-INSTAAR) measured $\delta^{13}C$ differences on Cape Grim air from the same flask as a function of flask collection date [From *Francey and Rayner*, 1998].

The inter comparison of the CO_2 mixing ratio between CSIRO and NOAA CMDL indicated a constant mean difference of 0.17 ppm ± 0.17 ppm [*Francey and Rayner*, 1998]. Compared to the inter calibration of CO_2 mixing ratio to 0.01 ppm for CSIRO in the 1997 WMO calibration exercise, the observed difference in the inter comparison between these two laboratories is much worse.

In 1995, the observed $\delta^{13}C$ difference from flask samples between CSIRO and INSTAAR was consistent with the CLASSIC high-pressure cylinder inter comparisons in the same period shown in Figure 4.2 (page 64). An advantage of the high frequency of the ICP becomes apparent in Figure 4.3 where it is seen that the CSIRO – INSTAAR $\delta^{13}C$ difference begins at slightly below zero and jumps to a positive value in 1994. As

mentioned previously, such a large offset of $\delta^{13}C$ measurements can correspond to a large error if applied globally.

These serious implications caused by relatively small measurement differences illustrate the problems associated with global measurement programs and the effects of inter calibration issues. Another example is the measurements of $\delta^{13}C$ during the 1980s. Over this period a gradual change of ~-0.02 to ~-0.03 ‰/year was observed for $\delta^{13}C$ by both *Francey et al.*, [1995] and *Keeling et al.*, [1995]. Excursions about this trend were correlated to El Niño Southern Oscillation (ENSO) events by *Keeling et al.*, [1995] but such variations were not present in the record of *Francey et al.*, [1995]. These differences are most likely due to the different fitting routines that were applied to the data, but the contribution and uncertainty due to calibration issues is uncertain and cannot be eliminated.

The most likely reasons for the discrepancies observed between laboratories that take part in the inter calibration and inter comparison exercises are that, some laboratories use different ion collection algorithms and calibration scales for calculating $\delta^{13}C$ [*Allison et al,*. 1995]. This causes problems as it can sometimes prevent many of these laboratories, which can measure an individual sample with high precision, from comparing measurements of the same sample at a lower precision [*Allison et al.,* 1995]. Therefore to help eliminate such problems, all laboratories presenting data should be rigorously inter calibrated, use comparable ion correction algorithms and assumptions about the isotopic composition of the primary standards, and report $\delta^{13}C$ and $\delta^{18}O$ according to agreed protocols.

With continued inter calibration and inter comparison measurements, the onset of problems can be quickly detected with confidence, and possible contributing factors may be determined. Such unexpected discrepancies between data from different measurement laboratories are clearly a major obstacle for the successful merging of atmospheric data. International calibration strategies such as GLOBAL-HUBS aim to overcome the present limiting factors of international calibration of atmospheric CO_2 measurements. This proposal, based on four globally distributed "HUB" laboratories, for the main calibrations and distributions of reference gases and technology, allow for frequent low-cost access to an internationally monitored calibration scale for all linked laboratories. To successfully model the global carbon cycle, such strategies are required to achieve the target spatial, temporal, inter-laboratory and network precision.

New techniques, such as the GC-IRMS technique presented here, need to be well calibrated and well inter calibrated. This is necessary not only for the reasons above, but

also to compare with the traditional techniques currently in use and further evaluate the performance of the new GC-IRMS technique. This is essential to enable the "seamless merging" of data from the new technique with that from the old. Differences between the techniques (*e.g.* N_2O-free isotopic measurements by GC-IRMS, and measurements containing N_2O with a subsequent correction by dual-inlet) may cause problems. In addition to high precision inter calibration exercises, concurrent inter comparison programs are also essential to establish the operational performance of a new technique (with respect to the inter calibration) and the long term stability of monitoring programs and measurement scales.

4.3 Strategy for these inter calibration and inter comparison exercises

The inter calibration exercise presented here was performed with CSIRO Atmospheric Research, Australia. An inter comparison program was also established with this laboratory. There were two main reasons for choosing CSIRO as the primary laboratory. First, CSIRO uses the smallest samples of any of the laboratories that have long established CO_2 isotope records. This allows for multiple analyses of inter calibration tanks to obtain the highest quality inter calibration data possible. In addition, the small sample requirements enable the use of inter calibration gases stored at low-pressure. This should help to eliminate the problems associated with CO_2 and regulators that *Da Costa and Steele* [1997] have observed. Second, freight costs were minimised because CSIRO is geographically the closest laboratory and small samples could be used for the both inter calibration and inter comparison exercises.

The inter calibration exercise was performed by circulating between CSIRO and NIWA a tank filled with gas of precisely determined composition. During each circulation, both laboratories performed multiple determinations of the tank. Due to the small sample usage of the two laboratories, the inter calibration gas was stored at low-pressure in a high-volume tank. To avoid problems with the use of regulators and CO_2 that have been previously observed by *Da Costa et al.*, [1997] a regulator was not used with this low pressure tank. The initial results from the inter calibration exercise presented in this chapter are from one tank of inter calibration gas. Many factors did not enable more tanks to be used in the inter calibration exercise. Furthermore, because a full inter calibration would take longer than the period available during the research for this PhD on-going programs have been established to enable this in the future.

Inter comparison programs with two other laboratories were established to further examine comparisons between operational measurement programs. These laboratories were: NOAA CMDL and INSTAAR, Boulder, Colorado, USA; and Scripps Institution of Oceanography (SIO), La Jolla, San Diego, California, USA.

Unfortunately, a "round robin" inter calibration nor inter comparison (where calibration gas or air samples in the same tank or flask are circulated between all laboratories for measurement at each) was not possible because larger volumes are required for round robin programs and the associated freight costs are large. Therefore, the inter comparisons between NIWA and the three other laboratories were performed independently.

On-going inter calibration and inter comparison exercises have been established by the author of this thesis and will continue into the future. These programs, together with the preliminary results, are now presented.

4.4 NIWA – CSIRO inter calibration exercise

4.4.1 Inter calibration gas preparation

Inter calibration gas was prepared at CSIRO and stored in a 44 litre stainless steel tank (S44L-001). Stainless steel bellows valves (Nupro Company, Willoughby, OH, USA) are fitted as a dual valve arrangement incorporating a stainless steel dip tube of 3.175 mm o.d. that extends into the center of the cylinder to allow effective flushing. A PTFE sealant is used on the threaded openings. Before filling, the tank was prepared using a steam cleaning process. This involved bubbling clean air through distilled water and flowing at a rate of ~100 ml/min through the tank which was heated in an oven at 100 °C. Steam cleaning took place overnight after which exposure to a high vacuum of $< 10^{-5}$ Pa was maintained for at least 8 hours. S44L-001 was filled with inter calibration gas to a pressure of ~200 kPa above ambient. The inter calibration gas was sub-sampled from a high-pressure whole-air sample from the CSIRO air-archive, which was originally collected in 1990 at Cape Grim, Australia by a procedure that has been previously described [*Francey et al.*, 1996].

After filling, multiple analyses were performed at CSIRO to obtain high precision measurements of CO_2 mixing ratio and isotopic composition. The tank was then freighted to NIWA for analyses and subsequently returned to CSIRO for analyses. This cycle was then repeatedly performed for continuing measurements for the inter calibration exercise between NIWA and CSIRO.

4.4.2 Inter calibration gas analysis

CSIRO CO_2 mixing ratio measurements were performed using a Carle series 400 GC-FID (after conversion to CH_4 with a heated (400 °C) nickel catalyst). For the CO_2 mixing ratio measurement, routine analysis, including flushing, uses ~30 ml (STP) of gas (this gas usage also includes additional measurements of CO, CH_4 and H_2 mixing ratio which are simultaneously measured) [*Francey et al.*, 1996]. These additional measurements provide further data to enable the integrity and stability of the inter calibration gas to be monitored. This is because relative drifts between some species that are consistent with mass-dependant fractionation and other species that are not consistent with mass-dependant fractionation, can indicate leakage [*Langfields et al.*, 1996].

For isotopic analysis at CSIRO, sample extraction of ~10 μl from 30 ml of CO_2 is performed by a MT Box-C gas preparation system, before introduction to a MAT 252 IRMS (Finnigan MAT, Bremen) via a dual-inlet system. For $\delta^{13}C$ and $\delta^{18}O$ measurements routine analysis, including flushing, uses ~50 ml (STP) of gas [*Francey et al.*, 1996].

Inter calibration measurements were performed on average ~9 times per laboratory session at CSIRO, using a total amount of ~720 ml (STP) gas per laboratory session.

NIWA analysis was performed using the technique described in Chapter 3, but modified slightly so that up to 12 aliquots were used in each analysis. Multiple analyses were performed (as by CSIRO) to improve the measurement statistics. The average session at NIWA per laboratory circulation was ~1440 ml (STP). This higher usage (compared to CSIRO) is because the sample introduction is performed to the pressure at which the sample is filled (~200 kPa above ambient). This usage will therefore reduce to ~720 ml as the calibration pressure lowers to ambient pressure.

As detailed in section 3.2 (page 36), both CSIRO and NIWA isotopic measurements are relative to the CG92 scale [*Allison and Francey*, 1999]. NIWA mixing ratio measurements are relative to the WMO X93 scale (also previously described in section 3.2, page 36), while CSIRO mixing ratio measurements are linked both directly and indirectly to NOAA CMDL [*Francey et al.*, 1996].

4.4.3 Results

The multiple analyses performed by NIWA and CSIRO during the inter calibration exercise enable the differences between NIWA and CSIRO (in addition to the stability of the inter calibration gas) to be examined. The measurement results (summarised in Figure 4.4) span two time frames. The first is the run-to-run time frame and variations on this

time scale (~days) are mostly indicative of measurement uncertainties. The second is the session-to-session time frame and variations over this time scale (~months) can be partly attributed to observed reference or inter calibration gas drifts, in addition to measurement uncertainties.

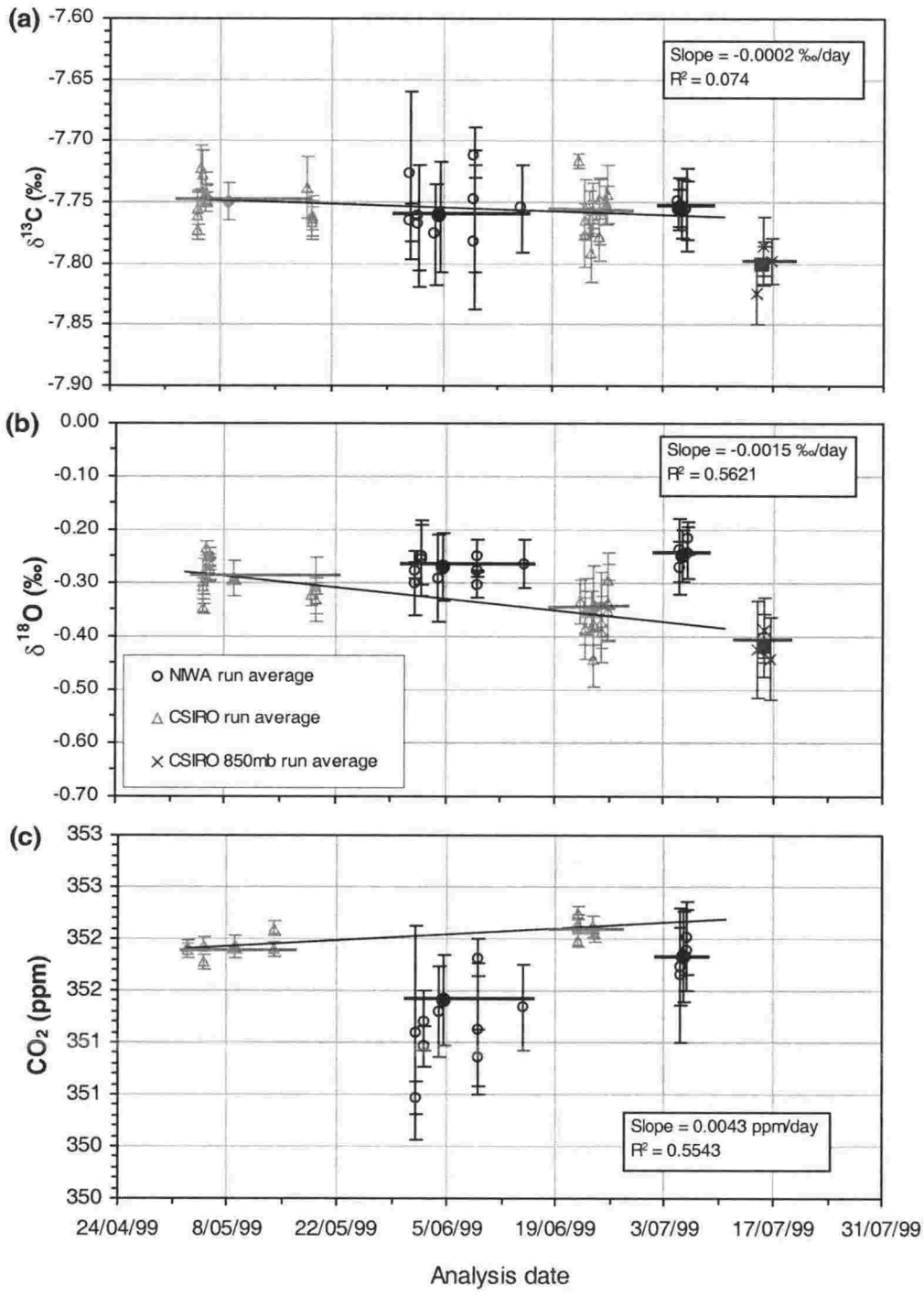

Figure 4.4 Inter calibration measurements of S44L-001 between NIWA and CSIRO for (a) $\delta^{13}C$ (b) $\delta^{18}O$ and (c) CO_2.

Run-to-run measurements for NIWA (hollow circles) and CSIRO (hollow triangles). Session-to-session measurements for NIWA (dark horizontal lines) and CSIRO (light grey horizontal lines) are shown. In addition, CSIRO measurements of S44L-001 at reduced pressure (850mb) are shown for run-to-run (crosses) and for the session average (dark grey horizontal line).

A valve failure in the automated extraction process during the second session of GC-IRMS measurements, lowered the pressure of the tank to ~85 kPa (850 mb). After return of S44L-001 to CSIRO at this sub-ambient pressure, isotopic measurements were performed but CO_2 mixing ratio measurements could not be made at CSIRO. Due to the deviation of the session average at reduced pressure from the observed drift rate for $\delta^{13}C$ (discussed below and shown in Figure 4.4 (a)) and the lack of CO_2 mixing ratio data at reduced pressure, these measurements at reduced pressure were not used in the calculation of the drift rates nor for the data that is summarised in Table 4.1. However, the reduced pressure may not be the sole cause for this difference because other unknown factors may be the cause and further measurements are therefore required to determine these.

From the first two CSIRO session measurements, the drift rates for: $\delta^{13}C$, $\delta^{18}O$, and CO_2 mixing ratio were observed to be (-0.0002 ± 0.0002) ‰/day, (-0.0015 ± 0.0006) ‰/day and (0.0043 ± 0.002) ppm/day respectively. For a high precision inter calibration exercise, the drift rates for $\delta^{18}O$ and CO_2 mixing ratio are of sufficient magnitude such that they must be accounted for. The $\delta^{13}C$ drift-rate has a small slope and this, combined with the uncertainty of the slope, mean that it is not useful to attempt to account for $\delta^{13}C$ drift. Additional statistical tests were not performed because other factors, which are discussed in the following text, have a much larger contribution to uncertainty, than the effect of a change in $\delta^{18}O$ and CO_2 mixing ratio slope as a result of the extrapolation of the observed CSIRO drift rates. To enable a direct comparison between CSIRO and NIWA inter calibration exercise measurements, CSIRO $\delta^{18}O$ and CO_2 mixing ratio measurements are extrapolated to the average date of the NIWA session. The inter calibration data are presented in Table 4.1.

Table 4.1 NIWA – CSIRO results for the inter calibration exercise from S44L-001.
To enable direct comparisons to be made, CSIRO session averages of $\delta^{18}O$ and CO_2 mixing ratio have been extrapolated to the average date at which analysis at NIWA was performed using the respective drift rates previously mentioned (the $\delta^{13}C$ drift rate was not significant). The values presented for the 'Average of Rounds 1 & 2' have also been extrapolated in this way. This explains why the value is not equal to the average of the values in the rows above Round 1 and Round 2. Errors (1 standard deviation) are calculated from the session averages and do not include uncertainty associated with the reference gas values. Δ is the difference between (NIWA-CSIRO) measurements. Mixing ratio measurements are to the X93 scale or the CSIRO scale as discussed in the following text.

		CSIRO	NIWA	Δ
Round 1	$\delta^{13}C$ (‰)	-7.75 ± 0.02	-7.76 ± 0.05	-0.01
	$\delta^{18}O$ (‰)	-0.33 ± 0.03	-0.27 ± 0.06	0.06
	CO_2 (ppm)	352.03 ± 0.10	351.41 ± 0.44 (X93)	-0.62
			351.86 ± 0.44 (CSIRO)	-0.17
Round 2	$\delta^{13}C$ (‰)	-7.76 ± 0.02	-7.76 ± 0.02	0.00
	$\delta^{18}O$ (‰)	-0.37 ± 0.04	-0.25 ± 0.05	0.12
	CO_2 (ppm)	352.16 ± 0.14	351.83 ±0.44 (X93)	-0.33
			352.28 ± 0.44 (CSIRO)	0.12
Average Of Rounds 1 & 2	$\delta^{13}C$ (‰)	-7.76 ± 0.02	-7.76 ± 0.04	0.00
	$\delta^{18}O$ (‰)	-0.38 ± 0.06	-0.26 ± 0.06	0.12
	CO_2 (ppm)	352.12 ± 0.14	351.4 ± 0.6 (X93)	-0.7
			351.9 ± 0.6 (CSIRO)	-0.2

Measurement uncertainties and the uncertainty associated with the reference gas values (section 3.2, page 36) must also be considered in the comparison of these preliminary inter calibration data. The initial two rounds of this inter calibration exercise between NIWA and CSIRO have shown inter laboratory agreement to less than or equal to 0.01 ‰ for $\delta^{13}C$. This inter-laboratory precision was higher than that obtained for any of the laboratories shown in Figure 4.2 for $\delta^{13}CO_2$ extracted from whole-air samples for dual-inlet analysis during the 1995 IAEA inter comparison exercise. The differences observed during dual-inlet analyses in the IAEA inter comparison (Figure 4.2) were up to ~0.1 ‰

and suggested that serious differences may exist between the extraction and analysis techniques for CO_2 from whole-air. Such problems were not observed for CO_2 extracted by GC-IRMS from these preliminary data at values close to the calibrated reference gases.

Reduced agreement for $\delta^{18}O$ was observed in the inter calibration exercise between NIWA and CSIRO compared to that for $\delta^{13}C$. In the first session, a difference of -0.060 ‰ was observed for $\delta^{18}O$ whereas in the second session a difference of -0.122 ‰ was observed. The significance of these differences are largely reduced when considering: the combined errors given in Table 4.1, and the errors associated with the assignment of the reference gas values (section 3.2, page 67).

Differences between the variations in NIWA and CSIRO measurements of the inter calibration gas were apparent (*i.e.* CSIRO observed a negative drift rate for $\delta^{13}C$ and $\delta^{18}O$, while NIWA observed a positive drift rate). These differences may be indicating that either a CSIRO or NIWA reference gas (or both) are drifting, however, due to the small amount of data obtained so far this is highly suggestive. These discrepancies will be further examined by the on-going inter calibration exercise established by the author of this work.

These measurements illustrate the inherent difficulties associated with inter calibration exercises because, although the averaged data may compare very well with small differences, the associated uncertainty greatly undermines the integrity of the inter calibration so that no significant conclusions can be drawn.

Differences between NIWA (X93) and CSIRO CO_2 mixing ratio measurements were -0.62 ppm in the first session, but decreased to -0.33 ppm in the second session. This inter laboratory precision GC-IRMS CO_2 mixing ratio measurements fall considerably short of the target inter laboratory precision of 0.05 ppm set by the WMO. If the CSIRO measurement* of the NIWA reference gas used (AIR1) is taken as the assigned value for the CO_2 mixing ratio of AIR1, rather than using the NIWA assigned value for AIR1, the differences reduce to -0.17 ppm for the first round and 0.12 ppm for the second round. Although increased agreement is achieved by using the CSIRO values for the reference gas (as expected) the inter laboratory precision for CO_2 mixing ratio still falls short of the WMO target inter laboratory precision of 0.05 ppm. Because frequent access to high precision measurements can be made at NIWA directly from the reference gas cylinder to the X93 scale, CSIRO mixing ratio values for the reference gas were not used further.

---

* AIR1 = 356.90 ± 0.07 ppm

During the first session, measurement precision was consistently lower than expected from the GC-IRMS technique. This was highlighted by the inter calibration exercise and the low precision was attributed to the following reasons:

1. Laboratory temperature variation was poor (~2 °C/hour). During the period of analysis a Finnigan MAT Kiel carbonate device was running on stand-by in the background. This had not been done before and the extra pumps and oven associated with the Kiel device, run hotter than the surrounding laboratory atmosphere and decrease the temperature stability in the region close to the SOV and COV. This is a bad position for temperature variation for GC-IRMS work and reproducibility is significantly affected (as discussed in section 3.8.3.2, page 51). Lower precision therefore results due to variations in the signal to noise ratio caused by the temperature fluctuations.
2. IRMS source pressure was running higher than normal. The source pressure was up to between 6.2 to 6.5 $\times 10^{-4}$ Pa. Pressures above 6.0 $\times 10^{-4}$ Pa are not recommended for the MAT 252 (*Brand*, personal communication, 1997). Higher source pressures have a greater fraction of contaminants in the ion source (*e.g.* H_2O) that contribute to loss of accuracy and precision (as discussed in section 3.8.2.1, page 47).
3. The IRMS source was in need of a bake out. This had not been done after last shutdown (~4 months before these measurements) in which contaminants were introduced into the IRMS. Therefore a larger fraction of these contaminants buried in the metallic surfaces of the IRMS are able to randomly desorb and interfere with the gas of interest during analysis (this may have contributed to the higher source pressure).
4. Sensitivity was down ~1500 molecules/ion versus 1100 molecules/ion (tuning unchanged). This affects precision (previously described in section 3.8.3.1, page 50).

Performing the inter calibration exercise enabled these problems to be determined and minimised, if not fixed, before the second round, which showed improved performance. In addition, these problems were rectified faster during the inter calibration exercise than would have otherwise been detected by routine measurements. This is because multiple analyses from the same tank better indicate problems in the performance of the technique, than do routine analysis of different flasks.

Despite the lowered performance in the first session measurements at NIWA, the inter calibration exercise between NIWA and CSIRO was successful and has demonstrated some important points for future work. These points are discussed in section 4.6.

As the gas preparation and analysis methods are different for routine samples compared to the inter calibration gas procedures, further operational ICPs are required to determine inter-laboratory precision from real atmospheric monitoring programs. These are presented in the following section.

4.5 Inter comparison Programs

The ICP commenced in this work between laboratories with long established atmospheric CO_2 measuring programs (CSIRO, NOAA CMDL, INSTAAR and SIO) is the first to unite all laboratories via an external laboratory with high frequency measurements (greater than 2 measurements per month) in an on going programme (previous "round-robin" WMO inter calibrations have been performed at low frequency, ~1 measurement per year). As discrepancies exist between CSIRO, NOAA CMDL, INSTAAR and SIO measurements that are outside the WMO and IAEA target precisions (*e.g.* Figure 4.1, 4.2 and 4.3 in section 4.2 of this chapter, from [*Francey and Rayner*, 1998]), inter comparisons with all three are of a great importance to obtaining inter-laboratory precision nearer (or within) these recommended target precisions.

The NOAA CMDL network utilises samples collected from the largest network of global atmospheric trace gas monitoring sites in the world and are already part of a well established ICP with CSIRO (*e.g.* Figure 4.3 [*Francey and Rayner*, 1998]) and Atmospheric Environment Service (AES), Canada [*Gaudry et al.*, 1996]). The ICP between CSIRO, NOAA CMDL and INSTAAR was established in 1991 [*Steele et al*, 1998] and forms the longest standing inter comparison of the mixing ratio and isotopic composition of atmospheric CO_2. Such established programs provide valuable records that the new ICPs introduced here can be compared to.

The collaborating laboratories chosen for these ICPs all maintain independent air sampling monitoring programs. Sharing air samples collected for these programs and performing analysis at the collaborating laboratories, allows the inter comparison measurements to be obtained.

4.5.1 Air Sample collection

For inter comparisons with CSIRO, air samples were both: collected at Baring Head, background air pollution station, New Zealand, and routed through the NIWA laboratory for analysis before freight to CSIRO; and collected at Cape Grim background air pollution

station, Tasmania, Australia and routed through the CSIRO laboratory for analysis before shipment to NIWA.

These CSIRO air samples are filled to and stored at a pressure of ~80 kPa in 0.5 litre glass flasks that are fitted with high vacuum valves and inert Teflon® PFA o-rings, (Glass Expansion Pty, Ltd. Victoria, Australia). The sampling procedure used at Baring Head has been previously described in section 3.3 (page 38). After analysis of these samples at NIWA and CSIRO the flasks are then filled at Cape Grim, Tasmania, Australia (40.7 °S, 144.7 °E). Most inter comparison samples were collected from the sampling mast (12.7 mm o.d. stainless steel) at an elevation of 104 m above sea level and 10 m above the station roof-deck. Furthermore, most of these samples were collected under 'baseline' conditions with winds coming from the pre-dominant south-west direction such that the air masses sampled between 190° and 280° were representative of clean southern ocean air. The Cape Grim site is further discussed in section 5.2.2 (page 108). Sample collection details are given further in *Francey et al.*, [1996]. To minimise inconsistencies NIWA and CSIRO sample collection procedures were as similar as possible (*e.g.* both filling procedures use $Mg(ClO_4)_2$ for chemical drying of the samples which is replaced after a measured weight gain of ~6 % due to absorption of H_2O).

The NOAA CMDL and INSTAAR ICP results presented here utilised a sub-set of samples collected in NIWA's Pacific Ocean voyages. These were filled to and stored at a pressure of ~150 kPa in 2 litre glass flasks that are made with ultra high vacuum valves and inert PTFE o-rings (Glass Expansion Pty, Ltd., Victoria, Australia). A reinforced Viton diaphragm pump (Thomas Industries Inc, Power Air Division, Sheboygan, WI, USA), powered by a 12 Volt battery filled the samples to the required pressure. Airlines were constructed from 6.35 mm o.d flexible Dekabon 1300 tubing (Furon Dekoron, Ohio, USA). Samples collected in the September 1998 voyage were dried by the same procedure as previously described for the NIWA – CSIRO ICP. Samples collected in March 1998 were not dried. Further description of these samples is presented in section 5.3.2.1 (page 125).

Due to laboratory commitments and freight costs, high frequency inter comparisons between NOAA CMDL, INSTAAR and NIWA were not initially possible. However continuing efforts established an ICP between these laboratories in mid-1999. For this ICP a similar procedure to that of the NIWA – CSIRO was established (*i.e.* samples were both: collected at Baring Head and routed through the NIWA laboratory before shipment to NOAA CMDL and INSTAAR; and collected at Niwot Ridge, Boulder, Colorado, USA and routed through the NOAA CMDL and INSTAAR laboratories before freight to

NIWA). The samples collected at Niwot Ridge (40.05 °N, 105.58 °W, 30 km west of Boulder, at an altitude of 3475 m) were filled to a pressure of ~41 kPa in 2.5 litre glass flasks [*Trolier et al.*, 1996]. The establishment of this on-going ICP will continue into the future to enable the long-term monitoring of the NOAA CMDL, INSTAAR and NIWA ICP.

Since 1973, samples have been collected for mixing ratio analysis at Baring Head as part of SIOs global monitoring network. Isotopic measurements from these air samples collected at Baring Head began in 1986. Sample pairs are collected by opening a greased stopcock on an evacuated 5 litre glass flask at the sampling site. No drying is performed during the collection process. The NIWA – SIO ICP was introduced by collecting an additional sample to the usual pair so that a group of three samples were collected. This extra flask was routed through the NIWA laboratory for analysis before shipment to SIO (the other two remain unanalysed by NIWA and are sent to SIO for analysis according to the long-established protocol).

4.5.2 Analysis techniques

NIWA analysis of inter comparison samples was performed with the technique described in Chapter 3. Routine analyses of only three aliquots of each sample were analysed in one measurement to obtain both CO_2 mixing ratio and isotopic composition. Sample usage from this analysis was ~90 ml for CSIRO samples and ~45 ml for NOAA CMDL and SIO samples. The total pressure change in each flask as a result of analysis was therefore relatively small.

CSIRO inter comparison analyses were performed as described in section 4.4.2 (page 69) except that routine analysis was performed, rather than the multiple analyses that were performed for inter calibrations previously described. Such routine analysis uses a total of ~80 ml for both mixing ratio and isotope measurements [*Francey et al.*, 1996].

For the NOAA CMDL and INSTAAR inter comparison, CO_2 mixing ratio measurements at NOAA CMDL are made by a Siemans Ultramat 3 NDIR. NOAA CMDL CO_2 mixing ratio analyses are reported relative to the X85 mole fraction scale from the WMO central CO_2 calibration laboratory and measurement precision is ~0.05 ppm [*Conway et al.*, 1994]. Isotope measurements are performed at INSTAAR using a VG-Optima IRMS. An automated extraction system is based on the methods proven for the previous SIRA Series II IRMS in which ~600 – ~800 ml of gas is extracted, yielding ~200 µl CO_2 for isotopic analysis [*Tans et al.*, 1998; *Troiler et al.*, 1996]. The overall

reproducibility for the Optima IRMS system (1 standard deviation for replicate analyses, in 1997) is 0.012 ‰ for $\delta^{13}C$ and 0.031 ‰ for $\delta^{18}O$ [*Tans et al.*, 1998].

For the SIO inter comparison, CO_2 mixing ratio measurements were performed by an Applied Physics Corporation NDIR using ~1 litre of gas. CO_2 mixing ratio values presented here were relative to their provisional X97 scale. Isotopic measurements were performed using a VG Prisim 2 IRMS using ~4 litres of gas. No ^{18}O corrections were made for the wet samples as it is assumed that the flask volume is large enough (5 litres) that ^{18}O exchange does not readily occur in the flask unless the sample is wet enough to cause condensation inside the flask (this is sometimes the case at very humid stations *e.g.* Samoa).

4.5.3 Results

4.5.3.1 NIWA – CSIRO

As was illustrated in the NIWA – CSIRO inter calibration, the measurement uncertainties of the two techniques must be considered when examining the NIWA – CSIRO inter comparison. The average uncertainties (standard deviations) for the GC-IRMS, dual-inlet IRMS and GC-FID measurements, in addition to the combined uncertainty of both techniques are shown in Table 4.2.

Table 4.2 Measurement uncertainties of NIWA GC-IRMS and CSIRO dual-inlet IRMS and GC-FID techniques.

Combined 1 σ and 2 σ are the sum of the NIWA and CSIRO uncertainties for 1 standard deviation and 2 standard deviations respectively.

	NIWA 1σ[a]	CSIRO 1σ[b]	Combined 1σ	Combined 2σ
$\delta^{13}C$ (‰)	0.02	0.01	0.03	0.06
$\delta^{18}O$ (‰)	0.04	0.02	0.06	0.12
CO_2 (ppm)	0.4	0.07	0.47	0.94

[a]From section 3.9 (page 52).

[b]From [*Francey et al.*, 1996].

The combined errors demonstrate how the relatively high precisions achieved by both laboratories (for $\delta^{13}C$ and $\delta^{18}O$) are reduced when comparing measurements between the two laboratories of the same flask. Of special note is the fact that GC-IRMS CO_2 mixing

ratio measurement uncertainty is larger than that for CSIRO. In addition to these measurement uncertainties, further uncertainty is added by the link to the calibration scales used by both NIWA and CSIRO (*e.g.* section 3.2, page 36).

The measured differences for the individual inter comparison flasks measured by NIWA and CSIRO are summarised in Figure 4.5. Some data have been rejected and are not shown. This applies for the following cases: 1) 2-sigma rejection of 'bad' pairs* 2) CO_2 mixing ratio measurements before October 1998†.

---

* CSIRO samples are rejected if the difference between the flask pair is larger than two times the estimated analytical precision. Approximately 10 % of samples collected at both Baring Head and Cape Grim were rejected for this reason.

† Before October 1998, the peak centering method relied on background m/e 44 levels. These levels were low (mV) and centering was neither accurate nor representative of typical detected sample levels. After October 1998, pure CO_2 from the IRMS bellows was used to perform a peak center at around 1.3 V (4.3 nA) m/e 44 before each analysis as previously described in section 3.6 (page 42). This enabled accurate analyses of CO_2 mixing ratios.

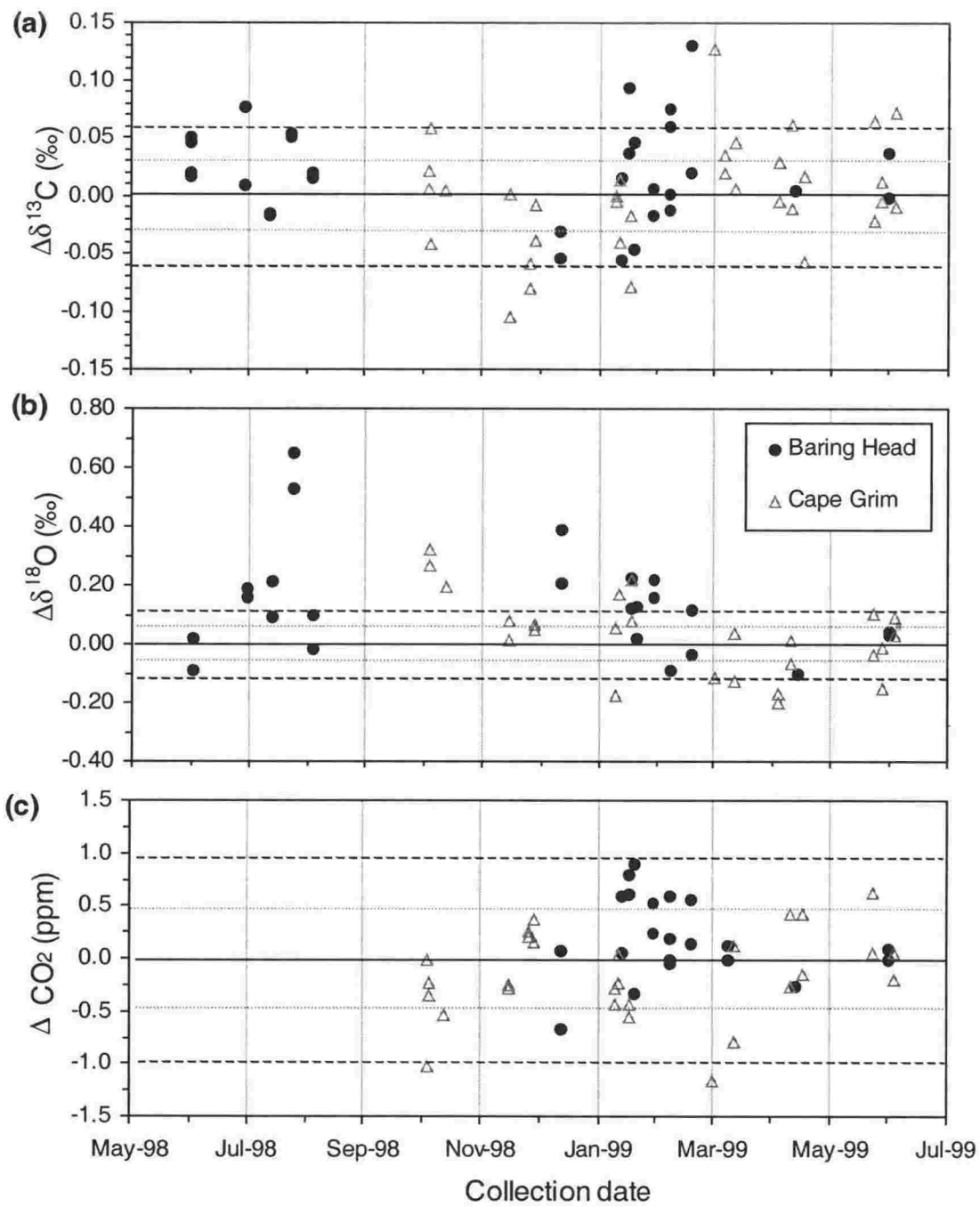

Figure 4.5 NIWA – CSIRO ICP differences for (a) $\delta^{13}C$ (b) $\delta^{18}O$ and (c) CO_2 mixing ratio. $\Delta\delta^{13}C$, $\Delta\delta^{18}O$ and ΔCO_2 are the differences between (NIWA-CSIRO) for each species. One standard deviation (light dashed lines) and two standard deviations (heavy dashed lines) indicate the combined technique precisions of NIWA GC-IRMS and CSIRO dual-inlet IRMS or GC-FID. Samples have been divided into those collected at Baring Head (solid circles) or Cape Grim (hollow triangles).

Considering the combined measurement uncertainties of the two techniques shown in Table 4.2, it is apparent that much of the variation observed may therefore be due to this combined uncertainty. The number and percentage of the total inter comparison flasks that lie within these combined uncertainties of the laboratories shown in Figure 4.5 are summarised in Table 4.3.

Table 4.3 The total number (n) and percentage of inter comparison samples that lie within 1σ and 2σ combined measurement uncertainties for the NIWA – CSIRO ICP.
The column headed "Both" is the total of Baring Head and Cape Grim.

		Baring Head	Cape Grim	Both
$\delta^{13}C$	1 σ	48 %	55 %	52 %
	2 σ	87 %	82 %	85 %
	n	31	34	65
$\delta^{18}O$	1 σ	25 %	32 %	29 %
	2 σ	50 %	56 %	53 %
	n	24	25	49
CO_2	1 σ	62 %	79 %	71 %
	2 σ	100 %	93 %	96 %
	n	21	28	49

Over 80 % of all measured NIWA – CSIRO flask inter comparisons were observed to lie within combined 2-sigma uncertainties of both techniques for $\delta^{13}C$ and CO_2 mixing ratio. However, the agreement was not as high for $\delta^{18}O$ and < 60 % of all inter comparison flask measurements were within combined 2-sigma uncertainties.

Samples collected at Cape Grim were observed to have a slightly higher percentage of ICP flasks within both 1-sigma and 2-sigma standard deviations for all species compared to those collected at Baring Head (with the exception of 2-sigma for $\delta^{13}C$ at Baring Head). Visual inspection of the ICP data shown in Figure 4.5 indicates that there appears to be no systematic offset between NIWA and CSIRO measurements of $\delta^{13}C$ as the scatter about zero is approximately uniform. Possible offsets for $\delta^{18}O$ and CO_2 may exist. These are further examined by calculating the mean and standard deviation of all ICP data presented in Figure 4.5 (Table 4.4).

Table 4.4 Average differences between (NIWA-CSIRO) ICP measurements.
Uncertainties shown are 1 σ standard deviations.
The row headed "Both" is the average of Baring Head and Cape Grim.

	$\Delta\ \delta^{13}C$ (‰)	$\Delta\ \delta^{18}O$ (‰)	$\Delta\ CO_2$ (ppm)
Both	0.01 ± 0.05	0.08 ± 0.16	0.0 ± 0.3
Baring Head	0.02 ± 0.04	0.12 ± 0.18	0.1 ± 0.2
Cape Grim	0.00 ± 0.05	0.03 ± 0.14	-0.2 ± 0.4

As previously discussed, the measurement uncertainties must be taken into consideration when examining the inter comparison data. The observed average difference for $\delta^{13}C$ at Baring Head and Cape Grim were small, but the uncertainties for $\delta^{18}O$ and CO_2 were larger. Compared to the inter calibration exercise with CSIRO, the inter comparison achieves similar agreement. These inter comparison data show excellent agreement compared to previous ICPs (*e.g.* NOAA CMDL, INSTAAR and CSIRO ICP has experienced $\delta^{13}C$ and CO_2 mixing ratio differences of ~ 0.04 ‰ and (~0.17 ± 0.17) ppm respectively [*Francey and Rayner*, 1998]). However, because of the relatively large scatter in the NIWA – CSIRO ICP data, the uncertainty associated with the average differences is greater than that for the CSIRO – NOAA CMDL ICP.

A larger average difference and variation was observed between NIWA and CSIRO for $\delta^{18}O$ than for $\delta^{13}C$ (Table 4.4). These differences may possibly be due to storage effects, which are examined in Figure 4.6.

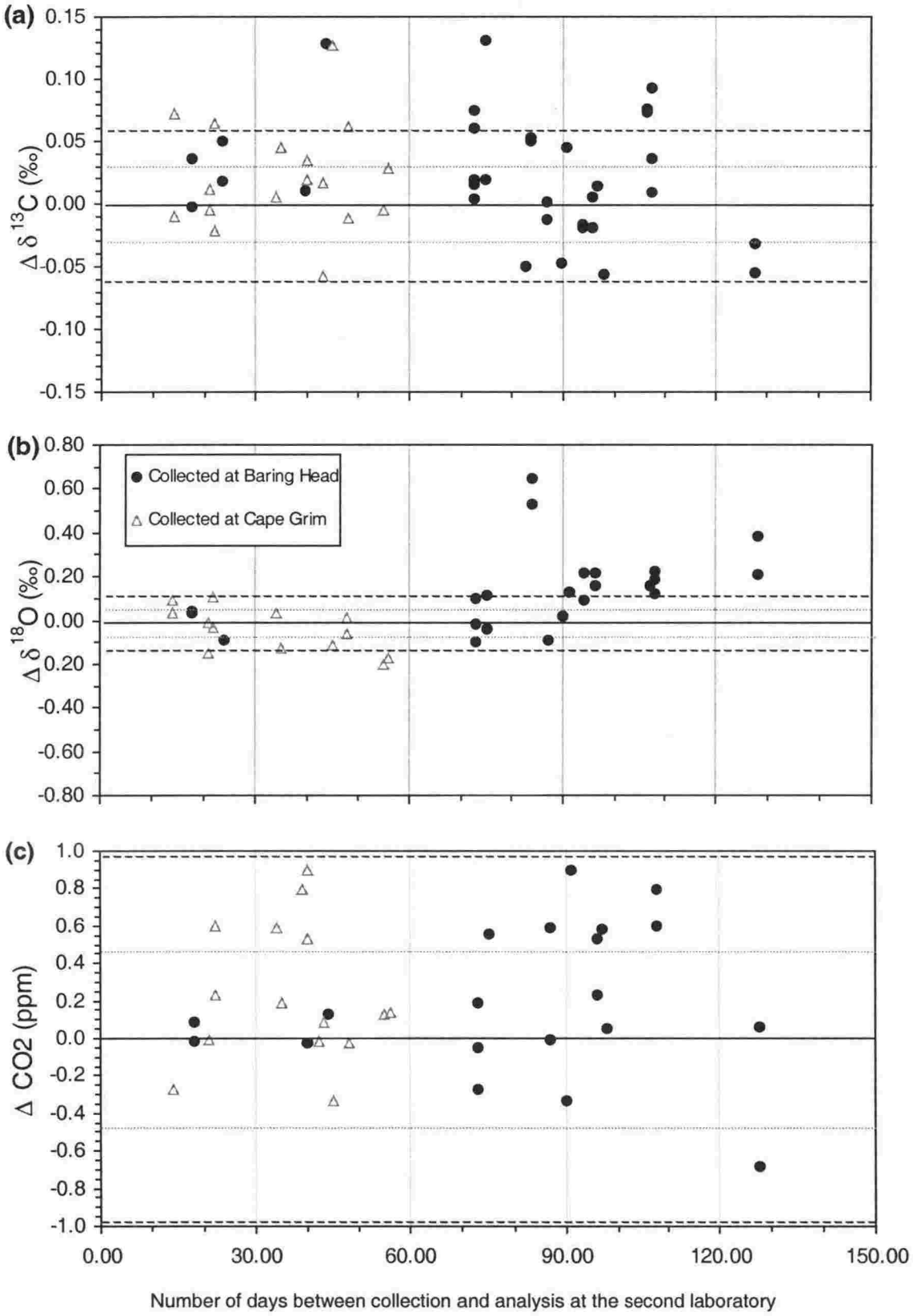

Figure 4.6 NIWA – CSIRO ICP differences as a function of the number of days between sample collection and analysis at the second laboratory.

Samples are separated into those collected at Baring Head (solid circles) and those collected at Cape Grim (hollow triangles). One standard deviation (light dashed lines) and two standard deviations (heavy dashed lines) indicate the combined technique precisions of NIWA and CSIRO.

$\delta^{13}C$ and CO_2 mixing ratio differences appeared to be non related to storage time for samples collected at Cape Grim and Baring Head. Only for $\delta^{18}O$ did the differences appear to be related to storage time (this was observed for samples collected at both Cape Grim and Baring Head). The differences for Cape Grim samples are less than those for the majority of flasks collected at Baring Head and the lack of measurements for storage periods less than ~60 days for samples collected at Baring Head is a problem. Likewise, for samples collected at Cape Grim, the lack of measurements that were performed more than 60 days after collection is also a problem. These different storage times are due to the fact that laboratories typically have different turn-around times for analysis.

Possible reasons for the observed differences may be due to inconsistencies between the sampling procedures at the two sites (*e.g.* less effective drying at one site and/or contamination of the sample with H_2O, would mean a higher chance for ^{18}O exchange between H_2O and CO_2 and resultant $\delta^{18}O$ fractionation [*Gemery et al,.* 1996]). Should this be the case, the observed negative drift rate for $\delta^{18}O$ for samples collected at Cape Grim is in the expected direction. Other possible explanations for some of the differences between the inter comparison samples collected at Baring Head and Cape Grim are that known inconsistencies exist in the ICP flasks. These differences may possibly be attributed to the fact that in addition to the 0.5 litre flasks, some 2 litre flasks were also used in the inter comparison. These NIWA 2 litre flasks have a higher flask surface area to volume ratio of ~0.04 m^2/l compared to ~0.07 m^2/l for the CSIRO 0.5 litre flasks. In addition, NIWA 2 litre flasks are collected to ~100 kPa and are fitted with Teflon® PTFE o-rings while the CSIRO 0.5 litre flasks are collected to ~80 kPa and are fitted with Teflon® PFA o-rings. These differences are most likely to be to small to be significant, but cannot be ruled out. To further examine these findings, additional storage tests between NIWA and CSIRO are required.

In addition to the inter comparison samples collected at Baring Head or Cape Grim which have been presented, other inter comparison measurements between NIWA and CSIRO were obtained. These were typically from NIWA reference gases and CSIRO primary standards. Some of these measurements were performed using reference and sample gas compositions that were much different (in terms of atmospheric composition). Such measurements showed reduced agreement (Table 4.5).

Table 4.5 Comparison of measurements for CSIRO Primary standard 941037.

Δ (NIWA ref gas – CSIRO) is equal to the difference between the composition of the NIWA ref gas used for the GC-IRMS measurements (AIR1 for the first case and AIR2 for the 2nd) and the CSIRO measured value for the Primary standard. Δ is the measured difference between the NIWA measured value and the expected value from the CSIRO measurements of the primary standard.

	Δ (NIWA ref gas – CSIRO)	Δ
$\delta^{13}C$ (‰)	0.276	-0.01
$\delta^{18}O$ (‰)	1.96	0.20
CO_2 (ppm)	-1.29	-0.29
$\delta^{13}C$ (‰)	-0.302	0.01
$\delta^{18}O$ (‰)	-0.609	0.27
CO_2 (ppm)	46.46	-2.70

The agreement for CO_2 mixing ratio was reduced when using the second NIWA reference gas with comparatively different composition to the CSIRO primary standard. A significant increase to the CO_2 mixing ratio difference was present when this second reference gas was used for the NIWA analyses. This gas that had a mixing ratio higher by almost 50 ppm decreased the agreement, and this may be a result of GC-IRMS non-linearity, which is further examined in Figure 4.7.

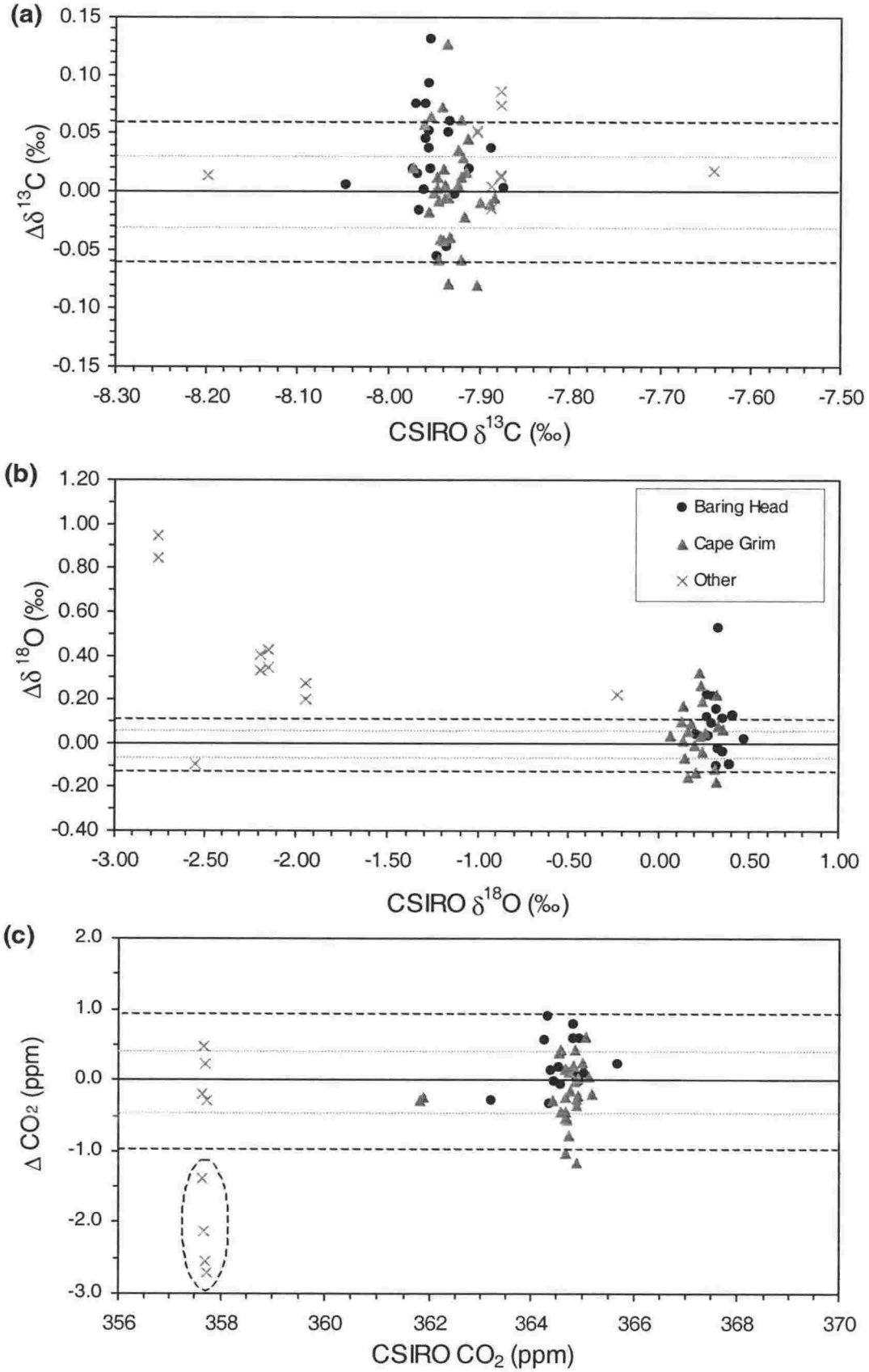

Figure 4.7 Differences between (NIWA-CSIRO) ICP flasks as a function of CSIRO measured values for (a) $\delta^{13}C$ (b) $\delta^{18}O$ and (c) CO_2 mixing ratio.

The circled data in (c) are discussed in the text.

GC-IRMS non-linearity for $\delta^{13}C$ was observed to be non-significant over the measured range from ~-8.2 ‰ to ~-7.6 ‰ because the range is small and the scatter is large. For the inter comparison flasks collected at Baring Head and Cape Grim, non-linearity for $\delta^{18}O$ and CO_2 was also not significant over the measured range for the same reason. However, for other $\delta^{18}O$ inter comparisons with the CSIRO primary standard measured at NIWA using AIR1 as the reference gas, GC-IRMS non-linearity was potentially observed. When reference – sample differences were up to ~2.5 ‰ for $\delta^{18}O$, the measured $\delta^{18}O$ difference increased up to ~1‰. Likewise when measuring the CSIRO primary standard relative to AIR2 at NIWA (reference – sample differences up to 50 ppm) the observed difference increased to between ~-1.5 and ~-2.8 ppm (circled in Figure 4.7(c)). When this gas was measured relative to AIR1, the agreement improved and the non-linearity was not significant.

Such non-linearities, highlight the need to use reference gases that have $\delta^{13}C$ and $\delta^{18}O$ values close to the current atmospheric composition. Furthermore, the importance of maintaining a minimised IRMS non-linearity is also highlighted.

A summary of this ICP and possibilities for future work are discussed in the summary and discussion at the end of this chapter.

4.5.3.2 NIWA – NOAA CMDL and INSTAAR

NIWA – NOAA CMDL and INSTAAR inter comparison data is presented in Figure 4.8. Some data have been rejected according to the criteria as previously described for the NIWA – CSIRO ICP (section 4.5.3.1, page 78), and are not shown in the figure. In addition, $\delta^{18}O$ values of the initial 4 flasks were collected wet during the March 1998 Pacific Ocean voyage and for $\delta^{18}O$, these data have also been rejected.

As was done for the NIWA – CSIRO ICP, combined 2-sigma measurement uncertainties are shown in the ICP differences plot. For the NIWA – NOAA CMDL and INSTAAR ICP combined 2-sigma measurement uncertainties shown for $\delta^{13}C$, $\delta^{18}O$ and CO_2 mixing ratio are 0.06 ‰, 0.12 ‰ and 0.9 ppm respectively.

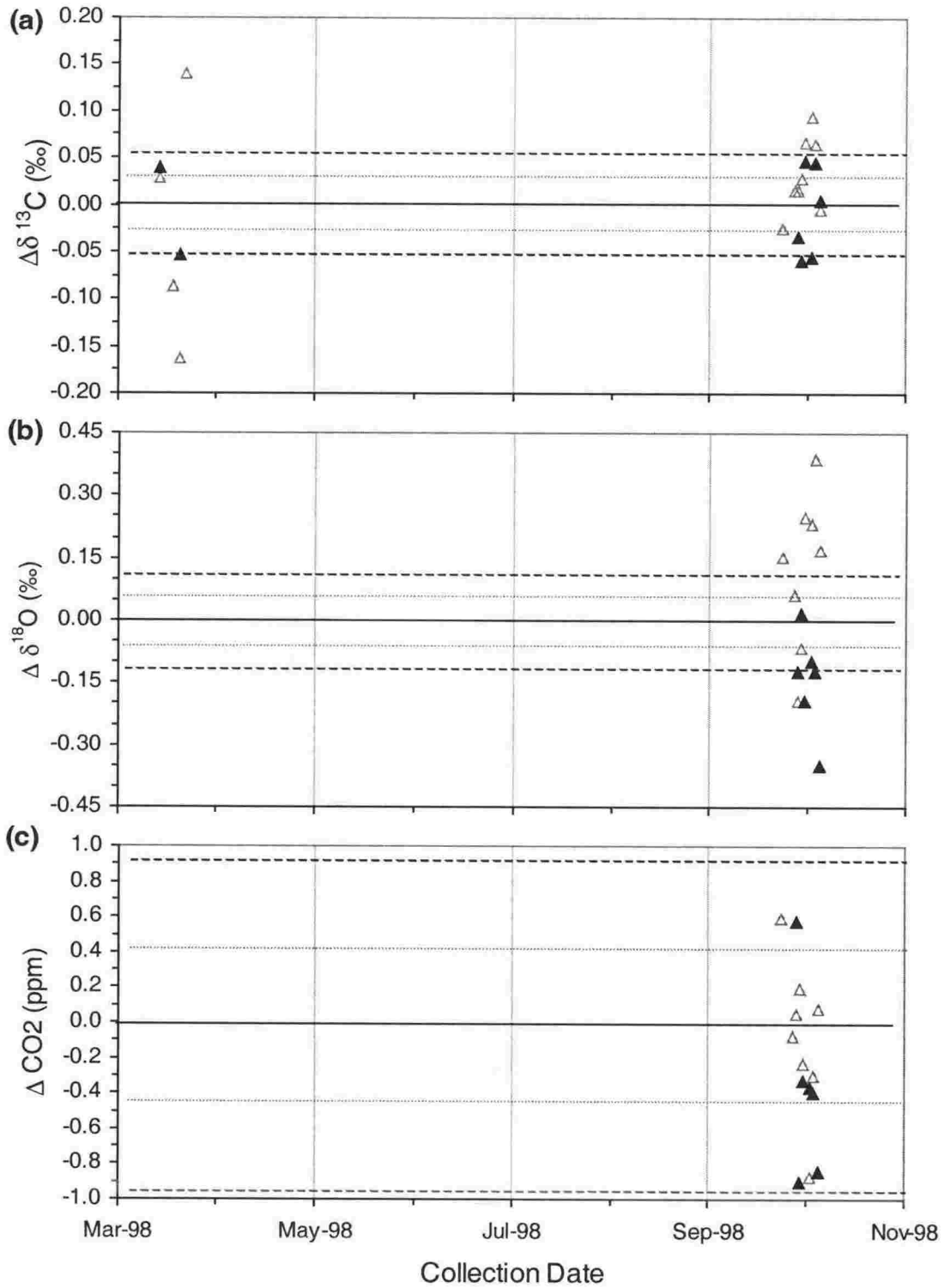

Figure 4.8 ICP differences between (a) NIWA-INSTAAR for $\delta^{13}C$ (b) NIWA-INSTAAR for $\delta^{18}O$ and (c) NIWA-NOAA CMDL for CO_2 mixing ratio.

Hollow triangles – difference from initial NIWA measurement. Solid triangles – difference from NIWA re-run measurement for samples which had enough pressure after INSTAAR and NOAA CMDL analysis. One standard deviation (light dashed lines) and two standard deviations (heavy dashed lines) indicate the combined technique precisions of NIWA GC-IRMS, NOAA CMDL NDIR and INSTAAR dual-inlet.

Considering the previously mentioned combined measurement uncertainties of the NIWA GC-IRMS, NOAA CMDL NDIR and INSTAAR dual-inlet IRMS techniques, it is apparent that much of the variation observed may therefore be due to the combined uncertainties. Although far less data have been obtained for this ICP, compared to that for the NIWA – CSIRO ICP, visual inspection of Figure 4.8 indicates that the level of agreement is similar to that of the NIWA – CSIRO ICP previously presented in Figure 4.5. (page 80).

The number and percentage of the total inter comparison flasks that lie within the combined uncertainties of the laboratories shown in Figure 4.8 are summarised in Table 4.6.

Table 4.6 The total number (n) and percentage of inter comparison samples which lie within 1σ and 2σ combined measurement uncertainties for the NIWA – NOAA CMDL and INSTAAR ICP.
Columns are headed: "initial" NIWA measurements, NIWA "Re-run" measurements after INSTAAR and NOAA CMDL analysis, and the total of "Both" initial and re-run measurements.

		Initial	**Re-run**	**Both**
$\delta^{13}C$	1 σ	50 %	13 %	35 %
	2 σ	50 %	63 %	55 %
	n	12	8	20
$\delta^{18}O$	1 σ	13 %	17 %	14 %
	2 σ	25 %	33%	29 %
	n	8	6	14
CO_2	1 σ	75 %	50 %	64 %
	2 σ	100 %	100 %	100 %
	n	8	6	14

100 % of all measured NIWA – NOAA CMDL inter comparisons were observed to lie within combined 2-sigma uncertainties of both techniques for CO_2 mixing ratio. The agreement for $\delta^{13}C$ was lower with over 50 % of inter comparison flask measurements within combined 2-sigma uncertainties. Agreement for $\delta^{18}O$ was further reduced with only ~30 % of inter comparison flask measurements within combined 2-sigma uncertainties.

Visual inspection of the ICP data shown in Figure 4.8 indicates no systematic offset between NOAA CMDL, INSTAAR and NIWA measurements because the scatter about

zero is approximately uniform. Further examinations of these differences are possible by calculating the mean differences and standard deviation of all data obtained (Table 4.7).

Table 4.7 Average differences between (NIWA-INSTAAR) measurements for $\delta^{13}C$ and $\delta^{18}O$ and (NIWA-NOAA CMDL) measurements for CO_2 mixing ratio from inter comparison flasks and 1 σ standard deviations.
The row headed Both is the average of the initial and re-run measurements.

	$\Delta\ \delta^{13}C$ (‰)	$\Delta\ \delta^{18}O$ (‰)	$\Delta\ CO_2$ (ppm)
Both	0.01 ± 0.07	0.01 ± 0.21	0.0 ± 0.6
Initial	0.01 ± 0.08	0.12 ± 0.18	0.2 ± 0.3
Re-run	-0.01 ± 0.05	-0.15 ± 0.12	-0.4 ± 0.8

These inter comparison data must be viewed with caution because the combined measurement uncertainties and the small number of inter comparison measurements must be considered. The observed average differences for $\delta^{13}C$ and CO_2 mixing ratio were small and within combined measurement uncertainties. Differences for $\delta^{18}O$ appeared to be large and a negative shift between the initial and re-run averages suggests possible storage problems. This is because the decrease in average $\delta^{18}O$ values may possibly be due to ^{18}O exchange between CO_2 and H_2O in the flasks [*Gemery et al.,* 1996] that may have occurred over the storage period between the NIWA re-run and NOAA CMDL, INSTAAR analysis (some flasks were stored for up to ~150 days before re-analysis at NIWA). However, due to the small amount of data obtained so far, storage effects for these flasks are not investigated further. One other possibility for some of the observed differences between the initial and re-run measurements are possible problems with extraction by GC-IRMS at reduced pressure after NOAA CMDL and INSTAAR analysis and further work would be required to investigate this possibility.

However, as the ICP results presented between NOAA CMDL, INSTAAR and NIWA are most likely the last to be performed using NIWAs 2 litre glass flasks, these findings may therefore not be applicable, or significant to the on-going ICP that has been established between these laboratories during this work. This is because the NOAA CMDL 2.5 litre flasks, which will be used in all further work, may not be prone to such problems.

The findings of this ICP and requirements for further work are discussed in the conclusions at the end of this chapter.

4.5.3.3 NIWA - SIO

NIWA –SIO inter comparison data are presented in Figure 4.9. Some data have been rejected according to the criteria as previously described for the NIWA – CSIRO ICP (section 3.4.3.1, page 78), and are not shown in the plot. The combined 2-sigma measurement uncertainties for the NIWA – SIO ICP shown on the following plot are 0.06 ‰, 0.12 ‰, and 0.9 ppm for $\delta^{13}C$, $\delta^{18}O$ and CO_2 mixing ratio respectively.

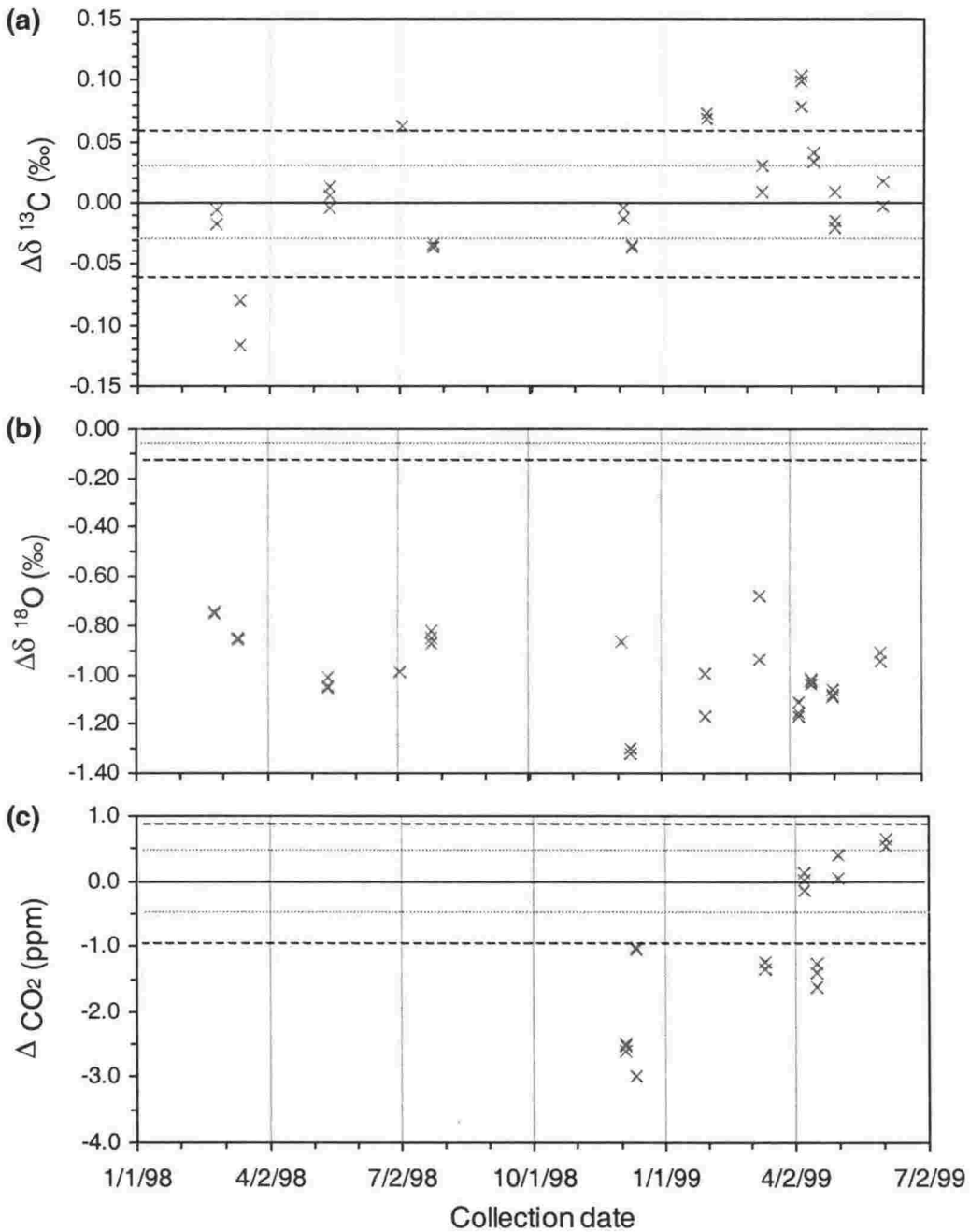

Figure 4.9 NIWA – SIO ICP differences for (a) $\delta^{13}C$ (b) $\delta^{18}O$ and CO_2 mixing ratio.
$\Delta\delta^{13}C$, $\Delta\delta^{18}O$ and ΔCO_2 are the differences between NIWA and SIO as measured by (NIWA- SIO) for each species. One standard deviation (light dashed lines) and two standard deviations (heavy dashed lines) indicate the combined technique precisions of NIWA GC-IRMS and SIO dual-inlet or NDIR.

Considering the previously mentioned combined measurement uncertainties of the NIWA and SIO techniques, it is apparent that much of the variation observed may therefore be due to this combined uncertainty for $\delta^{13}C$. However, for $\delta^{18}O$ and CO_2 mixing ratio there appears to be larger differences and possible offsets.

The number and percentage of the total inter comparison flasks that lie within the combined uncertainties shown in Figure 4.9 are summarised in Table 4.8.

Table 4.8 The total number (n) and percentage of inter comparison samples that lie within 1σ and 2σ combined measurement uncertainties for the NIWA – SIO ICP.

		SIO
$\delta^{13}C$	1 σ	46 %
	2 σ	71 %
	n	28
$\delta^{18}O$	1 σ	0 %
	2 σ	0 %
	n	29
CO_2	1 σ	27 %
	2 σ	39 %
	n	18

Seventy one percent of all measured NIWA – SIO inter comparisons were observed to lie within combined 2-sigma uncertainties for $\delta^{13}C$. The agreement for CO_2 mixing ratio was lower, with less than 50 % of inter comparison flask measurements within combined 2-sigma uncertainties. Agreement for $\delta^{18}O$ was observed to be much worse, with no inter comparison flask measurements within combined 2-sigma uncertainties.

Visual inspection of the ICP data shown in Figure 4.9 indicates that there appears to be no systematic offset between NIWA and SIO measurements for $\delta^{13}C$ as the scatter about zero is approximately uniform. An offset possibly exists for $\delta^{18}O$ and CO_2 mixing ratio which are further examined by calculating the mean differences and standard deviation of all data obtained (Table 4.9).

Table 4.9 Average differences between the (NIWA-SIO) ICP measurements.0

	$\Delta\ \delta^{13}C$ (‰)	$\Delta\ \delta^{18}O$ (‰)	$\Delta\ CO_2$ (ppm)
Average diff	0.01	-0.99	-0.9
Stdev	0.05	0.16	1.2

A large systematic offset between the NIWA and SOI analysed $\delta^{18}O$ values was observed. SIO $\delta^{18}O$ measurements are enriched compared to NIWA $\delta^{18}O$ measurements by ~1 ‰. Considering the SOI measurements are made after a long period of storage the difference therefore appears to be in the wrong direction, as after storage, $\delta^{18}O$ fractionates with water on the walls of the glass flasks and become more depleted [*Gemery et al.*, 1996]. The reason for this difference in the opposite direction to that expected is not yet known and more ICP (or inter calibration exercise) data are required to more fully investigate this discrepancy.

During the same period in which SIO CO_2 mixing ratio measurements were made at Baring Head, continuous NDIR measurements were also made. These measurements (described in section 5.2.1.1) are useful to help investigate the observed CO_2 mixing ratio differences between GC-IRMS and SIO NDIR measurements of the SIO 5 litre flasks (Figure 4.10)

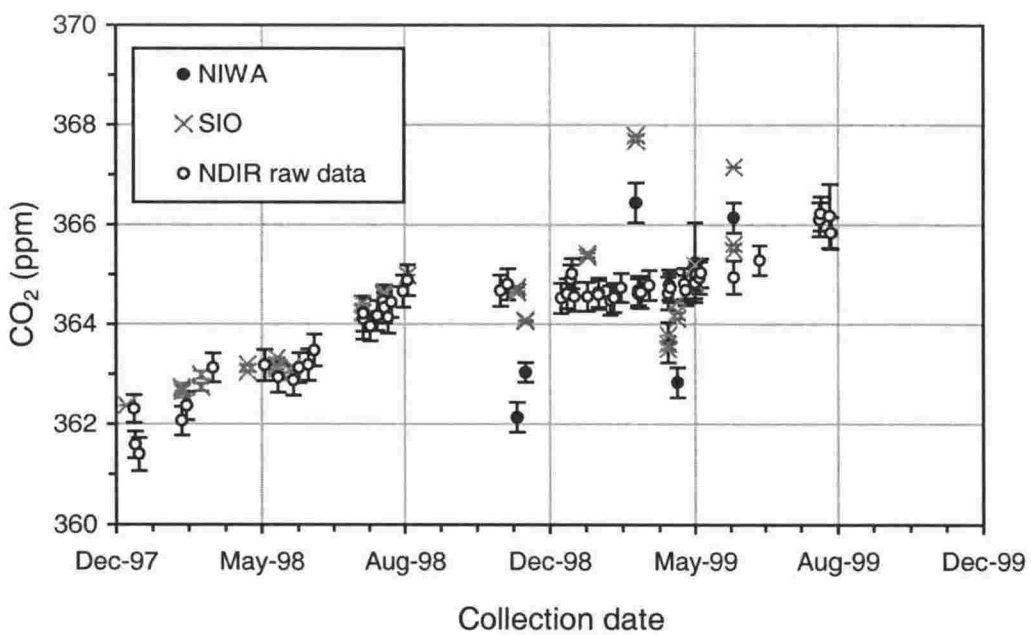

Figure 4.10 CO_2 mixing ratio measurements by NIWA GC-IRMS (solid circles) NIWA NDIR (hollow circles) and SIO (crosses).

Before August 1998, the agreement between the NIWA NDIR raw data that are collected on site at Baring Head and the SIO measurements is generally within measurement uncertainties. After November 1998, the scatter of the SIO flasks about the NIWA NDIR measurements increased and the magnitude of some of the difference became quite large (up to ~1.5 ppm). This decrease in agreement has occurred after the introduction of the GC-IRMS measurements to this program. However, the small amount of data makes it hard to draw any conclusions and the reasons for the increased differences can only be speculated (*e.g.* sample flask leakage or improper sample collection that may have altered the gas composition within some flasks before they were freighted to SIO). More data are therefore required to investigate these discrepancies.

Other possible reasons for the large average difference and variation observed between NIWA and SIO for $\delta^{18}O$ and CO_2 mixing ratio measurements (Table 4.9) are storage effects, which are examined in Figure 4.11.

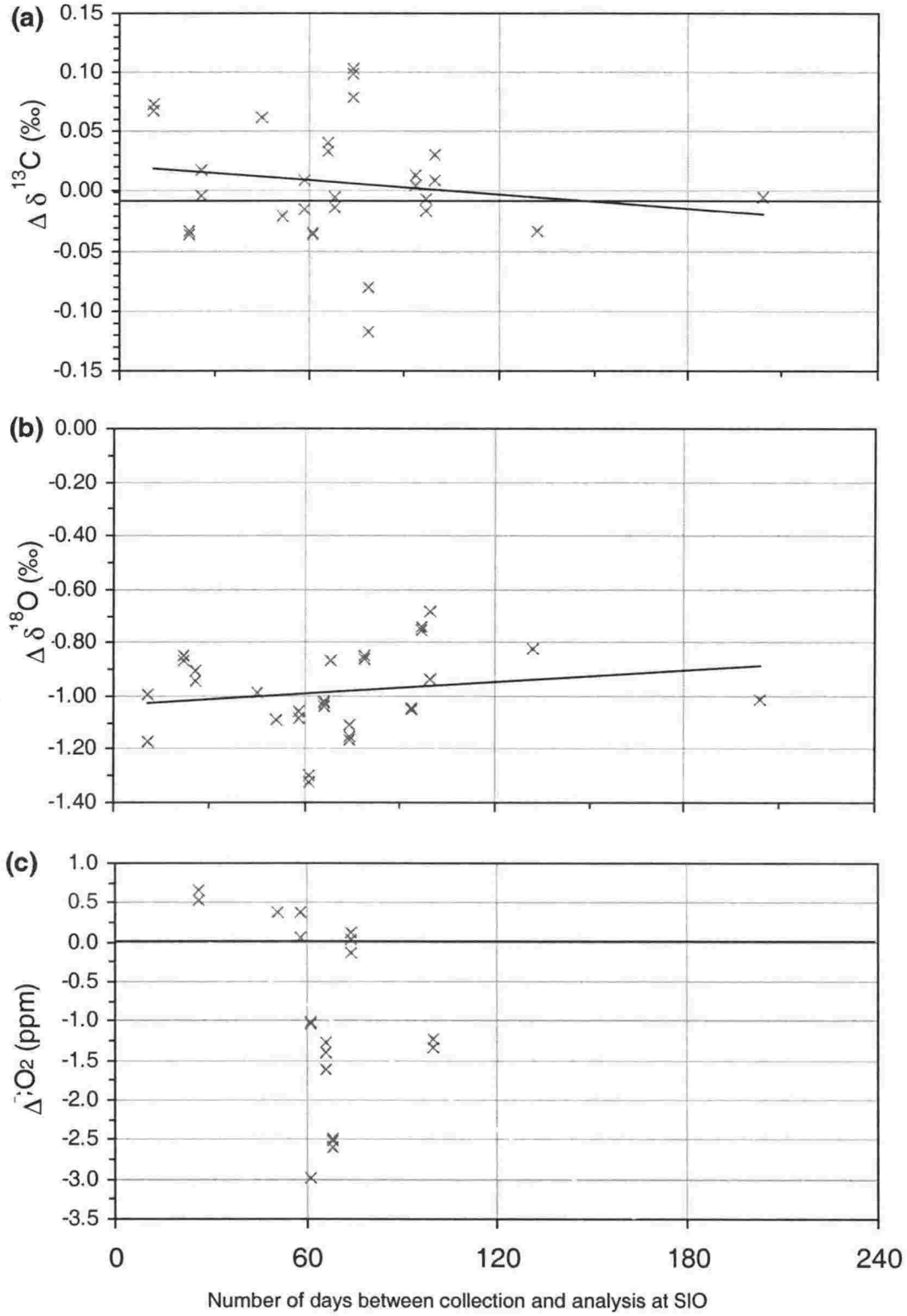

Figure 4.11 NIWA – SIO ICP differences as a function of the number of days between sample collection and analysis.

Despite being filled wet, the SIO 5 litre flasks appear to be relatively stable over the observed storage times for $\delta^{13}C$ and $\delta^{18}O$. CO_2 appears to be unstable, but the smaller amount of data lowers the significance of this finding.

Other possible reasons for the larger variations with the SIO ICP, compared to that with other laboratories, is that samples collected in flasks with greased stopcocks have been observed to have larger discrepancies compared to samples that are stored with Viton® o-rings [*Hudec et al.*, 1999]. This may however be a contributing factor but further work is required to more fully investigate such effects.

The findings and possibilities for future work are discussed in the summary and discussion at the end of this chapter.

4.6 Summary and discussion

NIWA – CSIRO Inter calibration exercise

Preliminary results from the high precision inter calibration exercise of the GC-IRMS technique using whole-air (with a composition close to that of the GC-IRMS reference gas used) stored in a tank at low pressure has been performed. The observed NIWA – CSIRO inter laboratory agreement to within 0.01 ‰ for $\delta^{13}C$ meets the IAEA inter laboratory target precision.

The preliminary results from the inter calibration exercise therefore indicate that GC-IRMS extraction and analysis of $\delta^{13}CO_2$ from inter calibration gas was not observed to be subject to the same problems that dual-inlet previously experienced when comparing measurements of whole-air in high-pressure cylinders. However, more results from the on-going inter calibration exercise are required to more fully investigate the agreement over a larger range of compositions. This will further add to the evaluation of the performance of the GC-IRMS technique with respect to traditional techniques.

The inter calibration exercise indicated that GC-IRMS technique was not subject to extraction and analysis problems for $\delta^{13}C$ for whole-air with similar composition to the reference gas used. This combined with the achievement of the inter-laboratory target precision for $\delta^{13}C$ by GC-IRMS is a successful result and the technique may potentially have large impacts for future work to enable the IAEA target precision to be obtained worldwide.

Agreement for $\delta^{18}O$ and CO_2 mixing ratio was lower than the IAEA and WMO target precisions. However, larger measurement uncertainties for these species meant that the differences between NIWA and CSIRO measurements were not statistically different.

Therefore, these preliminary results suggest that there is no systematic offset associated with dual-inlet measurements and the N_2O correction is currently being performed correctly at current atmospheric composition by CSIRO, however, additional data are

required to fully investigate the N_2O correction. This additional inter calibration data will be obtained by the on-going program established during the work of this thesis.

The initial inter calibration exercise of the GC-IRMS technique with CSIRO has been to a high inter laboratory precision and, at near atmospheric compositions, GC-IRMS is capable of performing accurate isotope ratio measurements to the CG92 scale. In addition, accurate, while less precise, CO_2 mixing ratio measurements can be performed to the X93 scale. The on-going inter calibration and inter comparison exercises established during the work of this thesis will ensure that this is monitored in the future.

Future work for the inter calibration exercise

The on-going inter calibration exercise established during this work will determine many performance measures that are beyond the scope of this thesis. These are:

- The long-term (decadal) performance of the technique.
- Evaluation of the N_2O correction for the dual-inlet method over large ranges of N_2O.

  This would be determined by using calibration gases that are composed of: CO_2 in "zero air" (no N_2O), and ambient levels of atmospheric CO_2 that have a range of N_2O levels.
- Evaluation and comparison of the non-linearity of the GC-IRMS and dual-inlet techniques. This will determine whether having the isotopic composition or the voltages they are ran at matched is most important.

  This would be determined by measuring 2 or more tanks (~5 tanks would be reasonable to obtain sufficient data without excessive analysis requirements) with the same N_2O, but with $\delta^{13}C$, $\delta^{18}O$ and CO_2 mixing ratio over a large range (~4 ‰ for $\delta^{13}C$ and $\delta^{18}O$ and ~50 ppm for CO_2).

In addition, new reference gases will need to be filled and calibrated before the old ones are exhausted. A suite of reference gases at and above current atmospheric levels will best achieve this. This is necessary to ensure on going successful calibration, inter calibration and operational use of the GC-IRMS technique in the future. As atmospheric CO_2 and N_2O levels rise, the current ratio of CO_2 to N_2O may not be maintained. N_2O corrections currently used by dual-inlet techniques may therefore change and any non-linearity problems associated with these measurements may affect the dual-inlet correction and reduce (or increase) the current agreement.

Inter comparison exercises

NIWA – CSIRO

The average difference observed for the flasks collected at Baring Head and Cape Grim over a one year period were: (0.01 ± 0.05) ‰ for $\delta^{13}C$, (0.08 ± 0.16) ‰ for $\delta^{18}O$, and (0.0 ± 0.3) ppm for $\delta^{13}C$. The $\delta^{13}C$ agreement observed during this ICP was higher than that previously observed for $\delta^{13}C$ ICP measurements between CSIRO and INSTAAR. A likely contributing factor to this excellent agreement between NIWA and CSIRO, compared to CSIRO and INSTAAR, is the fact that the NIWA measurement scale is based on the CSIRO measurement scale, whereas CSIRO and INSTAAR have independently maintained measurement scales. This agreement is encouraging for future inter calibration programs that would be based on such a strategy (*e.g.* GLOBAL-HUBS).

The average agreement for CO_2 mixing ratio was also excellent in the NIWA – CSIRO ICP, but the variation associated with this measurement was higher than that present in the CSIRO – NOAA CMDL ICP.

Non-linearity seems to be a limitation of the inter comparison measurements by the GC-IRMS technique for $\delta^{18}O$ and CO_2 mixing ratio measurements that are not close to the composition of the GC-IRMS reference gas used. This effect becomes significant when the differences between the compositions of the reference and sample gas becomes large (~2 ‰ and ~ 50 ppm for $\delta^{18}O$ and CO_2 mixing ratio respectively).

NIWA – NOAA CMDL and INSTAAR

The establishment of an ICP with NOAA CMDL and INSTAAR is a valuable contribution in itself. This is not a trivial point as it has taken over a year to establish and will be valuable in years to come (especially because of the link already established between CSIRO and NOAA CMDL and INSTAAR).

Inter comparisons of the new GC-IRMS technique with NOAA CMDL and INSTAAR were approximately the same as those observed during the NIWA and CSIRO ICP but their significance is reduced due to the low number of samples that were compared.

The possibility of storage problems was raised and this will need to be addressed and scrutinised carefully with the on-going ICP that has been established. The importance of high frequency measurements was also reinforced.

The ground work for this ICP has been performed during this thesis and the real value will come from this ICP over the next few years.

NIWA – SIO

Agreement for $\delta^{13}C$ between NIWA and SIO was observed when combined measurement uncertainties were considered.

An offset of (-0.99 ± 0.16) ‰ for $\delta^{18}O$ was not attributed to storage effects of the wet samples, but are most likely due to calibration scale offsets.

Future ICP work

To enable further checks on sample integrity and sample collection, the use of larger volume flasks in the CSIRO ICP would enable other species (*e.g.* N_2O) to be measured which would provide additional information that may prove useful.

Further development to reduce the uncertainty for GC-IRMS CO_2 mixing ratio measurements would be valuable as would efforts to reduced uncertainties for $\delta^{13}C$ and $\delta^{18}O$ to help achieve the IAEA and WMO target precisions.

Potential discrepancies due to the exchange of ^{18}O between H_2O and CO_2 that are accentuated by long storage periods between sample collection and analysis may possibly be mitigated by reducing laboratory turn-around times for analysis.

The inter comparison measurements presented here have shown that within combined measurement uncertainties, $\delta^{13}C$ measurements have agreed between CSIRO, INSTAAR and SIO. The 1995 IAEA inter comparison exercise between these three laboratories demonstrated that these laboratories disagreed. Therefore, the situation has either improved, or some unaccounted problem has been present in these inter comparison measurements.

Further work is therefore required to fully assess the current agreements or differences between these laboratories in an effort to achieve the IAEA and WMO target precisions.

Finally, the combination of future inter calibration and inter comparison measurements with the GLOBAL-HUBS inter calibration scheme should enable successful merging of atmospheric CO_2 data from the GC-IRMS and traditional techniques in the future. The increased spatial and temporal resolution that this merging facilitates would enable atmospheric CO_2 source –sink evaluations to be more accurately and precisely determined by global carbon cycle models in the future.

5 Applications

5.1 Introduction

In addition to the development of the GC-IRMS technique, previous chapters have presented inter calibration and inter comparison exercises that evaluated its performance with respect to traditional techniques.

This chapter demonstrates the successful use of the GC-IRMS technique by presenting results describing spatial and temporal variations of atmospheric CO_2 over the Pacific Ocean. Temporal variations at three Southern Hemisphere land-based monitoring sites (Baring Head, New Zealand; Cape Grim, Australia; and Arrival Heights, Antarctica) are presented and compared with each other. Spatial variations are then presented from ship-based collection sites in the Pacific region. To further increase understanding of the CO_2 variations over this region, additional measurements from upper-tropospheric air samples collected during a flight between New Zealand and Antarctica are also presented. In total, presented measurements cover a large latitudinal range over the Pacific Ocean from Arrival Heights, Antarctica (~78 °S), to the West Coast of the United States at ~35 °N (Figure 5.1).

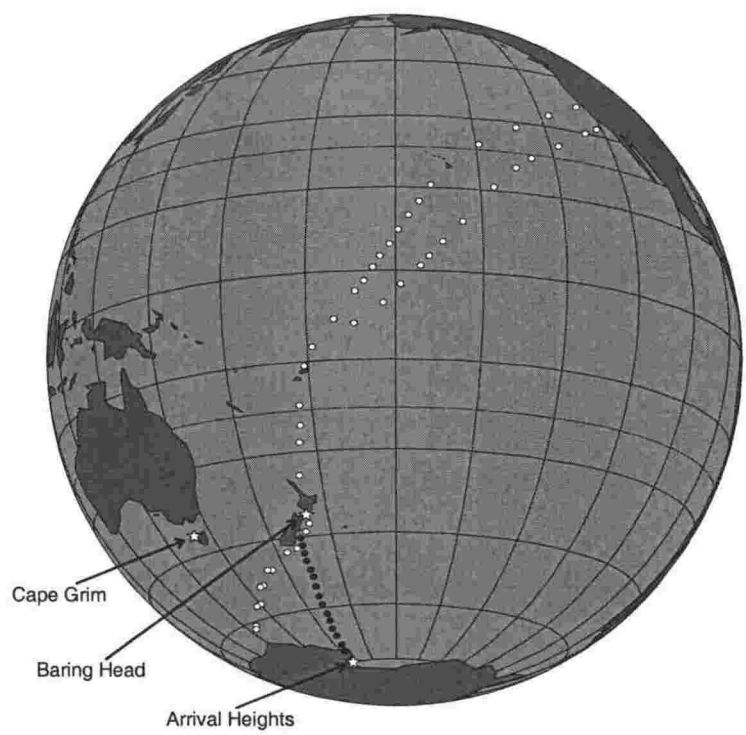

Figure 5.1 Pacific region sample collection sites.

Locations of long-term monitoring sites (stars), marine boundary layer measurements from ship voyages (white circles), and upper tropospheric air samples (black circles).

In addition, results are presented from a small-scale application of the technique for measurements of soil-respired CO_2. These measurements demonstrate the versatility and potential for a wide range of research that is possible with the new GC-IRMS technique.

5.2 Temporal variations of atmospheric CO_2 at Baring Head, Cape Grim and Arrival Heights

Monitoring the temporal variations of atmospheric CO_2 species enables the seasonal cycle and interannual variations to be determined. The integration of such observations from different sites enables the partitioning between the terrestrial biospheric and oceanic sources and sinks of atmospheric CO_2.

5.2.1 Baring Head, New Zealand

Baring Head background air pollution site is situated at 41.4 °S, 174.9 °E on the south coast of the North Island of New Zealand (Figure 5.2).

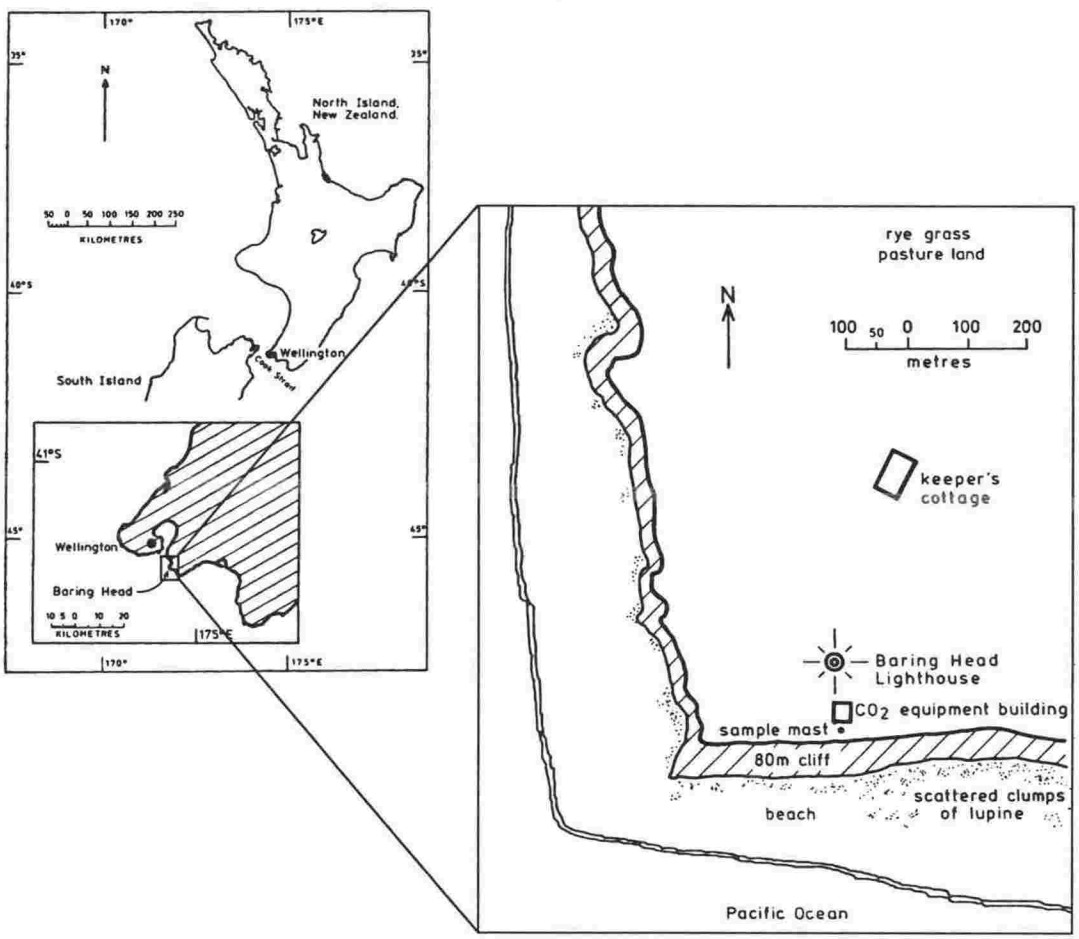

Figure 5.2 Location map and site plan of Baring Head, New Zealand.

Samples are collected from 85 meters above sea level through 12.7 mm o.d. stainless steel airlines that are attached to the sample mast and extend 10 meters above the top of the south facing cliff. The only vegetation between these air intakes and the ocean are scattered flax bushes (*Phormium tenax* and *Phormium cookianum*) on the cliff face and a 20 m stretch of lupine bushes (*Lupinus sp.*) on the beach below the cliff [*Lowe et al.*, 1979].

A statistical analysis of Baring Head air parcel back trajectories shows that ~10 % of these come from the Southern Ocean and ~30 % from the southerly sector [*Gomez*, 1996]. These southerly winds are onshore, have normally travelled long distances without any land contact, and are thus representative of clean Southern Ocean marine air. An example of such an air parcel back trajectory is given in Figure 5.3. Samples are only collected during winds from this southerly direction, as during periods of northerly airflow or airflow over the South Island of New Zealand, local sources and sinks of CO_2 potentially contaminate air at Baring Head.

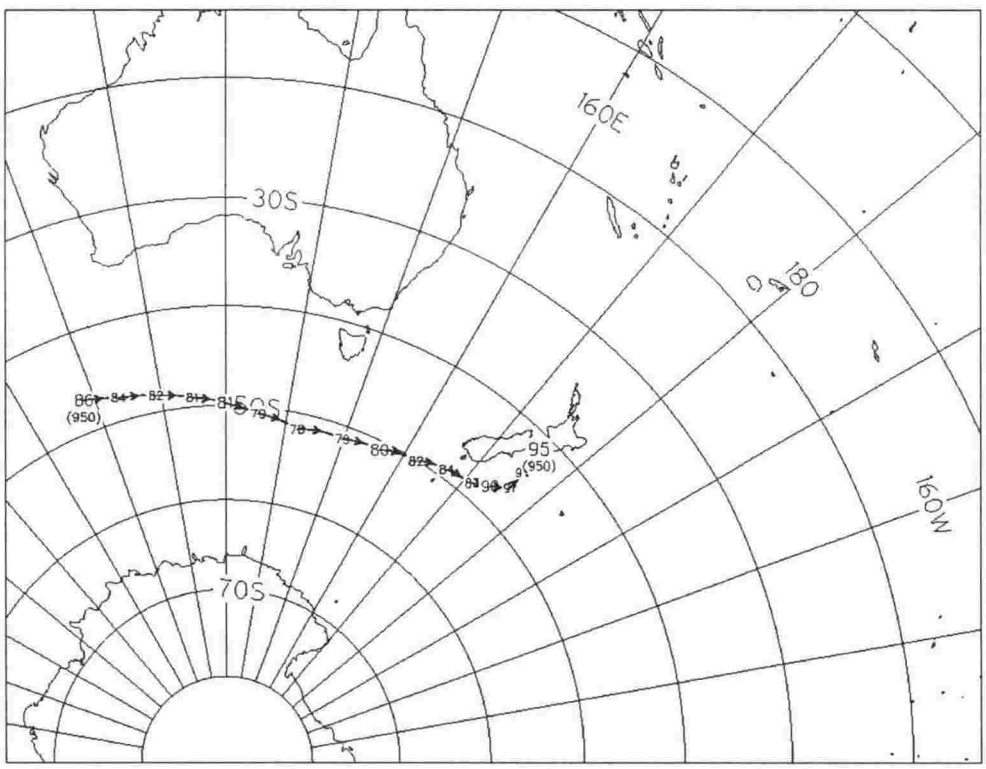

Figure 5.3 A 4-day back trajectory for an air parcel arriving at Baring Head on the 2nd May 1999. At intervals of 6 hours, the pressure level is shown in kPa, with larger numbers used every 24 hours. The numbers in paranthesis represent hPa. Back trajectories are calculated by analysis of forecasts produced by the New Zealand Meteorological Service as described by *Gordon* [1986]. Polar stereographic projection is used for the basemap.

5.2.1.1 History of CO_2 at Baring Head

Since the early 1970s, measurements of the atmospheric CO_2 mixing ratio have been made at Baring Head by an on-site continuous NDIR analyser [*Lowe et al.*, 1979; *Manning et al.*, 1994]. These measurements (Figure 5.4) show seasonality, in addition to a long-term trend over almost 30 years.

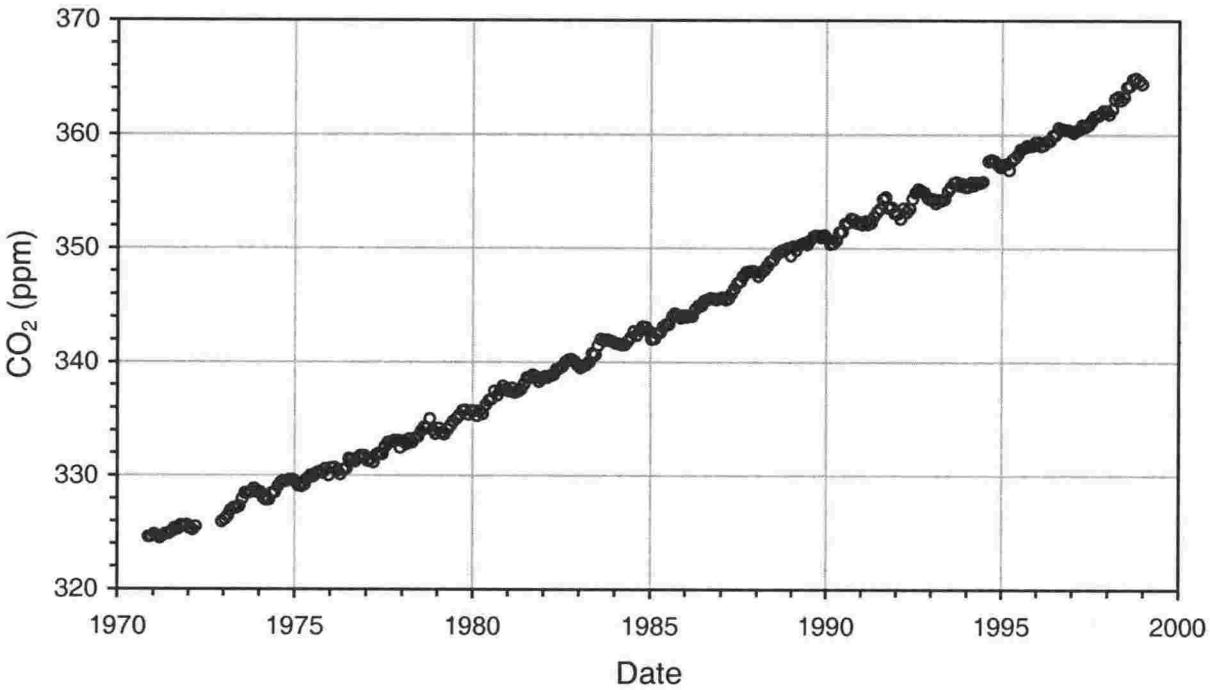

Figure 5.4 NDIR measurements of monthly mean CO_2 at Baring Head since the early 1970s. Data is collected during 'baseline' periods, which are defined as events in which the local wind direction is from the south, and the standard deviation of the minute-by-minute CO_2 level is <0.1 ppm for 6 or more hours. The first 17 months of data is from Makara Beach, ~24 km NW of Baring Head.

The monthly CO_2 record from Baring Head is typical of Southern Hemisphere sites. It shows a small seasonal amplitude of ~1 ppm with maxima occurring between August and October, and minima occurring between February to April. In addition, an average growth rate of ~1.4 ppm/year has been observed at Baring Head over the last 28 years. The seasonal cycle is in phase with, and of nearly the same amplitude as that observed at the South Pole [*Lowe et al.*, 1979]. This long-term record is valuable for comparisons of the measurements made by the new GC-IRMS technique presented in this work.

5.2.1.2 Air sample collection

For GC-IRMS analyses, NIWA routine air samples were collected in 2 litre glass flasks as previously described in section 3.3 (page 38).

CSIRO 0.5 litre inter comparison flasks collected at Baring Head (previously described in section 4.5.1, page 75) were also used for the construction of the Baring Head series.

5.2.1.3 Results

Results for baseline measurements of atmospheric CO_2 species at Baring Head are shown in Figure 5.5. Some data were rejected and are not shown in the plot. This applies for the following cases: 1) 2-sigma rejection of 'bad' pairs for the CSIRO inter comparison flasks*, 2) non-baseline samples†, 3) CO_2 mixing ratios before October 1998‡. In addition, ~3 % of samples that were collected were lost due to breakage and valve failures.

---

* CSIRO flasks are rejected if the difference between the flask pair is larger than two times the analytical precision. As previously mentioned in section 4.5.3.1 (page 79) ~10 % of the 0.5 litre samples collected at Baring Head were rejected for this reason.

† Samples collected at Baring Head were rejected if the back trajectories indicated contamination from either: Northerly flow, flow over the South Island of New Zealand, or flow that originated from the Australian continent. For this reason, approximately 20 % of the routine samples collected in 2 litre flasks were rejected, while less than 10 % of the 0.5 litre flasks were rejected. The higher percentage of 2 litre samples that were rejected reflects the proportion of these samples that were collected at additional times when no 0.5 litre flasks were collected.

‡ Previously described in section 4.5.3.1 (page 79).

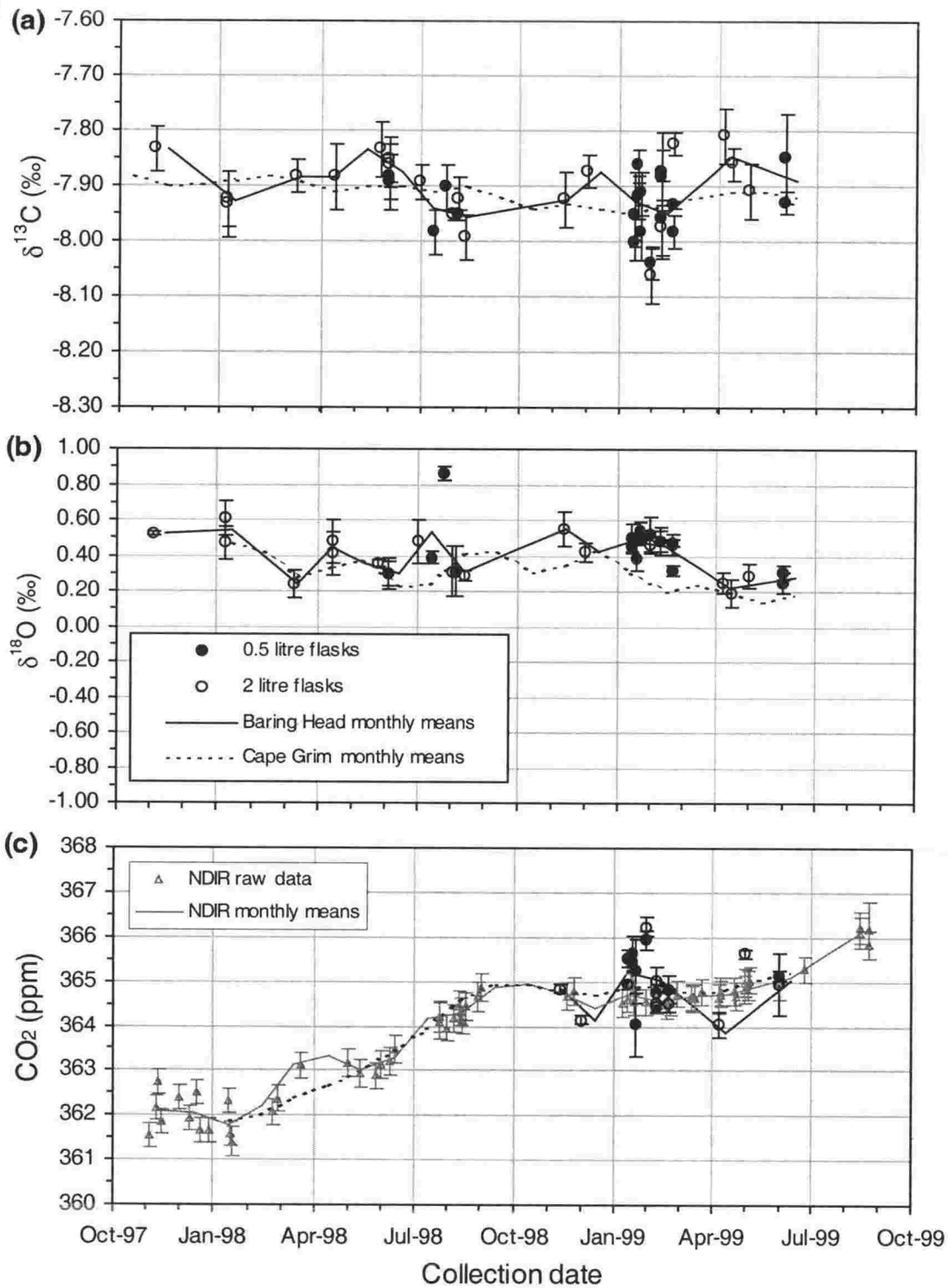

Figure 5.5 GC-IRMS measurements of (a) $\delta^{13}C$ (b) $\delta^{18}O$ and (c) CO_2 mixing ratio at Baring Head. Samples have been collected in either NIWA routine 2 litre flasks (hollow circles) or CSIRO 0.5 litre flasks (solid circles). Monthly means from GC-IRMS measurements are also shown (solid line). In addition, the CO_2 mixing ratio from NDIR measurements (hollow triangles) and NDIR monthly means (light line) are shown from November 1997 to July 1999. 1999 NDIR data are provisional and are subject to changes following full calibration that will be performed after the release of this thesis. Cape Grim monthly means are also shown (dashed line).

More flask measurements at Baring Head could not be obtained because of the low frequency of baseline conditions present during the monitoring period. This was partly due to the 1997-1998 El Niño, which reduced the frequency of southerly winds at Baring Head, especially from September 1998 to December 1998. The frequency of the NDIR raw data gives an approximate guide to the number of baseline periods (defined in section 5.2.1.1, page 104). In addition, the amount of raw data that the NDIR monthly means were constructed with are shown. This also gives an indication of how well the GC-IRMS monthly means capture the seasonal cycle. In some periods, the low frequency of the GC-IRMS data obtained lowers the significance of the variations observed in those periods (*e.g.* November and December, 1998). In other times, although the noise can be quite large, the GC-IRMS monthly means indicate general patterns which are discussed below.

Over the period of GC-IRMS measurements at Baring Head (~1.6 years), a weak seasonal cycle for $\delta^{13}C$, with maximum around May and minimum between August and December was observed. A peak to peak amplitude of ~0.1 ‰ for the seasonal cycle of $\delta^{13}C$ was observed by GC-IRMS measurements during 1998 and 1999. This signal is larger than previously observed signals at similar latitudes in the Southern Hemisphere (*e.g.* a seasonal cycle of ~0.05 ‰ has been previously observed at Baring Head between 1986 to 1990 by *Keeling et al.,* [1995] and also at Cape Grim between 1982 to 1992 by *Francey et al.,* [1995]). Published data by SIO for recent measurements at Baring Head are not yet available. However, variations in the trends measured by *Keeling et al.*, [1995] and *Francey et al.*, [1995] were evident and seasonal cycles approaching ~0.1 ‰ were observed (*e.g.* between 1987 and 1989 [*Francey et al.,* 1995]).

A seasonal cycle for $\delta^{18}O$ may exist at Baring Head but it was not prominent during the monitoring period and therefore not observed by the GC-IRMS measurements. The large variability in $\delta^{18}O$ observed at Baring Head has also been observed at similar latitudes [e.g., *Francey and Tans,* 1987; *Trolier et al.,* 1996] providing assurance that the GC-IRMS measurements are not excessively noisy for $\delta^{18}O$. In addition, the previously observed variations were of similar magnitude to that observed at Baring Head. The lack of trend in $\delta^{18}O$ at Baring Head was due to the strong opposing forces of respiration (depleted in ^{18}O) and photosynthesis (leaf water is enriched in ^{18}O) which vary considerably from year to year but balance over longer time scales [*Tans et al.*, 1998].

CO_2 mixing ratio increased by ~4 ppm over the 1.8 year period of NDIR data presented in Figure 5.5. Such an increase (~2.2 ppm/year) is higher compared to that previously observed at Baring Head (~1.4 ppm/year) and at other Southern Hemisphere sites (*e.g.* ~1.5 ppm/year was observed at: Amsterdam Island (38 °S), Cape Grim (41 °S), and at the

South Pole (90 °S) between ~1981 to ~1992 [*Conway et al.*, 1994]). After October 1998, and during the period of GC-IRMS measurements, CO_2 mixing ratios declined slightly and experienced a minimum between November 1998 and April 1999. CO_2 uptake by the biosphere during this active growth period causes this minimum over the summer months. The seasonal cycle at Baring Head normally has a seasonal cycle of up to 2 ppm, with a minima between February and April and a maxima between August and October [*Manning et al.*, 1994]. During April to September CO_2 mixing ratio rises very steeply because the rise of the seasonal cycle is combined with the increasing trend. During October to March the CO_2 mixing ratio levels off (or even declines) because the decline in CO_2 mixing ratio during the summer growth season approximately cancels out the increasing trend. The amplitude of the seasonal cycle of atmospheric CO_2 has been variable in the past with no seasonal cycle observed at all in some years (*e.g.* 1997-1998). The growth rate of atmospheric CO_2 has also varied over the last 40 years from between near-zero up to as high as ~2.5 ppm/year (*e.g.* Figure 2.10, page 21). Therefore, the cycle resolved in the GC-IRMS measurements and the relatively high growth rate is typical of this site.

Seasonal cycles in atmospheric CO_2 are mostly due to the effect of the terrestrial biosphere. During the summer growth season, the biosphere becomes a net sink for CO_2 because the uptake by photosynthesis draws down more CO_2 than that which is respired. In southern latitudes, the seasonal cycle for atmospheric CO_2 is small. This is because the oceans in the Southern Hemisphere mostly influence the CO_2 variation, rather than the terrestrial biosphere as in the Northern Hemisphere.

The seasonal cycle of CO_2 mixing ratio observed at Baring Head, with maxima between August to October and minima between February and April, was approximately anti-correlated to the $\delta^{13}C$ seasonal cycle, with minima between August to December and maxima in May. Such an anti-correlation is a reflection of photosynthesis and respiration (*e.g.* during the summer growth period, CO_2 mixing ratio falls, while $\delta^{13}C$ rises as uptake by plants leave behind atmospheric CO_2 which is more enriched in ^{13}C). The magnitude of this anti-correlation was small and approximately equal to that observed by independent measurements in the Southern Hemisphere [e.g., *Trolier et al.*, 1996].

5.2.2 Cape Grim, Australia

Since the establishment of the NIWA-CSIRO ICP in October 1998, GC-IRMS measurements have been made at Cape Grim, Australia. These measurements are

performed for a subset of the total number of air samples collected at Cape Grim for CSIRO's long-term monitoring program that began in 1976. The location of the Cape Grim site is shown in Figure 5.6. The collection details for these samples have previously been described in section 4.5.1 (page 75).

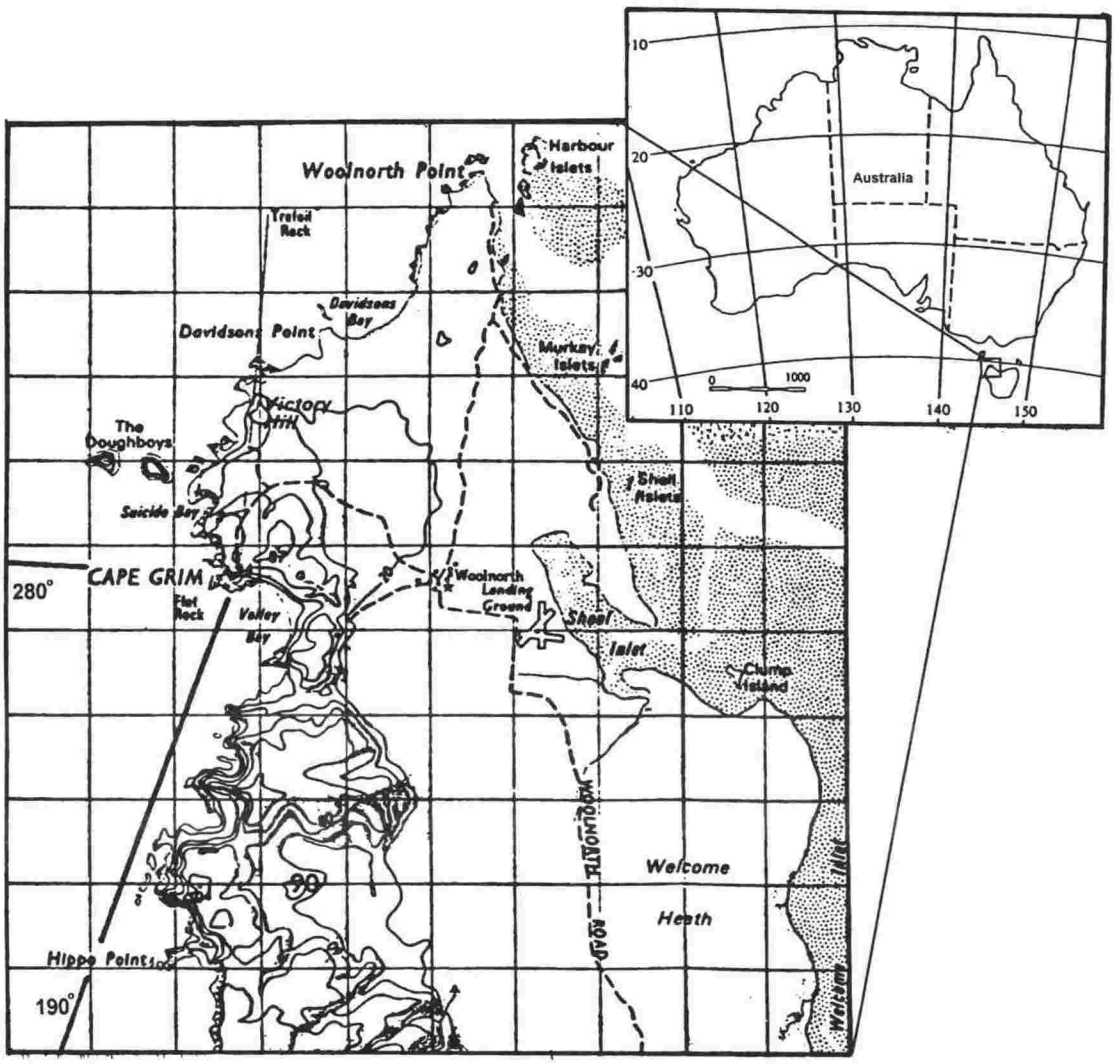

Figure 5.6 Location of Cape Grim, Tasmania Australia.

5.2.2.1 Results

Results of the GC-IRMS measurements at Cape Grim, in addition to the CSIRO dual-inlet measurements from the same flasks, and the monthly means since January 1998 are presented in Figure 5.7. Some data have been rejected according to the rejection criteria applied to the data in Figure 5.5 (detailed in section 5.2.1.3, page 105) and are not shown in the plot. In addition, individual flask measurements were rejected by CSIRO if residuals were greater than 3-sigma standard deviations from a smooth curve fitted to the entire data set.

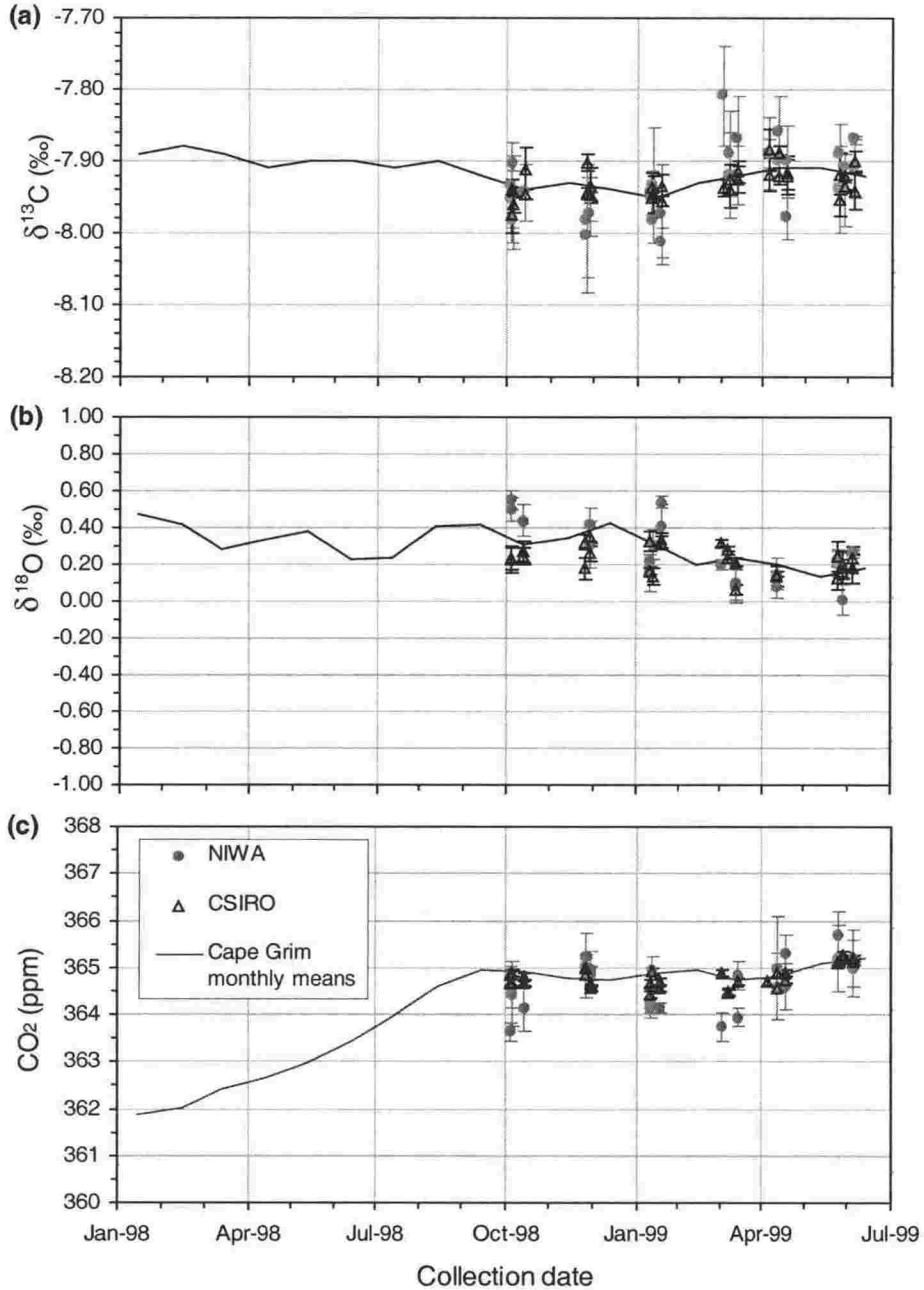

Figure 5.7 CSIRO dual-inlet measurements (hollow black triangles) and GC-IRMS measurements (solid circles) of (a) $\delta^{13}C$ (b) $\delta^{18}O$ and (c) CO_2 mixing ratio at Cape Grim.

The Cape Grim monthly means are constructed from the entire CSIRO data set which is not shown above.

During the period in which GC-IRMS measurements were obtained at Cape Grim, the CO_2 mixing ratio levelled off between October 1998 and May 1999 at ~364.8 ppm, indicating the seasonal cycle minimum during this time. $\delta^{13}C$ was approximately anti-correlated to CO_2 mixing ratio and $\delta^{18}O$ was observed to be variable with no significant trend. As indicated in Table 4.4 (page 82), NIWA and CSIRO measurements of air samples collected at Cape Grim compared with measurement differences of 0.00 ± 0.05 ‰ for $\delta^{13}C$, 0.03 ± 0.05 ‰ for $\delta^{18}O$ and –0.2 ± 0.4 ppm for CO_2 mixing ratio. The

differences between NIWA and CSIRO measurements of air samples collected at Cape Grim were therefore not statistically different and the CSIRO monthly means were used to represent Cape Grim. These CSIRO monthly means at Cape Grim are later compared with Baring Head and Arrival Heights in section 5.4.3 (page 133).

5.2.3 Arrival Heights, Antarctica

Arrival heights (77.8 °S, 166.7 °E) is located ~3800 km south of Christchurch, New Zealand on Ross Island, Antarctica (Figure 5.8).

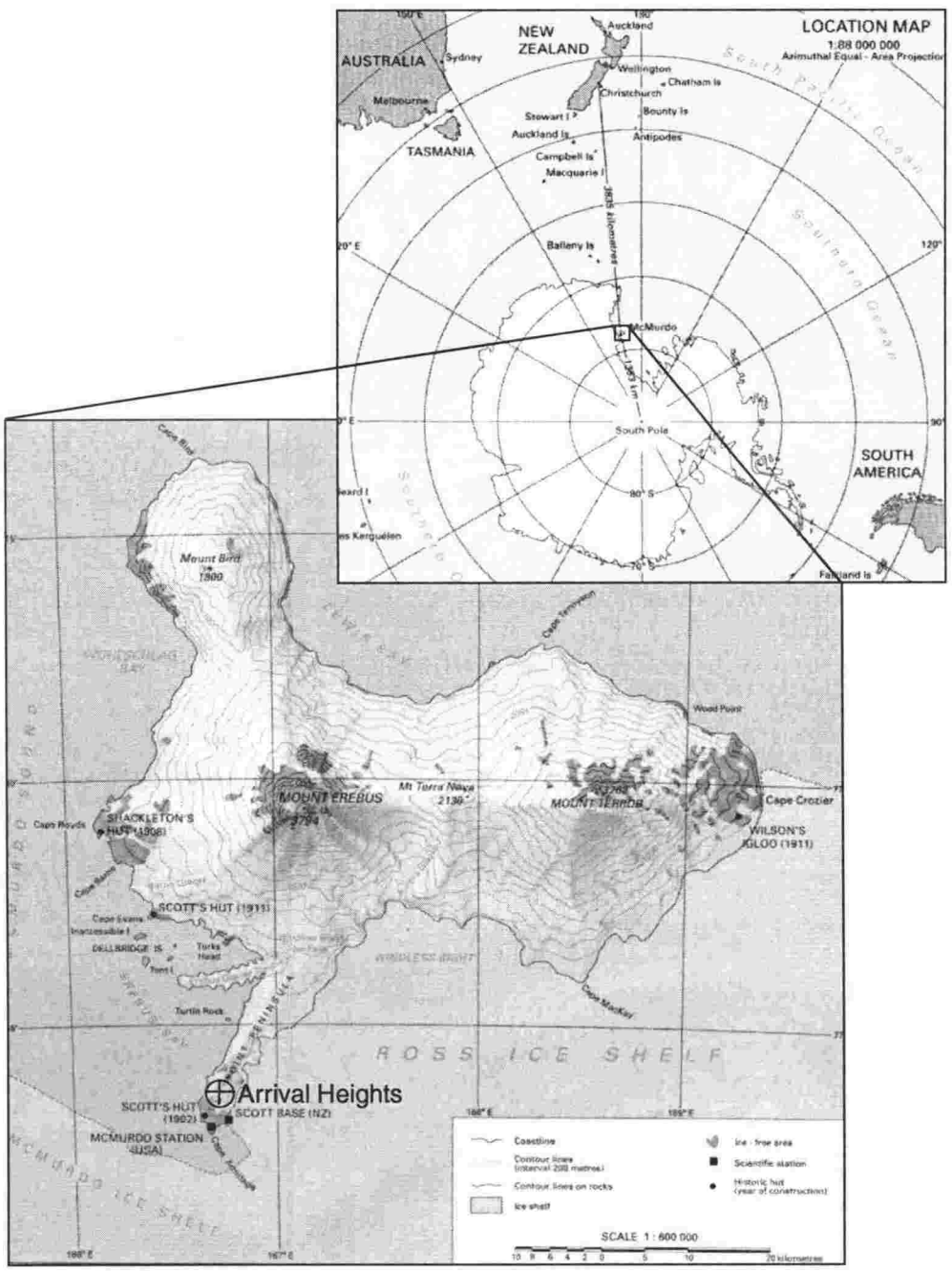

Figure 5.8 Location of Arrival Heights, Ross Island, Antarctica.

5.2.3.1 Air sample collection

Air samples were filled with a metal bellows pump (Senior Flexonics, Metal Bellows Division, Sharon, MA, USA) to a pressure of ~150 kPa. Samples were collected wet and stored in 2 litre stainless steel flasks. A stainless steel bellows valve (Nupro Company, Willoughby, OH, USA) is fitted to the flasks, the interior surfaces of which, are electro-polished. Samples were collected without chemical drying because during sample collection the average dew point was low (~-20 °C). At this temperature it was hoped that $\delta^{18}O$ would be stable as previously predicted [*Gemery et al.*, 1996]. To avoid contamination from nearby local sources of CO_2 (Scott Base and McMurdo Station) samples were only collected during baseline wind conditions at Arrival Heights, which are defined as winds between the SW, through N, to SE sectors.

5.2.3.2 Results

Other than the knowledge that samples were collected under baseline conditions, no further check on sample integrity exists. This is because reliable back trajectory calculations can not be easily determined at this latitude due to the lack of meteorological data and the high wind speeds in this region. Therefore, cautious interpretation of the data is required.

GC-IRMS measurements at Arrival Heights are presented in Figure 5.9. CO_2 mixing ratio data analysed before October 1998 have been rejected as previously described in section 4.5.3.1 (page 78).

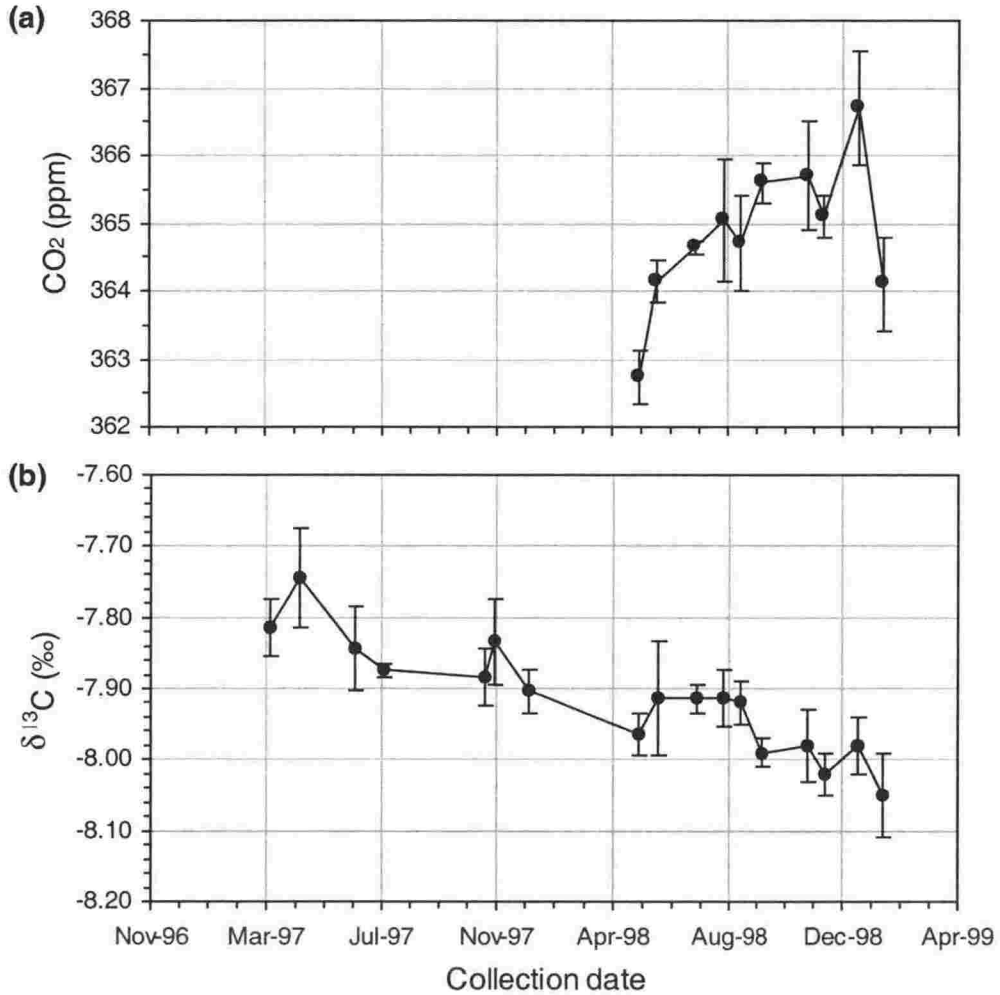

Figure 5.9 GC-IRMS measurements of (a) CO_2 mixing ratio and (b) $\delta^{13}C$ at Arrival Heights.

Measurements of $\delta^{18}O$ were found to be fractionated by as much as ~-9 ‰ and therefore were not included in Figure 5.9. *Gemery et al.*, [1996] recorded that for $\delta^{18}O$ in glass flasks to be stable, the dew point of the collected sample must be 2 °C or lower. In addition, the surface effects of quartz and Pyrex® glass flasks recorded by *Gemery et al.*, [1996] were significantly different with resultant $\delta^{18}O$ fractionations for these glass types of ~-2.5 ‰ and ~-8 % respectively. Assuming sample collection temperatures were accurate and samples were not collected in humid conditions, the Arrival Heights data therefore indicate that the possibly that the stability of $\delta^{18}O$ in stainless steel flasks is worse than that in glass flasks. This is because the samples were dried to a lower dew point than that required to avoid oxygen exchange, yet the resultant exchange of ^{18}O was larger than that observed in Pyrex flasks. However, the humidity referred to by *Gemery et al.*, [1996], is that within the flasks during storage, which can be significantly higher than ambient humidity during sampling (*e.g.* during freight where the flasks are cooled in the cargo hold which, in the case for Antarctic flights, may be extreme). Further tests are

therefore required to fully investigate the stability of $\delta^{18}O$ in stainless steel flasks for this Antarctic sampling program.

By visual inspection, the first CO_2 mixing ratio measurement in April 1998 and the last measurement in June 1999 appear to be low. Because the seasonality for CO_2 is almost the same at Baring Head and the South Pole [*Lowe et al.*, 1979] the seasonality at Arrival Heights is expected to be the same. In this case, a minimum between February and April and a maximum between August and October would be expected. Therefore the low value in May 1998, approximately coincides with the expected minimum. Excluding the point in January 1999, which is high compared to the adjacent measurements, the maximum would have occurred between September and November, which is close to the expected phase. Unfortunately the origin of these potentially high and low samples can not be determined and no further check of sample integrity nor possible reason for these values exist. A large and sharp rise in the CO_2 mixing ratio of ~4 ppm (or ~2.5 ppm with rejection of the April 1998 and June 1999 samples) was observed at Arrival Heights between May 1998 and January 1999. For this latitude, this rate of change is large because it exceeds: 1) the expected global trend and 2) the period in which the rate of change of the seasonal cycle is of the same sign as the expected global trend (*i.e.* the two signals are superimposed). In Antarctic regions a seasonal cycle of ~1 ppm is typically observed (*e.g.* at the Japanese Antarctic Station, Syowa (69.0 °S, 39.4 °E), a seasonal cycle of 1.1 ppm was present between 1984 to 1989 [*Nakazawa et al.*, 1991], and at the South Pole (90 °S) a seasonal cycle of ~1 ppm was present between 1981 to 1992 [*Conway et al.*, 1994]). *Keeling et al.*, [1989] observed the CO_2 mixing ratio to increase at ~1.3 ppm/year between 1970 to 1985 at the South Pole. Independent measurements at the South Pole by *Conway et al.*, [1994] observed an average increase at ~1.5 ppm/year between 1981 to 1992. The slightly larger growth rate observed by *Conway et al.*, [1994] indicates the increased emission of CO_2 in the late 1980s compared to the observations of *Keeling et al.* [1989] during the 1970s and early 1980s. However, larger variations in the global growth rate of atmospheric CO_2 have been previously observed, *e.g.* ~2.5 ppm/year between 1987 to 1988 and ~0.6 ppm/year in 1992 [*Conway et al.*, 1994]. Therefore, the magnitude of the variation measured at Arrival Heights by GC-IRMS is not an unlikely observation.

For $\delta^{13}C$, a decline of ~-0.22 ‰ was observed over the two year measurement period between March 1997 to March 1999 (~-0.11 ‰/year). Other research has measured a $\delta^{13}C$ trend in Antarctic regions that is smaller than this. For example, a $\delta^{13}C$ trend of -0.02 ‰/year from 1986 to 1990 was observed by *Murayama et al.*, [1998] and a $\delta^{13}C$ trend of ~-0.025 ‰/year was observed from 1977 to 1985 by *Keeling et al.*, [1989].

Variations within the $\delta^{13}C$ trends are however evident in these records (*e.g. Keeling et al.*, [1989] observed variations from ~-0.06 ‰/year between 1976 and 1983 to ~-0.13 ‰/year between 1983 and 1984). Because the GC-IRMS measurements do not temporally coincide with any other measurements and are too short to be representative of the long-trend, direct comparisons can not be made. However, previously measured variations suggest that it is likely that a real atmospheric event was observed. The cause of such an event, with a higher rate of decline for $\delta^{13}C$ than expected, indicate that a greater fraction of the excess CO_2 is from fossil fuel burning.

A seasonal cycle of ~0.04 ‰ for $\delta^{13}C$ was observed at Syowa, Antarctica between 1986 to 1990 by *Murayama et al.*, [1998] and was comparable to those made at the South Pole by *Keeling et al.*, [1989]. However, GC-IRMS measurements revealed no significant seasonal cycle for $\delta^{13}C$ over the observed period. Previous records have also observed periods in which no seasonal cycle was apparent (*e.g.* 1981 to 1982 [*Keeling et al.*, 1989]) and therefore more data are required to determine the seasonal variations at this location.

More data are required to better determine the trend and seasonal cycle of $\delta^{13}C$ and CO_2 mixing ratio at Arrival Heights.

Significant $\delta^{18}O$ variations in Antarctica have also been shown to exist by *Murayama et al.*, [1998]. Such measurements are useful because $\delta^{18}O$ has the potential to quantitatively separate respiration from photosynthesis in carbon cycle studies [*Tans et al.*, 1998]. Therefore, to ensure $\delta^{18}O$ stability so that this species may also be monitored at Arrival Heights, future sampling strategies should allow drying of the collected air samples (or collection in glass flasks as discussed by *Gemery et al.*, [1996] rather than the stainless steel flasks that have been used so far).

5.2.4 Comparison of Baring Head, Cape Grim, and Arrival Heights

Atmospheric CO_2 species from Baring Head, Cape Grim and Arrival Heights are compared in Figure 5.10.

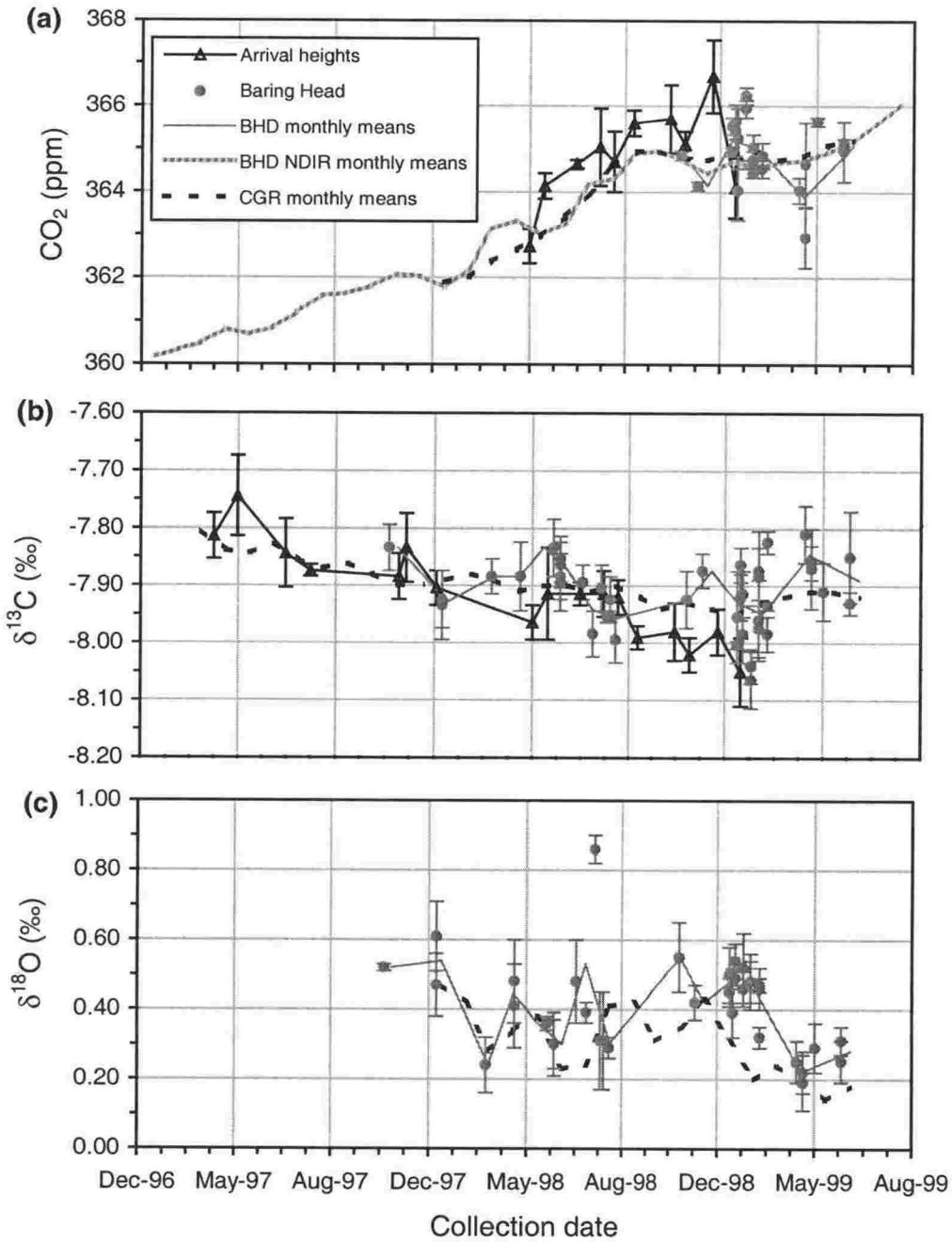

Figure 5.10 Comparison of atmospheric CO_2 species from air samples collected at Baring Head (solid grey circles), Arrival Heights (triangles) and Cape Grim monthly means (dashed black line).
BHD NDIR CO_2 mixing ratio monthly means (thick dashed line in (a)) and Baring Head monthly means (solid grey line) are also given.

Many of the differences between Baring Head and Cape Grim may be due to discrepancies associated with sample collection, storage effects, and measurement uncertainties. Much of the observed variation between Baring Head and Cape Grim may be attributed to the combined measurement uncertainties of NIWA and CSIRO (as was discussed in the NIWA-CSIRO inter comparison, section 4.5.3.1, page 78). GC-IRMS measurement uncertainty is also a potential cause for differences between Baring Head and Arrival Heights. However, differences that were larger than the combined

uncertainties of the NIWA and CSIRO techniques exist for $\delta^{18}O$ at Cape Grim. The lower sampling frequency at which the GC-IRMS measurements at Baring Head and Arrival Heights were obtained must also be borne in mind when comparing observations between the three locations. One other likely contributing factor is the different rejection criteria applied for fitting monthly means to the NIWA and CSIRO measurements. The Cape Grim monthly means were constructed with many measured data points, some of which are subject to 3-sigma rejection (previously discussed in section 5.2.2.1, page 109). GC-IRMS measurements at Baring Head and Arrival Heights were not frequent enough to allow such rejection. If it were possible to apply 3-sigma rejection to measurements at Baring Head and Arrival Heights, improved agreement may have resulted. Consider for example, the $\delta^{18}O$ value for Baring Head at the end of July 1998. This measurement was performed with satisfactory precision and the calculated back trajectory did not indicate that the sample airmass passed over land or any other contaminating source that would subject the sample to rejection. The inclusion of this point therefore raises the monthly mean, whereas for the Cape Grim series, the lack of such data keep the mean lower by ~0.3 ‰. Due to the proximity of Baring Head and Cape Grim, a small-scale variation with such a large effect seems unlikely. Further inter comparisons between NIWA and CSIRO (as in Chapter 4) may determine the reasons for such inconsistencies. Apart from this measurement, agreement of monthly means between Baring Head and Cape Grim is generally within ~0.05 ‰ for $\delta^{13}C$, 0.1 ‰ for $\delta^{18}O$, and 0.5 ppm for CO_2. Such non-systematic differences up to ~0.05 ‰ for $\delta^{13}C$ have been previously observed between Baring Head (measured by SIO) and Cape Grim (measured by CSIRO) between 1986 to 1991 [*Keeling et al.,* 1995] suggesting that the GC-IRMS technique has performed as well as the traditional dual-inlet technique for $\delta^{13}C$ measurements.

The CO_2 mixing ratio levelled off after October 1998 at Baring Head and Cape Grim due to the influence of terrestrial biospheric uptake during the growth season. The average growth rate over the period of observation was slightly higher than previously observed. Significant variations in past CO_2 growth rates have previously been observed (*e.g.* a global growth rate of ~2.5 ppm/year between 1987 to 1988 which dropped to ~0.6 ppm/year by 1992 [*Conway et al.,* 1994]. The cause of these particular different CO_2 growth rates was attributed to an increase of the Northern Hemisphere sink from ~3.9 GtC/year in 1991 to ~5.9 GtC/year in 1992. Variations in: the Southern Hemispheric sink, large-scale CO_2 sources over this region, or atmospheric transport, most likely account for the larger than expected CO_2 trend observed by the GC-IRMS measurements at Baring Head and Cape Grim.

A departure from the general agreement between Baring Head and Cape Grim was observed over the period between March and May 1998. During this time, an increase of CO_2 mixing ratio at Baring Head, to a maximum of ~1 ppm above that at Cape Grim was observed. This difference, which is larger than twice the combined measurement uncertainties from NIWA and CSIRO instruments, may have been due to regional variations because of an oceanic or atmospheric event (*e.g.* a variation in a local oceanic source or sink of CO_2 and/or predominant airflow patterns over such a region). Alternatively, the difference between Baring Head and Cape Grim may be a result of data rejection criteria discrepancies that possibly omit high frequency variations based on adjacent values (*e.g.* 3-sigma rejection at CSIRO). Furthermore, another possible reason is the occurrence of an undetected instrumental problem that may have occurred at one (or both) laboratories. The usefulness and value of ICPs discussed in Chapter 3 is highlighted by this example. If ICP data had been available over this time, further information would be available to help eliminate (or imply) reasons for the observed differences.

Until October 1998, a decline of ~0.1 ‰/year for $\delta^{13}C$ was observed at Cape Grim. Concurrently, an anti-correlated CO_2 mixing ratio growth of ~2 ppm/year was observed. Between November 1998 and April 1999, the CO_2 mixing ratio experienced a minimum of ~364.5 ppm, while $\delta^{13}C$ experienced a maximum of ~-7.95 ‰.

No systematic offset was observed between Baring Head and Cape Grim for any of the atmospheric CO_2 species monitored. Higher frequency and possibly higher precision sampling would be required to successfully determine longitudinal differences that may exist between Baring Head and Cape Grim.

Non-systematic differences were observed between measurements at Baring Head, Cape Grim and Arrival Heights. Between the months of May 1998 to January 1999, CO_2 mixing ratio measurements at Arrival Heights were ~1 ppm higher on average than those at Baring Head and Cape Grim. During January 1998 to June 1998 and August 1998 to January 1999, average $\delta^{13}C$ at Arrival Heights was observed to be depleted by ~0.05 to ~0.1 ‰ with respect to Baring Head and Cape Grim.

A similar comparison of measurements between Cape Grim, Syowa and the South Pole was made between 1984 to 1987 by *Nakazawa et al.*, [1991]. These measurements showed the amplitude and phase of seasonal cycles to be reasonably well related and variable from year-to-year. Furthermore, the amplitude was observed to increase going southwards from southern mid-latitudes where there are no sources and sinks of CO_2. The seasonal CO_2 cycle was delayed going southward, suggesting poleward transport of air. This is however contrary to the general circulation presented in Figure 2.3 (page 9) and

hence transport alone cannot explain all differences. Transport from the Northern Hemisphere in to the Southern Hemisphere from the upper troposphere in addition to downward transport of stratospheric air in the Antarctic region may also be responsible for the elevated CO_2 levels observed in Polar regions [*Nakazawa et al.*, 1991].

Interannual variations in global air temperature (Related to the El Niño Southern Oscillation, ENSO) which alter the terrestrial biosphere and oceanic sources and sinks of atmospheric CO_2 have been described as reasons for the observed variations in atmospheric CO_2 growth rate [*Keeling et al.*, 1995]. Other reasons may be attributed to Southern Ocean variability, which most likely accounts for the differences between Baring Head/Cape Grim and Arrival Heights. The Southern Ocean is potentially a very large sink for atmospheric CO_2 for several reasons. CO_2 solubility is higher in colder waters, high wind speeds over the Southern Ocean drive rapid gas exchange across the air-sea interface, and deep ocean mixing in the high southern latitudes provides an efficient connection between the atmosphere and the very large carbon reservoir in the deep ocean [e.g., *Siegenthaler and Sarmiento,* 1993; *Siegenthaler*, 1983]. The Southern Ocean therefore plays an important role in the global carbon cycle and its effects are not yet fully understood.

5.3 Spatial variations of atmospheric CO_2 in the marine boundary layer in the Pacific Ocean

Despite its importance, quantitative estimates of CO_2 uptake by the Southern Ocean remain poorly defined. This is because net fluxes are small, spread over large ocean areas, vary with time, and occur in an inhospitable environment. One of the greatest limitations to the determination of the Southern Ocean sink is the sparse data in this region [e.g., *Trolier et al.*, 1996]. Further measurements in the Southern Ocean are therefore useful to increase understanding. Measurements made from a NIWA research vessel in the Southern Ocean are now presented. These are later compared to samples collected in the upper-troposphere in section 5.3.4. Further measurements from ship voyages in the northern Pacific Ocean investigate other spatial variations of atmospheric CO_2 (section 5.3.2).

5.3.1 South Pacific Ocean

A NIWA research vessel (*R.V. Tangaroa*) was used as a platform for collecting samples in February 1999 on a voyage between Wellington, New Zealand (41 °S) and ~62 °S in the Southern Ocean. This voyage was for the purpose of the Southern Ocean Iron Enrichment Experiment (SOIREE). The aim of SOIREE was to travel into the Southern Ocean where it is hypothesised that although the Southern Ocean is very nutrient rich, iron limits the primary productivity of phytoplankton in this region. Iron was released into the ocean to fertilise a 50 km^2 "patch" and an array of measurements were performed to gain data to enable any iron-mediated affects on the patch to be determined (*e.g.* monitor carbon uptake as a result of increased phytoplankton productivity). The experiment was performed at ~61 °S, ~140 °E, south of the Antarctic Polar Front and North of the Southern Antarctic Circumpolar Current. Approximately 2 weeks were spent at the site before return to Wellington. To obtain transects, samples were collected during passage to and from the site. Only the southernmost sample on the northbound voyage was sampled within the approximate area of the patch.

5.3.1.1 Air sample collection

Sample collection procedures have been previously described in section 4.5.1 (page 75). Local contamination was avoided by sampling forward of the ships exhaust funnels 25 m above sea level from the highest point on the ship. Four samples were collected on the southbound voyage, before the iron release and the remaining seven were sampled on the return northbound voyage (~2 weeks later). On average the samples were collected at intervals of ~3.5 degrees of latitude. All samples were analysed at NIWA after a storage period of ~1 month.

5.3.1.2 Results

Air parcel back trajectories for the air samples collected during the Southern Ocean voyage are shown in Figure 5.11.

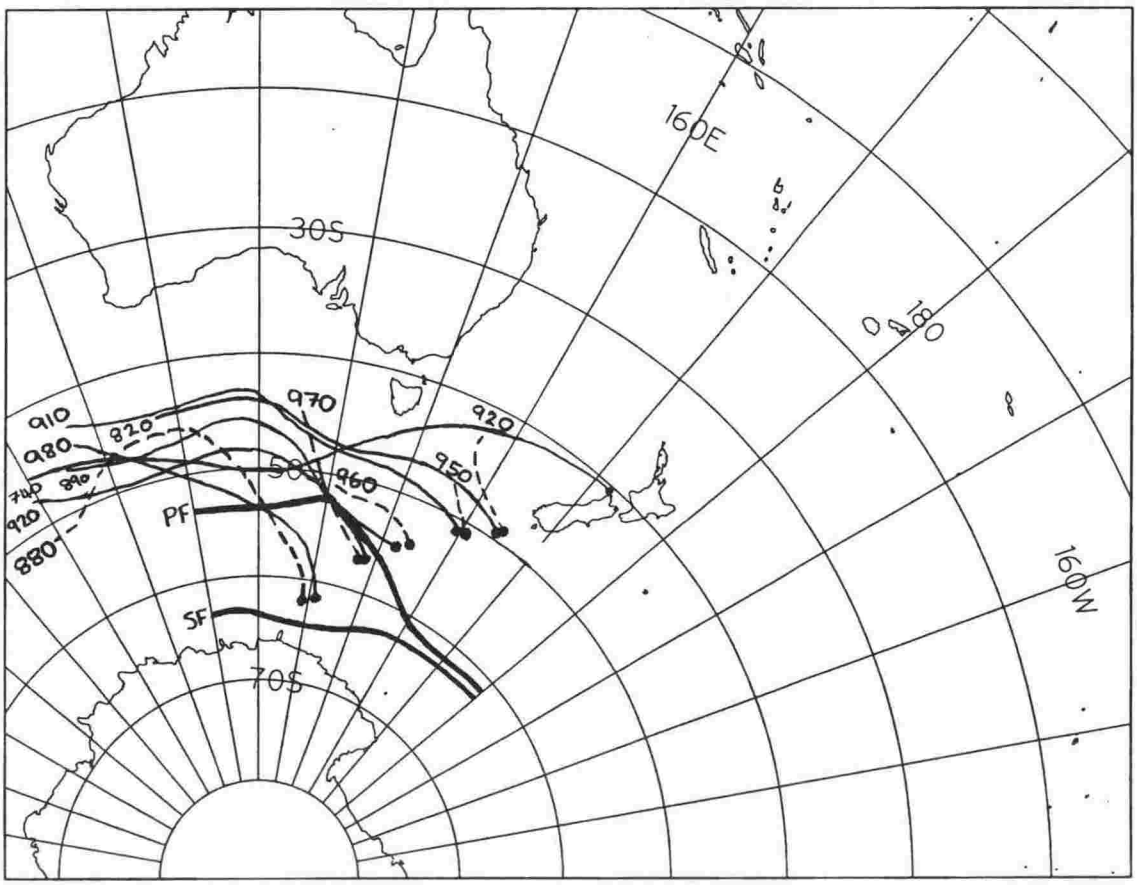

Figure 5.11 4-day back trajectories for air parcels arriving at *R.V. Tangaroa* at time of sample collection for the southbound voyage (dashed lines) and the northbound voyage (solid lines).
The back trajectories are calculated as previously described in Figure 5.3 (page 103). It was not possible to calculate the first 4 southbound back trajectories to 4 days due to missing data in the New Zealand Meteorological Service archived data. The pressure level of the air parcel at its origin (in most cases 4 days before collection) is shown in hPa. The positions of the Antarctic Polar Front (PF) and the Southern Antarctic Circumpolar Current Front (SF) are also shown.

The back trajectories indicate the origin of the airmass sampled. As can be seen most samples were collected from clean Southern Ocean air. The origin pressure level of the back trajectories is also shown, indicating that most air parcels were from below 800 hPa, while the last northbound sample descended from a relatively high level of ~740 hPa.

CO_2 mixing ratio, $\delta^{13}C$, and $\delta^{18}O$ measurements from the Southern Ocean voyage are shown in Figure 5.12.

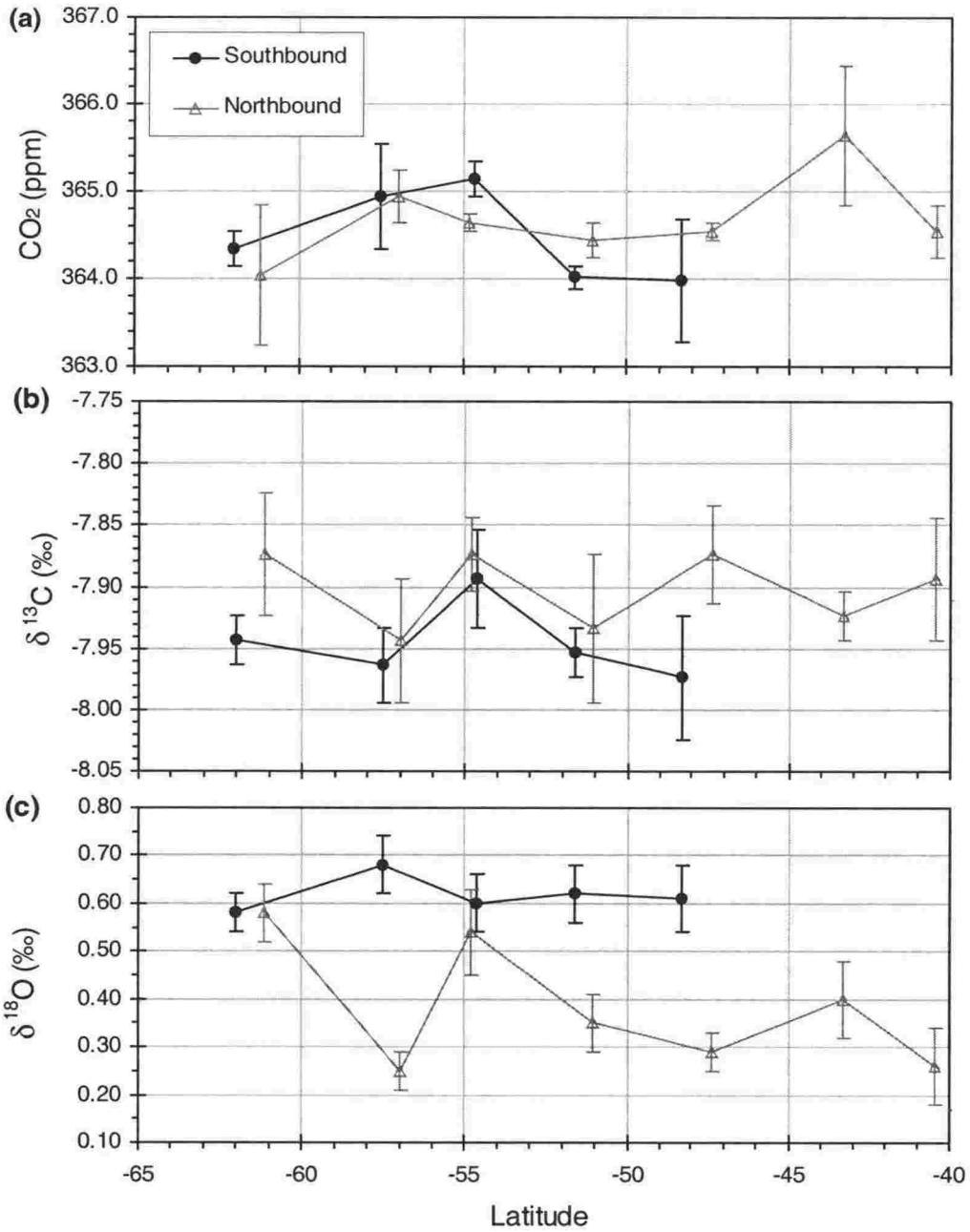

Figure 5.12 GC-IRMS measurements of (a) CO_2 mixing ratio (b) $\delta^{13}C$ and (c) $\delta^{18}O$ for the Southern Ocean voyage, February 1999.

During the southbound voyage, no significant trends were observed for all species over the region sampled. During the northbound voyage, an increase of ~0.7 ppm (~0.03 ppm/degree) was observed for CO_2 mixing ratio and $\delta^{13}C$ was on average ~0.05 ‰ higher than during the southbound voyage. However, variations between 51 °S and 58 °S were very similar, suggesting stability of this region during the two weeks between the voyages. The trough observed between ~43 °S and ~56 °S, where CO_2 mixing ratio was lower by up to ~1 ppm, is consistent with a sink in this region.

During the northbound voyage a decrease of ~-0.2 ‰ was observed for $\delta^{18}O$ (~-0.01 ‰/degree), whereas $\delta^{18}O$ for the southbound voyage was relatively constant at 0.6 ‰. $\delta^{18}O$ was observed to be up to ~0.4 ‰ more depleted during the northbound voyage, compared to the southbound voyage, and on average, an offset of ~-0.25 ‰ was present for $\delta^{18}O$ between these voyages.

The back trajectories indicate that, during the northbound voyage the sampled airmass was generally of a more southerly origin. The depleted $\delta^{18}O$ observed in this leg of the voyage may therefore be due to the depleted $\delta^{18}O$ in ocean surface water at high latitudes (which *Ciais et al.,* [1997a] attribute to the melting of ice sheets in summer and input of freshwater that is depleted in $\delta^{18}O$). In addition, the sample collected at 57 °S during the northbound voyage was observed to be depleted in $\delta^{18}O$ by ~0.25 ‰ compared to its adjacent samples. The back trajectory for this sample shows that the source level is ~920 hPa and that the airmass was subject to a lower average altitude during the 4 days before collection. Larger contact with the depleted surface water $\delta^{18}O$ values over this region may therefore provide an explanation for depleted $\delta^{18}O$ of this sample compared to the adjacent samples.

Back trajectory analyses indicate that air parcels sampled during the northbound voyage were from different origins than that sampled during the southbound voyage. An examination of the inverse CO_2 mixing ratio versus $\delta^{13}C$ plots, provides further information about these sources (Figure 5.13(a)). As a further check on the sample integrity, the correlation between CO_2 mixing ratio and condensation nuclei (CN^*) are also presented (Figure 5.13(b)).

---

* CN was collected during the SOIREE voyage using a TSI, model 3010, CN monitor to measure the concentration of airborne particles with diameter larger than 1 nm. 5 minute averages prior to the time of sample collection were used.

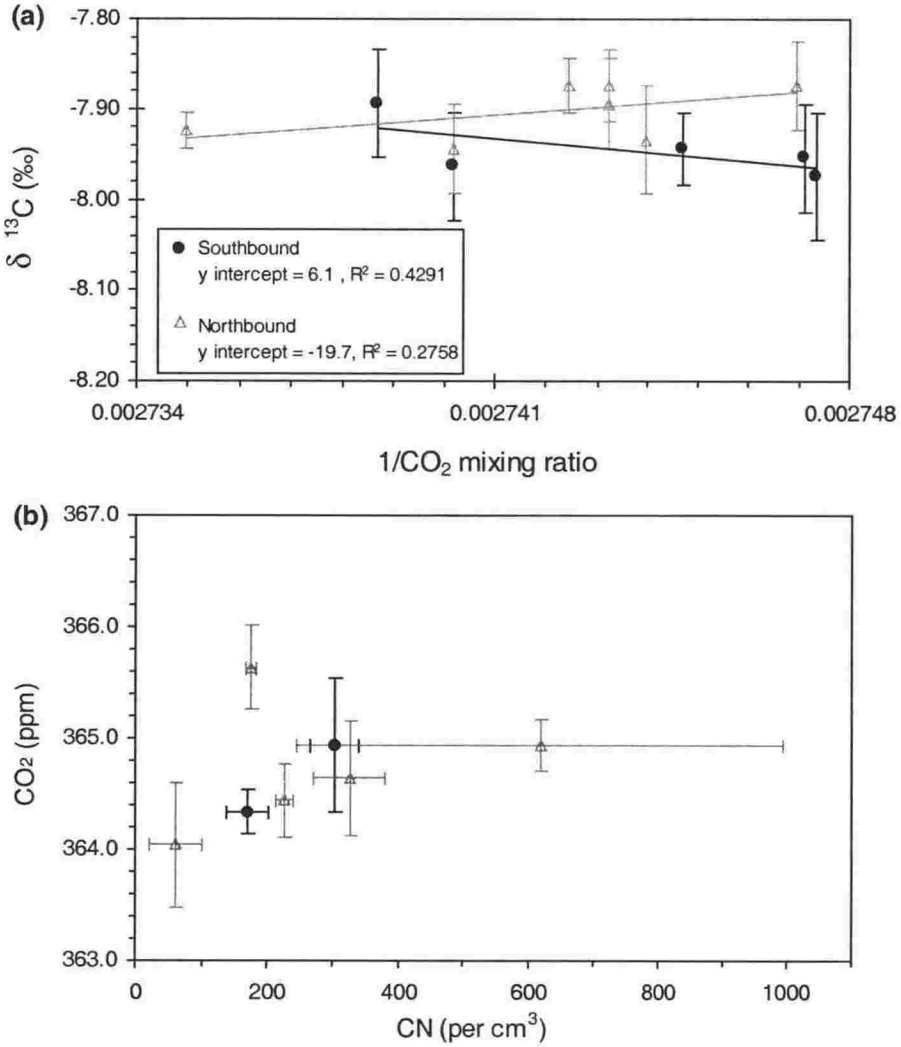

Figure 5.13 (a) $1/CO_2$ mixing ratio versus $\delta^{13}C$ and (b) CO_2 versus CN for the southbound (solid circles) and northbound legs (hollow triangles) for the Southern Ocean voyage, February 1999.

Because the coefficient of determination for the lines fitted to Figure 5.13(a) were low, source estimates of sufficient precision could not be determined for the northbound and southbound voyage. The high error is mainly due to the sparse data, rather than a problem with the measurement uncertainty. In addition, the integrity of the samples must be considered when considering each measurement (*e.g.* 10-day back trajectories would possibly allow rejection of the samples collected on the southbound voyage).

Except for two possible outliers, a relatively linear correlation between CO_2 mixing ratio and CN was observed. The first possible outlier, with a CO_2 mixing ratio of ~365.6 ppm is higher than adjacent samples. This higher mixing ratio cannot be attributed to a landmass or any other contaminating source by the 4-day back trajectories. Back trajectories beyond this time are not reliable at these southern latitudes. If they were possible, contamination from continental landmass (*e.g.* Australia) may have indicated

reason for rejection. The second possible outlier, with a high CN of ~600, indicates possible contamination but the large measurement uncertainty associated with this CN measurement lowers the significance of this higher value. CN measurements for the other samples collected during the southbound voyage could not be made because of instrument malfunction.

Other measurements in this region are also very sparse. However, they have shown relatively constant levels over this region (*e.g., Vay et al.*, [1999] observed a CO_2 mixing ratio of ~361 ± 1 ppm in September to October 1996). Previous isotopic measurements over this region were also relatively constant at ~-7.75 ‰ between January to March 1993 and ~-7.80 between July to September 1993 [*Francey et al.*, 1995]. The GC-IRMS measurements presented here therefore agree with these previous measurements when decadal trends and measurement uncertainties are considered.

5.3.2 Inter hemispheric CO_2 gradients

To investigate the Pacific region north of that examined during the Southern Ocean voyage, a container ship that makes frequent voyages between New Zealand and the West Coast of the United States of America was used as a platform for collecting whole-air samples representative of the Pacific Ocean region. Measurements from the Argentina Star (Blue Star Line Shipping Company, London – now part of P&O Nedlloyd) which made journeys from: Auckland, New Zealand to Los Angeles, USA via Suva, Fiji in March 1998; and Auckland, New Zealand to San Francisco, USA via Suva, Fiji and Honolulu, Hawaii, USA in September 1998 are presented.

5.3.2.1 Air sample collection

Sample collection procedures were identical to those previously described in section 4.5.1 (page 75). Local contamination was avoided by sampling forward of the ships exhaust funnels 25 m above sea level from either side of the ships bridge depending on the on-board wind direction. Samples were collected approximately every 5° of latitude from ~35° S to ~35° N and more frequently (approximately every 2.5°) near the ITCZ. During the first voyage in March 1998, samples were collected wet, whereas samples were chemically dried (as previously described in section 4.5.1) during the September 1998 voyage. All samples were analysed at NIWA after a typical storage period of ~2 months.

5.3.2.2 Results

Air parcel back trajectories and the position of the South Pacific Convergence Zone (SPCZ) and ITCZ for the Pacific voyages in March and September 1998 are shown in Figure 5.14.

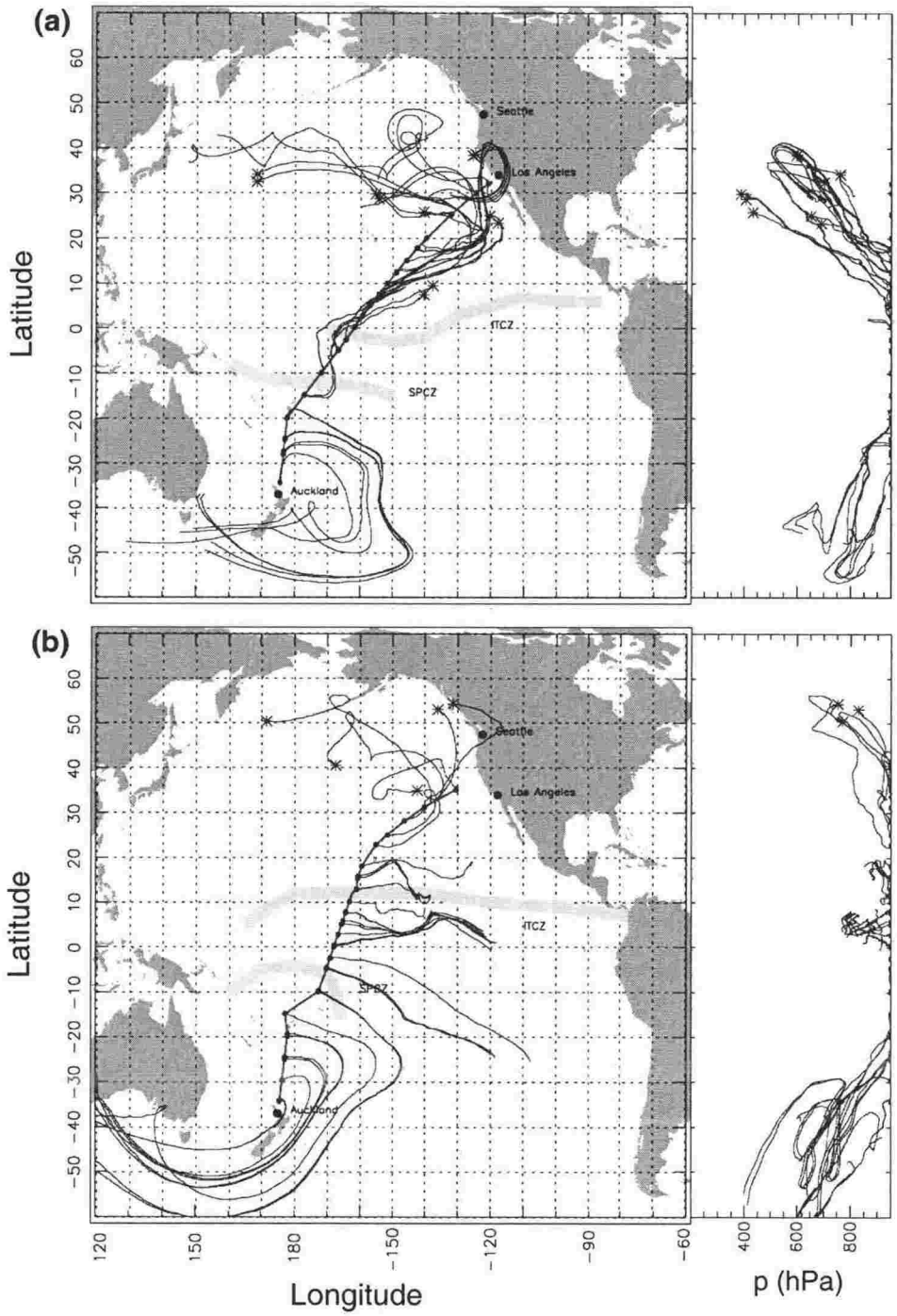

Figure 5.14 10-day back trajectories (LH panel) and pressure levels (RH panel) for air samples collected during the Pacific Ocean voyages in (a) March 1998 and (b) September 1998.

Errors associated with the back trajectories at 10 days are ~1 grid square horizontally and ~200 hPa vertically. The positions of the ITCZ and SPCZ are also shown. The back trajectories are calculated as previously described in Figure 5.3, page 103.

An independent check on the integrity of the calculated back trajectories was performed using the automated NASA algorithm that is the freely available by emailing the details of the required back trajectories (latitude, longitude, date, etc.) to [science@hyperion.gsfc.nasa.gov]. In this check, no significant differences were observed for most samples, but some 10-day back trajectories were offset horizontally and vertically from those presented here by up to ~2,000 km and ~200 hPa.

The back trajectories indicate the recent origin of the airmass sampled and give clues as to what processes have influenced it. CO_2 sources (*e.g.* the terrestrial biosphere, fossil fuel and biomass burning) contribute to the characteristics of an airmass relatively quickly (within hours). Because atmospheric CO_2 has a long lifetime compared to this, it retains these contributions and over time these contributions become so well mixed within the atmosphere that nearly the same growth rate is observed globally. However, within a relatively short time (~days), the characteristics of the airmass are altered by these sources so that the effect of any sources that were not far away at the time of sampling are relatively undiluted and clearly observed. Over a longer period (towards 10 days) the effects of sources and sinks are more diluted. However, if an airmass has only been exposed to a relatively homogeneous region (*e.g.* the mid-Pacific Ocean) mixing of the airmass with the surrounding atmosphere does not strongly dilute the airmass characteristics during its path and the longer back trajectory has higher confidence.

In March 1998, the SPCZ tended to separate the Pacific Ocean into two main regions such that south of the SPCZ the sampled air was from an origin between ~35 ^{o}S to ~50 ^{o}S and north of the SPCZ sampled air was from an origin between ~10 ^{o}N to ~40 ^{o}N. The samples collected between 10 ^{o}N and 20 ^{o}N passed over the Western Coast of the USA. However, the pressure levels for the collected samples indicate that for most samples, the sampled airmass has descended from ~600 to ~800 hPa. Two samples descended from ~400 hPa. In September, the SPCZ and ITCZ had shifted north by ~5 degrees and ~10 degrees respectively and tended to separate the Pacific Ocean into three main regions: 1) South of the SPCZ, sampled airmass was from south of New Zealand; 2) between the SPCZ and the ITCZ, the sampled airmasses were predominantly from the Eastern Pacific Ocean; and 3) North of the ITCZ, sampled airmasses were from regions north of ~10 ^{o}N. The pressure level of most collected samples in September were lower than those for March, especially north of the SPCZ.

CO_2 mixing ratio, $\delta^{18}O$ and $\delta^{13}C$ measurements from these voyages are shown in Figure 5.15.

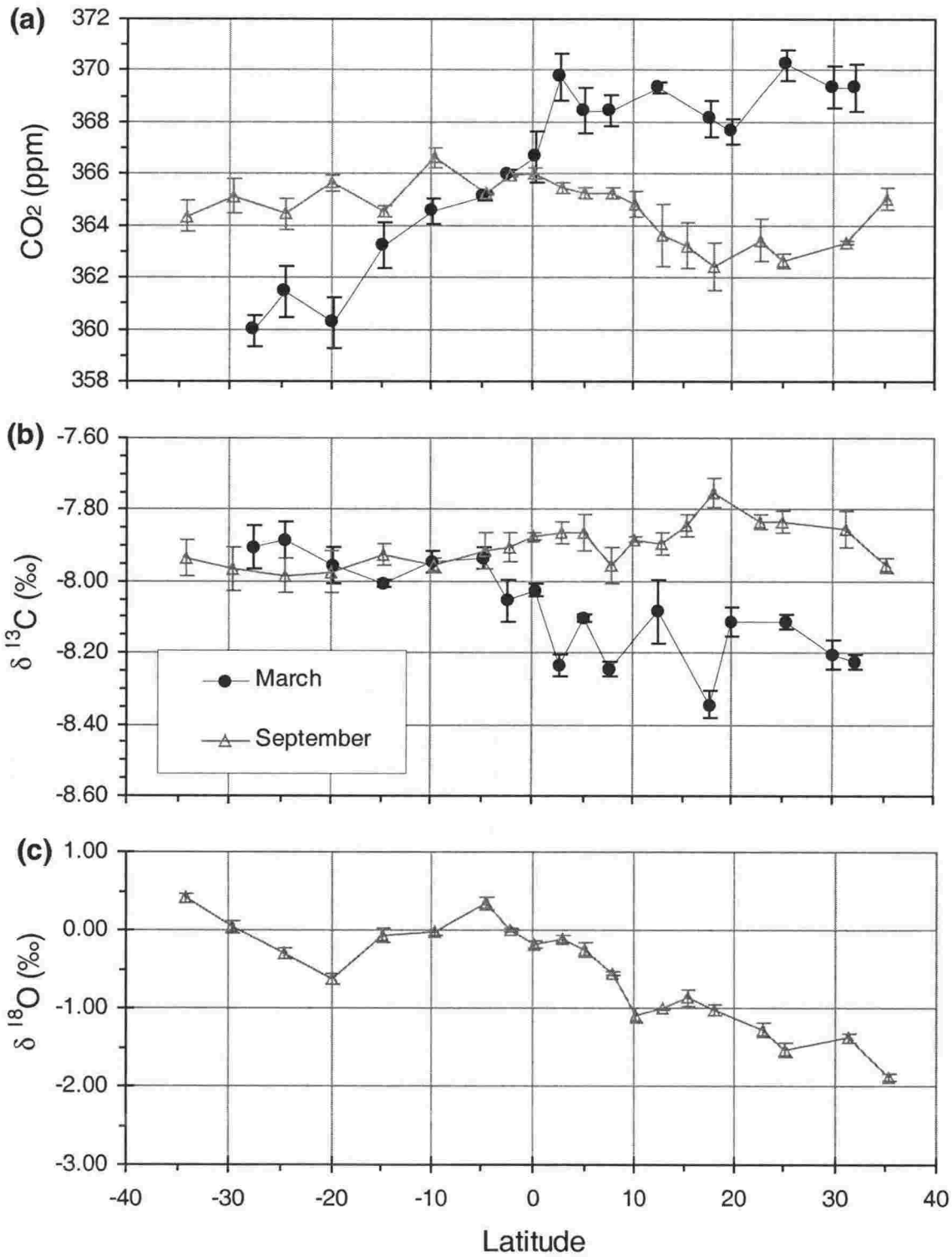

Figure 5.15 Inter hemispheric gradients of (a) CO_2 mixing ratio (b) $\delta^{13}C$ and (c) $\delta^{18}O$ in March 1998 (solid circles) and September 1998 (hollow triangles).

In March 1998 a strong inter hemispheric gradient was observed for CO_2 mixing ratio and $\delta^{13}C$. CO_2 mixing ratio increased from a relatively low value of ~360 ppm south of the SPCZ where back trajectories originated from the Southern Ocean, to high mixing ratio of ~370 ppm north of the SPCZ and ITCZ, where back trajectories originated from

the Northern Hemisphere. The steadily increasing CO_2 mixing ratios south of the SPCZ and ITCZ, and sharp rise north of the ITCZ imply that some meridional transport through the SPCZ was occurring, but that the ITCZ was acting as an effective barrier to such transport. It therefore appears that the 'barrier effect' of the SPCZ was low during March 1998, contrary to previous observations that it is usually strongest near this time of the year [*Vay et al.,* 1999]. Samples collected between 10 °N and 20 °N did not appear to be influenced by their passage over the West Coast of the USA, most likely because the air-parcels were still at relatively high levels (~400 to 600 hPa) as they passed over the continental land mass. This large inter hemispheric gradient for CO_2 mixing ratio of ~0.14 ppm/degree was anti-correlated to a $\delta^{13}C$ inter hemispheric gradient of ~-0.006 ‰/degree. The observed inter hemispheric gradient in March 1998 was most likely due to fossil fuel CO_2 release in the Northern Hemisphere winter, shown by the marked mixing ratio increase and more depleted isotopic signature that is associated with CO_2 of fossil fuel origin.

In September 1998, exactly six months later, the seasonal cycle is reversed. The terrestrial origin of the back trajectories and slightly depleted $\delta^{13}C$ values in the Northern Hemisphere (by ~0.2 to ~0.3 ‰) indicate a small fossil fuel release signal. The ~2.5 ppm lower mixing ratio north of the ITCZ and the high latitude origin of the back trajectories indicate that a large CO_2 uptake occurred during the Northern Hemisphere growth season. The large latitudinal decrease of ~2.3 ‰ for $\delta^{18}O$ in September 1998 (~0.03 ‰/degree) from ~35 °S to ~35 °N is typical of other observations over this region [e.g., *Francey et al.,* 1995]. The large latitudinal change of $\delta^{18}O$ between the Southern Hemisphere and the Northern Hemisphere is most likely due to the effect of plant photosynthesis and soil respiration which is larger in the Northern Hemisphere [*Tans et al.,* 1998; *Francey and Tans*, 1987; *Ciais et. al.,* 1997b]. CO_2 exchange with leaf (and possibly soil) water in the Northern Hemisphere is larger due to the larger landmass and is also accentuated by the summer growth season that occurs approximately between June and October.

Observations by *Vay et al.*, [1999] in September 1996 showed a relatively constant CO_2 mixing ratio of ~365 ppm between 40 °S and the Equator. The GC-IRMS measurements presented here for September 1998 are higher than this by ~4 ppm. About 3 ppm of this difference may be attributed to the global growth of CO_2 over this period (~1.5 ppm/year), but due to the variability of the CO_2 growth rate, this amount may be different. The remaining difference of ~1 ppm may be due to other reasons (*e.g.* decreased Pacific Ocean uptake in this region during the voyages, discrepancies between the sampling procedures between the observations, or calibration issues). Observations in 1993 over the entire

NOAA CMDL global network [*Ciais et al.*, 1995b] showed that from January to March $\delta^{13}C$ was ~-7.75 ‰ at 40 °S and decreased to ~-8.00 ‰ at 30 °N. In July to September the measurements showed an increase from ~-7.80 ‰ at 30 °S to ~-7.60 at 30 °N. These measurements agree with the GC-IRMS measurements presented here when decadal trends and measurement uncertainties are considered.

Because the two voyages were six months apart and within ~2 months of the maxima and minima of the seasonal cycles of CO_2 in both hemispheres, the extent of these cycles could be approximately estimated. For CO_2 mixing ratio and $\delta^{13}C$, the peak to peak amplitude of the seasonal cycle in the Northern Hemisphere was observed to be larger than that observed in the Southern Hemisphere. The observed seasonal cycles (~1.5 ppm and ~0.02 ‰ in the Southern Hemisphere, and ~7ppm and ~0.4 ‰ in the Northern Hemisphere for CO_2 mixing ratio and $\delta^{13}C$ respectively) were comparable to other data reported for this region [e.g., *Conway et al.*, 1994; *Trolier et al.*, 1996].

Estimates of the CO_2 source origin (terrestrial versus oceanic) are provided by plots of the inverse CO_2 mixing ratio versus $\delta^{13}C$ (Figure 5.16).

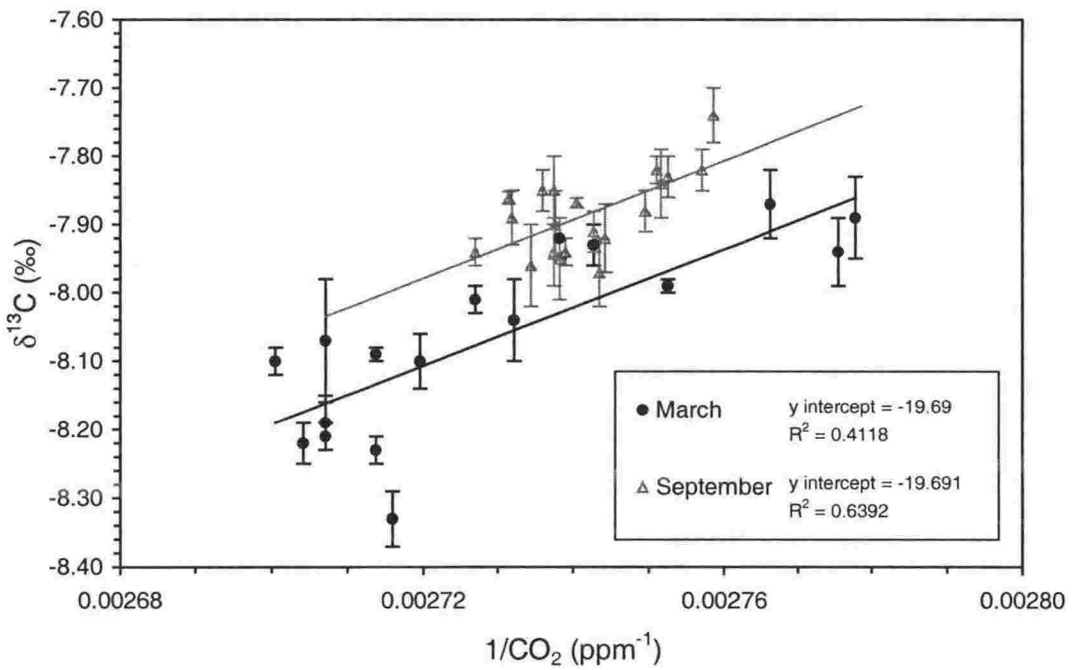

Figure 5.16 $\delta^{13}C$ versus $1/CO_2$ mixing ratio for air samples collected during Pacific Ocean voyages between 35 °S and 35 °N in March and September 1998.

The source signatures are a result of all contributing sources of the sampled airmass (*e.g.* oceanic and biospheric CO_2) and are indicated by the y intercepts of the inverse CO_2 mixing ratio versus $\delta^{13}C$ plot. The data presented here indicate that the sampled CO_2 is of

the same source for both voyages at ~-19.69 ‰. Such a source is predominantly due to the terrestrial biosphere [*Trolier et al.*, 1996].

More extensive and long-term measurements of the type presented here allow global carbon cycle models to calculate the partitioning of CO_2 between its various sources and sinks [*Francey et al.*, 1995]. In addition, the inter calibration and inter comparison exercises established during this work would enable the merging of such GC-IRMS data with that of established global networks in the future. This would increase the spatial and temporal resolution of measurements of atmospheric CO_2 and enable increased understanding of the global carbon cycle. Hence, performing this work in the future is an important task.

5.4 Upper-tropospheric CO_2 between New Zealand and Antarctica and comparison to marine boundary layer measurements

Measurements from aircraft are one of the most promising methods for determining spatial and temporal variations of atmospheric CO_2 species. This is because air samples collected on board aircraft are mostly free from the influence of regional sources and sinks of atmospheric CO_2 [*Nakazawa et al.*, 1992]. Measurements from upper-tropospheric air samples collected from a Royal New Zealand Air Force (RNZAF) C130 Hercules aircraft during a flight between New Zealand and Antarctica are now presented. These measurements are also compared to measurements made in the marine boundary layer at Baring Head, Cape Grim, and Arrival Heights and those from the Southern Ocean voyage.

5.4.1 Upper-tropospheric air sample collection

A computer-controlled portable flask sampling unit, consisting of two cases, was used for aircraft sample collection. The first case, which contains twenty 1 litre glass flasks fitted with ultra high vacuum valves and inert Teflon® PTFE o-rings, (Glass Expansion Pty, Ltd. Victoria, Australia) is linked to the second case. The second case contains a battery pack and a metal bellows pump (Senior Flexonics, Metal Bellows Division, Sharon, MA, USA) which is used to fill the flasks to a pressure of ~150 kPa. Samples can be collected at pre-determined latitudes by interfacing the unit to a Global Positioning Satellite (GPS) receiver or collected at operator selected times during the flight. Air samples were collected at an average altitude of ~8,700 m between New Zealand and Antarctica. The flight path during which samples were collected was essentially that of the

3,583 km distance between Christchurch, New Zealand and Ross Island, Antarctica shown in Figure 5.8 (page 111). Samples were collected without drying and were analysed within two months of collection.

5.4.2 Upper-tropospheric results

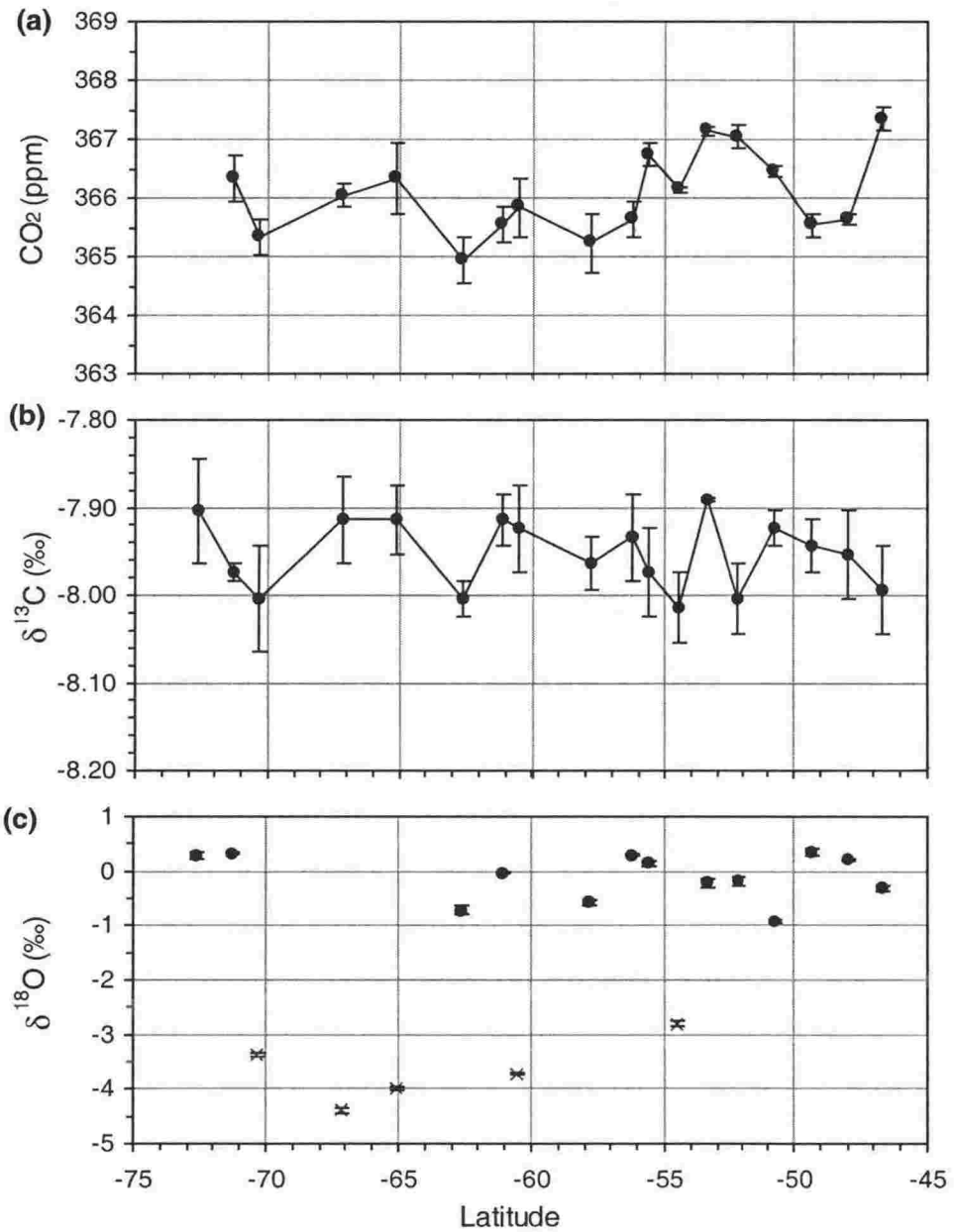

Figure 5.17 GC-IRMS measurements of (a) CO_2 mixing ratio (b) $\delta^{13}C$ and (c) $\delta^{18}O$ for upper-tropospheric air collected at ~8,700 m, between 45 °S and 75 °S, November 1998.
$\delta^{18}O$ measurements marked with a cross in (c) were rejected for the calculation of the trend line for $\delta^{18}O$.

Some of the observed variability in the upper-tropospheric air samples may be due to the fact that half of the samples were collected during the southbound flight, and half

during the northbound flight, 1 day later. Because the samples were collected without drying, very depleted $\delta^{18}O$ values were most likely due to contamination from H_2O and subsequent fractionation due to ^{18}O exchange. It is thought that the source of this H_2O was from ice-crystals in high-level cirrus clouds that that the aircraft passed through which may have later melted to form liquid H_2O that would be available for fractionation.

Over the latitudinal range measured, CO_2 increased by ~1 ppm. $\delta^{13}C$ and $\delta^{18}O$ trends were not significant when measurement uncertainties and the scatter of the data were considered.

5.4.3 Comparison of upper troposhperic and marine boundary layer measurements

Previously presented measurements in the Southern Ocean are now compared to upper-tropospheric measurements (Figure 5.18).

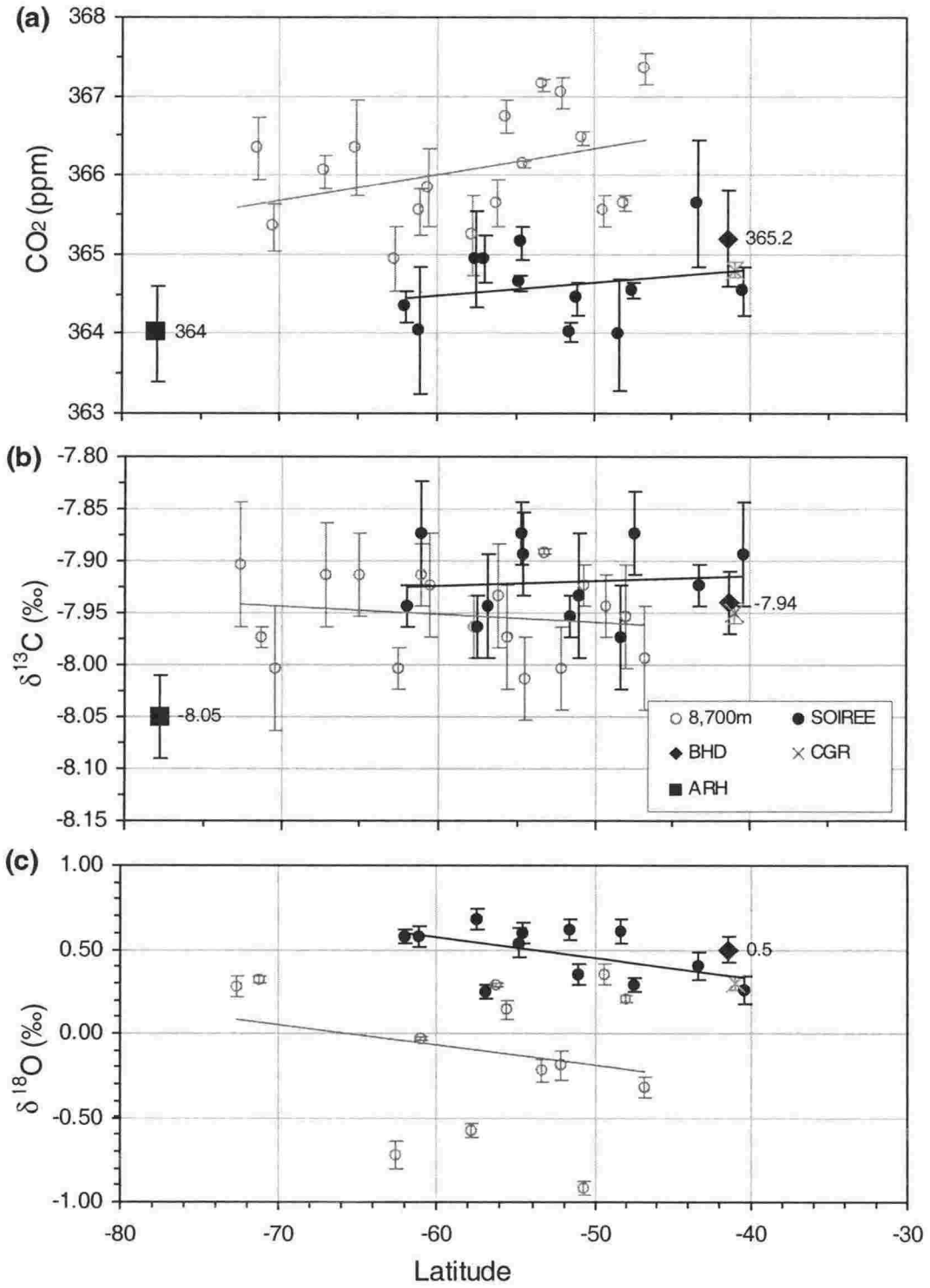

Figure 5.18 Comparison of Southern Ocean marine boundary layer measurements collected in February 1999 (SOIREE, solid circles) with upper-tropospheric air samples collected at 8,700 m in February 1998 (hollow circles).

In addition, average values in February 1999 for samples collected at Baring Head (solid diamond), Cape Grim (cross) and Arrival Heights (solid square) are given.

In the Southern Hemisphere, upper-tropospheric CO_2 mixing ratio levels are normally elevated with respect to surface measurements. This is for two reasons. First, the CO_2

sink at the surface of the Southern Ocean causes reduced CO_2 levels at the surface in this region. Second, Northern Hemisphere air is transported in to the upper-troposphere of the Southern Hemisphere, and top-down diffusion of this air results in elevated CO_2 levels in the upper-troposphere of the Southern Hemisphere [*Vay et al.,* 1999]. Compared to the levels observed during the Southern Ocean voyage, upper tropospheric air (although 1 year earlier) was elevated in CO_2 by ~1 ppm and depleted by ~0.02 ‰ for $\delta^{13}C$. However, if the marine boundary layer and upper-tropospheric samples were collected at the same time, the observed difference may have possibly been larger, due to the inclusion of the average CO_2 growth rate (~1.5 ppm/year) into the upper-tropospheric samples. However, CO_2 at Arrival Heights experienced a sharp decline to ~364 ppm in January 1999 and, as previously discussed in section 5.2.3.2 (page 112), the value shown in Figure 5.18 may be an outlier. Other research has shown that the seasonal cycle for upper tropospheric CO_2 lags that at the surface by ~1 month [*Nakazawa et al.,* 1992]. Comparing the observed CO_2 mixing ratio at Arrival Heights in December 1999 (~367 ppm) with the two most southern upper-tropospheric air samples (~365.5 ± 0.6 ppm), a higher CO_2 mixing ratio at Arrival Heights was observed in 1999 than was observed in the upper-troposphere in 1998. Furthermore, these two observations are approximately equal if the average growth rate of CO_2 is taken into consideration. Such agreement would be expected because the strong radiative cooling of Polar Regions causes widespread sinking of air, therefore transporting the upper tropospheric air that has elevated CO_2 to the lower troposphere.

The observed CO_2 gradients for the Southern Ocean samples were approximately equal to that observed over the entire land-based measurement range between Baring Head, Cape Grim and Arrival Heights. This gradient was also approximately equal to that observed in the upper-troposphere but was offset by ~-1.5 ppm. The Southern Ocean sink in this region most likely accounts for the lower surface values, but as previously discussed, transport of Northern Hemisphere air into the upper-troposphere of the Southern Hemisphere is also important.

With the exception of Arrival Heights, observed $\delta^{13}C$ were approximately equal at all sites (within measurement uncertainties). $\delta^{13}C$ at Arrival Heights was depleted by ~0.1 ‰. The upper-tropospheric air samples were collected a year before the measurement at Arrival Heights that is shown in Figure 5.18, but comparing a $\delta^{13}C$ measurement at Arrival Heights in February 1998 (~-7.92 ‰, interpolated from Figure 5.9, page 113) closer agreement is observed.

Observed latitudinal gradients for $\delta^{18}O$ were also approximately equal between the surface and the upper-troposphere. Upper tropospheric $\delta^{18}O$ measurements were depleted

by ~0.6 ‰ relative to surface measurements. Because of the lack of drying for the upper-tropospheric samples, their reduced integrity lowers the significance of this observation. However, because ocean water is depleted for $\delta^{18}O$ over this region [*Ciais et al.*, 1997b], $\delta^{18}O$ in atmospheric CO_2 collected near the surface would also be expected to be depleted in $\delta^{18}O$, rather than the enriched $\delta^{18}O$ measurements that were obtained over this region and the reason for the observation is unknown at present.

Further spatial and temporal measurements of $\delta^{13}C$, $\delta^{18}O$, and CO_2 mixing ratio are therefore required to more quantitatively understand the Southern Ocean region.

As demonstrated by the measurements presented in sections 5.2 and 5.3, the new GC-IRMS technique developed here has proven useful for monitoring atmospheric CO_2 and its stable isotopes over large spatial and temporal scales. This is what the technique was designed for. However, as the next section shows, the small sample requirements of the GC-IRMS technique ease the logistics for sample collection and provides opportunities for varied research.

5.5 Small-scale application: Soil-respired CO_2

An example of the application of the technique on a measurement scale many orders of magnitude smaller than those presented in the preceding sections of this chapter, is the analysis of soil-respired CO_2 sampled from chambers. Chamber-sampling studies of soil-respired CO_2 are potentially limited by the amount of sample required for analysis. This is because the sample volume withdrawn from the chamber must be minimised so that, after a sample is collected from the chamber, the chamber/soil pressure differential is small so as to avoid CO_2 from being "sucked" out of the ground. The small sample requirements of GC-IRMS allow this criteria to be met, while at the same time achieve relatively high precision.

In collaboration with Landcare Research, New Zealand, a pilot study of soil-respired CO_2 (respiration from roots, soil organic matter and recent inputs to soil organic matter) from a mountain beech forest was undertaken to identify how hydraulic limitation alters carbon fixation for the ecosystem in the study. Researchers at Landcare, New Zealand had found that older taller trees have lower stomatal conductances and lower photosynthesis rates due to differences in hydraulic pathway resistance. Based on the previous research by *Ehleringer and Cook* [1998], it was hypothesised that these differences should lead to variations in the discrimination of ^{13}C in photosynthesis. Assuming that this difference would be reflected in all of the recent organic matter in the ecosystem, this pilot study

investigated the hypothesis by measuring soil-respired CO_2 mixing ratio and $\delta^{13}C$ isotopic composition from young trees (~15 years of age) and from old trees (greater than 150 years old). Previous research by *Ehleringer and Cook* [1998], utilised samples collected in the forest canopy, which are difficult to obtain. Should this chamber sampling technique work, the logistics of sample collection will be considerably eased, and may allow for more extensive measurements to be made to increase understanding of photosynthetic processes in forest ecosystems.

The location of the sampling site was at Cragieburn Forest Park, ~60 km west of Christchurch, New Zealand. A Mountain Beech (*Nothofagus solandri var. cliffortioides*) forest was investigated in this study.

5.5.1 Air Sample collection

A chronosequence of measurements were taken from a closed-top, 3 litre chamber (footprint ~ 0.03 m^2) placed over the ground in each respective forest site. Over ~4.5 hours, 5 air samples were periodically collected from the chamber at each site. To ensure negligible soil/chamber pressure differentials, no more than 5 % of the volume of the chamber was removed for each sample. For this 3 litre chamber, 150 ml samples were collected at ambient pressure by attaching evacuated flasks to the chamber sample-port and opening the flask valve. Wet samples were collected for this initial study, as only CO_2 mixing ratio and $\delta^{13}C$ measurements were required.

5.5.2 Results

The results from this initial pilot study are shown in Figure 5.19.

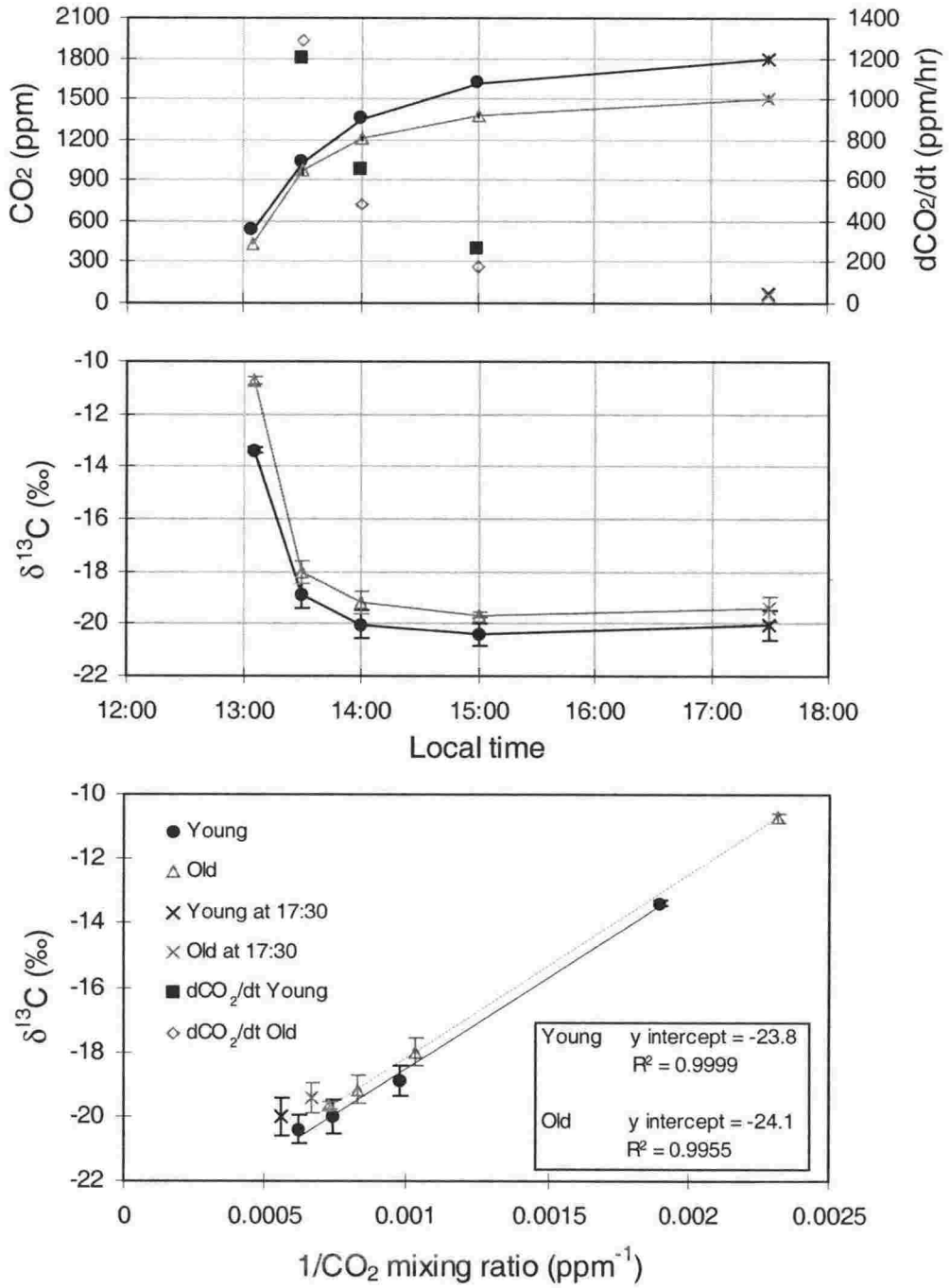

Figure 5.19 GC-IRMS measurements of (a) LH axis, CO_2 mixing ratio versus local time and RH axis, rate of CO_2 mixing ratio change dCO_2/dt (b) $\delta^{13}C$ versus local time and (c) $1/CO_2$ mixing ratio versus $\delta^{13}C$ for soil-respired CO_2 emitted into a chamber from young (solid circles) and old (hollow triangles) Mountain Beech trees at Cragieburn Forest Park.

Values at 17:30 are shown as crosses and are not used in the linear regression lines fitted to the remaining data.

During the period of collection CO_2 mixing ratio increased from ~500 ppm to almost 1800 ppm, while the isotopic ratio shifted from ~-11 ‰ to ~-20 ‰. A higher amount of CO_2 was respired by the more active younger forest compared to the older forest. This

higher activity was also reflected in the $\delta^{13}C$ isotope ratio which was on average depleted compared to the older forest by ~1 ‰. Of note is the first pair of samples, just after 13:00, that were collected approximately 10 minutes after the chamber was placed over the ground. For these two samples a significant proportion of the ambient atmosphere (which is more depleted for the younger forest) contributes to the observed signal. This accounts for the larger difference between the young and old forests that is present at this time compared to later times when the soil and recent organic matter in the ecosystem contribute more to the signal.

The isotopic signature of a CO_2 source ($\delta^{13}C_{source}$) that diffuses into and perturbs the original airmass ($\delta^{13}C_{perturbed}$, $CO_{2perturbed}$) is described by:

$$\delta^{13}C_{perturbed} = \delta^{13}C_{source} + m/CO_{2perturbed} \quad (5.1)$$

Therefore, the intercept from a plot of $\delta^{13}C$ versus the inverse of CO_2 mixing ratio (referred to as "Keeling plots") indicates the ecosystem ^{13}C discrimination. From Figure 5.19 (c), source signatures were (-23.8 ± 0.01) ‰ for the old forest and (-24.1 ± 0.1) ‰ for the young forest. The samples collected at 17:30 were not used in the linear regression because these samples have the largest uncertainty, experience a rise in $\delta^{13}C$ after 15:00, and are offset from the other samples on the Keeling plot. In addition it is thought that a pressure accumulation in the chamber may be present such that after 2 hours the integrity of measurements may be reduced [*Scott,* personal communication, 1999]. The reduced integrity after 2 hours is further highlighted by the non-linear rate of change of CO_2 mixing ratio after 2 hours shown in Figure 5.19(a).

Previous research has suggested that for coniferous trees, older forest stands have hydraulic limitations, which lower photosynthesis rates and leaf intracellular CO_2 values. This results in enriched leaf organic $\delta^{13}C$ [*Yoder et al.,* 1994] for older forests compared to younger forests. Based on previous measurements at Landcare Research, the amount of this enrichment was expected to be ~1.7 ‰, with source signatures for the young forest at ~-26 ‰ and ~-24.3 ‰ [*Scott*, personal communication, 1999]. The difference in $\delta^{13}C$ source signatures determined from this study was in the right direction, but the magnitude (~0.3 ‰) was smaller. Four reasons are likely to have contributed to the discrepancy between the observed and expected $\delta^{13}C$ source signatures. First, the source signal may change with seasonality. Further research is required to determine this possibility. Second, the number of samples collected for this pilot study was low. *Ehleringer and*

Cook, [1998] suggested that up to ~15 – 20 air samples are required for a reliable estimate of such source signatures. Collecting a higher number of air samples in future studies would therefore increase the reliability of these source determinations. In addition, the collection of a larger fraction of these samples in the period in which CO_2 mixing ratio and $\delta^{13}C$ gradients were largest (*i.e.* the first two hours) would be important to more accurately and precisely determine the source signatures from the $1/CO_2$ versus $\delta^{13}C$ plots. Third, the placement of only one chamber in each forest site assumes homogeneity within the forest which may not be true. Additional chambers in forest studies may therefore improve results. Fourth, the measurement uncertainties associated with some samples were relatively high. The high uncertainties associated with these pilot study measurements are partly due to the use of only one reference gas for these analyses (AIR2: CO_2 = 404.19 ppm and $\delta^{13}C$ = -8.192 ‰). When the composition of the sample and reference gas were within ~200 ppm and ~6.00 ‰, CO_2 mixing ratio and $\delta^{13}C$ precisions were ~2 ppm and ~0.1 ‰ respectively. But as the difference between the sample and reference gas became further apart (up to approximately 1500 ppm and -13.00 ‰), CO_2 mixing ratio and $\delta^{13}C$ precision decreased to ~20 ppm and ~0.6 ‰ respectively. However, because the biological signal was large, the precision obtained was sufficient to clearly observe the CO_2 mixing ratio and $\delta^{13}C$ signals versus time (Figure 5.19 (a) and (b)). The non-linearity problems highlighted in Figure 4.7 (page 86) may have been significant in this pilot study because of (reference – sample) differences of up to 1500 ppm for CO_2 mixing ratio and up to -13.00 ‰ for $\delta^{13}C$ were present. It is expected that using another reference gas that has a CO_2 mixing ratio and $\delta^{13}C$ isotopic composition of ~1,000 ppm and ~-15 ‰ respectively would yield a large improvement in obtainable precision for such studies and enable more accurate and precise $\delta^{13}C$ source signature determinations.

In the future, smaller sample volumes may be able to be analysed by GC-IRMS (*e.g.* by using lower volume valves and plumbing). If a lower volume is sampled from the chamber there would be less chance of "sucking" additional CO_2 out of the soil. Conversely, lower sample requirements could improve measurement precision if the same amount is sampled but more aliquots of this sample are analysed.

For future work, drying should be considered, as measuring and understanding $\delta^{18}O$ of CO_2 respired from soils is valuable for partitioning the Net Ecosystem Productivity (NEP) into its two components – photosynthesis and respiration [*Tans et. al.*, 1998]. This would be possible by drying the samples at collection, but would be more difficult to perform while maintaining the small sample usage requirements for this application. This may be

facilitated by simply analysing the samples within ~1 – 2 days of collection. However, other methods may be more effective and reliable. Such a method would be to employ a continuous low-flow sampling procedure, where a small pump passes the air sample through a Nafion drier membrane into the sample flask, which would be collected over a period of ~5 minutes.

This application of the GC-IRMS technique demonstrates its flexibility for varied applications that are made possible by the reduced sample requirements of this technique.

5.6 Summary and discussion

The new technique presented in this thesis has been applied to varied research from large scale studies of the distribution of CO_2 in the Pacific region to small-scale studies of forest soil-respired CO_2.

GC-IRMS measurements over a period of ~1.6 years determined the seasonal cycle of $\delta^{13}C$ in atmospheric CO_2 at Baring Head with maxima occurring around May, minima between August and December, and an amplitude of ~0.05 ‰. This seasonal cycle was approximately anti-correlated to CO_2 mixing ratio. $\delta^{18}O$ were variable and no significant seasonal cycle or trend was observed. These measurements were comparable to other measurements made at this, and other South Pacific sites by traditional techniques.

Further measurements were made at Cape Grim and the temporal variations between Cape Grim and Baring Head were examined. No significant differences were observed and further high precision and high frequency measurements are required to fully investigate the possibility of longitudinal differences between these two sites.

Measurements at Arrival Heights of $\delta^{13}C$ were performed over a period of ~2 years from March 1997 and the CO_2 mixing ratio was monitored for ~8 months from May 1998. A decline of ~-0.1 ‰/year was observed for $\delta^{13}C$ over this period which was larger than expected based on previous measurements at similar latitudes. Southern Ocean variability was the most likely reason for the observed differences between Arrival Heights and Baring Head/Cape Grim. Higher frequency sampling at all sites will help to eliminate seasonal cycle noise in future studies.

Spatial variations of atmospheric CO_2 were investigated between ~62 °S and ~32 °N in the Pacific Ocean by ship-based measurement programs. These data are consistent with a Southern Ocean sink of atmospheric CO_2 between ~43 °S to ~56 °S.

Inter hemispheric gradients between ~35 °S and ~32 °N of up to ~10 ppm and ~0.1 ‰ were observed for CO_2 mixing ratio and $\delta^{13}C$ in March 1998. Six months later, in

September 1998, smaller inter hemispheric gradients were observed for CO_2 mixing ratio and $\delta^{13}C$ because the effect of uptake in the growth season by the terrestrial biosphere in the Southern Hemisphere is small. Measurements of $\delta^{18}O$ in September indicated a large inter hemispheric gradient of ~-2.5 ‰, which was attributed to the strong effect of plant photosynthesis and soil respiration in the Northern Hemisphere. The observed measurements were comparable to previous measurements over this region.

Upper-tropospheric air was measured between New Zealand and Antarctica and was elevated in CO_2 mixing ratio and depleted in $\delta^{13}C$ compared to measurements made in the marine boundary layer. Transport of Northern Hemispheric air into this region and the Southern Ocean sink are important factors that help explain these vertical gradients. $\delta^{18}O$ was subject to fractionation as a result of H_2O contamination. Therefore, future measurements will require drying even at this high level of ~8,700 m to avoid the possibility of sampling of ice-crystals from high-level cirrus clouds.

A small-scale application of the technique for measurements of soil-respired CO_2 observed the biological signal from a chronosequence of samples collected from a small closed-top chamber. The combination of these measurements with $\delta^{13}C$ isotopic measurements allowed the source signatures to be determined for the young and old Mountain Beech forests. The difference between the young and old tree source signatures were in the right direction, but the magnitude was lower than expected. Collecting more samples, using an extra reference gas with an elevated higher CO_2 mixing ratio (~1,000 ppm) and a depleted $\delta^{13}C$ (~-15 ‰), and investigating the seasonality of the source signatures should resolve these discrepancies in further studies. These measurements demonstrated the technique's flexibility for applications that are very different to its original purpose for providing high precision isotopic analyses of background atmospheric CO_2.

The GC-IRMS measurements of many spatial and temporal variations that were comparable to measurements by traditional provides further evidence of the successful performance of this technique.

Future atmospheric sampling work will be improved by obtaining higher spatial and temporal resolution of collected samples. The inter calibration exercise and operational ICPs established by the work outlined in Chapter 4 of this thesis will allow the technique to remain comparable with other laboratories. This will enable the merging of data from spatial and temporal measurements into global carbon cycle models to help achieve the internationally important task of more accurately and precisely monitoring and predicting the future state of the Earth's atmosphere.

6 Summary and conclusions

6.1 GC-IRMS for atmospheric CO_2

6.1.1 The GC-IRMS technique

A new GC-IRMS technique has been developed for simultaneous analysis of the mixing ratio and isotopic composition of $\delta^{13}C$ and $\delta^{18}O$ in atmospheric CO_2. The technique avoids previous problems associated with traditional techniques by:

- completely separating N_2O from CO_2 so that previous corrections for this contaminant are no longer required.
- subjecting sample and reference gases to exactly the same extraction procedures so that introduced errors to the analysis procedure are systematic and therefore tend to cancel out.
- having small sample requirements to ease the logistics of sample collection.
- performing a simultaneous CO_2 mixing ratio measurement so that analysis by another instrument is eliminated, unless the required precision is higher than 0.4 ppm.
- Eliminating cryogen use for the extraction of CO_2 thus lowering the cost and workload required to perform the measurement.

The precision of the GC-IRMS technique when three 0.5 ml aliquots from a whole-air sample are analysed is:

- 0.02 ‰ for $\delta^{13}C$
- 0.04 ‰ for $\delta^{18}O$ and
- 0.4 ppm for CO_2 mixing ratio

This precision therefore meets the requirements to successfully monitor the isotopic composition of atmospheric CO_2.

The total sample usage is 45 ml for an air sample collected at ambient pressure. Of this, three 0.5 ml aliquots of the air sample are injected onto the GC column and from each of these ~0.8 nmol CO_2 enters the IRMS source. These sample requirements are up to three orders of magnitude smaller than those required by dual-inlet techniques.

Analysis of an air sample collected at ambient pressure can be performed without contamination so long as the sample flask volume is greater than 150 ml. This is currently limited by the inlet volume, which may be potentially further reduced with the use of very low volume valves and plumbing.

The technique performed at the theoretical maximum shot-noise-limited precision of 0.02 ‰ for $\delta^{13}C$. This can potentially be improved to 0.01 ‰ by reducing the open split ratio to enable more CO_2 (~3 nl) into the IRMS source. Better precision is possible if sample and reference gas volumes in the IRMS source are matched. However, small samples are analysed with higher precision by maintaining the reference gas volume relatively large.

To enable high precision important factors are:

- Maximisation of signal to noise ratios. This is achieved by minimising contamination of the system with laboratory air and maximising carrier gas purity (background m/e levels must be lower than ~2 pA). In addition, the open slit design must avoid sample dilution and the entrainment of laboratory air.
- Maximisation of reproducibility. Temperature and pressure effects must be reduced (less than 0.2 °C/hour) and the IRMS must be used with sensitivity maximised (greater than ~1,100 molecules/ion) and non-linearity minimised (less than ~0.1 ‰·$Volt^{-1}$ for $\delta^{13}C$ and <0.15 ‰·$Volt^{-1}$ for $\delta^{18}O$).

Further checks on the technique performance were carried out during inter calibration and inter comparison exercises with other laboratories and are discussed below in section 6.1.2.

Successful use of the technique was demonstrated by its the application over a large geographical region of the Pacific Ocean. The measurements obtained were consistent with previous measurements in this region. Further use of the technique for varied research utilising small sample requirements were also performed. These are discussed below in section 6.1.3.

When combined with successful inter calibration and inter comparison exercises with other laboratories, GC-IRMS is a very powerful technique to monitor global CO_2 mixing ratio and isotopic composition, both spatially and temporally. Such use, when merged with the existing measurements, would enable global carbon cycle modelling and climate change predictions to be performed with greater accuracy and confidence in the future.

6.1.2 Inter calibration and inter comparison exercises

Initial results from a high precision inter calibration exercise between the GC-IRMS technique and traditional techniques at CSIRO evaluated the performance of the GC-

IRMS technique. The IAEA target precision for $\delta^{13}C$ was achieved during the inter calibration exercise with CSIRO that utilised an inter calibration gas with a composition close to that of the ambient atmosphere and the GC-IRMS reference gas. Therefore, the extraction and analysis of CO_2 from whole-air in a low-pressure tank by GC-IRMS does not appear to be subject to the problems experienced by the dual-inlet technique in the 1995 IAEA inter comparison of whole air in high-pressure cylinders.

$\delta^{18}O$ and CO_2 mixing ratio demonstrated reduced agreement that was outside the IAEA and WMO target precisions. However, when measurement uncertainties were considered, the differences were not significant.

An ICP with CSIRO demonstrated better inter laboratory agreement than has previously been observed by other laboratories. For $\delta^{13}C$ the agreement was approximately the same as that observed during the inter calibration exercise, therefore indicating that no additional problems were introduced with the extraction and analysis of whole-air samples that were collected and stored in glass flasks.

Inter comparisons with NOAA CMDL and INSTAAR showed similar agreement to the ICP between NIWA and CSIRO. No significant conclusions can yet be drawn from these inter comparisons until further measurements are made.

Inter comparisons with SIO also showed good agreement for $\delta^{13}C$. A large offset of ~-0.99 ± 0.15‰ was observed between (NIWA-SIO) ICP measurements of $\delta^{18}O$ and the reasons for this are not yet clear.

The discrepancies observed in the ICPs may be attributed to the following possible reasons:

- Ineffective drying of collected air samples; this allows ^{18}O exchange between CO_2 and H_2O to occur, with loss of $\delta^{18}O$ stability.
- Long-term storage in sample flasks; this facilitates ^{18}O exchange between CO_2 and H_2O to occur over a longer period so that the fractionation can become large enough to account for some of the differences observed between the laboratory measurements.
- GC-IRMS non-linearity; this causes loss of agreement when comparing whole-air samples or other gases (*e.g.* primary standards) that have different CO_2 mixing ratio and $\delta^{18}O$ compositions by up to ~50 ppm and ~2.5 ‰ respectively, from the reference gases used to perform the analysis.

- Small numbers of inter comparison samples; this limits the significance of observed differences (or agreement).
- Different data rejection criteria that exist between laboratories; this can sometimes cause differences in the temporal variations observed at land-based monitoring sites because one laboratory may reject data that the other does not and this affects monthly mean values.
- Inconsistencies within calibration scales; these can introduce offsets to laboratory data sets.

Resolution of these problems should improve future ICPs.

These preliminary inter comparison data suggest agreement between all three laboratories for $\delta^{13}C$. This is in contrast to a previous IAEA inter comparison of these laboratories in 1994 that showed large inter laboratory differences for $\delta^{13}C$ of up to 0.1 ‰. Assuming differences were not smaller than that detectable, this finding suggests that the inter calibration situation has improved between these laboratories or that some unaccounted problem has been present in these measurements.

Further work is therefore necessary, and the combination of on-going inter calibration and inter comparison measurements that have been established during this work, with the implementation of the GLOBAL-HUBS inter calibration scheme will most likely enable IAEA and WMO target precisions to be met. This will allow worldwide merging of atmospheric CO_2 data from GC-IRMS and traditional techniques in the future. The increased spatial and temporal resolution as a result of this merging will allow atmospheric CO_2 source – sink evaluations to be more accurately and precisely determined by global carbon cycle models in the future.

6.1.3 Applications

Temporal variations of atmospheric CO_2 species at Baring Head, Cape Grim and Arrival Heights were monitored by GC-IRMS. The CO_2 mixing ratio and $\delta^{13}C$ seasonal cycle were successfully observed at Baring Head with an amplitude of ~1 ppm and ~0.05 ‰ respectively. $\delta^{18}O$ showed a large variation. A decline of ~-0.1 ‰/year for $\delta^{13}C$ was observed at Arrival Heights and reasons for this large trend, compared to other measurements, are not yet clear. Higher frequency sampling at these sites should help to more accurately monitor change at these sites. Further work is therefore required to investigate differences between these sites in the Southern Hemisphere.

Spatial variations in the Pacific Ocean region were investigated and in the Southern Ocean, relatively constant levels for CO_2 species as a function of latitude were observed. Gas exchange with ocean water was important in this region because ocean water at high latitudes has depleted $\delta^{18}O$, due to its freshwater content, and samples from low levels experiencing greater exchange with this water therefore had depleted $\delta^{18}O$ compared to samples from higher levels. The sparse data in the Southern Ocean is the biggest limitation to these and other measurements of atmospheric CO_2 species.

Inter hemispheric gradients were observed from two Pacific Ocean ship voyages between ~32 °S and 35 °N. The position and intensity of the SPCZ and ITCZ were important for the strength of these gradients in equatorial regions. The larger seasonal cycle of atmospheric CO_2 mixing ratio and $\delta^{13}C$ in the Northern Hemisphere was clearly resolved. These measurements compared well with previous data obtained in the region.

Upper-tropospheric CO_2 collected during flights between New Zealand and Antarctica was elevated in CO_2 mixing ratio and depleted in $\delta^{13}C$. Even at altitudes of ~8,700 m, H_2O contamination (possibly from the collection of ice-crystals in high-level cirrus clouds) and resultant ^{18}O exchange between CO_2 and H_2O occurred. Drying of all further samples would therefore eliminate this problem. The transport of Northern Hemisphere air into the upper troposphere of the Southern Hemisphere is important in this region. This transport, in addition to the CO_2 sink at the surface of the Southern Ocean, accounts for the differences between upper tropospheric and surface based measurements in this region.

A small-scale application of the technique for analysing soil-respired CO_2 collected in 150 ml flasks at ambient pressure was performed successfully. The precision and accuracy of CO_2 source determinations can be increased in the future by collecting more samples (which are easily analysed by the automated GC-IRMS technique) and using an additional reference gas that has a similar composition to that of the samples.

6.2 Further work

Recently, mixing ratio measurements of other important trace gases such as CH_4 and CO have also been complemented by determinations of their stable isotopic composition. These data have provided additional constraints on the budgets and removal mechanisms of these gases [e.g., *Tyler et al.*, 1999; *Lowe et al.*, 1997]. Traditionally, IRMS analysis of these gases has been performed after conversion to CO_2 and/or pre-concentration. The GC-IRMS technique developed by this work can be used as a "front end" for the analysis

of such gases. This "modular approach" to important greenhouse gases is summarised below in Figure 6.1 and work has already begun at NIWA to develop high precision GC-IRMS measurements of atmospheric CH_4 [*Brailsford*, in preparation]. Previous methods for non methane hydrocarbons (NMHCs) [*Rudoulph et al.*, 1997] are easily accommodated by this modular approach presented below and higher performance would be possible by the use of the technique presented in this thesis for the analysis of the extracted CO_2. The large sample requirements traditionally required for dual-inlet analysis of CH_4 (~35 to 50 litres) and CO (~300 litres) would be reduced considerably for GC-IRMS analysis. N_2O is another important greenhouse gas and presently isotope measurements of this gas are difficult to perform. Such measurements can be performed by GC-IRMS as complete separation from CO_2 is possible. Further research of N_2O pathways in soil, through either nitrification or de-nitrification, would also be possible with the GC-IRMS technique to provide information about these processes of which little is currently known.

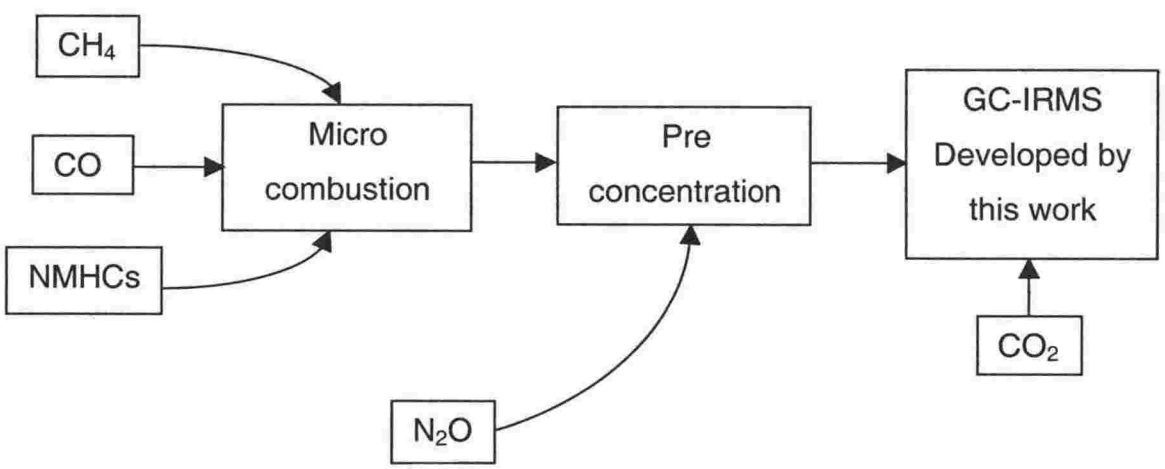

Figure 6.1 Modular approach to GC-IRMS for further work.

Potentially, the linking of a GC-IRMS system with GCs for the analysis of other mixing ratios would enable a complete suite of greenhouse gas mixing ratio and isotopic ratio determinations to be performed simultaneously from one air sample in an automated procedure without the use of cryogen. This has large advantages for atmospheric monitoring programs to extend the number of species monitored with a reduction in human workload and required consumables.

Other areas of research that may potentially benefit from the applications of this technique are biological and ecosystem studies (*e.g.* plant respiration and agricultural N_2O source sink determinations). In addition, biomedical measurements of $\delta^{13}C$ in breath

samples for diagnosis of metabolic disorders and infections (*e.g. Helicobacter pylori,* responsible for stomach ulcers and implicated in stomach cancer [e.g., *Koletzko et al.*, 1995; http://www.helico.com], carbohydrate malabsorption, abnormal liver function and variations in bile acid metabolism [*Esler*, 1997]) would be easily performed by GC-IRMS and these measurements would be more economical than dual-inlet IRMS measurements that are normally performed. Recent developments in FTIR [*Esler*, 1997] are also available for these measurements but are performed with lower precision than is possible with GC-IRMS.

6.3 Overall conclusion

GC-IRMS is a reliable technique that yields sufficient precision to provide useful determinations of the isotopic composition of atmospheric CO_2. These measurements are N_2O-free and therefore avoid previous problems in correcting for its isotopomers. In addition, useful CO_2 mixing ratio measurements are simultaneously performed. When combined with successful inter calibration and inter comparison exercises with other laboratories, GC-IRMS is a very powerful technique to monitor global CO_2 mixing ratio and isotopic composition, both spatially and temporally. Such use, when merged with the existing measurements, would enable global carbon cycle modelling and climate change predictions to be performed with greater accuracy and confidence in the future.

6.4 References

Allison, C.E., and Francey, R.J., High precision stable isotope measurements of atmospheric trace gases, in *Reference and intercomparison materials for stable isotopes of light elements*, pp. 131-153, International Atomic Energy Agency, Vienna, 1995.

Allison, C.E., R.J. Francey, and H.A.J. Meijer, Recommendations for the reporting of stable isotope measurements of carbon and oxygen in CO_2 gas, in *Reference and intercomparison materials for stable isotopes of light elements*, pp. 155-162, International Atomic Energy Agency, Vienna, 1995.

Allison, C.E., and Francey, R.J., $\delta^{13}C$ of atmospheric CO_2 at Cape Grim: The in situ record, the flask record, air standards and the CG92 calibration scale, in *Baseline Atmospheric Program Australia 1996*, edited by A.L. Dick, N.A. Derek, and W. Bouma, Bureau of Meteorology and CSIRO Division of Atmospheric Research, Aspendale, 1999.

Becker, J.F., T.B. Sauke, and M. Loewenstein, Stable isotope analysis using tunable diode laser spectroscopy, *Applied optics*, *31*, 1921-1927, 1992.

Brenna, J., T.N. Corso, H.J. Tobias, and R.J. Caimi, High-precision continuous flow isotope ratio mass spectrmetery, *Mass Spectrometery Reviews*, *16*, 227-258, 1997.

Ciais, P., P.P. Tans, J.W.C. White, M. Trolier, R.J. Francey, J.A. Berry, D.R. Randall, P.J. Sellers, J.G. Collatz, and D.S. Schimel, Partitioning of ocean and land uptake of CO_2 as inferred by $\delta^{13}C$ measurements from the NOAA Climate Monitoring and Diagnostics Laboratory Global Air Sampling Network, *Journal of Geophysical Research*, *100* (D3), 5051-5070, 1995a.

Ciais, P., P.P. Tans, M. Trolier, J.W.C. White, and R.J. Francey, A Large Northern Hemisphere Terestrial CO_2 Sink Indicated by the $^{13}C/^{12}C$ Ratio of Atmospheric CO_2, *Science*, *269*, 1098 - 1102, 1995b.

Ciais, P., A.S. Denning, P.P. Tans, J.A. Berry, D.R. Randall, J.G. Collatz, P.J. Sellers, J.W.C. White, M. Trolier, A.J. Harro, A.J. Meijer, R.J. Francey, P. Monfray, and M. Heimann, A three-dimensional synthesis study of $\delta^{18}O$ in atmospheric CO_2 1. Surface fluxes, *Journal of Geophysical Research*, *102* (D5), 5857-5872, 1997a.

Ciais, P., P.P. Tans, A.S. Denning, R.J. Francey, M. Trolier, A.J. Harro, A.J. Meijer, J.W.C. White, J.A. Berry, D.R. Randall, J.G. Collatz, P.J. Sellers, P. Monfray, and M. Heimann, A three-dimensional synthesis study of $\delta^{18}O$ in atmospheric CO_2 2. Simulations with the TM2 transport model, *Journal of Geophysical Research*, *102* (D5), 5873-5883, 1997b.

Clarke, H.T., Isotopes in Biochemistry: Historical Background, in *The use of isotopes in biology and medicine*, edited by H.T. Clarke, The University of Winsconsin press, Winsconsin, 1948.

Conway, T.J., P.P. Tans, L.S. Waterman, K.W. Thoning, D.R. Kitzis, K.A. Masarie, and N. Zhang, Evidence for interannual variability of the carbon cycle from the NOAA CMDL global air sampling network, *Journal of Geophysical Research*, *99*, 22,831-22,855, 1994.

Craig, H., Isotopic standards for carbon and oxygen and correction factors for mass spectometric analysis of carbon dioxide, *Geochimica Cosmochimica Acta*, *12*, 133-149, 1957.

Da Costa, G. and Steele, P., A low flow analyser system for making measurements of atmospheric CO_2, in *Report of the ninth WMO meeting of experts on carbon dioxide concentration and related tracer measurement techniques*, edited by Roger Francey, World Meteorological Organization Global Atmosphere Watch, No. 132, Aspendale, Victoria, Australia, 1997.

Ehleringer, J.R., and Cook, C.S., Carbon and oxygen isotope ratios of ecosystem respiration along an Oregon conifer transect: preliminary observations based on small-flask sampling, *Tree Physiology*, *18*, 513-519, 1998.

Esler, M.B., High precision measurement of atmospheric trace gases using Fourier transform infrared spectroscopy, University of Wollongong, 1997.

Etheridge, D.M., L.P. Steele, R.L. Langenfelds, R.J. Francey, J.M. Barnola, and V.I. Morgan, Natural and anthropogenic changes in atmospheric CO_2 over the last 1000 years from air in Antarctic ice and firn, *Journal of Geophysical Research*, *101* (D2), 4115-4128, 1996.

Francey, R.J. and Tans, P. P, Latitudinal variations in oxygen-18 in atmospheric CO_2, *Nature*, *327*, 495-497, 1987.

Francey, R.J., P. Tans, C.E. Allison, I. Enting, J.C. White, and M. Trolier, Changes in oceanic and terrestrial carbon uptake since 1982, *Nature*, *373*, 326-330, 1995.

Francey, R.J., L.P. Steele, R.L. Langenfelds, M.P. Lucarelli, C.E. Allison, D.J. Beardsmore, S.A. Coram, N. Derek, F.R. de Silva, D.M. Etheridge, P.J. Fraser, R.J. Henry, B. Turner, E.D. Welch, D.A. Spencer, and L.N. Cooper, Global atmospheric sampling laboratory (GASLAB): Supporting and extending the Cape Grim trace gas programs, in *Baseline Atmospheric Program Australia 1993*, edited by R.J. Francey, A.L. Dick, and N. Derek, pp. 8-29, Bureau of Meteorology and CSIRO Division of Atmospheric Research, Melbourne, 1996.

Francey, R.J., and Rayner, P.J., Constraining the carbon budget from global to regional scales - the measurement challenge, in *First anniversary workshop of the Max Plank Institut fur Biogeoghie*, Jena, Germany, 1998.

Francey, R.J., L.P. Steele, R.L. Langfields, L.N. Cooper, C.E. Allison, N.B.A. Trivett, and V. Hudec, CSIRO trace gas measurements from Canadian sites, *Canadian Baseline Program Summary of Progress to 1998,* Atmospheric Environment Service, Environment Canada, Toronto, 1999.

Francey, R.J., C.E. Allison, D.M. Etheridge, C.M. Trudinger, I.G. Enting, M. Leuenberger, R.L. Langfields, E.A. Michel, and L.P. Steele, A 1000-year high precision record of $\delta^{13}C$ in atmospheric CO_2 , *Tellus* (5th International CO_2 conference issue), 51B, 170-193, 1999.

Francey, R.J., *Personal communication*, CSIRO Division of Atmospheric Research, Melbourne, Australia, August 1999.

Friedli, H., H. Lotscher, H. Oeschger, U. Siegenthaler, and B. Stauffer, Ice core record of the $^{13}C/^{12}C$ ratio of CO_2 in the last two centuries, *Nature, 324*, 237-238, 1986.

Gaudry, A., P. Monfray, M. Trolier, C. Flehoc, P. Ciais, and S.G. Jennings, A preliminary comparison of $\delta^{13}C$ measurements in CO_2 from Mace Head, Ireland, *Climate Monitoring and Diagnostics laboratory Summary Repot No. 23, 1994-1995,* U. S. Department of Commerce. National Oceanic and Atmospheric Administration, Boulder, 1996.

Gemery, P.A., Troiler, M., and White, J. W. C., Oxygen isotope exchange between carbon dioxide and water following atmospheric sampling using glass flasks, *Journal of Geophysical Research, 101* (D9), 14,415-14,420, 1996/6.

Gomez, A., Baring Head Atmospheric Data Summary, NIWA, Wellington, 1996.

Gonfiantini, R., W. Stichler, and K. Rozanski, Standards and intercomparison materials distributed by the International Atomic Energy for stable isotope measurements, in *Reference and intercomparison materials for stable isotopes of light elements*, pp. 13-29, International Atomic Energy Agency, Vienna, 1995.

Halstead, R.E., and Nier, A. O., Gas flow through a mass spectrometer viscous leak, *The Review of Scientific Instruments, 21*, 1019-1021, 1950.

Hoefs, J., *Stable isotope geochemistry*, 201 pp., Springer, Berlin, 1997.

Hudec, V., K. Higuchi, and N.B.A. Trivet, Flask CO_2 measurements, *Canadian Baseline Program Summary of Progress to 1998,* Atmosphere Environment Services, Environment Canada, Toronto, 1999.

IPCC, *Climate change 1994: Radiative forcing of climate change*, 339 pp., Cambridge University Press, Cambridge, 1995.

IPCC, *Climate change 1995: The science of climate change*, 572 pp., Cambridge University Press, Cambridge, 1996.

Keeling, C.D., Industrial production of carbon dioxide from fossil fuels and limestone, *Tellus, XXV*, 174-198, 1973.

Keeling, C.D., R.B. Bacastow, A.F. Carter, S.C. Piper, T.P. Whorf, M. Heimann, W.G. Mook, and H. Roeloffzen, A three dimensional model of atmospheric CO_2 transport based on observed winds: 1. Analysis of observational data, in *Geophysical Monograph 55*, pp. 165-236, American Geophysical Union, 1989.

Keeling, C.D., T.P. Whorf, M. Wahlen, and J. van der Plicht, Interannual extremes in the rate of rise of atmospheric carbon dioxide since 1980, *Nature, 375*, 666-670, 1995.

Koletzko, S., M. Haish, I. Seebooth, B. Braden, K. Hengels, B.A. Koletzko, and P. Hering, Isotope selective non-dispersive infrared spectrometery for detection of Helicobacter pylori infection with ^{13}C urea breath test, *Lancet, 345* (961-962), 1995.

Langfields, R.L., P.J. Fraser, r.J. Francey, L.P. Steele, L.W. Porter, and C.E. Allison, The Cape Grim air archive: the first seventeen years, 1978 – 1995, in *Baseline Atmospheric Program Australia 1995-1995*, edited by R.J. Francey, A.L. Dick, and N. Derek, pp. 53-70, Bureau of Meteorology and CSIRO Division of Atmospheric Research, Melbourne, 1996.

Leckrone, K.J., and Hayes, J.M., Efficiency and temperature dependence of water removal by membrane dryers, *Analytical Chemistry, 69*, 911-8, 1997.

Leckrone, K.J., and Hayes, J.M., Water-induced errors in Continuous-Flow carbon isotope ratio mass spectrometery, *Analytical Chemistry, 70*, 2737-2744, 1998.

Lowe, D.C., P.R. Guenther, and C.D. Keeling, The concentration of atmospheric carbon dioxide at Baring Head, New Zealand, *Tellus, 31*, 58-67, 1979.

Lowe, D.C., M.R. Manning, G.W. Brailsford, and A.M. Bromley, The 1991-1992 atmospheric methane anomaly: Southern Hemisphere ^{13}C decrease and growth rate fluctuations, *Geophysical Research Letters, 24,* 857-860, 1997.

Mak, J.E., and Brenninkmeijer, C. A. M., Compressed air sample technology for isotopic analysis of atmospheric carbon monoxide, *Journal of Atmospheric and Oceanic Technology*, *11*, 425-431, 1994.

Manahan, S.E., *Environmental chemistry*, 811 pp., Lewis Publishers, Ann Arbor, 1994.

Manning, M.R., A.J. Gomez, and K.P. Pohl, Atmospheric CO_2 record from in-situ measurements at Baring Head, *pp 174-178. In Trends '93*, edited by T.A. Boden, D.P. Kaiser, R.J. Sepanski and F.W. Stoess, A compendium of data on global change, ORNL/CDIAC-65, Carbon Dioxide Information Analysis Center, Oak Ridge National Laboratory, Oak Ridge, Tenn, USA, 1994.

Matthews, D.E., and Hayes, J. M., Isotope-ratio-monitoring gas chromatography-mass spectrometry, *Analytical Chemistry*, *50*, 1465-1473, 1978.

McKinney, C.R., J. M. McCrea, S. Epstein, H. A. Allen, and H. C. Urey, Improvements in mass spectrometers for the measurement of small differences in isotopic abundance ratios, *The Review of Scientific Instruments*, *21*, 724-730, 1950.

Merritt, D. A., and Hayes, J. M., Factors Controlling Precision and Accuracy in Isotope-Ratio-Monitoring Mass Spectrometry, *Analytical Chemistry*, *66* (14), 2336-2347, 1994.

Merritt, D.A., J.M. Hayes, and D.J. Des Marais, Carbon isotopic analysis of atmospheric methane by isotope-ratio-monitoring gas chromatography-mass spectrometry, *Journal of Geophysicl Research*, *100* (D1), 1317-1326, 1995.

Mook, W.G., and Jongsma, J., Measurement of the N_2O correction for $^{13}C/^{12}C$ ratios of atmospheric CO_2 by removal of N_2O, *Tellus*, *39B*, 96-99, 1987.

Murayama, S., T. Nakazawa, A. Shuhji, and M. Shinji, Variations of the carbon and oxygen isotopic ratios of atmospheric CO_2 at Syowa Station, *Meteorological and Geophysical Abstracts*, *49*, 4-110, 1998.

Murnick, D.E., and Peer, B. J., Laser-based analysis of carbon isotope ratios, *Science*, *263*, 945-947, 1994.

Nakazawa, T., S. Aoki, S. Murayama, M. Fukabori, T. Yamanouchi, H. Murayama, M. Shiobara, G. Hashida, S. Kawaguchi, and M. Tanaka, The concentration of atmospheric carbon dioxide at the Japanese Antarctic station, Syowa, *Tellus*, *43B*, 126-135, 1991.

Nakazawa, T., S. Muruyama, K. Miyashita, S. Aoki, and M. Tanaka, Longitudinally different variations of lower tropospheric carbon dioxide concentrations over the North Pacific Ocean, *Tellus*, *44B*, 161-172, 1992.

Nier, A.O., and Gulbransen, E. A., Variations in the relative abundances of the carbon isotopes, *Journal of American Chemical Society*, *61*, 697-698, 1939.

Peixoto, J.P., and Oort, A. H., *Physics of climate*, 520 pp., American Institute of Physics, New York, 1992.

Petterson, D.W., and Hayes, J. M., *Contempory topics in analytical and clinical chemistry*, 217-252 pp., Plenum Publishing, New York, 1978.

Ricci, M.O., K.H. Merrit, and J.M. Hayes, Aquisition and processing of data for isotope-ratio-monitoring mass spectrometery, *Organic Geochemistry*, *21*, 561-572, 1194.

Rudolph, J., D.C. Lowe, R.J. Martin, and T.S. Clarkson, A novel method for the compound specific determination of $\delta^{13}C$ in volatile organic compounds at ppt levels in ambient air, *Geophysical Research Letters*, *24* (6), 659-662, 1997.

Sano, M., Y. Yotsui, H. Abe, and S. Sasaki, A new technique for the detection of metabolites labelled by the isotope ^{13}C using mass fragmentography, *Biomedical Mass Spectrometry*, *3*, 1-3, 1976.

Santrock, J., S.A. Studley, and J.M. Hayes, Isotopic analyses based on the mass spectrum of carbon dioxide, *Analytical Chemistry*, *57*, 1444-1448, 1985.

Scott, N. A, *Personal communication*, Landcare Research, Palmerston North, New Zealand, September 1999.

Siegenthaler, U., Uptake of excess CO_2 by an outcrop-diffusion model of the ocean, *Journal of Geophysical Research, 88*, 3,599-3,608, 1983.

Siegenthaler, U. and Oeschger, H., Biospheric CO_2 emissions during the past 200 years reconstructed by deconvolution of ice core data, *Tellus, 39B*, 140-154, 1987.

Siegenthaler, U. and Sariemento, J. L. Atmospheric carbon dioxide and the ocean, *Nature, 365*, 119-125, 1993.

Sturman, A. P., and Tapper, N. J., *The weather and Climate of Australia and New Zealand*, 476pp., Oxford University Press, Auckland, 1996.

Steele, L.P., Beardsmore, D. J., Pearman, G. I. and Da Costa, G. A., Baseline carbon dioxide monitoring, in *Baseline Atmospheric Program Australia 1995-1995*, edited by R.J. Francey, A.L. Dick, and N. Derek, pp. 103, Bureau of Meteorology and CSIRO Division of Atmospheric Research, Melbourne, 1996.

Steele, L.P., R.J. Francey, R.L. Langfields, C.E. Allison, M.P. Lucarelli, P.P. Tans, E.J. Dlugokencky, T.J. Conway, P.C. Novelli, K.A. Massarie, J.W.C. White, and M. Trolier, An operational intercalibration experiment between CMDL and CSIRO to measure several atmospheric trace species, U. S. Department of Commerce. National Oceanic and Atmospheric Administration, Boulder, 1996.

Svec, H.J., Mass spectrometery - ways and means. A historical prospectus, *International Journal of Mass Spertrometery and Ion Processes, 66*, 3-29, 1985.

Tans, P.P., P.S. Bakwin, L. Bruhwiler, T.J. Conway, E.J. Dlugokencky, D.W. Guenther, D.F. Hurst, D.R. Kitzis, P.M. Lang, K.A. Masarie, J.B. Miller, P.C. Novelli, C. Prostko-Bell, K.W. Thoning, B.H. Vaughan, J.W.C. White, D. Yakir, and C. Zhao, *Climate Monitoring and Diagnostics Laboratory Summary Report No. 24 1996-1997*, U. S. Department of Commerce. National Atmospheric Administration, Boulder, 1998.

Trolier, M., J.W.C. White, P.P. Tans, K.A. Masarie, and P.A. Gemery, Monitoring the isotopic composition of atmospheric CO_2: Measurements from the NOAA Global Air Sampling network, *Journal of Geophysical Research, 101* (D20), 25,897-25,916, 1996.

Tyler, S.C., H.O. Ajie, M.L. Gupta, R.J. Cicerone, D.R. Blake, and E.J. Dlugokenchy, Carbon isotopic composition of atmospheric methane: A comparison of surface level and upper tropospheric air, *Journal of Geophysical Research, 104*, 13,895-13,910, 1999.

Vay, S.A., B.E. Anderson, T.J. Conway, G.W. Sachse, J.E. Collins, D.R. Blake, and D.J. Westberg, Airborne observations of the tropospheric CO_2 distribution and its controlling factors over the South pacific basin, *Journal of Geophysical Research, 104* (D5), 5663-5676, 1999.

Warneck, P., *Chemistry of the atmosphere*, 753 pp., Academic Press, San Diego, 1988.
WMO, Environmental pollution monitoring and research program, World Meteorological Organization, Geneva, 1987.

Weiss, R. F., Determination of carbon dioxide and methane by dual catalyst Flame Ionization Chromatography and nitrous oxide by Electron Capture Detector, *Journal of Chromatographic Science*, 19, 611-616, 1981.

Yoder, B.J., M.G. Ryan, R.H. Waring, A.W. Schoettle, and M.R. Kaufmann, Evidence of reduced photosynthetic rates in old trees, *Science*, *40*, 513-527, 1994.